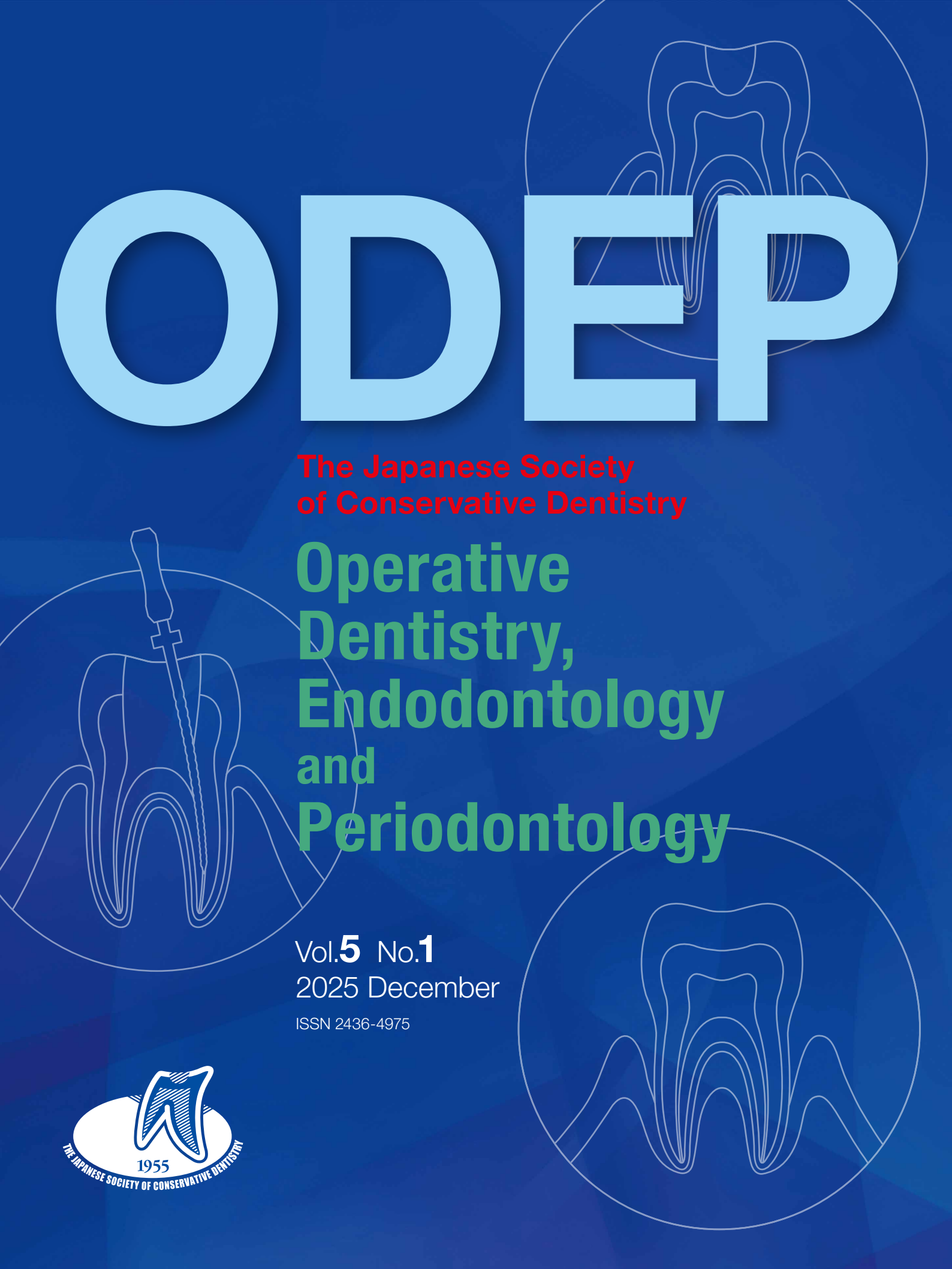

ODEP

The Japanese Society of Conservative Dentistry

Operative Dentistry, Endodontology and Periodontology

Vol.5 No.1
2025 December
ISSN 2436-4975

1955
THE JAPANESE SOCIETY OF CONSERVATIVE DENTISTRY

NISHIKA

Bioceramic material

バイオセラミックスが
封鎖性と生体親和性を向上

根管充填シーラとして

充填法
- シングルポイント法 *
- 側方加圧法
- 垂直加圧法

誰が練っても
いつも同じ仕上がり

歯科用覆髄材料・
歯科用根管充填シーラ

ニシカ キャナルシーラー® BGmulti

覆髄材として

ペーストにパウダーを
混ぜると覆髄にも
使いやすい性状に。

[包装・標準価格]
ペースト：1本［A材 4.5g(2.5mL)、B材4.5g(2.5mL)］・12,000円／パウダー：1個［2g］・9,800円／
セット：ペースト1本、パウダー1個・21,000円

管理医療機器 一般的名称：歯科用覆髄材料・歯科用根管充填シーラ　医療機器認証番号：302ADBZX00055000　製造販売元：日本歯科薬品株式会社

＊シングルポイント根管充填用ツール「BGフィル」を販売しています。詳しくは、特設サイトをご覧ください。

【特設サイト】

NISHIKA 日本歯科薬品株式会社
本　社 山口県下関市竹崎町4-7-24 〒750-0025
営業所 大阪・東京・福岡
https://www.nishika.co.jp/
お問合せ・資料請求《お客様窓口》
0120-8020-96

第二弾 演者発表！【早割申込】受付中

GC友の会70周年記念

第6回国際歯科シンポジウム

2026.10.3 SAT ▷ 4 SUN

会場：東京国際フォーラム（東京都千代田区）

英知の結集

80億人の笑顔を育む歯科医療

Gather Knowledge, Create “8 billion” Smiles!

THE 6TH INTERNATIONAL DENTAL SYMPOSIUM

国内講師


Dr. Akihiko Katayama


Prof. Akikazu Shinya


Ms. Akiko Katayama


Ms. Akiko Kobayashi


Prof. Akimasa Tsujimoto


Dr. Akira Hasuike


Dr. Akira Makino


Dr. Akira Suzaki


Dr. Akiyoshi Funato


Prof. Atsuo Amano


Prof. Atsushi Saito


Ms. Ayako Shiinoki


Ms. Chieko Hayashi


Ms. Chiharu Kanno


Dr. Dai Kawanabe


Prof. Eriko Marukawa


Dr. Gen Takahashi


Prof. Hajime Matsumura


Prof. Haruka Tohara


Prof. Hidefumi Maeda


Dr. Hidehiro Abe


Dr. Hidetoshi Aimiya


Ms. Hikari Tanimoto


Dr. Hirofumi Tashiro


Mr. Hirofumi Yokota


Dr. Hirohiko Hirano


Dr. Hiroki Suzuki


Prof. Hiroshi Egusa


Dr. Hiroshi Ishii


Mr. Hiroyuki Kito


Dr. Hiroyuki Saida


Dr. Hitoshi Higuchi


Dr. Ikuhisa Okuno


Ms. Izumi Nishio


Dr. Kakuhiro Fukai


Dr. Kan Ushijima


Prof. Kaoru Kusano


Dr. Katsuhiko Akiyama


Dr. Katsu Takahashi


Dr. Katsushi Sato

Dr. Katsuyuki Atsumi

Dr. Kazuki Nagata

Dr. Kazunori Otani

Prof. Keiichi Hosaka

Dr. Kensuke Sakai

Mr. Ken Takahashi

Dr. Kentaro Imamura

Dr. Kentaro Okuno

Dr. Kiyoe Shimizu

Dr. Kohei Teramoto

Prof. Koichiro Matsuo

Dr. Kotaro Fujimaki

Prof. Kyoko Oka

Prof. Manabu Kanazawa

Ms. Mari Nobeta

Ms. Masae Nakazawa

Dr. Masahiro Minami

Dr. Masao Yamazaki

Prof. Masashi Miyazaki

Prof. Masayuki Tsukasaki

Ms. Miho Yokota

Ms. Mika Shinonaga

Dr. Mitsuteru Kawamura

Dr. Miyuki Hamano

Ms. Nami Katayama

Mr. Naoki Hayashi

Dr. Naoto Ito

Dr. Noriko Tonogi

Ms. Noriko Yamamoto

Ms. Noriko Yura

Dr. Ryosuke Hayashi

Dr. Ryuichi Kondo

Dr. Ryuichi Takaoka

Ms. Sakura Miyamoto

Prof. Satoshi Imazato

Dr. Satoshi Kawai

Dr. Seiichiro Ono

Ms. Seira Ito

Dr. Shigeru Daimon

Prof. Shinya Murakami

Dr. Shogo Maekawa

Prof. Shouji Hironaka

Dr. Shu Hoshi

Dr. Shunsuke Fukuba

Dr. Tadahiko Nakano

Prof. Takanori Iwata

Prof. Takayuki Ueda

Dr. Takeshi Sasaki

Dr.Takuya Minamino

Dr. Teppei Tsukiyama

Dr. Tetsuji Aoshima

Dr. Tetsuya Mizukami

Dr. Tetsuya Uchiyama

Dr. Tokuo Matsui

Dr. Tomohiro Ishikawa

Dr. Tomoyoshi Shimoyama

Dr. Toshiki Takamizawa

Dr. Toshio Ohkawa

Ms. Yaeko Kakinuma

Dr. Yasuhiro Kizu

Dr. Yasuhiro Sasao

Mr. Yasunari Araki

Prof. Yasunori Ayukawa

Prof. Yasushi Shimada

Dr. Yoichi Taniguchi

Dr. Yoji Sato

Dr. Yoshiaki Sakurai

Dr. Yoshihiro Iwano

Ms. Yoshiko Tsukamoto

Mr. Yoshinori Yamamoto

Dr. Yoshitaka Nara

Dr. Yudai Ogawa

Dr. Yuichiro Ihara

Dr. Yuiko Niizuma

Ms. Yuki Ohara

Dr. Yukihiro Kosaka

Ms. Yuki Shioura

Dr. Yukiko Koke

Ms. Yuko Shimoda

Dr. Yumiko Shibahara

Ms. Yumiko Tanigaki

Ms. Yuriko Chiba

Dr. Yusuke Ninomiya

海外講師

Dr. Anthony Mak

Prof. Anton Sculean

Prof. Bart Van Meerbeek

Dr. Bharat Agrawal

Prof. Bora Korkut

Dr. Celine Higton

Dr. Chia Cheng Lu

Prof. Chooryung J. Chung

Dr. Diana Boangar

Dr. Dimitrios Spagopoulos

Prof. Falk Schwendicke

Prof. Hom-Lay Wang

Prof. Ivana Miletić

Dr. James Tsoi

Dr. Javier Tapia Guadix

Mr. Jin Gu Kim

Prof. Joseph Sabbagh

Dr. Julia Garcia Baeza

Prof. Katrin Bekes

Prof. Marco Ferrari

Prof. Marleen Peumans

Dr. Michelle Lee

Dr. Michel Lee Gall

Dr. Mohamad Al Husini

Dr. Paul S. Rosen

Prof. Pekka Vallittu

Dr Robert L. Waugh

Dr. Roberto Sorentino

Dr. Roland Frankenberger

Dr. Stefano Troiani

Mr. Yu Yo Lin

第6回国際歯科シンポジウム 特設サイト

最新情報は特設サイトおよびInstagramにて随時更新いたします。

https://www.gc.dental/japan/6thsymposium

instagram

NEO DENTAL CHEMICAL PRODUCTS CO., LTD.

RENEW

素材の品質も 性能の一部です。

1本で覆髄から裏層まで！

DirectCapping+BaseLiner CAVIOS with MTA

トドイテ タレナイ

新黒Sチップ 標準添付

MTA成分「ネオホワイトピュア®」を配合したスムーズで切れの良い、歯質へのなじみが高い直接覆髄裏層材です。MTAの効果発現を促す処方により光重合裏層材としての理工学的性質に加え、直接覆髄材としての性能を有します。
1本で覆髄にも裏層にも使える２in１製材です。
従来のMサイズチップに代わり新たにＳサイズ遮光チップを標準添付しました。
微細な部分への到達性が高まっただけでなく、適応量がより細かくコントロール可能となり、同時にペーストの垂れも低減されました。

光重合 覆髄+裏層材

D-Cavios® MTA

ネオホワイトピュア® 配合

1.5g入シリンジ　1本
先端チップ　15本 **(Sサイズ)**
標準価格 6,500円

補充用　ネオ ブラックチップ(S)　30本　NEW
一般医療機器
医療機器届出番号　13B1X00154000013　標準価格 2,000円

※従来のMサイズは単品でお求めいただけます。

覆髄+裏層 2in1
D-キャビオス®MTA

医療機器認証番号　304ADBZX00054000
歯科用覆髄材料（歯科裏層用高分子系材料）
管理医療機器

製造販売業者
ネオ製薬工業株式会社
〒150-0012　東京都渋谷区広尾3丁目1番3号
Tel. 03-3400-3768（代）　Fax. 03-3499-0613

LA2507

コンポジットレジン修復の Management

審美修復を極めるための基本の「き」

宮崎真至 著

- A4判／124頁／カラー
- 定価 9,900円（本体 9,000円＋税10%）
- ISBN978-4-263-44769-7
- 注文コード：447690

詳しい内容は
二次元コードの
リンク先から!

- 長年, コンポジットレジン修復の普及に取り組んできた著者が贈る, 上達のためのバイブル的テキスト！
- 筆者の蓄積してきた知識とテクニックを, 理解しやすい図をもって解説. 実際の臨床例だけでなく, 模型も用いてステップを示しています.
- 修復の臨床において何を観るのか, 観たものをどう具現化し, そしてどのような材料で完成させていくのか, その詳細を理解し, 眼前の症例に即時対応できるようになります.

MMコンポジットレジン修復の集大成！

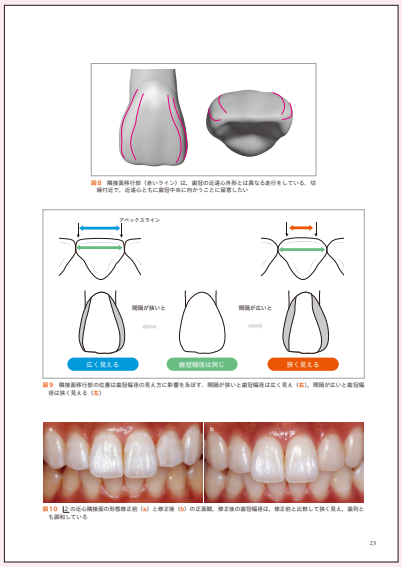

修復のためのポイントは図を使用して解説

臨床のステップは模型を用いて分かりやすく

臨床の実際も明確な写真で提示

医歯薬出版株式会社 〒113-8612 東京都文京区本駒込1-7-10 TEL03-5395-7630 FAX03-5395-7633 https://www.ishiyaku.co.jp/

OPERATIVE DENTISTRY, ENDODONTOLOGY AND PERIODONTOLOGY

Vol. 5, No. 1 DECEMBER 2025

CONTENTS

Published
by
THE JAPANESE SOCIETY OF CONSERVATIVE DENTISTRY (JSCD)
c/o Oral Health Association of Japan (Kōkūhoken kyōkai)
1-43-9, Komagome, Toshima-ku, Tokyo 170-0003
Japan

Editorial Board of Operative Dentistry, Endodontology and Periodontology (2025)

Dec, 2025

Original Article

ODEP 5 (1) : 1〜10, 2025

Development of a Biphasic Calcium Phosphate Root Canal Sealer

Yasutoshi OJIMA

Nihon University Graduate School of Dentistry at Matsudo

Abstract

Purpose: The purpose of root canal filling in endodontic treatment is to tightly seal the root canal in three dimensions following root canal enlargement and washing to prevent re-infection. Bioceramic sealers currently in clinical use in the field of endodontic treatment include calcium silicate cement sealers containing mineral trioxide aggregate (MTA) and bioactive glass sealers containing calcium silicate glass. These show good sealing properties, biocompatibility, antibacterial effects due to their basicity, and precipitation of hydroxyapatite (HA: $Ca_{10}(PO_4)_6(OH)_2$) on the material surface. This study focused on biphasic calcium phosphate (BCP), a type of bioceramic material in which α-tricalcium phosphate and tetracalcium phosphate are evenly dispersed within the same particle, and investigated the material properties of adhesive resin sealer with different amounts of added BCP.

Methods: BCP was prepared from dicalcium phosphate anhydrous and calcium carbonate. The adhesive resin sealer was MetaSEAL Soft Paste (MS). BCP was added to MS in differing amounts, and the flow, film thickness, setting time, solubility and disintegration, and radiopacity of the resulting BCP adhesive resin sealers were investigated. BCP adhesive sealers were also immersed in human simulated body fluid (SBF), and observations for precipitation on the material surface using a scanning electron microscope (SEM), energy dispersive X-ray spectroscopy (EDS) using an SEM, and microscopic Fourier transform infrared spectroscopy (FTIR) were carried out for component analysis. In addition, root apex sealing tests were carried out using extracted human teeth.

Results: With increased amounts of BCP, flow decreased, and there was no significant difference in film thickness. Setting time increased with 5–10 wt% BCP and decreased with 20–40 wt% BCP. No disintegration was seen in any of the conditions, and solubility increased with 5–30 wt% BCP and decreased with 40 wt% BCP. Radiopacity decreased with increasing amounts of added BCP. The SEM observations showed plate-like crystals, and the results of the EDS and FTIR analyses suggested that they were calcium-deficient apatite. In the root apex sealing test, 5 wt% BCP sealer showed the same sealing properties as MS.

Conclusion: The material properties of BCP sealer were comparable to those of MS. The precipitation of calcium phosphate crystals suggests that the sealer has properties that involve mineralization in the root dentin.

Key words: biphasic calcium phosphate, adhesive resin sealer, root canal filling material

Corresponding author: Chiaki KOMINE, Department of Operative Dentistry, Nihon University School of Dentistry at Matsudo, 870-1, Sakaecho, Nishi-2, Matsudo, Chiba 271-8587, Japan

TEL: +81-47-360-9358, FAX: +81-47-360-9358, E-mail: komine.chiaki@nihon-u.ac.jp

Received for Publication: October 23, 2024/Accepted for Publication: November 29, 2024

DOI: 10.11471/odep.2025-001

Introduction

In endodontic treatment, root canal filling is carried out after root canal enlargement or forming and disinfection by sterilization. The root canal is tightly sealed in three dimensions with root canal filling material to prevent the entry of bacteria or harmful substances[1,2]. Materials used for root canal fillings are required to have a wide range of properties, including tissue affinity, chemical and physical stability, non-absorbability, density, radiopacity, and promotion of healing with osteoid scars[1,2], and it has been reported that there are no materials that satisfactorily meet all of these requirements[1,3]. Nonetheless, the development of dental materials for use in dental therapy has been remarkable. Bioceramics in particular offer higher stability and tissue affinity than metals or polymers, and they show virtually no decay or rejection. Bioceramic sealers that are used in clinical practice in the field of endodontic therapy include calcium silicate cement sealers containing mineral trioxide aggregate (MTA) and bioactive glass sealers containing calcium silicate glass[3,4]. These materials have features that include good sealing properties, biocompatibility, antibacterial effects due to their basicity, and precipitation of hydroxyapatite (HA: $Ca_{10}(PO_4)_6(OH)_2$) on the material surface[3,5–9]. Calcium phosphate materials, of which HA is the best-known example, are also bioceramic materials[3], and they are used in clinical practice due to their excellent biocompatibility, hard tissue mineralization, and bone regeneration[10–13]. To date, they have been reported to be effective in the field of endodontic therapy as a root canal filing material[3,14,15] and a pulp capping material[16–18].

Recent years have seen the development of biphasic calcium phosphate (BCP), a material in which α-tricalcium phosphate (α-TCP: α-$Ca_3(PO_4)_2$) and tetracalcium phosphate (TTCP: $Ca_4(PO_4)_2O$) are evenly dispersed at the molecular level within the same particle[13,19]. BCP sets in a short time and subsequently precipitates HA[10,11,13,19]. In a study using BCP as a retrograde root canal filling material after apicoectomy, Nakamura et al.[19] reported that there was no significant difference in sealing performance compared with MTA.

The present study focused on adhesive resin sealer as a component material for the development of a root canal filling material with adhesive properties that loses none of the characteristics of BCP. Adhesive resin sealers are root canal filling materials that are known to have high adhesion with root canal dentin[20]. Research has been carried out into the use of bioceramic materials with adhesive resin[21–23], and studies with MTA have shown that a surface layer of apatite forms when it is immersed in human simulated body fluid (SBF)[21], but the polymerization rate is reduced, which may affect adhesion to dentin[22]. In the present study, adhesive resin sealers containing varying amounts of BCP were prepared, and the effects of different amounts of BCP on the material properties of the sealers were examined for the purpose of developing a new adhesive resin sealer that has the characteristics of BCP and retains the adhesive properties of adhesive resin sealers.

Materials and Methods

1. Experimental materials

1) Preparation of BCP

BCP was prepared according to the method of Sugawara[13]. Dicalcium phosphate anhydrous ($CaHPO_4$) and calcium carbonate ($CaCO_3$) were prepared to a Ca/P molar ratio of 1.8, and the mixture was heated to 1,500℃ for 6 h in an electric furnace (ECSH-2027, Siliconit, Saitama, Japan). After cooling to room temperature, the sintered material was ground in a planetary ball mill to obtain BCP powder with a mean particle diameter of 12.65 μm.

2) Preparation of BCP-containing adhesive resin sealers

Commercially available adhesive resin sealer (MS: MetaSEAL Soft Paste, Sun Medical, Shiga, Japan) was mixed for 10 s according to the manufacturer's instructions (Table 1), and BCP was added to the mixed paste to 0 (control), 5, 10, 20, 30, and 40 wt% to prepare the different BCP-containing adhesive resin sealers (BCP sealers) for the experiment.

2. Experimental methods

1) Evaluation of material properties

The following measurements were made on each of the BCP sealers, in accordance with the Japanese Industrial Standard (JIS) for each measurement item[24,25].

(1) Flow

Each BCP sealer (0.05 mL) was placed on the center

Table 1 Materials used in this study

Root canal sealer	Code	Composition
MetaSEAL Soft Paste	MS	Base Paste：4-META, HEMA, dimethacrylates, water, organic filler CataPaste：HEMA, dimethacrylates, bismuth carbonate oxide, silica, aromatic amine

4-META；4-Methacryloxyethyl trimellitate anhydride, HEMA；2-Hydroxyethyl methacrylate

of a glass plate (40×40×5 mm^3), and 180 s after the start of mixing, a glass plate was placed on top with a pressure load of 120 g. Ten minutes after the start of mixing, the diameters of the compressed, disc-shaped samples were measured, and the mean of the maximum and minimum diameters was taken to be the flow (mm). This test was conducted three times.

(2) Film thickness

Each BCP sealer was left to stand on a 200 mm^2 glass plate, and another glass plate was placed on top. Then, 180 s after the start of mixing, a load of 150 N was applied, and 10 min from the start of mixing, the thickness was measured with a micrometer (ID-C150XB, Mitutoyo, Kanagawa, Japan). The measured value with the thickness of the two glass plates subtracted was taken to be the film thickness (μm). This test was conducted three times.

(3) Setting time

Each BCP sealer was filled into a stainless-steel ring (diameter 10 mm, height 2.0 mm) and left in an incubator (temperature 37±1℃, relative humidity 95±5%). From 2 min after the end of mixing, a Vicat needle (mass 100.0 g, diameter 2.0 mm) was dropped onto the surface of the sample, and the time until there was no change in depth of the indentation of the surface of the sample was taken to be the setting time (min). This test was conducted three times, and measurements were taken at 5-min intervals.

(4) Solubility and disintegration

Each BCP sealer was filled into a polytetrafluoroethylene split-ring mold (diameter 20 mm, height 1.5 mm) placed on a glass plate, a glass plate was pressed onto the ring, and this was placed in an incubator (temperature 37±1℃, relative humidity 95±5%). The ring and glass plates were removed after 48 h, and the two specimens thus produced were weighed. These two specimens were placed in a previously weighed vessel so that they were not touching, 50 mL of purified water was added, and the vessel was placed in an incubator (temperature 37±1℃, relative humidity 95±5%). After 24 h, disintegration of the specimens was checked, and the results were taken to be the disintegration of the material. The water in the vessel was then evaporated in an incubator (110℃). The vessel was weighed, the pre-experiment weight of the vessel was subtracted to give the weight of the residue, and the solubility (%) was calculated as the percentage of the original weight of the specimen made up by the residue. This test was conducted twice.

(5) Radiopacity

A disc-shaped specimen of each BCP sealer made by filling it into a stainless-steel ring (diameter 10 mm, height 1.00 mm) and an aluminum step wedge were placed on the same fluorescent imaging plate, and X-ray images were taken using a high-frequency portable X-ray device (Acrobio, Tokyo, Japan) at 50 kV with a focal length of 350 nm. Using the digital files thus obtained, the gray values were measured by software (Adobe Photoshop, Adobe, CA, USA) and compared with the gray values of the aluminum step wedge to give the radiopacity. This test was conducted three times.

2) Component analysis of the surface of samples immersed in SBF

BCP sealer containing 0, 5, and 10 wt% BCP was filled into a polytetrafluoroethylene split-ring mold (diameter 8 mm, height 1 mm) and placed on a glass plate with a plastic sheet on top, and this was placed in an incubator (temperature 37±1℃, relative humidity 95±5%) for 48 h. The surface area of the two specimens was calculated. The volume of human SBF to be used was calculated according to the following equation:

$Vs = 100\ mm \times Sa$

where

Vs is the volume of SBF (mm^3), and

Sa is the surface area of the specimen (mm^2).

The calculated amount of SBF was poured into a plastic container, each sample was immersed in the

SBF, and the container was placed in an incubator (temperature 37±1℃, relative humidity 95±5%). After 28 days of immersion, the sample was removed from the incubator, and the remaining SBF on the surface of each sample was washed off with purified water to give the SBF immersion sample[26].

(1) Scanning electron microscope observation and energy dispersive X-ray spectroscopy of sample immersed in SBF

The samples were Pt coated, and observations of the surface of each sample were carried out using a scanning electron microscope (SEM: JSM-IT200, JEOL, Tokyo, Japan) at an acceleration voltage of 15 kV[26]. Elemental analysis of the precipitated crystalline parts was carried out by energy dispersive X-ray spectroscopy (EDS). Measurements were taken three times, and the Ca/P ratio was calculated from the mean.

(2) Fourier transform infrared spectroscopy of the surface of the sample immersed in SBF

Using microscopic Fourier transform infrared spectroscopy (FTIR: Spectrum Two, PerkinElmer, CT, USA), measurements of each sample were made under the following analysis conditions: infrared measurement, ATR method; wavenumber range, 4,000 cm^{-1} to 450 cm^{-1}; detector, DTGS; resolution, 4 cm^{-1}; and cumulative number of measurements, 4. Spectral analysis and peak calculations were carried out using dedicated software (Panorama Ver 4.0 Analytical Software, LabCognition Analytical Software, Köln, DEU).

3) Root apex sealing test

Eighteen human front teeth with no extreme curvature that had been stored in water immediately after extraction were used (approved by the Ethics Review Board of Nihon University School of Dentistry at Matsudo, approval no. EC24-24-001A-1). Samples for the root apex sealing tests were prepared by cutting off the crown so that the length of the remaining root was 10 mm, the root canal was formed using NiTi rotary files (JIZAI, Mani, Tochigi, Japan) in the order #25, 04 taper, #25, 06 taper, #35, 04 taper, and #35, 06 taper attached to an endo motor (X-Smart Plus, Dentsply Sirona, NC, USA: forward rotation, 300 rpm, 1 N torque) with a working length of 9 mm. Files were replaced every 10 root canals. According to Kamiyama's method[27], root canal formation was carried out under NaClO solution (Dental Antiformin, Nippon Shika Yakuhin, Yamaguchi, Japan), and the root canal was washed with 5 mL each of NaClO solution and EDTA solution (Smearclean, Nippon Shika Yakuhin), in that order. A final wash was carried out with 3 mL of purified water, after which the root canal was dried with a paper point. The formed root canals were then randomly allocated to three groups, six per group, and filled with 0, 5, or 10 wt% BCP sealer. Filling was carried out with an endo nozzle (Sun Medical). After root canal filling, the crowns were temporarily sealed with hydraulic cement (Caviton, GC, Tokyo, Japan), and left for 24 h at a temperature of 37℃ and relative humidity of 95±5%. The hydraulic cement was then removed, and the root was immersed in SBF. After 28 days, the root was removed from the SBF and washed with purified water. An acrylic tube was fixed to the top of the root sample (Superbond, Sun Medical), 2 mL of 1% methylene blue solution was injected into the acrylic tube, and the tooth was placed with the root apex immersed in 3 mL of purified water (Fig. 1). After 28 and 56 days, the purified water was collected, the absorbance was measured using a microplate reader (iMark Microplate Reader, Bio-Rad Laboratories, CA, USA), and the amount of leakage was calculated. The purified water was completely replaced after each measurement.

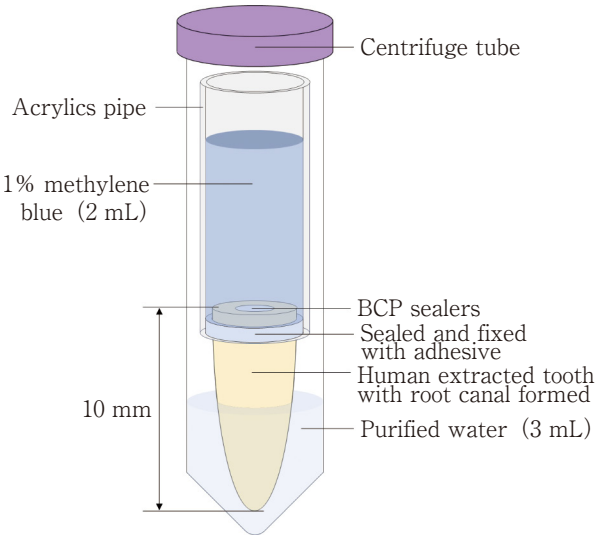

Fig. 1 Schematic diagram of the dye leakage test

After completion of the leakage test, the sample was sectioned horizontally with the tooth axis at 2.5, 5.0, and 7.5 mm from the root apex, and observed using a digital microscope (VHX-900, KEYENCE, Osaka, Japan). Samples with abnormal root canal morphology, such as fracture lines, low incomplete bifurcation root canals, and

Table 2 Physical properties of BCP sealers and requirements of the JIS standard

Property	0 wt%	5 wt%	10 wt%	20 wt%	30 wt%	40 wt%	n	JIS requirements
Flow (mm)	23.14±0.34[a]	20.00±1.17[b]	13.46±1.36[c]	12.23±1.57[c]	11.37±2.27[c]	10.61±0.98[c]	3	≥17
Film thickness (μm)	17.67±2.31	16.00±6.24	20.33±6.03	26.33±17.04	20.00±5.57	32.00±21.52	3	≤50
Setting time (min)	158.33±54.85[b]	370.00±17.32[a]	330.00±25.98[a]	123.33±11.55[bc]	41.67±5.77[cd]	33.33±5.77[d]	3	
Solubility (%)	0.59±0.42[a]	2.24±0.10[b]	2.76±0.29[b]	4.54±0.25[c]	5.90±0.32[d]	5.13±0.14[cd]	2	≤3.0
Radiopacity (mm Al)	9.30±0.02[a]	8.70±0.11[b]	8.78±0.06[b]	8.12±0.04[c]	7.74±0.15[d]	7.29±0.05[e]	3	≥3

All values are mean±SD.
The different letters indicate significant differences (Scheffé, $p<0.05$).

fins, were excluded from the results.

4) Statistical analysis

Measurements are expressed as mean±standard deviation values, and differences in means were examined by one-way analysis of variance (ANOVA) and Scheffé multiple comparison test, with the significance level set at 0.05. Statistical analysis was carried out using BellCurve for Excel (Social Survey Research Information, Tokyo, Japan).

Results

1. Material properties

The results of the tests of material properties are shown in Table 2.

1) Flow

Flow showed a tendency to decrease with increasing amount of BCP in the sealer. Only 5% BCP sealer met the JIS standard of flow ≥17 mm[24].

2) Film thickness

No significant differences with respect to the control were found. All samples met the JIS standard of film thickness ≤50 μm[24].

3) Setting time

The samples with 5 and 10 wt% BCP showed longer setting time than the control, but setting time decreased with 20–40 wt% BCP sealers.

4) Solubility and disintegration

No disintegration was found in any of the conditions. Solubility tended to increase with increasing amount of BCP in the 5–30 wt% BCP sealers, but it decreased from 30 to 40 wt% BCP. Sealers with 5 and 10 wt% BCP met the JIS standard of solubility ≤3.0%[24].

5) Radiopacity

Radiopacity showed a tendency to decrease with increasing amount of BCP in the sealer. All samples met the JIS standard of radiopacity ≥3 mm Al[24].

2. Component analysis of the surface of samples immersed in SBF

1) SEM observation and EDS analysis

SEM images and EDS analysis results for each type of sample after immersion in SBF are shown in Fig. 2. Plate-like crystals were seen with the BCP sealers, and the EDS results showed that Bi decreased, whereas Ca and P increased with respect to the control in the BCP sealers. The Ca/P ratio is shown in Table 3. It increased significantly with 5 and 10 wt% BCP sealers compared to controls.

2) FTIR analysis

The pattern for each type of sample after immersion in SBF is shown in Fig. 3. In the sealers with BCP added, absorbance bands due to PO_4^{3-} were observed in the regions of 1,017 cm^{-1}, 962 cm^{-1}, and 600 cm^{-1}. The absorbance bands showed no clear differences in both peaks and waveforms between the 5 wt% BCP sealer and the 10 wt% BCP sealer. These absorbance bands were not seen in the control.

3. Root apex sealing test

The results for dye leakage are shown in Table 4. At 56 days, the 5 wt% BCP sealer showed no significant difference from the control, but the 10 wt% BCP sealer showed an increase in dye leakage.

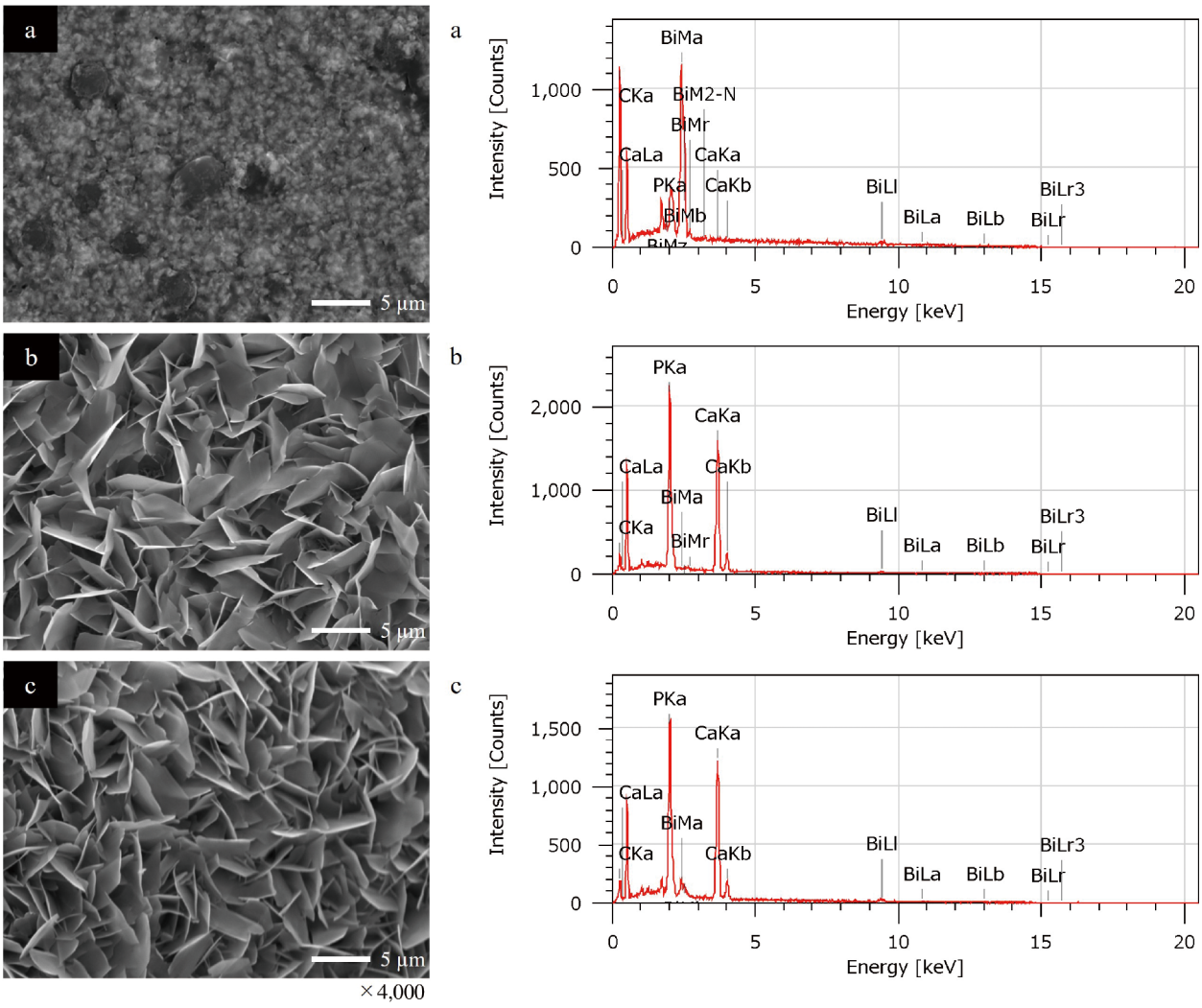

Fig. 2 SEM images and EDS microanalyses of the mixing conditions
a : 0 wt%, b : 5 wt%, c : 10 wt%

Table 3 EDS Ca/P molar ratio

	0 wt%	5 wt%	10 wt%
Ca/P	0.11±0.12[a]	1.34±0.04[b]	1.53±0.10[b]

All values are mean±SD. (n=3)
The different letters indicate significant differences (Scheffé, $p<0.05$).

Discussion

In the evaluation of material properties, the effects of adding BCP to MS were examined. This study was conducted in accordance with JIS standards, which also determined the number of experiments to be performed[24]. The experimental results showed differences in setting behavior among 5–10%, 10–30%, and 30–40 wt% BCP. MS contains the acidic monomer 4-methacryloxyethyl trimelliate anhydride (4-META), and this may have undergone an acid-base reaction with BCP, which exhibits basicity, thus impeding the polymerization of MS. At 5–10 wt% BCP, the decrease in flow, the increase in setting time, and the solubility all became greater. However, it appears that, because the amount of BCP was ≤10 wt%, the setting was the MS reaction of radical curing, and the effects of the acid-base reaction were therefore slight. At 10–30 wt%, the only change was reduction in setting time. This was probably the result of an increase in the proportion of setting due to the acid-base reaction and a decrease in the proportion due to radical polymerization as the amount of BCP increased. At 30–50 wt%, solubility decreased and

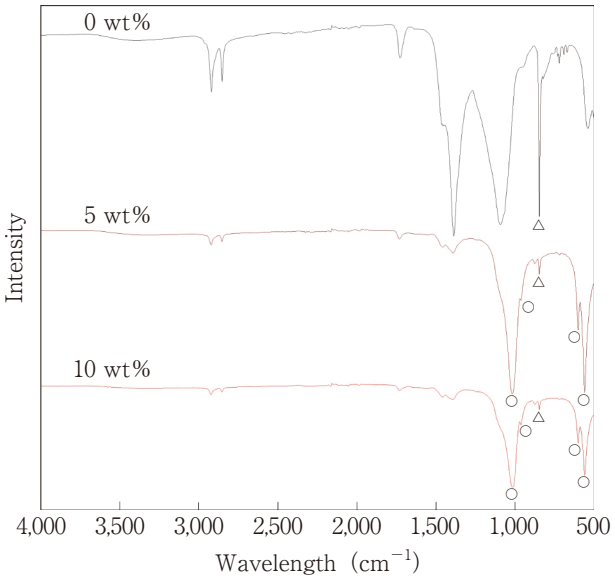

Fig. 3 FTIR spectra of BCP sealers
○ : due to $(HPO_4)^{2-}$, △ : due to $(CO_3)^{2-}$

setting time decreased to 26.3% and 21.1% of the control, respectively, from which it appears that the setting changed from mainly radical polymerization to an acid-base reaction. With film thickness, the results showed no relationship to the amount of BCP. Film thickness may have been less affected by the amount of BCP than flow because the mean size of BCP particles, 12.65 μm, was smaller than the film thickness of the control. With radiopacity, BCP is known to have no radiopacity, however, when 40 wt% of BCP was added to MS, it exhibited 78.3% radiopacity compared with MS alone. This indicates that the sealer can meet the requirements as a sealer even when the amount of BCP blended is increased. The above results show that formulations of BCP up to 10 wt% meet the conditions for a sealer for root canal filling.

Based on the foregoing, component analysis of precipitates and root apex sealing tests were carried out using samples of 5 and 10 wt% BCP sealers. The results of the SBF immersion test showed plate-like crystalline precipitates with the BCP sealers. The Ca/P ratios of the precipitates were lower than 1.67, the theoretical ratio of HA. However, because SBF contains Na^+, K^+, Mg^{2+}, Ca^{2+}, Cl^-, HCO_3^-, HPO_4^{2-}, and SO_4^{2-} [26], it was considered that there was partial substitution of Na^+, K^+, and Mg^{2+} at the Ca^{2+} position, of HPO_4^{2-} and CO_3^{2-} at the PO_4^{3-} position, and of Cl^- and CO_3^{2-} at the OH^- position in the process of re-precipitation as *in vivo*. In the FTIR analysis, the peaks characteristic of MS in the region of 845 cm^{-1} and 1,385 cm^{-1} disappeared, and absorbance bands due to PO_4^{3-} were found in the regions of 1,017 cm^{-1}, 962 cm^{-1}, and 600 cm^{-1}. These bands are characteristic of calcium phosphate[28]. These results suggest that the precipitates obtained from the immersion tests were calcium phosphate crystals, and it may be inferred from the Ca/P ratio that they were calcium-deficient apatite. It was also feared that the conversion to calcium phosphate would be inhibited by the monomer when BCP was added to the adhesive resin sealer. However, SEM and FTIR results showed calcium phosphate precipitation. Therefore, it was shown that the conversion to calcium phosphate was possible in the presence of the monomer, as reported by Matsuya et al.[29], which blended TTCP, a component of BCP, with poly (methyl vinyl ether-maleic acid).

MS includes 4-META, an acidic functional monomer, and the 4-META self-adhesive system allows MS to penetrate the root canal wall and polymerize so that it bonds to the root canal dentin, exhibiting good sealing properties[30]. In addition, MS is known to have hydrophilic properties and to expand on water absorption[31]. Calcium phosphate cement is also known to expand slightly in volume when converted to HA[32]. Thus, the water absorption and expansion properties of the BCP sealer are considered to be maintained. It therefore appears that the BCP sealers had the MS characteristics of adhesiveness and expansion on water absorption together with sealing properties from the precipitate deposited as a result of reaction with SBF. However, the amount of leakage was significantly greater with the 10 wt% BCP sealer. Takezawa et al. reported the expansion coefficient of calcium phosphate cement to be 0.08%[32], while Ori reported a water absorption expansion coefficient of self-adhesive 4-META-containing methacrylate resin-based sealer to be 6.0%[31]. In short, the expansion rate of BCP is considered to be lower than that of MS. Moreover, the resin tags decreased in a BCP amount-dependent manner, since BCP is not involved in its formation. Therefore, it was considered that the increase in the amount of BCP inhibited the decrease in water-absorption expansion and adhesion.

MS has the characteristics of sealing due to expansion on water absorption and adhesion with the root canal wall, and the present results suggest that BCP

Table 4 Leakage amount in the dye leakage test for BCP sealers (μg/mL)

Soaking period (day)	0 wt%	5 wt%	10 wt%
28	0.23±0.08[a]	1.04±0.16[b]	0.43±0.18[a]
56	0.27±0.10[a]	1.21±0.19[ab]	2.87±2.60[b]
n	5	6	5

All values are mean±SD.
The different letters indicate significant differences (Scheffé, $p<0.05$).

sealers may be expected to have improved sealing properties, because the addition of BCP causes bonding with the dentin of the root canal. Since calcium phosphate crystals have excellent biocompatibility, a good long-term prognosis can be expected. With bioceramic sealers, it has been reported that sealers containing calcium silicate glass have significantly higher leakage volume than MS[20]. In the present study, the leakage volume with 5 wt% BCP sealer showed no significant difference from that of the control, suggesting that it will have the same clinical applications as MS. In addition, root canal filling is usually performed using the apical barrier technique in cases where the root apex of the re-root canal treatment is greatly enlarged[3,33]. Various MTA formulations have been used for forming apical plugs, but difficulties when carrying out filling have been identified. Since the present results suggest that the flow and the setting time of BCP sealers can be adjusted by increasing the amount of BCP, application of BCP sealers to the apical barrier technique may be possible.

The above results suggest that BCP sealers will be useful as root canal filling materials because they retain a similar level of sealing properties to MS, and they precipitate calcium phosphate crystals in contact with body fluids. In this experiment, it was conducted using BCP with an average particle size of 12.65 μm according to Sugawara's method[13]. It has been reported that the average particle size affects the material properties[19].

Therefore, it is believed that changing the average particle size of the BCP used will affect the material properties and leakage volume of the BCP blended sealer. Although these results showed the material properties of BCP sealers, the relationship between their biocompatibility and pharmacological effects such as antibacterial action due to basicity remains unknown. Therefore, further investigation is needed to clarify the optimum conditions for a BCP sealer for root canal filling.

Conclusion

BCP, which comprises α-TCP and TTCP, was added to the adhesive resin sealer MS to give it bioactive properties, and the relationship between the amount of BCP added and the effect on the adhesive resin sealer was examined. The following conclusions were obtained.

1. The optimum amount of BCP meeting the JIS standard was less than 10 wt%.
2. Precipitation of calcium phosphate crystals was found in SBF with 5 and 10 wt% BCP sealers.
3. With root apex sealing, 5 wt% BCP sealer showed the same level of performance as MS.

These findings suggest that BCP sealer exhibits excellent properties as a root canal filling material, and that the addition of BCP imparts bioactive characteristics.

Acknowledgements

The authors would like to express their deepest gratitude to Professor Chiaki Komine and former Professor Satoshi Hirayama of the Department of Operative Dentistry, Nihon University School of Dentistry at Matsudo, for their advice and guidance throughout the conduct of this study, as well as their sincere appreciation to the members of the Department of Operative Dentistry and the Department of Histology for their kind cooperation.

Conflicts of Interest

The authors declare no conflict of interest related to this paper.

References

1) Komabayashi T, Colmenar D, Cvach N, Bhat A, Primus C, Imai Y. Comprehensive review of current endodontic sealers. Dent Mater J 2020; 39: 703–720.
2) Khandelwal A, Janani K, Teja K, Jose J, Battineni G, Riccitiello F, Valletta A, Palanivelu A, Spagnuolo G. Periapical healing following root canal treatment using different endodontic sealers: A systematic review. Biomed Res Int 2022; doi: 10.1155/2022/3569281
3) Al-Haddad A, Che Ab Aziz ZA. Bioceramic-based root canal sealers: A review. Int J Biomater 2016; doi: 10.1155/2016/9753210
4) Sfeir G, Zogheib C, Patel S, Giraud T, Nagendrababu V, Bukiet F. Calcium silicate-based root canal sealers: A narrative review and clinical perspectives. Materials (Basel) 2021; 14: 3965; doi: 10.3390/ma14143965.
5) Giacomino CM, Wealleans JA, Kuhn N, Diogenes A. Comparative biocompatibility and osteogenic potential of two bioceramic sealers. J Endod 2019; 45: 51–56.
6) Washio A, Morotomi T, Yoshii S, Kitamura C. Bioactive glass-based endodontic sealer as a promising root canal filling material without semisolid core materials. Materials (Basel) 2019; 12: 3967; doi: 10.3390/ma12233967
7) Hanada K, Morotomi T, Washio A, Yada N, Matsuo K, Teshima H, Yokota K, Kitamura C. In vitro and in vivo effects of a novel bioactive glass-based cement used as a direct pulp capping agent. J Biomed Mater Res B Appl Biomater 2019; 107: 161–168.
8) Murata K, Washio A, Morotomi T, Rojasawasthien T, Kokabu S, Kitamura C. Physicochemical properties, cytocompatibility, and biocompatibility of a bioactive glass based retrograde filling material. Nanomaterials 2021; 11: 1828; doi: 10.3390/nano11071828
9) Washio A, Nakagawa A, Nishihara T, Maeda H, Kitamura C. Physicochemical properties of newly developed bioactive glass cement and its effects on various cells. J Biomed Mater Res B Appl Biomater 2015; 103: 373–380.
10) Chow LC. Development of self-setting calcium phosphate cements. JCS-Japan 1991; 99: 954–964.
11) Wang P, Zhao L, Chen W, Liu X, Weir MD, Xu HHK. Stem cells and calcium phosphate cement scaffolds for bone regeneration. J Dent Res 2014; 93: 618–625.
12) Lu J, Yu H, Chen C. Biological properties of calcium phosphate biomaterials for bone repair: a review. RSC Adv 2018; 8: 2015–2033.
13) Sugawara A. Physical properties and hydroxyapatite formation of fast self-setting biphasic calcium phosphate cement. J Hard Tissue Biol 2020; 29: 173–182.
14) Imamura Y, Tanaka Y, Nagai A, Yamashita K, Takagi Y. Self-sealing ability of OCP-mediated cement as a deciduous root canal filling material. Dent Mater J 2010; 29: 582–588.
15) Jacob GM, Kumar A, Varughese JM, Varghese NO, Varma PRH, Komath M. Periapical tissue reaction to calcium phosphate root canal sealer in porcine model. Indian J Dent Res 2014; 25: 22–27.
16) Shinkai K, Taira Y, Suzuki M, Kato C, Ebihara T, Wakaki S, Seki H, Shirono M, Ogisu T, Yamauchi J, Suzuki S, Katoh Y. Dentin bond strength of a new adhesive system containing calcium phosphate experimentally developed for direct pulp capping. Dent Mater J 2009; 28: 743–749.
17) Bresciani E, Wagner WC, Navarro MFL, Dickens SH, Peters MC. In vivo dentin microhardness beneath a calcium-phosphate cement. J Dent Res 2010; 89: 836–841.
18) Zakaria MN, Cahyanto A, El-Ghannam A. Calcium release and physical properties of modified carbonate apatite cement as pulp capping agent in dental application. Biomater Res 2018; 22: 35; doi: 10.1186/s40824-018-0146-6
19) Nakamura T, Hayashi M, Tamura M, Kaketani M, Ito T, Takamizawa T, Suzuki Y, Yasukawa T, Sugawara A, Takeichi O. Utility of biphasic calcium phosphate cement as a seal for root-end filling. Dent Mater J 2023; 42: 412–417.
20) Ito S, Kado T, Furuichi Y. Evaluation of root canal sealing and removal of resin-based sealers. JJEA 2023; 44: 27–35.(in Japanese)
21) Watanabe T, Wanibe H, Yamamoto M, Nakata K, Hoshika T, Nishitani Y, Yoshiyama M, Kawai T, Nakamura H. Development of adhesive root canal sealer containing mineral trioxide aggregate (MTA). J J Dent Mater 2009; 28: 378, Abst. No.P132.(in Japanese)
22) Nishitani Y, Hoshika T, Morimoto S, Watanabe T, Wanibe H, Yamamoto M, Nakata K, Takahashi K, Kawai T, Nakamura H, Yoshiyama M. Development of adhesive root canal sealer inducing hard tissue formation. J J Dent Mater 2009; 28: 380, Abst. No.P134.(in Japanese)
23) Tatsuyama S, Takashi Y, Katsumata A, Kajihara T, Hoshika T, Imai K, Nishitani Y. Effect of cell growth on adhesive root canal sealer containing portlamd cement. J Jpn Assoc Regenerative Dent 2017; 15: 3–9.(in Japanese)
24) Japanese Industrial Standard. JIS T 6522: 2015. Dental root canal sealing materials.(in Japanese)
25) Japanese Industrial Standard. JIS T 6006: 2018. Dentistry-test method for determining radio-opacity of materials.(in Japanese)
26) International Organization for Standardization. ISO 23317: 2014. Implants for surgery—In vitro evaluation for apatite-forming ability of implant materials.

27) Kamiyama C, Kawano S, Takeda S, Yoshida T. Application of α-TCP/Te-CP cement to root canal sealer. Jpn J Conserv Dent 2015; 58: 124–142.(in Japanese)
28) Camila CAL, Pedro HJOL, Veridiana RN, Paula D. Fourier transform infrared spectroscopy (FTIR) application chemical characterization of enamel, dentin and bone. Appl Spectrosc Rev 2018; 53: 747–769.
29) Matsuya Y, Matsuya S, Antonucci JM, Takagi S, Chow LC, Akamine A. Effect of powder grinding on hydroxyapatite formation in a polymeric calcium phosphate cement prepared from tetracalcium phosphate and poly (methyl vinyl ether-maleic acid). Biomaterials 1999; 20: 691–697.
30) Sui M, Young KK, Hiraishi N, Junqi L, David HP, Franklin RT. Evaluation of the true self-etching potential of a fourth generation self-adhesive methacrylate resin-based sealer. J Endod 2009; 35: 870–874.
31) Ori T. Physical properties of adhesive root canal sealers. Jpn J Conserv Dent 2011; 54: 233–241.(in Japanese)
32) Takezawa Y, Doi Y, Shibata S, Wakamatsu N, Kamemizu H, Goto T, Iijima M, Moriwaki Y, Uno K, Kubo F, Haeuchi Y. Self-setting apatite cement Ⅱ. Hydroxyapatite as setting accelerator. J J Dent Mater 1987; 6: 426–431.(in Japanese)
33) Rao AS, Mathur R, Shah NC, Malge R, Sathnoorkar S, Chandrasekhar T. Evaluation of extrusion and apical seal of thermafil™ obturation with and without MTA as an apical barrier in comparison with lateral condensation technique: An in vitro study. Int J Clin Pediatr Dent 2020; 13: 40–44.

Original Article

ODEP 5 (1) : 11～19, 2025

Changes in the Colors and Surface Structures of Bovine Enamel Using Three Different In-office Bleaching Agents

Takako EGUCHI[1], Hiroki SUGITO[1,2], Yukie KUSAKA-YOSHINO[3], Yumiko NAGAI[1], Mihoko TADA[1], Akiko HARUYAMA[2] and Takashi MURAMATSU[2]

[1]Department of Dental Hygiene, Tokyo Dental Junior College
[2]Department of Operative Dentistry, Cariology and Pulp Biology, Tokyo Dental College
[3]GC Corporation R&D. Mfg

Abstract

Purpose: Dental patients' esthetic expectations have been increasing, and bleaching has rapidly gained popularity in clinical practice. Two main bleaching methods are currently available: at-home bleaching and in-office bleaching. In-office bleaching has been increasingly recommended because it provides immediate results and is performed by dental professionals. However, adverse effects, such as the development of a chalky white appearance and reduced acid resistance of the enamel, have been reported. Therefore, the present study examined changes in enamel color and surface roughness after in-office bleaching using bleaching agents with different concentrations of hydrogen peroxide.

Methods: Bovine mandibular anterior teeth were used in this study. Three types of in-office bleaching agents with different hydrogen peroxide concentrations were tested (experimental groups P, T, and H). An LED light-curing unit was employed as the light source. Color measurements were conducted using a microspectrophotometer and brightness and chromaticity (L^*, a^*, and b^*) within the CIE1976$L^*a^*b^*$ color space were assessed. Color differences after bleaching were calculated. Enamel surface roughness was measured using a 3D laser scanning microscope, and roughness values were obtained before and after bleaching. Enamel surfaces were also examined using scanning electron microscopy (SEM).

Results: After bleaching, L^* and a^* values significantly increased in all groups. b^* values slightly decreased in groups P and T, and slightly increased in group H. No significant differences were observed after bleaching in group P. These results showed a clear bleaching effect in all groups, regardless of the hydrogen peroxide concentration. ΔE^*ab values in all groups also indicated a significantly strong bleaching effect. SEM observations of the enamel surface after bleaching revealed a smooth appearance in groups P and T and a roughened surface in group H, in which the bleaching agent had a higher hydrogen peroxide concentration. Furthermore, surface roughness showed significant changes after bleaching in all groups.

Conclusion: The hydrogen peroxide concentration in in-office bleaching agents affected the enamel surface structure and color changes.

Key words: bleaching agents, hydrogen peroxide concentration, in-office bleaching

Corresponding author: Hiroki SUGITO, Department of Dental Hygiene, Tokyo Dental Junior College, 2-9-18, Kanda-Misakicho, Chiyoda-ku, Tokyo 101-0061, Japan
TEL: +81-3-6380-9105, FAX: +81-3-6380-9635, E-mail: sugito@tdc.ac.jp
Received for Publication: January 9, 2025/Accepted for Publication: March 12, 2025
DOI: 10.11471/odep.2025-002

Introduction

The maintenance of dental and oral health preserves and improves general health[1]. Good dental and oral health is an essential factor for quality of life. Therefore, awareness of dental and oral health has increased. To control the risk of developing oral diseases, such as dental caries and periodontal disease, individuals need to be aware of their oral environment and initiate behavioral changes to optimize self-care for specific issues[2]. Esthetic improvements often serve as a trigger for enhancing self-awareness and motivation for self-care[2,3]. Esthetic demands have recently been increasing and teeth bleaching has rapidly gained popularity in clinical practice.

The main bleaching methods currently performed are at-home bleaching and in-office bleaching. With at-home bleaching, carbamide peroxide decomposes into urea and hydrogen peroxide on the tooth surface, and active oxygen released during this process acts on the substances responsible for discoloration and staining[4]. A drawback of this method is that it requires a long application period, e.g., approximately one to two weeks[5].

In contrast, in-office bleaching involves the application of a bleaching agent, primarily consisting of hydrogen peroxide, to the surface of the enamel by a dentist, or a dental hygienist under the supervision of a dentist. Light or heat is applied to accelerate the chemical reactions that break down enamel stains and discoloration[6]. An immediate bleaching effect is possible, even with an irregular tooth alignment. However, when high concentrations of hydrogen peroxide are used for bleaching, a chalky white (chalk-like opacity) appearance may develop on the teeth, resulting in a less translucent whiteness[7]. Furthermore, tooth structures and the surrounding tissues may be adversely affected[8].

The adverse effects of at-home bleaching include tooth sensitivity during and after the procedure, gingival whitening due to contact with the bleaching agent, and pain[8]. After three months of at-home bleaching, patients have reported not only tooth sensitivity and gingival pain, but also thermal sensitivity in response to cold and heat stimuli in daily life[8]. In-office bleaching using agents with high concentrations of hydrogen peroxide may reduce acid resistance of enamel, which may adversely affect the tooth structure[9].

A previous study reported that in-office bleaching may lead to a bleaching effect of up to 50 μm in depth from the surface as the number of bleaching sessions increases. However, this process also causes structural changes in the enamel[10]. Limited information is currently available on the impact of various hydrogen peroxide concentrations in bleaching agents on enamel[10,11], and many aspects remain unclear.

Therefore, the present study investigated the effects of bleaching agents with different hydrogen peroxide concentrations on color changes and enamel surface roughness after in-office bleaching.

Materials and Methods

1. Sample preparation

Twenty-four frozen extracted bovine mandibular anterior teeth were used. After thawing, teeth were sectioned using a diamond band saw (Maruto Co., Ltd., Tokyo, Japan) under water irrigation. The cervical and incisal sides were cut to extract the central enamel portion of the crown. The diameter of samples was adjusted to approximately 1 cm in order to match the 8-mm diameter of the light irradiation device used during the bleaching procedure.

1) Samples for color change observations

The labial enamel surface of tooth crowns was polished with waterproof abrasive paper (#400, Sankei Co., Ltd., Tokyo, Japan) to ensure that the polished surface was parallel to the measurement platform. Fifteen samples with exposed fresh enamel were prepared[12,13].

2) Samples for surface structure observations

After sectioning, the labial enamel surface of tooth crowns was sequentially polished with waterproof abrasive papers (#400, #1000, #2000, and #4000) to ensure that the polished surface was parallel to the measurement platform. Nine samples were prepared. After polishing, half of each sample was covered with sticky wax (GC Corporation, Tokyo, Japan) to establish a reference surface and experimental surface on the same tooth[12,13].

2. Experimental groups and processing method

There were three experimental groups (Table 1). Each bleaching agent was handled according to the methods specified by the respective manufacturers and previous studies[14-16]. An LED light-curing unit (G-Light

Table 1 A list of components of the bleaching agents used in this study

Group	Main components	Hydrogen peroxide concentration	Light irradiation	Product name
P	Solution 1：Liquid Hydrogen peroxide 85% phosphoric acid Sodium pyrophosphate Decahydrate Purified water Solution 2：Liquid Titanium dioxide Synthetic magnesium silicate Sodium Purified water	3.5%	Approx. 5 min.	PYRENEES（Morita）
T	Syringe A：Colorless transparent liquid Hydrogen peroxide Syringe B：Translucent gel Carbamide peroxide Glycol Vinyl polymer Reactor：Yellowish-white liquid Visible light-responsive titanium oxide Distilled water Ethanol Gingiva protection resin：Blue paste Methacrylate-based resin Filler	23%	60 seconds/teeth	TiON in Office（GC）
H	Powder： Aerosil Metal salts Indicator Others Liquid： 35% hydrogen peroxide solution Others	35%	Around 3 min.	Shofu HiLite（Shofu）

Prepared based on the catalog and package insert of each product

Prima II Plus, GC Corporation) was used for bleaching. The irradiation output of the device was checked each time before bleaching, and mode 20 (normal mode) was used for irradiation.

Group P was treated with a bleaching agent containing 3.5% hydrogen peroxide and titanium dioxide was the main component（PYRENEES, Nissin Dental Products, Kyoto, Japan). The bleaching agent was applied to samples with a brush. Samples were then irradiated for 2 minutes with the tip of the irradiator 1 mm away from the bleaching agent-coated surface. After bleaching, the surfaces were thoroughly rinsed and dried. This treatment cycle was performed three times[14].

Group T was treated with a bleaching agent containing 23% hydrogen peroxide and titanium dioxide was the main component（TiON in Office, GC Corporation). Bleaching was performed as follows. After applying the reactor and drying, a mixed gel from syringes A and B was applied, and teeth were irradiated for 10 minutes using LED visible light[15].

Group H was treated with a bleaching agent containing 35% hydrogen peroxide as the main component (Shofu HiLite, Shofu Inc., Kyoto, Japan). Bleaching was performed as follows. One scoop of powder and two

drops of liquid were mixed for 30 seconds to a uniform paste using a spatula provided in the kit. The paste was applied at a thickness of 1–2 mm onto samples. After standing for approximately 6 minutes, samples were irradiated using the LED visible light for 3 minutes. The paste was removed 1 minute later[16].

Samples in each group were randomly assigned. Each group included five samples for the color change analysis and three for the surface structure analysis.

3. Observation methods

1) Color changes

Color measurements were performed before and after bleaching using a microspectrophotometer (MSP-300H, Nippon Denshoku Industries, Tokyo, Japan). In each sample, color was measured at five central locations, and the average value was used. Measurements were expressed using the CIE1976$L^*a^*b^*$ color space, with L^*, a^*, and b^* values being calculated. Baseline values before bleaching were designated as L^*_0, a^*_0, and b^*_0 and those after bleaching as L^*_1, a^*_1, and b^*_1[13].

Differences between values before and after bleaching were defined as ΔL^*, Δa^*, and Δb^* and the standard deviation was calculated. Specifically, brightness ΔL^* was calculated using the formula $\Delta L^* = \Delta L^*_1 - \Delta L^*_0$. The chroma representing red-green tones, Δa^*, and the chroma representing yellow-blue tones, Δb^*, were calculated using the same formula.

Furthermore, the color difference value ΔE^*ab was calculated using the following formula to evaluate color changes.

$$\Delta E^*ab = [(\Delta L^*)^2 + (\Delta a^*)^2 + (\Delta b^*)^2]^{1/2}$$

2) Surface changes observed under SEM

Using a vacuum deposition device (VC-100S, Vacuum Device Inc., Mito, Japan), carbon was deposited onto samples. Observations were conducted using a scanning electron microscope (SEM : SU6600, Hitachi High-Tech Corporation, Tokyo, Japan) at an accelerating voltage of 15 kV. The magnification for imaging was set at × 1,000[12].

3) Surface roughness observed using a 3D laser microscope

Surface roughness was measured using a 3D laser microscope (LEXT OLS4000, Olympus Corporation, Tokyo, Japan).

Surface roughness was evaluated using the arithmetic mean roughness (Sa). Measurements were taken at five locations each on the reference surface and experimental surface for each sample, and the mean value ± standard deviation was calculated. The measurement area was set to 645×645 μm, with a cut-off value of 80 μm[13,17]. The difference between Sa values before and after bleaching was calculated and defined as ΔSa.

4. Statistical analysis

Data were analyzed using Statcel4 (OMS Publishing, Tokyo, Japan). To examine the significance of differences in values before and after bleaching with each bleaching agent, a paired t-test was performed with significance set at $p<0.05$. To examine differences in values among the three groups after bleaching, normality was confirmed using Bartlett's test, followed by a one-way analysis of variance to confirm significance. Multiple comparison testing was then conducted using the Tukey-Kramer method, with significance set at $p<0.05$.

Results

1. Color changes

The results obtained on L^*, a^*, and b^* are shown in Tables 2 to 4. L^* and a^* values significantly increased in all three groups after bleaching ($p<0.05$). b^* values slightly decreased in groups P and T, and slightly increased in group H. Moreover, significant differences were observed in groups T and H, whereas no significant difference was observed in group P.

Comparisons between the three groups, based on differences between values before and after bleaching, are shown in Fig. 1 to 3. Differences for each group were denoted as ΔL^*, Δa^* and Δb^*. A significant difference was observed in Δb^* between groups P and H and between groups T and H ($p<0.01$), whereas no significant differences were noted in ΔL^* or Δa^*.

Color difference values (ΔE^*ab) are shown in Fig. 4. ΔE^*ab values were 3.89 for group P, 4.41 for group T, and 3.09 for group H. No significant difference was observed among the three groups.

2. SEM observations

SEM images of the enamel surface are shown in Fig. 5. Comparisons to the reference surfaces of each group (Fig. 5-a, c, e) revealed that the enamel surface had a smoother appearance after bleaching in group P (Fig. 5-b) and a slightly smoother appearance in group T (Fig. 5-d). Conversely, the enamel surface after bleach-

Table 2 L^* values of the enamel surface before and after bleaching (mean±SD)

	L^*_0	L^*_1	Statiscal difference#
Group P	82.17±0.25	84.29±1.07	Significant
Group T	79.82±0.88	83.15±0.66	Significant
Group H	70.4±0.25	72.6±0.70	Significant

L^*_0 : Before bleaching, L^*_1 : After bleaching
: Statistical difference between L^*_0 and L^*_1 for each group ($p<0.05$)

Table 3 a^* values of the enamel surface before and after bleaching (mean±SD)

	a^*_0	a^*_1	Statiscal difference#
Group P	−1.61±0.06	−1.24±0.08	Significant
Group T	−1.59±0.62	−1.21±0.03	Significant
Group H	−2.33±0.04	−1.66±0.11	Significant

a^*_0 : Before bleaching, a^*_1 : After bleaching
: Statistical difference between a^*_0 and a^*_1 for each group ($p<0.05$)

Table 4 b^* values of the enamel surface before and after bleaching (mean±SD)

	b^*_0	b^*_1	Statiscal difference#
Group P	0.38±0.28	−0.1±0.39	No significant
Group T	−0.15±0.28	−1±0.46	Significant
Group H	−3.74±0.23	−3.04±0.52	Significant

b^*_0 : Before bleaching, b^*_1 : After bleaching
: Statistical difference between b^*_0 and b^*_1 for each group ($p<0.05$)

ing was rougher in group H than in groups P and T (Fig. 5-f).

3. Surface roughness observations by the 3D laser microscope

Surface roughness measurements are shown in Table 5. After bleaching, significant differences were observed in all groups. Surface roughness slightly decreased in groups P and T, and slightly increased in group H. Although changes in surface roughness were observed after bleaching in each group, no significant differences in ΔSa values were noted between the groups (Fig. 6).

Discussion

Teeth bleaching is very popular in Japan and is considered a simple cosmetic treatment. Moreover, bleaching is regarded as "minimal intervention dentistry" because it does not involve cutting the teeth. Additionally, with the establishment of specialized whitening clinics and the certification of whitening coordinators at professional societies[18], the demand for bleaching is expected to increase in Japan.

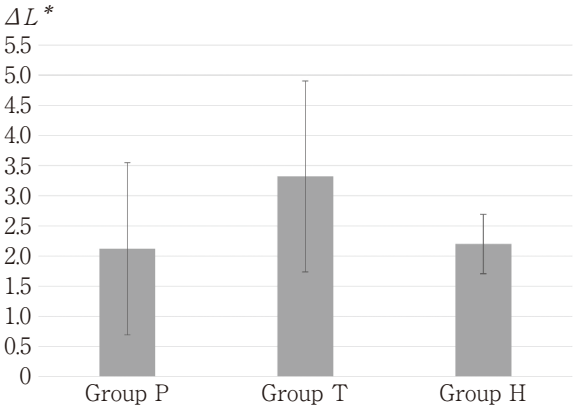

Fig. 1 Color changes measured by ΔL^* values
Bars : SD

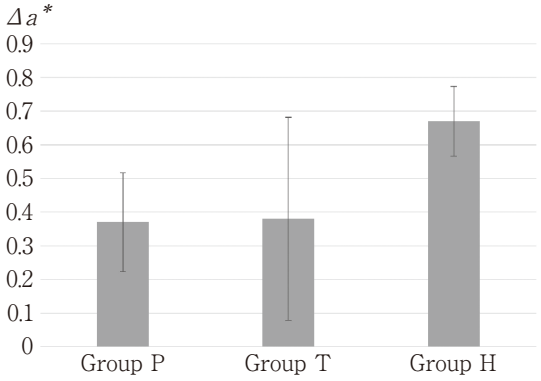

Fig. 2 Color changes measured by Δa^* values
Bars : SD

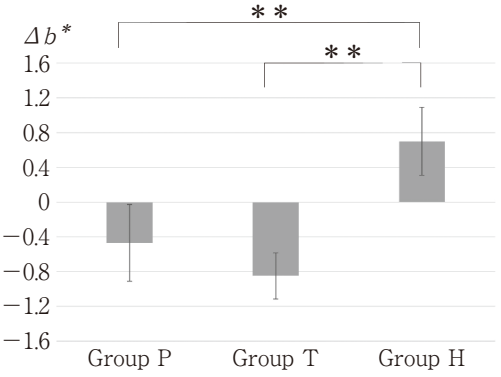

Fig. 3 Color changes measured by Δb^* values
Bars : SD. ＊＊ : $p<0.01$

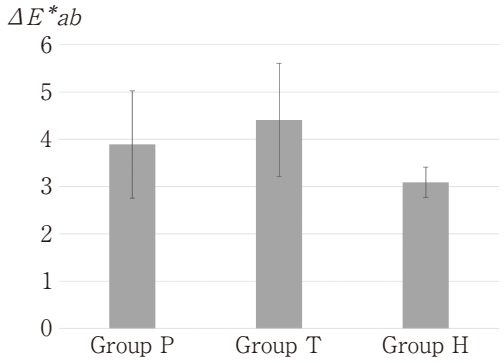

Fig. 4 Color differences measured by ΔE^*ab

Bars : SD

Table 5 Sa values of the enamel surface before and after bleaching (mean±SD, μm)

	Sa_0	Sa_1	Statiscal difference#
Group P	0.11±0.02	0.04±0.01	Significant
Group T	0.05±0.01	0.04±0.01	Significant
Group H	0.03±0.01	0.1±0.02	Significant

Sa_0 : Before bleaching, Sa_1 : After bleaching

: Statistical difference between Sa^*_0 and Sa^*_1 for each group ($p<0.05$)

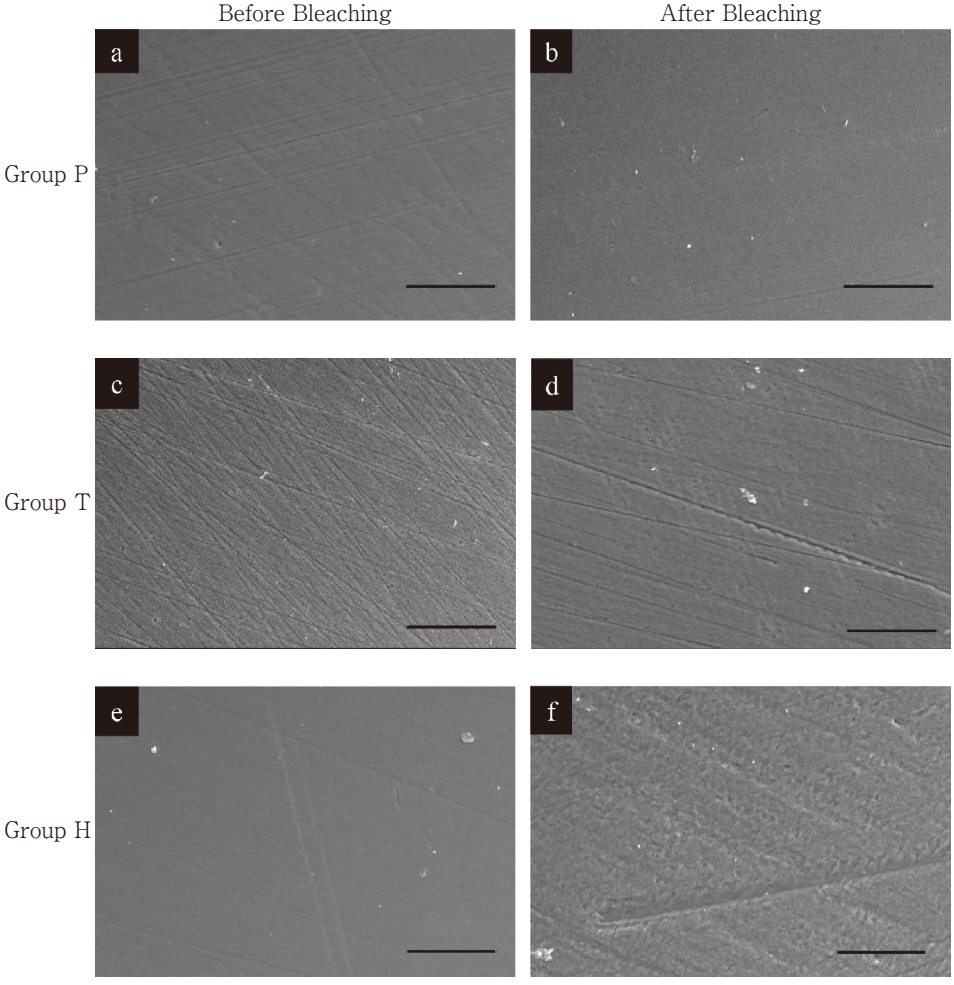

Fig. 5 SEM images of enamel surfaces before and after bleaching

a : Before bleaching in group P, b : After bleaching in group P exhibiting a smooth appearance, c : Before bleaching in group T, d : After bleaching in group T exhibiting a slightly smoother appearance, e : Before bleaching in group H, f : After bleaching in group H exhibiting a roughened surface

Bars : 25 μm

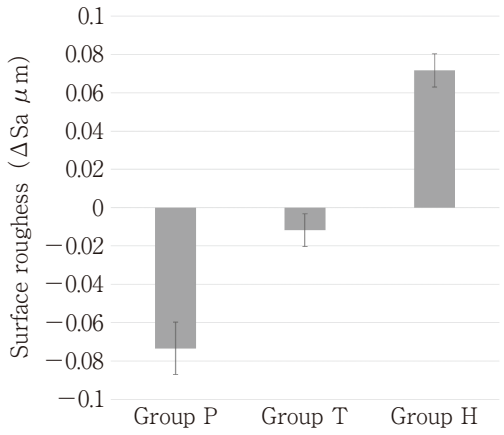

Fig. 6 Surface roughness changes after bleaching
Bars : SD

The present study investigated color changes and the enamel surface structure after in-office bleaching. Experiments were conducted assuming a single-visit bleaching session, and changes in both color and the enamel surface structure were observed after bleaching. Enamel surface structure changes were similar to those previously reported[11]. A roughened surface was observed after bleaching in group H, which utilized an agent with a higher hydrogen peroxide concentration.

The color changes noted in the present study were consistent with those described in previous studies[5,8,19]. In all three experimental groups, significant increases were observed in L^* values after bleaching, suggesting improvements in both brightness and whiteness. However, no significant differences were noted between the groups, indicating that agents with different hydrogen peroxide concentrations provided similar outcomes. Additionally, color changes in the present study were similar to those previously reported[5,8,19]. ΔE^*ab values were high in all groups (P, T, and H), indicating a clear bleaching effect. However, no significant differences were detected between the groups.

Titanium dioxide in the bleaching agents used in the present study has been reported to be applicable for teeth bleaching[20]. When exposed to ultraviolet light, it generates active oxygen, such as OH・radicals, which decompose a number of organic compounds[21].

The bleaching agent in group P was induced to react with visible light at wavelengths of 400 to 420 nm by the addition of a low concentration of hydrogen peroxide to titanium dioxide, which only reacts to ultraviolet light. Therefore, the photocatalytic activity of titanium dioxide is induced by irradiation with violet to blue visible light, and bleaching proceeds due to the oxidizing effects of the OH・radicals generated[14]. The LED light-curing unit used in the present study emits violet light (at approximately 400 nm), which is suitable for teeth bleaching. Therefore, although the bleaching agent used in group P contained a low concentration of hydrogen peroxide, the presence of titanium dioxide and the use of a light irradiator to induce its photocatalytic activity produced an equivalent amount of OH・radicals to that by the agent with a high concentration of hydrogen peroxide in group H, with no significant difference in their bleaching effects.

On the other hand, the bleaching agent used in group T employs a visible light-responsive titanium oxide photocatalyst, which activates hydrogen peroxide and decomposes colored substances following its irradiation with visible light[22]. In the present study, the bleaching agent used in group T had a hydrogen peroxide concentration of 23%. However, the presence of titanium dioxide, the use of a light irradiator to activate its photocatalytic properties, and a longer duration of bleaching than in the other groups, resulted in no significant differences in their bleaching effects[23].

Therefore, although hydrogen peroxide concentrations differed among the groups, the use of titanium dioxide as a photocatalyst and the duration of light exposure resulted in the generation of a large amount of OH・radicals, yielding the same bleaching effects.

Surface roughness significantly differed after bleaching in all groups, indicating that the bleaching agents affected the enamel surface under the bleaching conditions used in this study.

The critical pH for enamel demineralization is 5.5[24,25]. The pH of the bleaching agent used in group H is approximately 4 to 5. Kobayashi et al.[26] reported no significant changes in the enamel surface after 3 minutes of treatment with a bleaching agent; however, a bubbling rough surface structure was noted with further bleaching. Nakazawa et al.[14] also showed that surface roughness slightly increased after bleaching, which may have been due to the effects of the pH of the agent, similar to the present study. On the other hand, the pH of the bleaching agents used in groups P and T was approximately 6. Surface roughness slightly decreased in groups P and T, which is consistent with

previous findings[14]. Kimura et al.[27] reported no significant changes in the enamel surface structure after bleaching, suggesting that the pH of the bleaching agents used in groups P and T did not markedly affect the enamel surface structure. Therefore, surface roughness appears to vary depending on the pH of the bleaching agent, but did not significantly differ after a single bleaching treatment in this study.

Notably, group H showed increases in the surface roughness values after bleaching, suggesting that the enamel surface became rougher. This may be attributed to the high hydrogen peroxide concentration of 35% in the bleaching agent used in group H, which resulted in a lower pH, further contributing to enamel surface roughness[28]. Therefore, the enamel surface was rougher after bleaching in group H than in the other groups, causing light scattering, which led to the bleaching effect being visually recognizable.

In the present study, experiments were conducted under the assumption of a single-visit in-office bleaching procedure. Since repeated bleaching may increase the leaching of calcium and phosphate[10], the effects of bleaching agents under different conditions, including multiple in-office bleaching visits, need to be investigated in the future. It is important to note that there were large standard deviations in the results obtained within each group, which may be due to an insufficient sample size. Therefore, further studies with a larger sample size are warranted.

Conclusion

The present study examined color and enamel surface changes after bleaching with a single-visit in-office bleaching procedure using agents with various hydrogen peroxide concentrations. L^* and a^* values significantly increased in all three groups after bleaching. Moreover, b^* values slightly decreased in groups P and T, and slightly increased in group H. However, no significant differences were observed in group P. Therefore, a clear bleaching effect was observed in all three groups regardless of hydrogen peroxide concentrations. ΔE^*ab values in all groups indicated significantly strong bleaching effects, suggesting effectiveness. SEM observations of enamel surfaces revealed a smooth appearance after bleaching in groups P and T, and a roughened enamel surface in group H, which used an agent containing a higher hydrogen peroxide concentration. Furthermore, surface roughness showed significant changes after bleaching in all groups.

Conflicts of Interest

Yukie Kusaka-Yoshino is an employee of GC Corporation and receives compensation from the company.

References

1) Fukai K. Introduction and summary overview. Fukai K (editor-in-chief). The current evidence of dental care and oral health for achieving healthy longevity in an aging society 2015. Japan Dental Association: Tokyo, 2015. 6–11.
2) Kressin NR, Boehmer U, Nunn ME, Spiro A 3rd. Increased preventive practices lead to greater tooth retention. J Dent Res 2003; 82: 223–227.
3) Goldstein RE, Garber DA. A new role for restorative dentistry. Complete Dental Bleaching. 1st ed. Quintessence Publishing: Chicago; 1995. 1–23.
4) Goldstein RE, Garber DA. Nightguard vital bleaching. Complete Dental Bleaching. 1st ed. Quintessence Publishing: Chicago; 1995. 71–100.
5) Nie J, Tian FC, Wang ZH, Yap AU, Wang XY. Comparison of efficacy and outcome satisfaction between in-office and home teeth bleaching in Chinese patients. J Oral Sci 2017; 59: 527–532.
6) Goldstein RE, Garber DA. In-office bleaching of vital teeth. Complete Dental Bleaching. 1st ed. Quintessence Publishing: Chicago; 1995. 57–69.
7) Al-Qunaian TA. The effect of whitening agents on caries susceptibility of human enamel. Oper Dent 2005; 30: 265–270.
8) Tsubura S. Clinical evaluation of three months' nightguard vital bleaching on tetracycline-stained teeth using Polanight 10% carbamide gel: 2-year follow-up study. Odontology 2010; 98: 134–138.
9) Smidt A, Weller D, Roman I, Geralia I. Effect of bleaching agents on microhardness and surface morphology of tooth enamel. Am J Dent 1998; 11: 83–85.
10) Cimilli H, Pameijer CH. Effect of carbamide peroxide bleaching agents on the physical properties and chemical composition of enamel. Am J Dent 2001; 14: 63–66.
11) Al-Salehi SK, Wood DJ, Hatton PV. The effect of 24h non-stop hydrogen peroxide concentration on bovine enamel and dentine mineral content and microhardness. J Dent 2007; 35: 845–850.
12) Miake Y, Nozue S, Moriguchi M, Yamazaki T, Sawada T, Yanagisawa T. The ability of xylitol containing gum with calcified seaweed in preventing demineralization of

tooth surfaces. J Hard Tissue Biol 2011; 20: 87–92.
13) Sugito H, Eguchi T, Tanaka R, Haruyama A, Muramatsu T. The effects of dietary pH changes on tooth staining of the enamel surface. ODEP 2023; 3: 80–85.
14) Nakazawa T, Kato J, Hirai Y. Comparison of bleaching effects between low-concentration hydrogen peroxide with titanium dioxide and high-concentration hydrogen peroxide. Jpn J Conserv Dent 2007; 50: 373–378.(in Japanese)
15) Lu L, Yoshikawa K, Komatsu O, Hirota Y, Hattori Y, Inoue C, Yasuo K, Tanimoto H, Iwata N, Wu B, Yamamoto K. Evaluation of a tooth bleaching system incorporating titanium dioxide: Influence of the concentration of hydrogen peroxide and titanium dioxide on bleaching effect. J Oasaka Dent Univ 2013; 47: 209–214.
16) Kyaw KY, Otsuki M, Hiraishi N, Segarra MS, Tagami J. Effect of application of desensitizers before bleaching on change of tooth shade. Dent Mater J 2019; 38: 790–797.
17) Eguchi T, Satou R, Miake Y, Sugihara N. Comparison of resistance of dentin to erosive acid after application of fluoride to teeth. J Hard Tissue Biol 2020; 29: 193–202.
18) Japan Academy of Esthetic Dentistry. Accreditation. https://www.jdshinbi.net/en/accreditation/(cited 2024.10.31)
19) Yoshino F. Application of titanium dioxide photocatalyst reaction in a tooth-bleaching agent. Bull Kanagawa Dent Coll 2011; 39: 45–47.
20) Nonami T, Ishibashi K, Ishibashi T, Kondo O. Bleaching with TiO2 photocatalyst and its biocompatibility. Jpn J Dent Esthet 2001; 13: 251–255.(in Japanese)
21) Fujishima A, Honda K. Electrochemical photolysis of water at a semiconductor electrode. Nature 1972; 238: 53–58.
22) Kishi A, Otsuki M, Sadr A, Ikeda M, Tagami J. Effect of light units on tooth bleaching with visible-light activating titanium dioxide photocatalyst. Dent Mater J 2011; 30: 723–729.
23) Tagami J, Senda A, Otsuki M, Nikaido T, Nakajima M, Tomoda S, Yamada M, Kawai T. Clinical evaluation of an office bleaching system containing visible light activating titanium oxide photocatalyst (TiON in Office). Jpn J Conserv Dent 2011; 54: 131–141.(in Japanese)
24) Stephan RM, Miller BF. A quantitave method for evaluating physical and chemical agents which modify production of acids in bacterial plaques on human teeth. J Dent Res 1943; 22: 45–51.
25) Stephan RM. Intra-oral hydrogen-ion concentrations associated with dental caries activity. J Dent Res 1944; 23: 257–266.
26) Kobayashi T, Mega J, Mishima H, Kozawa Y, Gotoh H, Koike K, Mizukawa K. Vital teeth bleaching: Structural analysis of the enamel surface treated with Hi Lite™. J Jpn Prosthodont Soc 1995; 39: 303–307.(in Japanese)
27) Kimura Y, Imai H, Sato Y, Sato M, Yamazaki N, Yamada M, Amano Y, Masuda Y, Yamada Y, Kameda A, Koba K. Bleaching effect and influence on teeth of various bleaching materials. Jpn J Conserv Dent 2011; 54: 162–168.(in Japanese)
28) Lewinstein I, Hirschfeld Z, Stabholz A, Rotstein I. Effect of hydrogen peroxide and sodium perborate on the microhardness of human enamel and dentin. J Endod 1994; 20: 61–63.

Original Article

ODEP 5 (1) : 20～31, 2025

Type H Vessels Are Progressively Lost in a Mouse Model of Periodontitis : A 3D Tissue-clearing Analysis of Alveolar Bone

Satoru SHINDO, Shin NAKAMURA[1], Risa SHINDO, Tomoya UEDA, Donald PHAM[2], Tetsuya ADACHI[3], Motoki OKAMOTO[4], Maiko SUZUKI, Yoshitaka HOSOKAWA[5], Ikuko HOSOKAWA[5], Hideki SHIBA[6], Hajime SASAKI[7], Saynur VARDAR[2] and Toshihisa KAWAI

Department of Oral Science and Translational Research, College of Dental Medicine, Nova Southeastern University
[1]Department of Patho-physiology/Periodontal Science, Okayama University Faculty of Medicine, Dentistry and Pharmaceutical Sciences
[2]Department of Periodontology, College of Dental Medicine, Nova Southeastern University
[3]Department of Dental Medicine, Graduate School of Medical Science, Kyoto Prefectural University of Medicine
[4]Department of Restorative Dentistry and Endodontology, Osaka University Graduate School of Dentistry
[5]Department of Conservative Dentistry, Tokushima University Graduate School of Biomedical Sciences
[6]Department of Biological Endodontics, Graduate School of Biomedical and Health Sciences, Hiroshima University
[7]Department of Cariology, Restorative Sciences, and Endodontics, School of Dentistry, University of Michigan

Abstract

Purpose: Type H vessels, a specialized subtype of bone-forming vasculature first identified in long bones, are now recognized as critical regulators of angiogenesis-osteogenesis coupling. Defined by high expression of CD31 and endomucin (EMCN), these vessels contribute to both physiological bone growth and pathological bone loss. Although recent studies have identified type H vessels in alveolar bone, their three-dimensional (3D) organization and responses to inflammation remain poorly understood. Here, we aimed to establish a reproducible methodology for visualizing and quantifying type H vessels in murine alveolar bones under both healthy and inflammatory conditions, utilizing a mouse model of periodontitis.

Methods: Experimental periodontitis was induced in C57BL/6 mice by placing 5-0 silk ligatures around the maxillary second molar for 0, 3, 7, or 14 days. For 3D vascular analysis, maxillary bone samples underwent tissue clearing with the X-CLARITY system to achieve optical transparency while preserving the antigenicity of the molecules of interest. Type H vessels were identified by dual immunofluorescence staining for CD31 and EMCN, followed by confocal microscopy. The captured digital images were reconstructed for quantification using Imaris software. Alveolar bone loss and microstructural changes were evaluated using micro-computed tomography (micro-CT). Gingival tissues were harvested to assess inflammatory or osteoblast-associated gene expression by qPCR. In parallel, bone marrow-derived endothelial cells (BMECs) were stimulated with recombinant TNF-α or rIL-1β, and changes in EMCN and CD31 expression were analyzed by qPCR and flow cytometry.

Corresponding author: Satoru SHINDO, Department of Oral Science and Translational Research, College of Dental Medicine, Nova Southeastern University, 3200 South University Drive, Fort Lauderdale, FL 33328, USA
TEL: +1-954-935-4006, E-mail: sshindo1@nova.edu
Received for Publication: September 12, 2025/Accepted for Publication: October 8, 2025
DOI : 10.11471/odep.2025-003

Results: The clearing protocol yielded optically transparent maxillary alveolar bone while preserving tissue architecture and immunoreactivity. Confocal imaging revealed abundant $CD31^{+}EMCN^{+}$type H vessels in the control healthy periodontal tissue. Quantitative 3D analysis revealed a time-dependent reduction in type H vessel volume following ligature-induced periodontitis in mice. Strikingly, regions exhibiting diminished type H vasculature spatially coincided with areas of alveolar bone resorption identified by micro-CT and with elevated gingival *Tnf* and *Il1b* expression, indicating a link between vascular rarefaction and inflammatory bone loss. In parallel, the expression of osteogenic markers, including *Alpl*, *Col1a1*, and *Bglap*, was significantly decreased during murine periodontitis. *In vitro*, both recombinant TNF-α and IL-1β suppressed the expression of EMCN, a hallmark molecule of type H vessels, in BMECs.

Conclusion: This study provides the first 3D visualization and quantitative characterization of type H vessels in murine alveolar bone with or without periodontitis using a tissue-clearing-based approach. We demonstrate that inflammatory conditions associated with periodontitis cause marked loss of type H vasculature, thereby disrupting angiogenesis-osteogenesis coupling. These findings underscore the possible role of the vascular niche in periodontal disease pathogenesis and suggest that therapeutic preservation or restoration of type H vessels could represent a novel strategy to prevent inflammation-driven alveolar bone loss and enhance periodontal regeneration.

Key words：type H vessels, periodontitis, tissue clearing

Introduction

Bone is a highly vascularized tissue in which angiogenesis and osteogenesis are tightly coordinated[1–3]. The vasculature not only provides oxygen and nutrients but also delivers instructive signals that regulate bone remodeling and regeneration[4,5]. In 2014, Kusumbe et al. identified a specialized capillary subtype in long bones associated with active bone formation, termed type H vessels, characterized by high expression of CD31 and endomucin (EMCN). These vessels are distinguished by their high expression of CD31 and EMCN[6], in contrast to other capillary subtypes in the diaphyseal region—where bone formation is largely complete—that display low expression of both markers (so-called type L vessels). Type H vessels are particularly enriched in the metaphyseal and endosteal regions, where they play a critical role in supporting osteoprogenitor cell expansion and tightly coupling angiogenesis with osteogenesis[6,7].

Type H vessels have since been shown to play critical roles in skeletal development and homeostasis. Their abundance declines with age, correlating with reduced bone formation and osteoporosis[6,8]. Experimental stimulation of type H vessels through Notch signaling or hypoxia-inducible factor (HIF) pathways has been shown to restore bone mass in murine models[9,10]. Endothelial cells within type H vessels secrete angiocrine factors, including vascular endothelial growth factor (VEGF), bone morphogenetic proteins (BMPs), platelet-derived growth factor subunit B (PDGF-BB), and slit guidance ligand 3 (SLIT3), which stimulate osteoprogenitor recruitment and differentiation, thereby enhancing bone formation[11–14]. Furthermore, alterations in type H vessel formation are implicated in pathological contexts such as fracture healing defects, glucocorticoid-induced osteoporosis, and spondylarthritis[12,15,16]. Collectively, these studies suggest that type H vasculature is a critical regulator of skeletal health and a potential therapeutic target.

Although the role of type H vessels in long bone biology is increasingly well characterized, their contribution to craniofacial bone homeostasis and pathology remains largely undefined. This represents a critical gap in knowledge, as craniofacial bones fundamentally differ from long bones by undergoing intramembranous rather than endochondral ossification[17,18]. In particular, alveolar bone is widely recognized to develop through intramembranous ossification[19,20], highlighting the likelihood of distinct vascular-skeletal interactions within the periodontal bone compartment. Understanding this relationship is particularly important in the context of periodontitis, a highly prevalent chronic inflammatory bone lytic disease initiated by dysbiotic microbial communities and amplified by aberrant host immune responses[21,22].

Although osteoclast-mediated bone resorption is the primary pathological effector mechanism[23,24], vascular changes are also observed in periodontal tissues, including abnormal angiogenesis and vessel leakage[25,26]. Type H vessel formation has been reported to play an important role in alveolar bone formation[27,28]. However, how type H vessels respond to inflammatory conditions, in relation to the level of bone destruction, remains an unresolved question.

Conventional histology is limited in studying the vascular microenvironment of alveolar bone due to its mineralized nature and the two-dimensional (2D) constraints of sectioning. Advances in tissue clearing technologies such as X-CLARITY have recently enabled three-dimensional (3D) visualization of vasculature in intact organs, including bone[29–31]. These approaches render tissues optically transparent while preserving immunoreactivity, thereby allowing deep-tissue imaging with confocal or light-sheet microscopy. Such methods provide a powerful opportunity to investigate the spatial organization and dynamics of type H vessels in alveolar bone, but to date, few studies have systematically applied them to the context of periodontitis.

Here, we established a method combining tissue clearing, confocal immunofluorescence, and volumetric analysis to visualize and quantify type H vessels in murine alveolar bone. Using the ligature-induced periodontitis model, we investigated whether inflammatory bone loss is associated with alterations in type H vessel formation. We hypothesized that periodontitis leads to a reduction in type H vasculature, thereby impairing angiogenesis-osteogenesis coupling in the periodontal microenvironment. Our findings demonstrate that type H vessels are present in healthy alveolar bone, which are significantly diminished during periodontitis, providing new insights into the vascular contribution to periodontal disease and suggesting novel therapeutic avenues.

Materials and Methods

1. Animals

Eight-week-old male C57BL/6J mice (Jackson Laboratory, Bar Harbor, ME, USA) were used in all experiments. Animals were housed under specific pathogen-free conditions with ad libitum access to food and water, under a 12-h light/dark cycle. All experimental procedures were approved by the Institutional Animal Care and Use Committee (IACUC) of Nova Southeastern University (Protocol #TK7) and performed in accordance with NIH guidelines for the care and use of laboratory animals.

2. Ligature-induced periodontitis model

Experimental periodontitis was induced as previously described[32,33]. Briefly, under anesthesia with ketamine/xylazine (100 mg/kg and 10 mg/kg, i.p.), a 5–0 silk ligature (ETHICON, J & J, New Brunswick, NJ, USA) was placed around the maxillary second molar and maintained for 3, 7, or 14 days. Mice were sacrificed at each time period for tissue collection. Gingival tissues surrounding the maxillary molars were harvested for RNA extraction, while maxillary bone tissues were collected for micro-computed tomography (micro-CT) analysis and tissue clearing.

3. Micro-CT analysis

Maxillae were dissected, fixed in 10% formaldehyde overnight at 4℃, and scanned using a SkyScan 1276 micro-CT system (Bruker, Billerica, MA, USA). Scanning parameters were 65 kV, 385 μA, and 9-μm voxel resolution. Images were reconstructed with NRecon software (Bruker) and analyzed using CTAn (Bruker). Regions of interest (ROI) included the interproximal alveolar bone between the first, second, and third molars. Bone volume fraction (BV/TV) was quantified.

4. Tissue clearing

Murine maxillary bones were fixed in 10% formaldehyde overnight at 4℃, followed by decalcification in 10% EDTA at 37℃ for 4 days. After thorough washing with PBS, samples were incubated in X-CLARITY Polymerization Initiator and Hydrogel Solution (Logos Biosystems, Anyang, South Korea) at 4℃ for 24 h. Polymerization was then carried out using the X-CLARITY Polymerization System under vacuum (−90 kPa) at 37℃ for 3 h. Following polymerization, tissues were washed in PBS and subjected to lipid removal using the X-CLARITY Tissue Clearing System II (1.2 A, 37℃, 50 rpm) for 8 h. Cleared tissues were rinsed in PBS (3×5 min) and further incubated in PBS overnight at room temperature before subsequent immunostaining.

5. Immunofluorescence staining

Cleared maxillae were incubated with primary antibodies against Vio R667-conjugated CD31 (anti-mouse, REAfinity clone REA782, Miltenyi Biotec, Cat# 130–

123-935, 1 : 50) and FITC-conjugated endomucin antibody (clone V.5C7, Santa Cruz Biotechnology, Dallas, TX, USA, sc-53941 FITC, 1 : 50) in staining solution (6% BSA, 0.2% TritonX-100 and 0.01% sodium azide in PBS) for 4 days at 37℃ with gentle agitation. After staining, tissues were washed three times in distilled water (5 min each) at room temperature. Samples were then incubated twice in fresh mounting solution (Logos Biosystems) for 1 h each at room temperature before being fully submerged in fresh mounting solution for imaging.

6. Confocal microscopy and 3D reconstruction

Imaging was performed using a Zeiss LSM880 confocal microscope (Carl Zeiss, Oberkochen, Germany). Z-stack images were acquired at 2-μm intervals, covering a total thickness of 300-500 μm within the alveolar bone. Three-dimensional reconstruction and volumetric analyses were carried out using Imaris software (version 10.2; Oxford Instruments, Concord, MA, USA). Type H vessels were identified as $CD31^+EMCN^+$ capillaries. For all samples, the quantified region of interest was defined as the alveolar bone located between the first and second molars.

7. Quantitative polymerase chain reaction (qPCR)

Total RNA was extracted from murine gingival samples or mouse bone marrow-derived endothelial cells (BMECs) using the PureLink RNA Mini Kit (Thermo Fisher Scientific, Waltham, MA, USA), following the manufacturer's protocol. The first strand cDNA was assembled from 100 ng of sample RNA using a Verso cDNA Synthesis Kit (Thermo Fisher Scientific). Amplification reactions were performed by Taqman Fast Advanced Master Mix (Thermo Fisher Scientific) or SYBR Green Master Mix (Thermo Fisher Scientific). The resultant cDNA was amplified by specific probes (Thermo Fisher Scientific) for *Gapdh* (Mm99999915_g1), *Tnfa* (Mm00443258_m1), *Il1b* (Mm00434228_m1), *Alpl* (Mm00475834_m1), *Col1a1* (Mm00801666_g1), *Bglap* (Mm03413826_mH), *Emcn* (Mm00497495_m1), and *Pecam1* (Mm01242576_m1) on a QuantStudio 3 (Thermo Fisher Scientific). The ratios of mRNA levels to those of the control gene were calculated using the ΔCt method ($2^{-\Delta\Delta Ct}$).

8. BMEC culture

Primary mouse BMECs were purchased from Cell Biologics (Chicago, IL, USA; Cat. No. C57-6221) and cultured in Complete Endothelial Cell Medium (Cell Biologics; M1168) according to the manufacturer's instructions. BMECs were maintained at 37℃ in a humidified incubator with 5% CO_2, and the culture medium was refreshed every 48 h. When cells reached 70-85% confluence, they were passaged using trypsin-EDTA (Thermo Fisher Scientific). Experiments were performed with cells at passages between 5 and 10 to ensure preservation of endothelial phenotype. For cytokine stimulation assays, BMECs were seeded in 12-well plates at a density of 2×10^5 cells per well. Subsequently, BMECs treated with recombinant mouse TNF-α or IL-1β (10 or 100 ng/mL; Biolegend, San Diego, CA, USA) for 3, 6, or 12 h for qPCR or 48 h for flow cytometry.

9. Flow cytometry

BMECs cultured in 6-well plates were detached using Accutase (Thermo Fisher Scientific) for 5 min at 37℃, gently triturated, and washed with FACS buffer (PBS containing 2% FBS and 2 mM EDTA). A total of 1×10^6 cells per sample were incubated for 30 min on ice with anti-EMCN antibody conjugated to Alexa Fluor 488 (Santa Cruz Biotechnology) and anti-CD31 antibody conjugated to Alexa Fluor 647 (Santa Cruz Biotechnology). Corresponding isotype control antibodies conjugated to Alexa Fluor 488 or Alexa Fluor 647 (Biolegend) were included to establish gating thresholds. After staining, cells were washed twice with FACS buffer and analyzed on a BD LSRFortessa flow cytometer (BD Biosciences, Franklin Lakes, NJ, USA) using FlowJo software version 10 (BD Biosciences).

10. Statistical analysis

All quantitative data are presented as mean±standard deviation (SD). Statistical significance was determined using unpaired two-tailed Student's *t*-tests for two groups or one-way ANOVA with Tukey's post hoc test for multiple comparisons. A value of $p<0.05$ was considered statistically significant. Analyses were performed using GraphPad Prism 10.0.1 (GraphPad Software, Boston, MA, USA).

Results

1. Successful tissue clearing and detection of type H vessel in murine maxillary alveolar bone

To enable 3D visualization of vascular networks

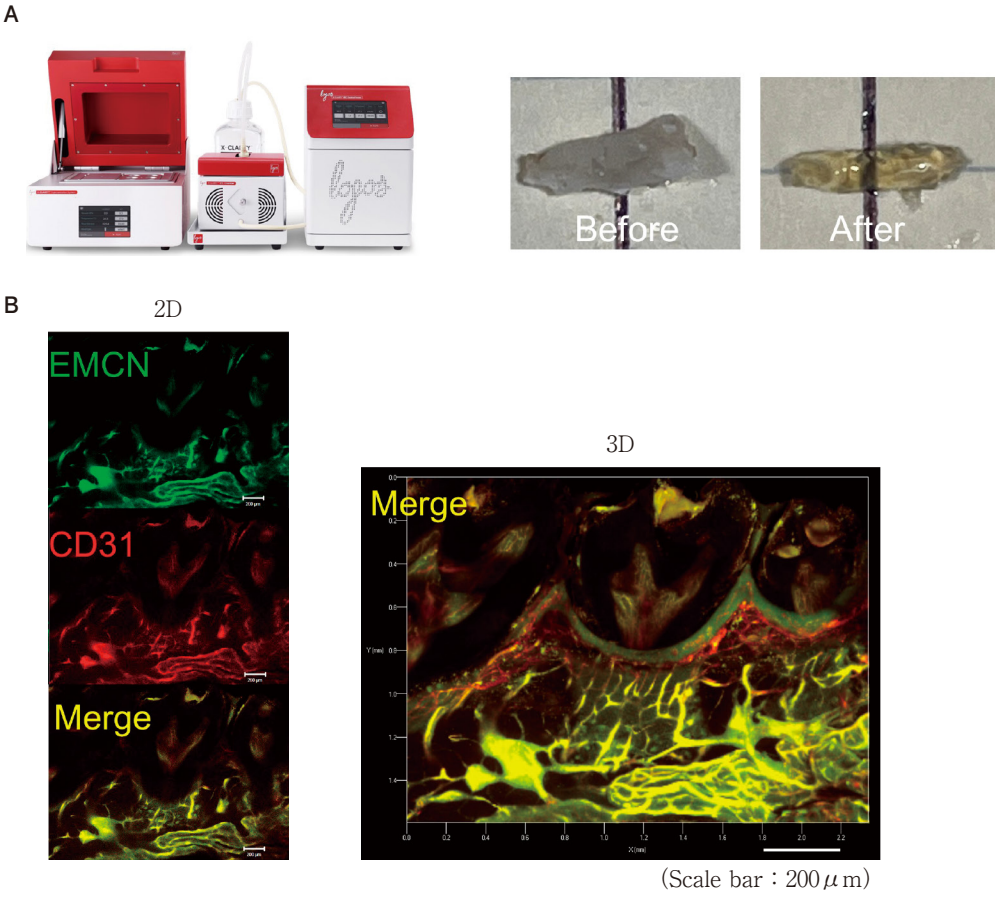

Fig. 1 3D visualization of type H vessels in murine alveolar bone
(A) Transparent alveolar bone tissue was prepared using the X-CLARITY tissue clearing system. (B) Cleared tissue was immunostained with anti-CD31 and anti-EMCN antibodies to identify type H vessels. 3D reconstruction and visualization were performed using Imaris software. Scale bar indicates 200 μm.

within alveolar bone, we optimized a tissue clearing protocol using the X-CLARITY system. Following electrophoretic lipid removal, cleared maxillary bone samples were incubated in the mounting solution (Logos Biosystems) to achieve refractive index matching. Murine maxillae were rendered optically transparent (Fig. 1A). The cleared tissues maintained their structural integrity. They permitted deep-tissue penetration of fluorophore-conjugated antibodies, providing a foundation for subsequent 3D type H vascular imaging, which indicated $CD31^{+}EMCN^{+}$ vessels in murine alveolar bone (Fig. 1B).

2. Time-dependent bone loss, vascular rarefaction, inflammation and osteoblastogenesis in ligature-induced periodontitis

Micro-CT analysis revealed progressive alveolar bone loss following ligature placement around the maxillary second molar for 3, 7, or 14 days. Bone volume fraction (BV/TV) was significantly reduced compared with non-ligated controls, with the greatest resorption observed on day 14 ($p<0.05$, one-way ANOVA with Tukey's multiple comparisons test) (Fig. 2), confirming the reproducibility and progressive nature of the ligature-induced periodontitis model. Concomitant with bone resorption, 3D confocal analysis demonstrated a time-dependent reduction in type H vessels ($p<0.05$, one-way ANOVA with Tukey's multiple comparisons test) (Fig. 2). Importantly, regions of reduced type H vasculature spatially corresponded with alveolar bone resorption identified by micro-CT, indicating that vascular rarefaction is tightly coupled to inflammatory bone loss. Supporting this relationship, qPCR analysis of gingival tissues showed progressive upregulation of *Tnfa* and *Il1b* expression over the same time course. The

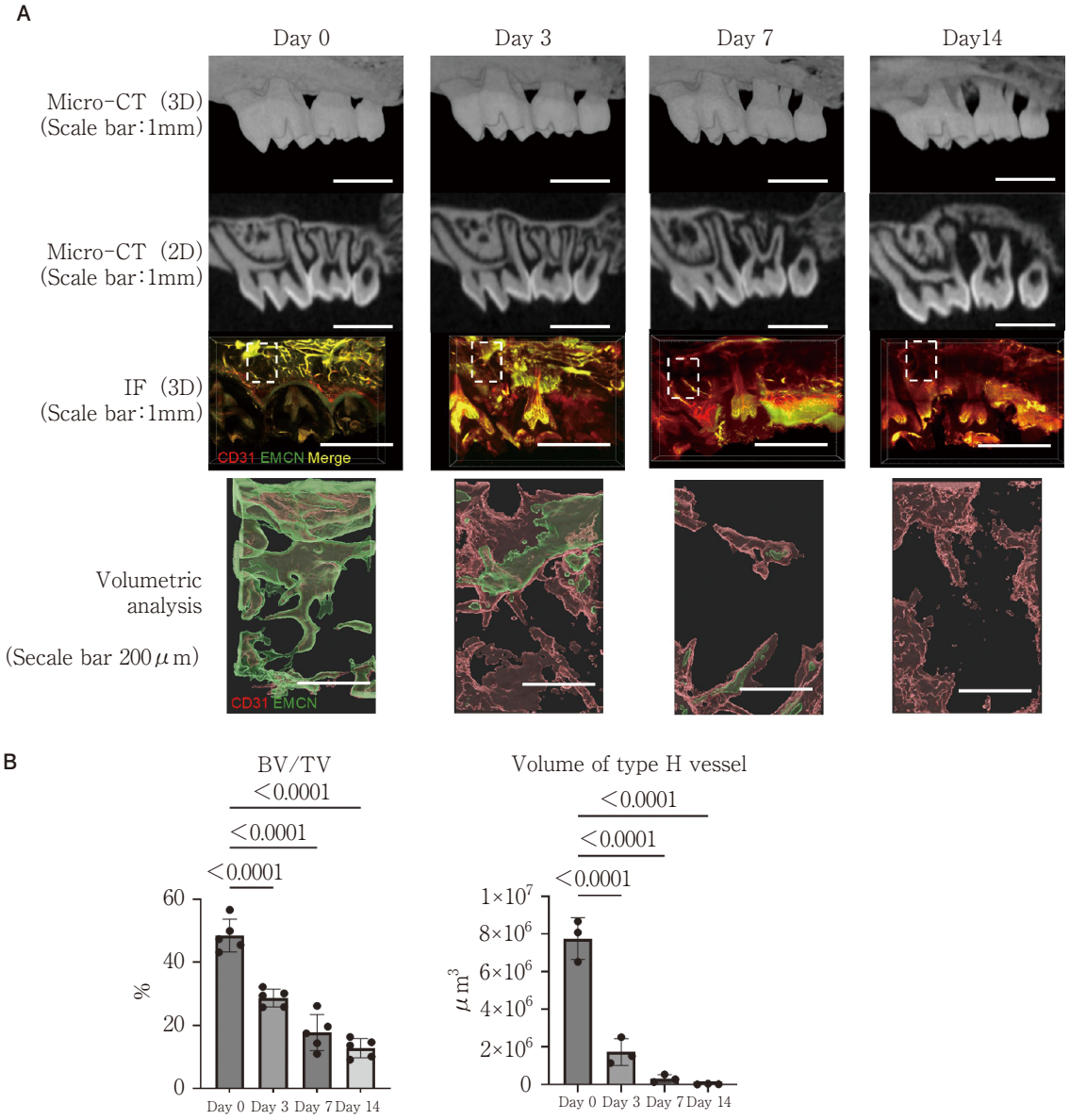

Fig. 2 Correlation between type H vessel formation and periodontal bone loss

(A) Bone volume and type H vessel formation were analyzed in the ligature-induced periodontitis model at days 3, 7, and 14 using micro-CT and immunofluorescence (IF) combined with tissue clearing technology, respectively. Scale bar : 1 mm or 200 μm. (B) Quantification of bone volume and type H vessel volume.

temporal increase in pro-inflammatory cytokines paralleled the decline in type H vessel volume, linking inflammatory signaling to vascular deterioration and alveolar bone loss ($p<0.05$, one-way ANOVA with Tukey's multiple comparisons test) (Fig. 3A). Furthermore, qPCR analysis of osteoblast-related genes, including *Alpl*, *Col1a1*, and *Bglap*, revealed marked downregulation during the progression of periodontitis ($p<0.05$, one-way ANOVA with Tukey's multiple comparisons test) (Fig. 3B). These results suggest that the reduction of type H vessels impairs osteoblastogenesis, thereby contributing to inflammatory bone loss.

3. Pro-inflammatory cytokine suppression of the type H phenotype in BMECs

While CD31 expression remained largely unchanged under TNF-α stimulation, a modest reduction was observed in IL-1β-treated BMECs ($p<0.05$, one-way ANOVA with Tukey's multiple comparisons test) (Fig.

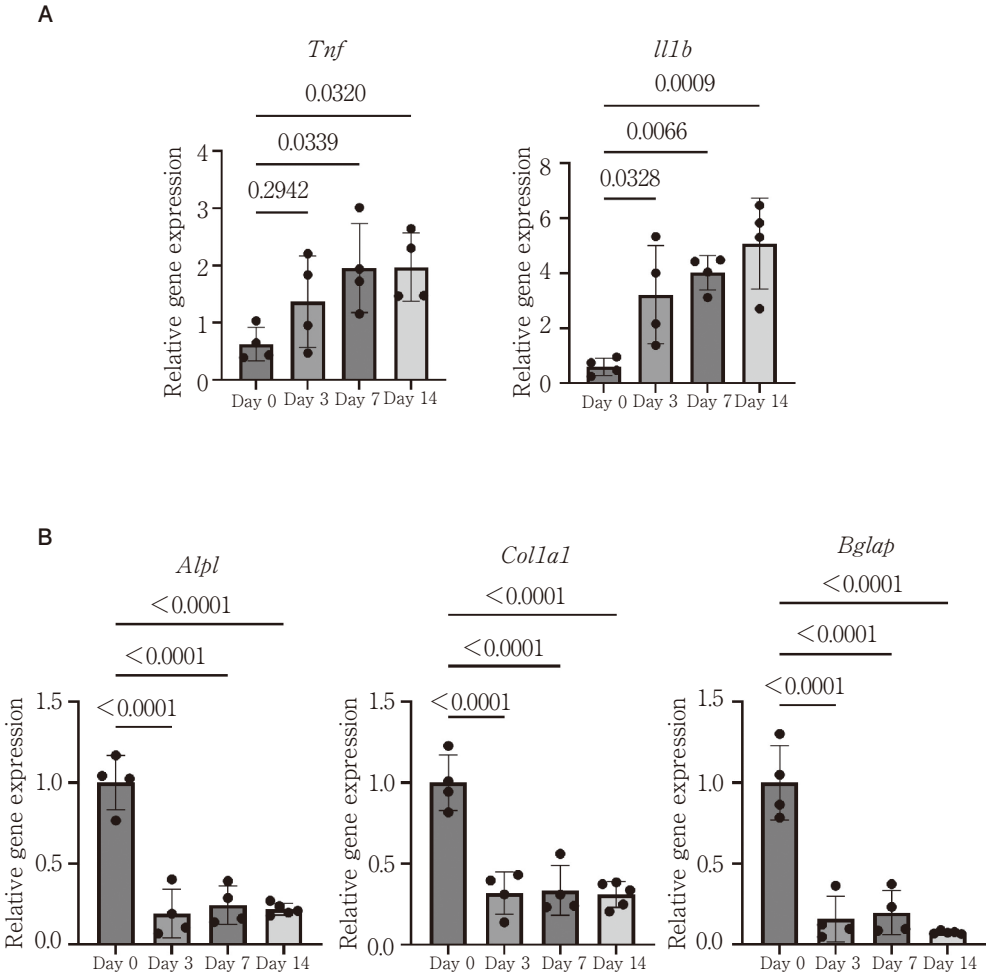

Fig. 3 Gene expression of inflammation and osteoblastogenesis in periodontitis
(A) Gene expression of *Tnf* and *Il1b* in murine gingival tissue was assessed by qPCR.
(B) Gene expression of *Alpl*, *Col1a1*, and *Bglap* was analyzed by qPCR.

4). Consistent with the transcriptional results, flow cytometry demonstrated that EMCN protein expression was significantly reduced by both TNF-α and IL-1β, whereas CD31 levels were relatively preserved ($p<0.05$, unpaired two-tailed Student's *t*-test) (Fig. 5). These findings indicate that inflammatory cytokines preferentially disrupt the type H-associated endothelial phenotype. Collectively, these results support the *in vivo* observation that pro-inflammatory mediators contribute to the rarefaction of type H vessels during periodontitis.

Discussion

In this study, we provide the first 3D visualization and quantitative analysis of type H vessels in murine alveolar bone and demonstrate their progressive rarefaction during ligature-induced periodontitis in mice. Using tissue clearing combined with confocal imaging and volumetric reconstruction, we established a reproducible methodology to interrogate the periodontal vascular network (Fig. 1). Our findings show that alveolar bone resorption is closely associated with the loss of type H vasculature, and that pro-inflammatory cytokines such as TNF-α and IL-1β directly suppress the type H-associated endothelial phenotype *in vitro*. Together, these data highlight the importance of the vascular niche in periodontal disease pathogenesis and identify type H vessels as a potential therapeutic target.

Type H vessels, defined by high expression of CD31 and EMCN, were first identified in long bones, where they provide a specialized vascular niche that supports osteoprogenitor proliferation and couples angiogenesis

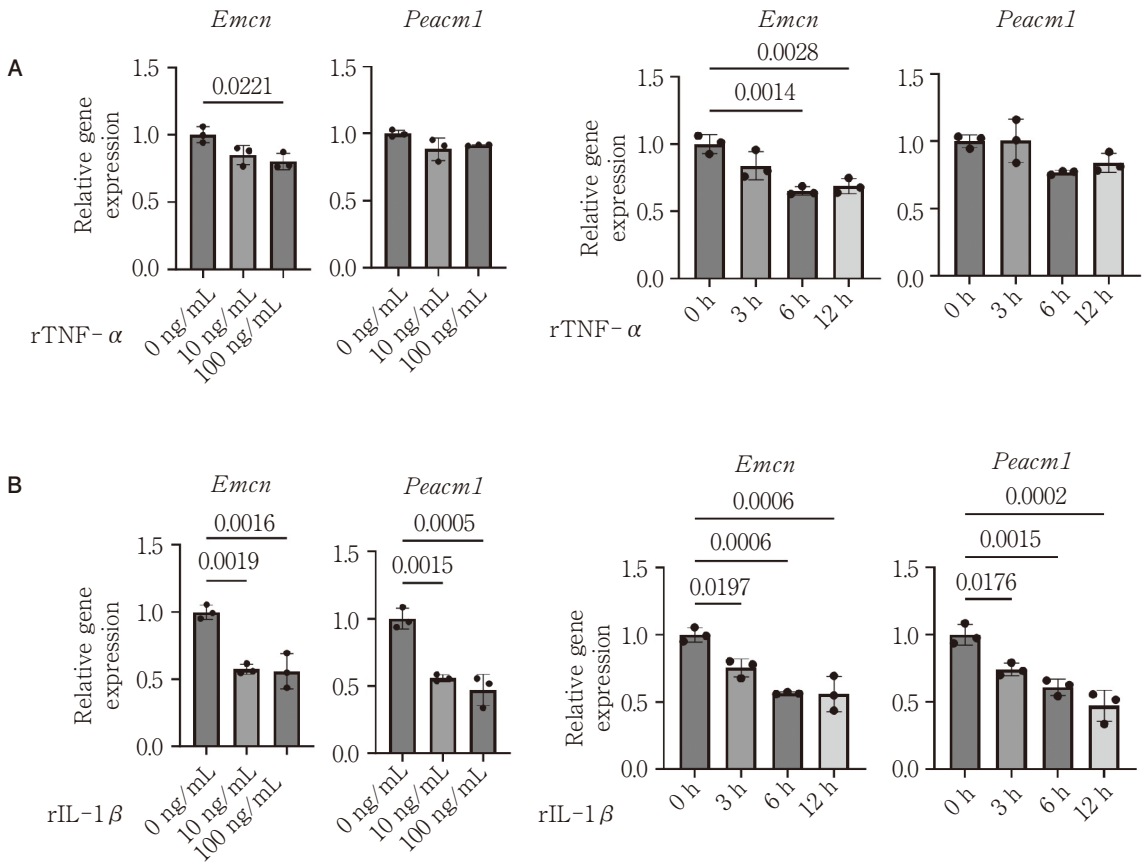

Fig. 4 Effects of inflammatory cytokines on CD31 and EMCN gene expression in BMECs
(A) BMECs were treated with recombinant TNF-α (10 or 100 ng/mL) for 3, 6, or 12 hours. *Pecam1* and *Emcn* expression levels were quantified by qPCR. (B) BMECs were treated with recombinant IL-1β (10 or 100 ng/mL) for 3, 6, or 12 hours, and *Pecam1* and *Emcn* expression levels were analyzed by qPCR.

with osteogenesis[6]. Subsequent studies demonstrated that the abundance of type H vessels declines with aging and osteoporosis, contributing to skeletal fragility[8,34,35]. More recent studies further demonstrated that occlusal force preserves alveolar bone homeostasis by promoting type H angiogenesis within the periodontal ligament niche[27], and that systemic inhibition of cathepsin K (CTSK) in pre-osteoclasts protects against ligature-induced periodontal bone loss in mice by enhancing type H vessel formation[36]. Our findings build on these observations by extending the relevance of type H vasculature to the alveolar bone compartment, showing that type H vasculature is present within the periodontal region but is progressively lost under inflammatory conditions (Figs. 2B and 3A). The reduction of osteoblast-related genes (*Alpl, Col1a1, Bglap*) observed in parallel with vascular deterioration further supports the concept that type H vessels play a central role in maintaining osteoblastogenesis in alveolar bone (Fig. 3B). Previous studies have established that type H endothelial cells promote bone formation by secreting angiocrine factors such as PDGF-B and SLIT3[11–14]. Our findings suggest that inflammatory disruption of type H vessels disrupts osteoblast maturation, thereby impairing angiogenesis-osteogenesis coupling and accelerating periodontal bone loss. Although the murine ligature model recapitulates key features of human periodontitis, species-specific differences may limit direct translational applicability. Notably, type H vessels have been identified as important indicators of bone mass in humans, underscoring their conserved and critical role in coupling angiogenesis with osteogenesis[37]. However, their presence and functional significance within human periodontal tissues remain largely unknown.

Our data revealed that reductions in type H vessel volume correlate temporally with alveolar bone resorption and increased gingival expression of *Tnfa* and *Il1b*. These findings are consistent with the concept that

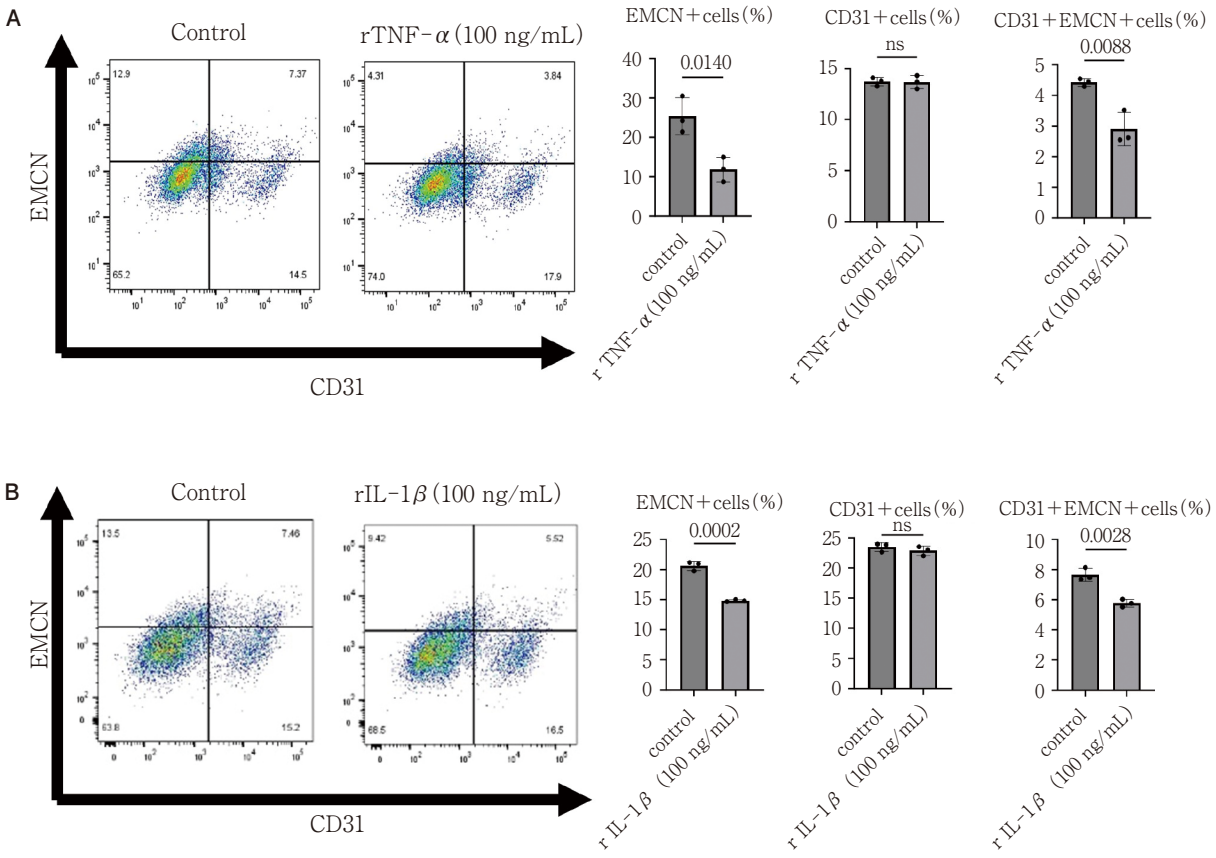

Fig. 5 Effects of inflammatory cytokines on CD31 and EMCN protein expression in BMECs
(A) BMECs were treated with recombinant TNF-α (100 ng/mL) for 48 hours. Protein expressions of CD31 and EMCN were assessed by flow cytometry. (B) BMECs were treated with recombinant IL-1β (100 ng/mL) for 48 hours, and CD31 and EMCN protein expressions were analyzed by flow cytometry.

inflammation exerts direct detrimental effects on the bone-forming vasculature. Indeed, previous studies have shown that TNF-α and IL-1β impair endothelial function, inhibit angiogenesis, and disrupt vascular homeostasis[38,39]. Moreover, TNF-α or IL-1β stimulation downregulates cell surface expression of EMCN in human umbilical vein endothelial cells (HUVECs), while concurrently upregulating adhesion molecules such as ICAM-1 and VCAM-1, thereby promoting a pro-inflammatory endothelial phenotype[40]. This observation is consistent with our finding that TNF-α or IL-1β selectively reduces EMCN expression in murine BMECs, indicating that inflammatory cytokines may drive vascular rarefaction by disrupting the type H endothelial phenotype (Fig. 4 and 5). Notably, a recent study demonstrated that LPS suppresses EMCN expression in HUVECs, supporting the concept that inflammation is closely associated with the reduction of type H vessel formation[41]. This suggests that inflammatory signaling preferentially disrupts the vascular subtype responsible for osteo-angiogenic coupling. Our findings provide mechanistic support for the *in vivo* observation that type H vessel rarefaction is a defining feature of inflammatory alveolar bone loss. Nevertheless, our analysis was limited to TNF-α and IL-1β, and additional inflammatory mediators may also contribute to this vascular rarefaction. Further mechanistic studies will be required to elucidate the precise pathways underlying the reduction of type H vessels.

Traditional histology offers only 2D assessment of vasculature and often distorts spatial relationships between bone and vessels. In contrast, our approach using tissue clearing and 3D confocal imaging preserved anatomical integrity and enabled volumetric quantification of vascular subtypes within intact alveolar bone (Fig. 2). These methodological advances complement recent efforts by applying optical clearing to study skeletal and dental tissues[42,43]. As shown in Fig.

2A, the vasculature within dental pulp tissue was also clearly visualized using the tissue-clearing approach, highlighting the broad applicability of this methodology. However, a key limitation is the absence of a suitable contrast agent for precise localization of mineralized bone, which remains a challenge to be addressed through future methodological and engineering advances. Periodontitis is a leading cause of tooth loss worldwide, yet current therapies focus largely on antimicrobial and anti-inflammatory strategies without directly addressing the vascular-osteogenic interface[44-46]. Our findings suggest that therapeutic approaches aimed at preserving or restoring type H vessels may help prevent or reverse alveolar bone loss. Strategies that enhance angiogenesis or stabilize EMCN expression could represent promising avenues for future regenerative therapies[47,48]. While our findings demonstrate an association between type H vessel loss and bone resorption, causal relationships remain to be established. Future studies employing genetic or pharmacologic tools to selectively preserve or expand type H vessels *in vivo* will be essential to determine whether vascular restoration is sufficient to promote periodontal regeneration.

Conclusion

In summary, we have demonstrated that ligature-induced periodontitis leads to progressive alveolar bone loss accompanied by rarefaction of type H vessels, and that inflammatory cytokines directly suppress the type H endothelial phenotype. By linking vascular decline with inflammatory bone resorption, our study provides novel insights into the vascular contribution to periodontal disease pathogenesis and identifies type H vessels as a promising therapeutic target for bone regeneration strategies.

Conflict of interest

The authors declare no conflict of interest to disclose.

Acknowledgement

This work was supported by NIH/NIDCR (DE-027851, DE-028715, DE-331851, DE-032907, DE-027648, DE-034069, DE030213, & DE-034154).

References

1) Chen D, Tian W, Li Y, Tang W, Zhang C. Osteoblast-specific transcription factor Osterix (Osx) and HIF-1α cooperatively regulate gene expression of vascular endothelial growth factor (VEGF). Biochem Biophys Res Commun 2012; 424: 176–181.
2) Filipowska J, Tomaszewski KA, Niedźwiedzki Ł, Walocha JA, Niedźwiedzki T. The role of vasculature in bone development, regeneration and proper systemic functioning. Angiogenesis 2017; 20: 291–302.
3) Stegen S, Carmeliet G. The skeletal vascular system-Breathing life into bone tissue. Bone 2018; 115: 50–58.
4) Rafii S, Butler JM, Ding BS. Angiocrine functions of organ-specific endothelial cells. Nature 2016; 529: 316–325.
5) Ramasamy SK, Kusumbe AP, Adams RH. Regulation of tissue morphogenesis by endothelial cell-derived signals. Trends Cell Biol 2015; 25: 148–157.
6) Kusumbe AP, Ramasamy SK, Adams RH. Coupling of angiogenesis and osteogenesis by a specific vessel subtype in bone. Nature 2014; 507: 323–328.
7) Ramasamy SK, Kusumbe AP, Wang L, Adams RH. Endothelial Notch activity promotes angiogenesis and osteogenesis in bone. Nature 2014; 507: 376–380.
8) Xie H, Cui Z, Wang L, Xia Z, Hu Y, Xian L, Li C, Xie L, Crane J, Wan M, Zhen G, Bian Q, Yu B, Chang W, Qiu T, Pickarski M, Duong LT, Windle JJ, Luo X, Liao E, Cao X. PDGF-BB secreted by preosteoclasts induces angiogenesis during coupling with osteogenesis. Nat Med 2014; 20: 1270–1278.
9) Kusumbe AP, Ramasamy SK, Itkin T, Mäe MA, Langen UH, Betsholtz C, Lapidot T, Adams RH. Age-dependent modulation of vascular niches for haematopoietic stem cells. Nature 2016; 532: 380–384.
10) Peng Y, Wu S, Li Y, Crane JL. Type H blood vessels in bone modeling and remodeling. Theranostics 2020; 10: 426–436.
11) Sivaraj KK, Adams RH. Blood vessel formation and function in bone. Development 2016; 143: 2706–2715.
12) Xu R, Yallowitz A, Qin A, Wu Z, Shin DY, Kim JM, Debnath S, Ji G, Bostrom MP, Yang X, Zhang C, Dong H, Kermani P, Lalani S, Li N, Liu Y, Poulos MG, Wach A, Zhang Y, Inoue K, Di Lorenzo A, Zhao B, Butler JM, Shim JH, Glimcher LH, Greenblatt MB. Targeting skeletal endothelium to ameliorate bone loss. Nat Med 2018; 24: 823–833.
13) Langen UH, Pitulescu ME, Kim JM, Enriquez-Gasca R, Sivaraj KK, Kusumbe AP, Singh A, Di Russo J, Bixel MG, Zhou B, Sorokin L, Vaquerizas JM, Adams RH.

Cell-matrix signals specify bone endothelial cells during developmental osteogenesis. Nat Cell Biol 2017; 19: 189–201.
14) Hu K, Olsen BR. Osteoblast-derived VEGF regulates osteoblast differentiation and bone formation during bone repair. J Clin Invest 2016; 126: 509–526.
15) Kaaij MH, van Hamburg JP, van Rooijen CCN, Grüneboom A, Kan YY, Pots D, Schett G, van Ruijven LJ, van Duivenvoorde LM, Huitema LFA, Baeten DLP, Tas SW. Contribution of type H blood vessels to pathologic osteogenesis and inflammation in an experimental spondyloarthritis model. Arthritis Rheumatol 2023; 75: 1152–1165.
16) Ruan Z, Yin H, Wan TF, Lin ZR, Zhao SS, Long HT, Long C, Li ZH, Liu YQ, Luo H, Cheng L, Chen C, Zeng M, Lin ZY, Zhao RB, Chen CY, Wang ZX, Liu ZZ, Cao J, Wang YY, Jin L, Liu YW, Zhu GQ, Zou JT, Gong JS, Luo Y, Hu Y, Zhu Y, Xie H. Metformin accelerates bone fracture healing by promoting type H vessel formation through inhibition of YAP1/TAZ expression. Bone Res 2023; 11: 45.
17) López JM. Bone development and growth. Int J Mol Sci 2024; 25: 6767.
18) Jin SW, Sim KB, Kim SD. Development and growth of the normal cranial vault: An embryologic review. J Korean Neurosurg Soc 2016; 59: 192–196.
19) Tokavanich N, Chan B, Strauss K, Castro Andrade CD, Arai Y, Nagata M, Foretz M, Brooks DJ, Ono N, Ono W, Wein MN. Control of alveolar bone development, homeostasis, and socket healing by salt-inducible kinases. J Bone Miner Res 2025; 40: 656–670.
20) Brăescu R, Săvinescu SD, Tatarciuc MS, Zetu IN, Giuşcă SE, Căruntu ID. Pointing on the early stages of maxillary bone and tooth development—histological findings. Rom J Morphol Embryol 2020; 61: 167–174.
21) Hajishengallis G. Periodontitis: from microbial immune subversion to systemic inflammation. Nat Rev Immunol 2015; 15: 30–44.
22) Kinane DF, Stathopoulou PG, Papapanou PN. Periodontal diseases. Nat Rev Dis Primers 2017; 3: 17038.
23) Kawai T, Matsuyama T, Hosokawa Y, Makihira S, Seki M, Karimbux NY, Goncalves RB, Valverde P, Dibart S, Li YP, Miranda LA, Ernst CW, Izumi Y, Taubman MA. B and T lymphocytes are the primary sources of RANKL in the bone resorptive lesion of periodontal disease. Am J Pathol 2006; 169: 987–998.
24) Wisitrasameewong W, Kajiya M, Movila A, Rittling S, Ishii T, Suzuki M, Matsuda S, Mazda Y, Torruella MR, Azuma MM, Egashira K, Freire MO, Sasaki H, Wang CY, Han X, Taubman MA, Kawai T. DC-STAMP is an osteoclast fusogen engaged in periodontal bone resorption. J Dent Res 2017; 96: 685–693.
25) Booth V, Young S, Cruchley A, Taichman NS, Paleolog E. Vascular endothelial growth factor in human periodontal disease. J Periodontal Res 1998; 33: 491–499.
26) Yucel-Lindberg T, Båge T. Inflammatory mediators in the pathogenesis of periodontitis. Expert Rev Mol Med 2013; 15: e7.
27) Chen Y, Yin Y, Luo M, Wu J, Chen A, Deng L, Xie L, Han X. Occlusal force maintains alveolar bone homeostasis via type H angiogenesis. J Dent Res 2023; 102: 1356–1365.
28) Yan ZQ, Wang XK, Zhou Y, Wang ZG, Wang ZX, Jin L, Yin H, Xia K, Tan YJ, Feng SK, Xie PL, Tang SY, Fang CY, Cao J, Xie H. H-type blood vessels participate in alveolar bone remodeling during murine tooth extraction healing. Oral Dis 2020; 26: 998–1009.
29) Cai R, Pan C, Ghasemigharagoz A, Todorov MI, Förstera B, Zhao S, Bhatia HS, Parra-Damas A, Mrowka L, Theodorou D, Rempfler M, Xavier ALR, Kress BT, Benakis C, Steinke H, Liebscher S, Bechmann I, Liesz A, Menze B, Kerschensteiner M, Nedergaard M, Ertürk A. Panoptic imaging of transparent mice reveals whole-body neuronal projections and skull-meninges connections. Nat Neurosci 2019; 22: 317–327.
30) Susaki EA, Tainaka K, Perrin D, Kishino F, Tawara T, Watanabe TM, Yokoyama C, Onoe H, Eguchi M, Yamaguchi S, Abe T, Kiyonari H, Shimizu Y, Miyawaki A, Yokota H, Ueda HR. Whole-brain imaging with single-cell resolution using chemical cocktails and computational analysis. Cell 2014; 157: 726–739.
31) Tainaka K, Kubota SI, Suyama TQ, Susaki EA, Perrin D, Ukai-Tadenuma M, Ukai H, Ueda HR. Whole-body imaging with single-cell resolution by tissue decolorization. Cell 2014; 159: 911–924.
32) Shindo S, Pierrelus R, Ikeda A, Nakamura S, Heidari A, Pastore MR, Leon E, Ruiz S, Chheda H, Khatiwala R, Kumagai T, Tolson G, Elderbashy I, Ouhara K, Han X, Hernandez M, Vardar-Sengul S, Shiba H, Kawai T. Extracellular release of citrullinated vimentin directly acts on osteoclasts to promote bone resorption in a mouse model of periodontitis. Cells 2023: 1109; 12.
33) Ishii T, Ruiz-Torruella M, Ikeda A, Shindo S, Movila A, Mawardi H, Albassam A, Kayal RA, Al-Dharrab AA, Egashira K, Wisitrasameewong W, Yamamoto K, Mira AI, Sueishi K, Han X, Taubman MA, Miyamoto T, Kawai T. OC-STAMP promotes osteoclast fusion for pathogenic bone resorption in periodontitis via up-regulation of permissive fusogen CD9. Faseb J 2018; 32: 4016–4030.
34) Liu X, Chai Y, Liu G, Su W, Guo Q, Lv X, Gao P, Yu B, Ferbeyre G, Cao X, Wan M. Osteoclasts protect bone blood vessels against senescence through the angiogenin/plexin-B2 axis. Nat Commun 2021; 12: 1832.

35) Peng Y, Lv S, Li Y, Zhu J, Chen S, Zhen G, Cao X, Wu S, Crane JL. Glucocorticoids disrupt skeletal angiogenesis through transrepression of NF-κB-mediated preosteoclast Pdgfb Transcription in young mice. J Bone Miner Res 2020; 35: 1188–1202.
36) Zhou H, Zhang YF, Zhang QQ, Liu F, Zhang JY, Chen Y. Cathepsin K inhibition alleviates periodontal bone resorption by promoting type H vessel formation through PDGF-BB/PDGFR-β axis. Oral Dis 2024; 30: 5335–5348.
37) Wang L, Zhou F, Zhang P, Wang H, Qu Z, Jia P, Yao Z, Shen G, Li G, Zhao G, Li J, Mao Y, Xie Z, Xu W, Xu Y, Xu Y. Human type H vessels are a sensitive biomarker of bone mass. Cell Death Dis 2017; 8: e2760.
38) Madge LA, Pober JS. TNF signaling in vascular endothelial cells. Exp Mol Pathol 2001; 70: 317–325.
39) Carmeliet P, Jai RK. Principles and mechanisms of vessel normalization for cancer and other angiogenic diseases. Nat Rev Drug Discov 2011; 10: 417–427.
40) Zahr A, Alcaide P, Yang J, Jones A, Gregory M, dela Paz NG, Patel-Hett S, Nevers T, Koirala A, Luscinskas FW, Saint-Geniez M, Ksander B, D'Amore PA, Argüeso P. Endomucin prevents leukocyte-endothelial cell adhesion and has a critical role under resting and inflammatory conditions. Nat Commun 2016; 7: 10363.
41) Li J, Kou N, Shi X, Kong L, Chen W, Yang X, Zhao Y, Zhao J, Wang F. Inhibition of soluble epoxide hydrolase reverses bone loss in periodontitis by upregulating EMCN and inhibiting osteoclasts. Stem Cell Res Ther 2024; 15: 451.
42) Jing D, Yi Y, Luo W, Zhang S, Yuan Q, Wang J, Lachika E, Zhao Z, Zhao H. Tissue clearing and its application to bone and dental tissues. J Dent Res 2019; 98: 621–631.
43) Tazawa K, Sasaki H. Three-dimensional cellular visualization in mouse apical periodontitis using combined whole-mount staining and optical tissue clearing. J Oral Biosci 2023; 65, 132–135.
44) Shi R, Zhu Y, Lu W, Zhai R, Zhou M, Shi S, Chen Y. Nanomaterials: innovative approaches for addressing key objectives in periodontitis treatment. RSC Adv 2024; 14: 27904–27927.
45) Hashim NT, Babiker R, Chaitanya N, Mohammed R, Priya SP, Padmanabhan V, Ahmed A, Dasnadi SP, Islam MS, Gismalla BG, Rahman MM. New insights in natural bioactive compounds for periodontal disease: Advanced molecular mechanisms and therapeutic potential. Molecules 2025: 807; 30.
46) Zhu Y, Tao C, Goh C, Shrestha A. Innovative biomaterials for the treatment of periodontal disease. Front Dent Med 2023; 4: 1163562.
47) Liu L, Zheng CX, Zhao N, Zhu T, Hu CB, Zhang N, Chen J, Zhang KC, Zhang S, Liu JX, Zhang K, Jing H, Sui BD, Jin Y, Jin F. Mesenchymal stem cell aggregation-released extracellular vesicles induce CD31 (+) EMCN (+) vessels in skin regeneration and improve diabetic wound healing. Adv Healthc Mater 2023; 12: e2300019.
48) Bai J, Li L, Kou N, Bai Y, Zhang Y, Lu Y, Gao L, Wang F. Low level laser therapy promotes bone regeneration by coupling angiogenesis and osteogenesis. Stem Cell Res Ther 2021; 12: 432.

Original Article

ODEP 5 (1) : 32～43, 2025

Exploring the Potential of New Regenerative Endodontic Procedures for Dentin-pulp Complex Regeneration after Pulpectomy of Immature Teeth

Kayoko KITAJIMA, Hanae MINATO, Hiroko IDA-YONEMOCHI[1],
Masafumi YARITA, Rie YAMADA, Kyoko ARAI, Kota SHIMIZU[2],
Tomonori SATOH[3] and Masaru IGARASHI[4]

Department of Endodontics, The Nippon Dental University School of Life Dentistry at Niigata
[1]Division of Anatomy and Cell Biology of the Hard Tissue, Department of Tissue Regeneration and Reconstruction, Niigata University Graduate School of Medical and Dental Sciences
[2]Comprehensive Dental Care, Niigata Hospital, The Nippon Dental University
[3]Division of General Dentistry 1 (Endodontics), The Nippon Dental University Hospital
[4]The Nippon Dental University School of Life Dentistry

Abstract

Purpose: This study aimed to investigate a new regenerative endodontic procedure (REP) that uses platelet-rich plasma (PRP) as a scaffold for the regeneration of the dentin-pulp complex following pulpectomy of immature teeth.

Methods: Molars of 6-week-old male Wistar rats were subjected to pulpectomy. After root canal shaping, the canals were treated with ethylenediaminetetraacetic acid (EDTA) for one minute, then rinsed with sodium hypochlorite (NaOCl), and under microscopic examination, removal of canal contents and hemostasis were confirmed. PRP was prepared by centrifuging whole blood collected from the rats twice and injecting it into the root canal up to the cervical area. Mineral trioxide aggregate (MTA) was packed on the PRP, and the top of the MTA was filled with a resin-based backfilling material and composite resin. After 4 and 8 weeks of treatment, the specimens were fixed in 4% paraformaldehyde solution, demineralized with EDTA, and embedded in paraffin to obtain 5-μm serial sections. The specimens were chemically and immunologically stained and observed under an optical microscope.

Results: An increase in the root length was observed in all rats. Most of the root canals were periodontal ligament-like tissues, but regeneration of the dentin-pulp complex was confirmed in one of six cases. Pulps containing odontoblasts, pulp cells, blood vessels, nerves, and dentin-containing odontoblast-like protrusions were also observed. This hard tissue was formed with uniform thickness throughout the entire root canal wall, from just below the cervical MTA to the apex, and the root length and thickness increased.

Conclusions: This method of applying PRP for pulpectomy in immature teeth suggests the possibility of a new endodontic therapy that regenerates the dentin-pulp complex.

Key words: regenerative endodontic procedure, dentin-pulp complex, platelet-rich plasma, non-vital teeth, immature teeth

Corresponding author: Kayoko KITAJIMA, Department of Endodontics, The Nippon Dental, University School of Life Dentistry at Niigata, 1-8, Hamaura-cho, Niigata 951-8580, Japan
TEL: +81-25-211-8171, E-mail: kitajima@ngt.ndu.ac.jp
Received for Publication: August 14, 2025/Accepted for Publication: October 15, 2025
DOI: 10.11471/odep.2025-004

Introduction

Root development is maintained through apexogenesis in vital immature teeth. In contrast, non-vital teeth undergo apexification; however, there is no evidence of continuous root formation or the addition of dentin to the root canal wall, and the remaining root remains thin, increasing the risk of root fracture. A new method known as pulp revascularization has been developed[1,2]. After disinfecting root canal, Banchs et al.[2] stimulated apical periodontal tissues to induce bleeding, and then filled mineral trioxide aggregate (MTA) cement on top of the formed blood clot, resulting in root growth and narrowing of the root canal. However, experimental studies on pulp revascularization have shown the formation of irregular cementum- and bone-like hard tissues without sufficient dentin regeneration by odontoblasts[3]. These findings are consistent with those of previous animal experiments[4–8] and case reports[9–12].

Numerous studies have explored regenerative endodontic procedures (REPs)[13]. Although immunohistological studies have been conducted[14–17], high-quality histological evidence following REPs in non-vital teeth remains limited. Austah et al.[15] suggested the presence of nerves, blood vessels, lymph vessels, and antigen-presenting cells within dental pulp tissue, as well as regeneration of the dentin-pulp complex. However, full dentin-pulp complex regeneration throughout the root canal has not yet been achieved. Attempts have been made to regenerate the pulp of immature teeth with necrotic pulp using platelet-rich plasma (PRP)[18]. This study aimed to investigate the potential of PRP as a scaffold for pulp regeneration therapy after pulpectomy in immature teeth.

Materials and Methods

This study was approved by the Ethics Committee for Animal Experiments of Nippon Dental University School of Life Dentistry at Niigata (approval number: 194).

1. Animal experiments

Six-week-old male Wistar rats (n=12) were used as experimental animals. The study included six cases at 4 weeks and six cases at 8 weeks, with six experimental cases each using PRP and six control cases on the contralateral jaw for revascularization. Of the five root canals in the maxillary M1, the mesial root canal was used for both the experimental and control groups. The remaining four root canals of the M1 tooth not used in the experiment underwent pulpotomy.

Under rubber dam isolation, the working length of each mesial root canal was determined by referring to the apical indication value on the electrical root canal length measurement device (Root ZX mini, Morita, Japan). The pulp was removed using a pulling needle #00 (MANI, Japan). To eliminate odontoblast cells, enlargement of the root canal walls was performed using H-files #10, #15, and #20 (MANI) and a NiTi rotary file (PROTAPER F1: DENTSPLY Maillefer, Ballaigues, Switzerland) connected to an endo motor (X-SMART: DENTSPLY Maillefer). 17% ethylenediaminetetraacetic acid (EDTA) was applied to the root canal for 1 min. Next, 20 mL 6% sodium hypochlorite (NaOCl) was used to flush the root canal for 5 min, and the canal was dried using a paper point. PRP was prepared from whole blood collected from the rats using a two-step centrifugation method[19]. The entire blood sample was collected in a sterile glass tube containing citrate solution as an anticoagulant. The sample was then centrifuged at 600 ×*g* for 7 min and the precipitated blood cells were removed. Then, a second centrifugation was performed at 2,000 ×*g* for 5 min. PRP was then added to the cervical region of the tooth.

MTA (PROROOT MTA, DENTSPLY Maillefer) was applied to all treated surfaces, and composite resin filling was performed after covering the upper part with a resin-based backfilling material. The control group underwent revascularization by removing the pulp from the root canal, inserting an H-file approximately 1 mm beyond the working length to induce bleeding and form a blood clot, and applying MTA to the root canal opening.

2. Preparation of tissue sections

After perfusion fixation in 4% paraformaldehyde solution, decalcification with EDTA-2N solution, and paraffin embedding, 5-μm serial thin-sectioned slices were prepared. Hematoxylin and eosin staining (HE), Schmorl staining (SH)[20,21], and immunostaining for osteopontin (OPN), dentin matrix protein 1 (DMP1), nestin (NES), and neuron cytoplasmic protein 9.5 (PGP 9.5) were performed. The sections were observed under an optical microscope.

3. Immunostaining method

OPN was detected using rabbit anti-OPN polyclonal antibody (1 : 5,000; LSL-LB-4225, Cosmo Bio, Japan), DMP1 was detected using rabbit anti-DMP1N polyclonal antibody (1 : 100; ab8235, Abcam, Cambridge, UK), NES was detected using mouse anti-nestin monoclonal antibody (1 : 500; MAB353, Millipore Temecula, CA, USA), and PGP 9.5 was detected using rabbit anti-PGP 9.5 polyclonal antibody (14730-1-AP, Proteintech Japan, Japan). For OPN, DMP1 and PGP 9.5, biotinylated anti-rabbit IgG (BA-1000, Vector Laboratories, Burlingame, CA, USA) and an Avidin-Biotin Peroxidase Complex (Vectastain ABC Kit, Vector Laboratories) was applied. For NES, an Envision+/Horseradish Peroxidase System (K5027, Dako, Japan) was used. For final visualization, the sections were treated with 0.05 M Tris-HCl buffer (pH 7.6) containing 0.04% 3-3'-diaminobenzidine tetrahydrochloride and 0.0002% H_2O_2. The immunostained sections were counterstained with hematoxylin. The primary antibody was replaced with phosphate-buffered saline to serve as an immunohistochemical negative control.

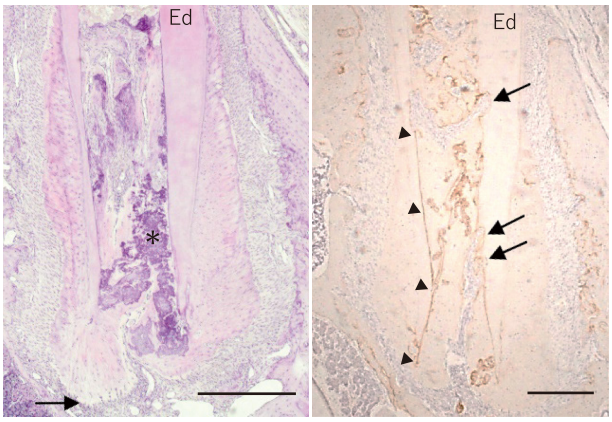

Fig. 1 Histological findings at 4 weeks and 8 weeks in the revascularization (control) group

A : Revascularization (Cont.), 4 weeks (HE), bar : 500 μm. Arrow : Formed cement-like hard tissue, * : Bone-like hard tissue.

B : Revascularization (Cont.), 8 weeks (OPN), bar : 500 μm. OPN-positive reaction observed between the root canal wall after root canal preparation and the formed hard tissue (arrowheads). Absorption cavity and multinucleated giant cells confirmed on the root canal wall with weak OPN-positive reaction (arrows).

Results

In the control group at 4 weeks, hard tissue was formed within the root canal, and bone-like hard tissue was observed in all cases (Fig. 1A). At 8 weeks, internal resorption was observed in part of the root canal wall (Fig. 1B).

In the 4-week group (Fig. 2), in which PRP was applied to the root canal, immature pulp-like tissue was observed within the root canal, with hard tissue forming during the process (Fig. 2A, yellow arrow). These tissues tested positive for NES, OPN, and DMP1 (Fig. 2C-F). At the time of the procedure, growth lines (Fig. 2A, yellow arrowhead) indicating root growth were observed along the thin root canal wall at the apical end, which was immature and exhibited a blunderbuss-like shape (Fig. 2A, white arrow; Fig. 2B, red arrow) at the time of the procedure. Hard tissue formed on the canal side, resulting in nearly parallel root canal walls at the apical region and confirming root elongation and increased root diameter (Fig. 2A, B, black arrow). Within the root canal, the formation of tissue containing vascular structures and stellate-shaped cells was observed. NES-positive reactions were confirmed around the newly formed cells within the root canal (Fig. 2C, arrow). Although the odontoblasts in the root canal wall had disappeared due to the root canal enlargement and formation, NES-positive, projection-like structures extending from the root canal wall into the deep dentin were observed (Fig. 2C, arrowhead). Newly formed hard tissue on the root canal wall (Fig. 2D, black arrowhead) showed OPN-positive staining. Along the root canal wall, near the boundary between areas with and without hard tissue formation, OPN-positive, roughly circular structures were observed (Fig. 2D, arrow). Slight OPN-positive staining was detected within the coronal dentin where hard tissue had not formed (Fig. 2D, red arrowhead). Tissue extending from the root canal tissue surrounded by the newly formed hard tissue showed NES-positive staining (Fig. 2E, arrow), and DMP1-positive staining was observed around the apex (Fig. 2F, arrow).

A particularly interesting finding was observed in one case at 8 weeks (Fig. 3, 4). Following root canal enlargement, shaping, and irrigation, new hard tissue of consistent thickness was confirmed to have formed throughout the entire root canal wall, from the apex to

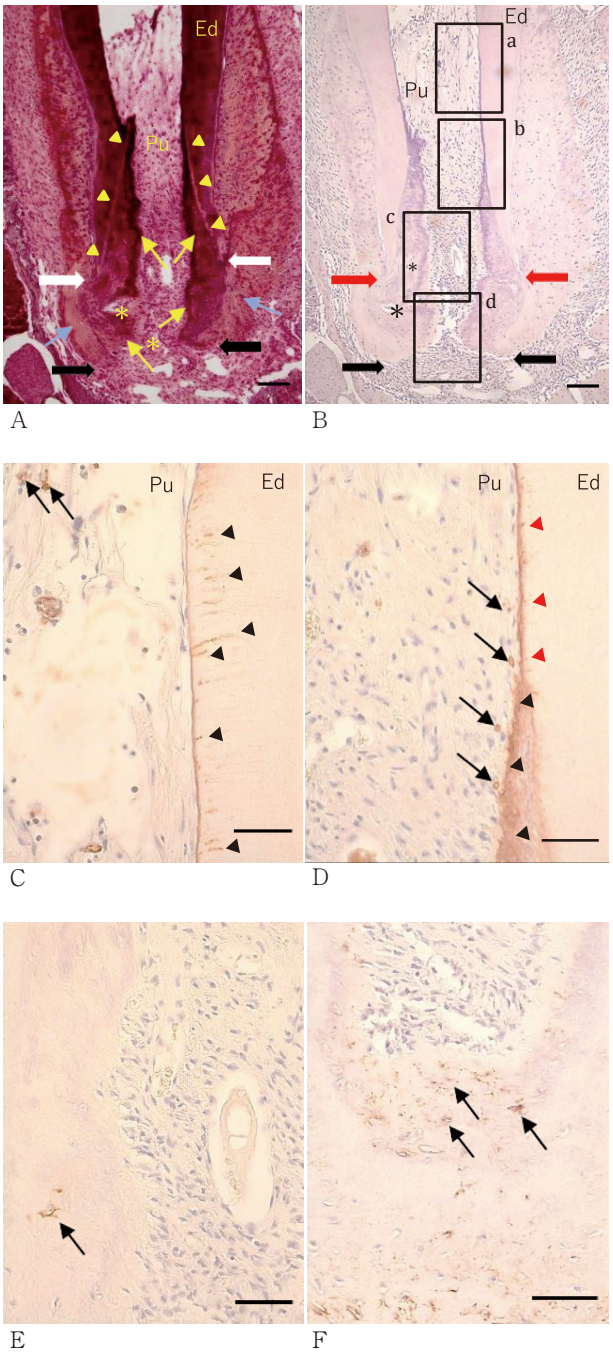

A : SH (bar ; 100 μm). White arrows : The apical portion of the tooth root exhibited a blunderbuss-shaped canal due to incomplete root development at the time of procedure. Black arrows : Root apex 4 weeks after the procedure. Blue arrows : Periodontal tissue around the root apex 4 weeks after the procedure. Yellow arrows : Hard tissue formed in the direction of the newly formed pulp-like tissue from the blunderbuss-shaped opening. Yellow arrowheads : Growth line. In the periapical region of the root canal, which remained open in a blunderbuss-like shape, complex tissue formation was observed in the interior of the root canal along the growth line. The root canal walls, which had been dilated like a blunderbuss, became almost parallel, confirming root elongation and increased root diameter. ＊ : Newly formed pulp-like tissue embedded within the newly formed hard tissue.

B : Another serial section of Fig. 2A (HE×100, bar ; 100 μm) Red arrows : The blunderbuss-shaped opening of the root canal at the time of the procedure. Black arrows : Root apex 4 weeks after the procedure. ＊ : Newly formed pulp-like tissue embedded within the newly formed hard tissue.

C : Enlarged image of part (a) in Fig. 2B (NES, bar : 50 μm) Arrowheads : Protrusion-like structure of odontoblast showing NES positivity. Arrows : NES positive reaction around cells in newly formed pulp-like tissue. Odontoblast cell bodies on the surface of the root canal wall disappeared because of pulpectomy, root canal enlargement, and root canal cleaning.

D : Enlarged image of part (b) in Fig. 2B (OPN, bar : 50 μm) Black arrowheads : OPN-positive reaction in the newly formed hard tissue. Red arrowheads : OPN-positive reaction on the crown side of the newly formed tissue. Black arrows : OPN-positive reaction in newly formed pulp-like tissue adjacent to the hard tissue.

E : Enlarged image of part (c) in Fig. 2B (NES, bar : 50 μm) Arrow : NES-positive tissue within the newly formed hard tissue (corresponding to ＊in Fig. A and B).

F : Enlarged image of part (d) in Fig. 2B (DMP1, bar : 50 μm) Arrows : DMP1-positive reaction within the newly formed hard tissue.

Ed, existing dentin ; Pu, newly formed pulp-like tissue ; SH, Schmorl ; HE, hematoxylin and eosin ; NES, nestin ; OPN, osteopontin ; DMP1, dentin matrix protein

Fig. 2 Histological findings at 4 weeks in the PRP application group

the neck, where odontoblasts had been removed (Fig. 3A, E). This resulted in increased root canal wall thickness and root length. Odontoblast-like cells were observed in a regular arrangement adjacent to the newly formed hard tissue surface (Fig. 3A–D, J, K; 4A–L). Lumen-like vascular structures (Fig. 3B) and PGP 9.5-positive nerve-like tissue (Fig. 3J, K) were identified within this newly formed tissue in the root canal. Within the newly formed hard tissue directly beneath the MTA applied to the cervical region, a radial structure resembling pulp horns was observed (Fig. 3B, F, I). A band-like OPN-positive reaction was confirmed at the border between the existing dentin and the newly formed hard tissue (Fig. 4A–D). DMP1-positive reactions were observed in the newly formed hard tissue, showing a strong reaction on the root canal side (Fig.

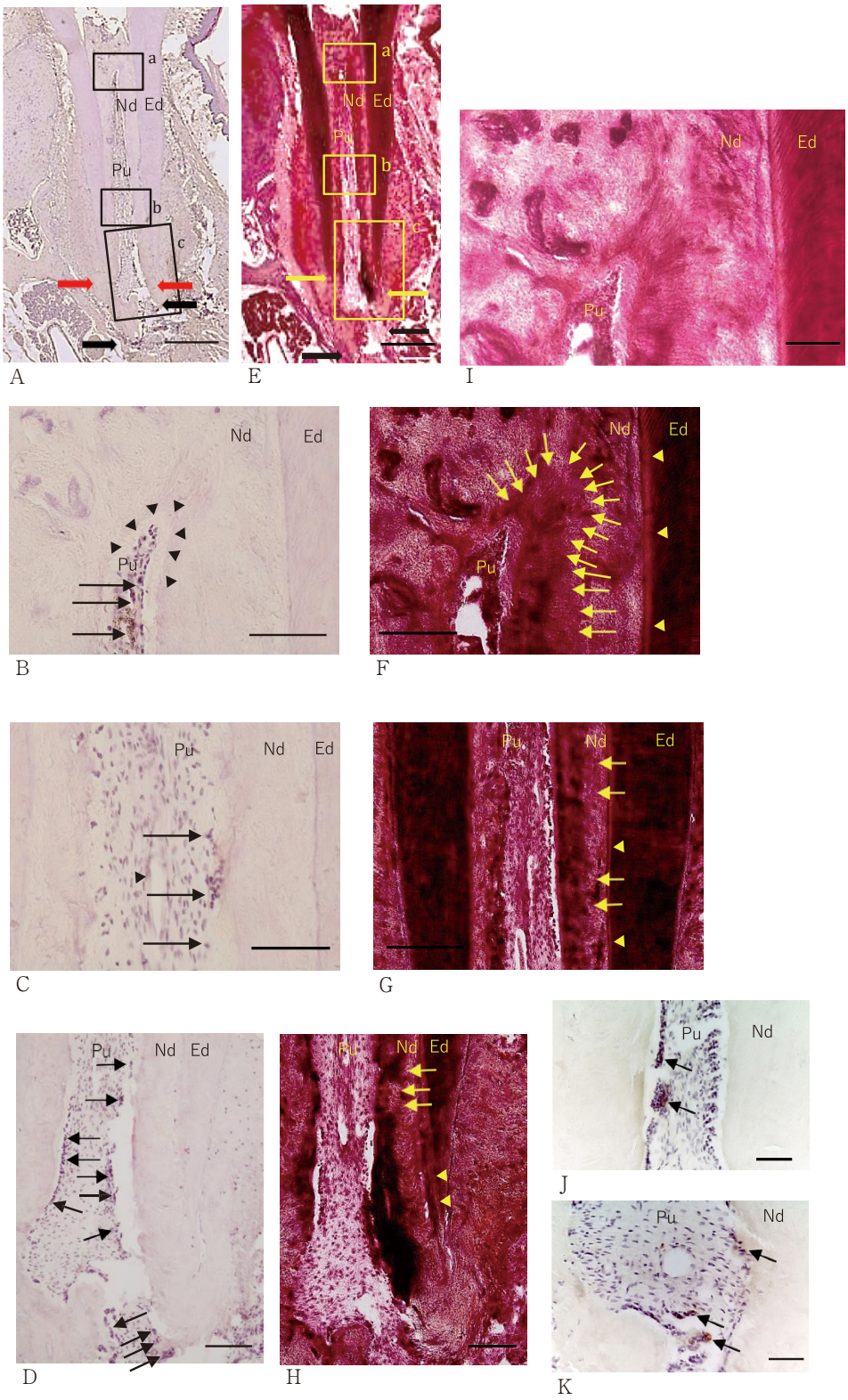

Fig. 3 Histological findings at 8 weeks in the PRP-applied group : HE, SH, and PGP 9.5 staining

Fig. 3 Figure legend

A : HE (bar ; 500 μm)

Red arrows : The blunderbuss-shaped opening at the time of the procedure. Black arrows : Root apex 8 weeks after the procedure.

B : Enlarged image of part (a) in Fig. 3A (HE, bar : 100 μm)

Arrows : Odontoblast-like cells seen in the newly formed pulp-like tissue. Arrowheads : Pulp horn-like structure directly below the MTA.

C : Enlarged image of part (b) in Fig. 3A (HE, bar : 100 μm)

Arrows : Odontoblast-like cells seen in the newly formed pulp-like tissue. Arrowhead : Blood vessels in the newly formed pulp-like tissue.

D : Enlarged image of part (c) in Fig. 3A (HE, bar : 100 μm)

Arrows : Odontoblast-like cells seen in the newly formed pulp-like tissue.

E : SH (bar ; 500 μm)

Yellow arrows : The blunderbuss-shaped opening at the time of the procedure. Black arrows : Root apex 8 weeks after the procedure.

F : Enlarged image of part (a) in Fig. 3E (SH, bar : 500 μm)

Arrows : Radial odontoblast protrusions forming a pulp horn-like structure. Arrowheads : Growth line.

G : Enlarged image of part (b) in Fig. 3E (SH, bar : 500 μm)

Arrows : Radial odontoblast protrusions running perpendicular to the existing dentin wall. Arrowheads : Growth line.

H : Enlarged image of part (c) in Fig. 3E (SH, bar : 500 μm)

Arrows : Odontoblast protrusions running perpendicular to the existing dentin wall. Arrowheads : Growth line.

I : Magnified image of the pulp horn-like structure in Fig. 3F (SH, bar : 50 μm)

J : PGP 9.5 (bar ; 50 μm)

Arrows : PGP 9.5-positive cells in the newly formed pulp-like tissue.

K : PGP 9.5 (bar ; 50 μm)

Arrows : PGP 9.5-positive cells in the root apex.

Ed, existing dentin ; Nd, newly formed dentin ; Pu, newly formed pulp-like tissue ; HE, hematoxylin and eosin ; SH, Schmorl ; PGP 9.5, neuron cytoplasmic protein 9.5

4E–H). NES-positive reactions were confirmed both in odontoblast-like cells arranged regularly along the root canal wall and in protrusions extending into the newly formed hard tissue (Fig. 4I–L).

Taken together, these results showed that in the control revascularization group, the soft tissue within the root canal resembled the periodontal ligament tissue. In both the 4- and 8-week groups, the newly formed calcified tissue consisted of cementum-like hard tissue with a laminar structure or irregularly shaped bone-like hard tissue. In the experimental group treated with PRP, pulp-like findings were observed in the 4-week group, whereas clear pulp tissue regeneration was confirmed in the 8-week group. Although the newly formed tissue was primarily cementum-like dentin, distinct dentin regeneration was observed around the entire circumference of the cervical region to the root apex at 8 weeks in one case (Table 1).

Discussion

OPN is an extracellular matrix protein used to identify odontoblasts, and it is also expressed by immune cells such as macrophages, neutrophils, and dendritic cells. It functions as a cell adhesion protein and is involved in cell adhesion and wound healing. Furthermore, it initiates the process of forming the undulating margin when osteoclasts begin bone resorption, and it also promotes cell survival by regulating apoptosis. DMP1 regulates the formation of the calcified matrix. It is an extracellular matrix protein and is essential for proper calcification of bone and dentin. NES is a neural stem cell-specific molecule also gaining attention in nerve regeneration medicine.

In the 4-week example shown in Fig. 2D, OPN-positive, roughly circular structures are observed along the surface of the newly formed hard tissue wall, and the formation of OPN-positive tissue is also confirmed

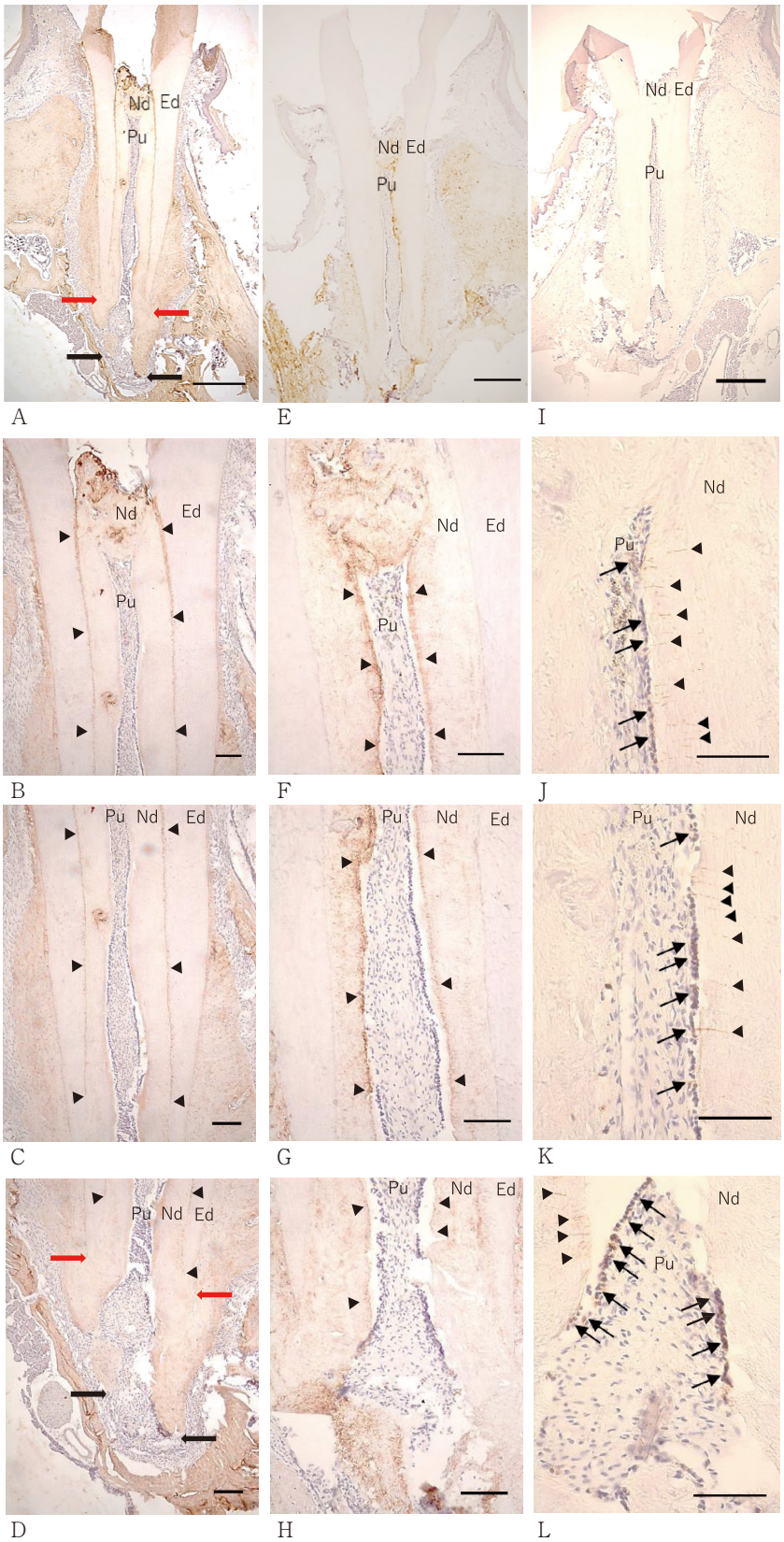

A : OPN (bar ; 500 μm), B : OPN (bar ; 100 μm, crown side), C : OPN (bar ; 100 μm, central root), D : OPN (bar ; 100 μm, apical root)

Red arrows : The blunderbuss-shaped opening at the time of the procedure. Black arrows : Root apex 8 weeks after the procedure. A clear OPN-positive reaction (arrowheads) is observed forming a continuous band from the root tip to the cervical area of the tooth, located between the existing dentin wall (Ed) and the regenerated dentin (Nd) after the root canal enlargement.

E : DMP1 (bar ; 500 μm), F : DMP1 (bar ; 100 μm, crown side), G : DMP1 (bar ; 100 μm, central root), H : DMP1 (bar ; 100 μm, apical root)

Arrowheads : DMP1-positive reaction observed in the newly formed dentin-like hard tissue.

I : NES (bar ; 500 μm), J : NES (bar ; 100 μm, crown side), K : NES (bar ; 100 μm, central root), L : NES (bar ; 100 μm, apical root)

Arrows : NES-positive reaction is observed around the odontoblasts-like cells along the canal wall in the newly formed pulp-like tissue. Arrowheads : NES-positive odontoblasts are observed along the dentin tubule-like structures in the newly formed dentin-like tissue.

Ed, existing dentin ; Nd, newly formed dentin-like tissue ; Pu, newly formed pulp tissue ; OPN, osteopontin ; DMP1, dentin matrix protein 1 ; NES, nestin

Fig. 4 Histological findings at week 8 in the PRP-applied group : OPN, DMP1, and NES staining

Table 1 Regenerative tissue findings observed at 4 and 8 weeks

		Revascularization (Cont.) Healing pattern		PRP Healing pattern	
age	Sample No.	Newly formed mineralized tissue	Intracanal tissue	Newly formed mineralized tissue	Intracanal tissue
4W	1	CEM-DAMT and OSD-DAMT	PDL-like	CEM-DAMT	PDL-like
	2	CEM-DAMT and OSD-DAMT	PDL-like	CEM-DAMT	PDL-like
	3	CEM-DAMT and OSD-DAMT	PDL-like	CEM-DAMT, ID	IP-like
	4	CEM-DAMT and OSD-DAMT	PDL-like	CEM-DAMT	PDL-like
	5	CEM-DAMT and OSD-DAMT	PDL-like	CEM-DAMT	PDL-like
	6	CEM-DAMT and OSD-DAMT	PDL-like	CEM-DAMT	PDL-like
8W	1	CEM-DAMT and OSD-DAMT	PDL-like	CEM-DAMT	PDL-like
	2	CEM-DAMT and OSD-DAMT	PDL-like	CEM-DAMT and OSD-DAMT	PDL-like
	3	CEM-DAMT and OSD-DAMT	PDL-like	Dentin	Pulp
	4	CEM-DAMT and OSD-DAMT	PDL-like	CEM-DAMT	PDL-like
	5	CEM-DAMT and OSD-DAMT	PDL-like	CEM-DAMT	PDL-like
	6	CEM-DAMT and OSD-DAMT	PDL-like	CEM-DAMT and OSD-DAMT	PDL-like

CEM-DAMT：cementum-like dentin-associated mineralized tissue
OSD-DAMT：osteodentin-like dentin-associated mineralized tissue
PDL：periodontal ligament. ID：immature dentin. IP：immature pulp

within the newly formed hard tissue itself. This likely results from the secretion of acid phosphoproteins of the dentin matrix. Odontoblast differentiation is expected to occur, leading to dentin formation. In the tooth at 4 weeks, no clearly morphologically defined odontoblasts were identified within the tissue formed in the root canal. However, it is conceivable that odontoblast differentiation will occur in the future, promoting dentin formation. This may represent an immature pulp stage preceding the formation of a complete pulp. DMP1 is dentin matrix acidic phosphoprotein 1, which is thought to be involved in proper dentin mineralization. DMP1-positive reactions have been confirmed in newly formed hard tissue, suggesting the potential for increased calcification in the future.

In the tooth at 8 weeks, DMP1-positive reactions were continuously observed from the apical region to the cervical region. Meanwhile, NES-positive reactions, a marker for neural stem cells, were observed in pulp-like tissue embedded within the newly formed hard tissue. Furthermore, PGP 9.5, a neuronal cell marker, showed positive reaction in the newly formed tissue apical region and newly formed tissue, supporting the regeneration of the dentin-pulp complex alongside nerve and blood vessel regeneration.

MTA is a hydraulic cement primarily composed of calcium silicate, exhibiting excellent sealing properties, antibacterial activity, and high biocompatibility. It promotes proliferation of surrounding cells by releasing calcium ions. Specifically, calcium hydroxide generated by MTA through its hydration reaction is known to promote cell proliferation, contributing to cell survival and growth, and to induce hard tissue formation. Hard tissue newly formed immediately beneath the applied MTA at the 8-week mark exhibited radially oriented dentin tubule-like structures, accompanied by odontoblast-like processes observed along their course. Although the mechanism underlying the formation of these pulp horn-like structures remains unclear, the abundant hard tissue formation likely resulted from MTA's effect of promoting hard tissue formation. Fibroblast growth factor (FGF) contained in PRP is thought to play a crucial role in the proliferation and differentiation processes of a wide range of cells and tissues, and is believed to have effectively promoted angiogenesis and wound healing. Transforming growth factor beta (TGF-β) is a type of cytokine that regulates cell proliferation, differentiation, and apoptosis. It acts on normal fibroblasts to induce transformation and is a cell proliferation inhibitory factor. These factors are aggregated within PRP, and their combined action is thought to have led to the regeneration of the den-

tin-pulp complex in the 8-week group.

Hargreaves et al.[22] suggested that the periapical tissues of immature roots contain more stem cells than the systemic circulating blood. In immature roots, even if the pulp in the root canal is removed or necrotic, a small amount of pulp tissue may remain in the root canal wall in a blunderbuss-like shape, or the dental papilla cells may contain stem cells.

Edanami et al.[23] performed REP after sectioning the living pulp at four different heights and found that when a larger amount of pulp remained, dentin and osteoid-like dentin were formed. Conversely, when the pulp remnants were minimal, cementum- and osteoid-like hard tissues were formed. Beyond the root apex, cementum-like hard tissue and endosteal bone were formed. During pulp revascularization, which induces bleeding at the root tip, a cementum or bone-like hard tissue is formed.

This study explored the use of regenerative medicine after pulpectomy and found that cementum- and bone-like hard tissues were formed in some areas; however, regeneration of the dentin-pulp complex throughout the root canal wall was also confirmed. In immature teeth, it is hypothesized that cell differentiation, proliferation, vascularization, and matrix formation may be stimulated by the action of growth factors and other substances present at high concentrations in PRP. Moreover, dentin formation may have been promoted by the stem cells remaining in the root tip, which remained open in a blunderbuss-like shape.

In this study, the root canal wall was enlarged and odontoblast cells were removed. OPN staining was performed to confirm that the regeneration of the dentin-pulp complex was not due to residual odontoblasts in the upper part of the root canal wall. Saito et al.[24] reported that when dentin was cut, odontoblasts became inactive, new odontoblasts appeared, a new matrix formed on the dentin surface, and OPN was deposited at the interface. OPN plays a role in both cell adhesion and bone calcium adhesion; without it, dentin is not formed, even if odontoblasts are formed[24]. In this study, a continuous band of OPN-positive reactions was observed between existing dentin and regenerated tissue formed from the apical to cervical regions (Fig. 4 A–D). This finding suggests that odontoblasts from the dilated root tip to the cervical region of the tooth were deactivated because of root canal shaping, and that new odontoblasts migrated to the area to form dentin. Thus, regenerated dentin is formed by newly migrated cells rather than existing odontoblasts. Odontoblasts are thought to originate from preodontoblasts derived from the root apex papilla tissue. DMP1 is dentin matrix acidic phosphoprotein 1, which is thought to be involved in proper dentin mineralization. In this study, DMP1-positive reactions were continuously observed from the apical region to the cervical region. Meanwhile, NES-positive reactions, a marker for neural stem cells, were observed in the pulp tissue embedded within the regenerated dentin. Furthermore, PGP 9.5, a neuronal cell marker, showed positive staining in the apical region and regenerated pulp. Additionally, stellate-shaped cells, were observed in the tissue formed within the root canal, suggesting they are derived from mesenchymal stem cells. These findings strongly indicate that regeneration of the dentin-pulp complex occurred in this study. Notably, dentin, which contains projections of odontoblasts and has a pulp horn-like structure, was regenerated under MTA filled in the cervical surface of the PRP. Torabinejad et al.[18] reported that PRP contains three to five times the number of platelets in circulating blood, along with various growth factors that are beneficial for the regeneration of the dentin-pulp complex. Furthermore, Sonoyama et al.[25] showed that the dental papilla contains many undifferentiated mesenchymal cells that have the potential to differentiate into odontoblasts, and reported similarities between dental papilla cells and odontoblasts.

In this study, bleeding was not induced from outside the root apex. After pulpectomy and root canal shaping to remove odontoblastic bodies, the teeth were treated with NaOCl and EDTA, which is believed to be a significant methodological aspect. Martin et al.[26] investigated the effect of NaOCl concentration on the survival of stem cells of the apical papilla (SCAPs) and the expression of dentin sialo phosphoprotein (DSPP), and found that 1.5% NaOCl increased DSPP expression. Trevino et al.[27] reported that SCAP survival was highest when 1.5% NaOCl was used, followed by 17% EDTA. Growth factors near the dentin root canal wall are released, facilitating the differentiation of stem cells into the dental papilla or residual pulp tissue at the root tip, which remains open in a blunderbuss-like shape. Under the influence of PRP, these cells may be induced

to differentiate into odontoblasts and arranged on the surface of the root canal wall. Regenerated dentin exhibited a regular tubular structure running vertically along the surface of the root canal wall.

Recent findings indicated that dentin is a reservoir of growth factors and cytokines[28]. These factors become soluble when the hard tissue is demineralized using EDTA, NaOCl, and other substances[29–33]. Smith et al.[29] demonstrated that when dentin is treated with EDTA, the calcified portion is dissolved, and growth factors are released, promoting the differentiation of precursor or stem cells. In this study, growth factor release was promoted by treating dentin with 20 mL 17% EDTA for 1 min and NaOCl for 5 min, which likely enhanced the effect of PRP.

In the initial pulp revascularization procedure reported by Iwaya et al.[1], intentional bleeding was not induced. Radiographic images showed root elongation and increased root canal wall thickness, likely due to the proliferation of granulation tissue in the root canal. Although the structure of the formed hard tissue was unknown, the smooth root canal walls in the X-ray images suggested dentin-pulp complex regeneration, as seen in this study. In regenerating the dentin-pulp complex during the pulpectomy of an immature tooth, critical factors include the pulp cutting position, the presence of a scaffold such as a blood clot or PRP, and adherence to the root canal wall surface. It is difficult to accurately assess the condition of periapical tissues using clinical radiographs alone. Therefore, in future regenerative therapies, it is important to utilize stem cells present in the apical region and use PRP or other scaffolds that can consistently provide sufficient quantities to the cervical region without damaging the apical region, thereby reliably inducing physiological tooth growth and apical closure.

In this study, root canal preparation and root canal irrigation with EDTA and NaOCl were performed on immature teeth, followed by REP using PRP. This approach resulted in confirmed root lengthening and root diameter enlargement, along with the formation of hard tissue consisting of tubules containing odontoblasts and their filament-like structures, regularly arranged along the root canal walls. Furthermore, dentin formation was observed beneath MTA, which has a structure similar to pulp horns, and the formation of nerves, blood vessels, and immune system cells within the newly formed tissue in the root canal was noted. Therefore, it is considered that the dentin-pulp complex was regenerated.

However, the readings of the electric root canal length-measuring device tend to be unstable in immature teeth. Furthermore, even slight differences in the cutting position can easily affect the results for the small teeth of small animals.

Besides PRP as a scaffold, there are many other issues to be examined, such as the use of platelet-rich fibrin (PRF) and methods for adjusting it, as well as the appropriate concentration and action time of EDTA and NaOCl.

This was a pilot study, and further research is warranted to obtain stable results. However, it was confirmed that the dentin-pulp complex was regenerated. In immature teeth, even in cases where the pulp has been removed, it is worth trying this procedure before apexification, bearing in mind that the apical region, which is open in a blunderbuss-like shape, may contain many stem cells.

Future advancements in surgical techniques may further enhance the feasibility of regenerating the dentin-pulp complex after pulpectomy of immature teeth.

Conclusion

In immature teeth, after pulpectomy, root canal preparation, and cleaning with EDTA and NaOCl, the application of PRP suggested the possibility of regeneration of the dentin-pulp complex. Further detailed studies are necessary to establish a stable surgical procedure.

Conflict of Interest

The authors declare no conflict of interest related to this paper.

Acknowledgments

The authors thank Dr. Hayato Oshima from the Division of Anatomy and Cell Biology of Hard Tissue, Department of Tissue Regeneration and Reconstruction, Niigata University Graduate School of Medical and Dental Sciences, Japan.

Funding Sources

This study was partially funded by a Grant-in-Aid for Scientific Research (C) (grant number 17K11720). The funding

body played no role in the design of the study, collection, analysis, and interpretation of data, or in writing of the manuscript.

References

1) Iwaya S, Ikawa M, Kubota M. Revascularization of an immature permanent tooth with apical periodontitis and sinus tract. Dent Traumatol 2001; 17: 185–187.
2) Banchs F, Trope M. Revascularization of immature permanent teeth with apical periodontitis: new treatment protocol? J Endod 2004; 30: 196–200.
3) Minato H, Kitajima K, Arai K, Igarashi M. Revascularization after pulpectomy of immature molars in rats. Jpn J Conserv Dent 2019; 62: 27–38.
4) Thibodeau B, Teixeira F, Yamauchi M, Caplan DJ, Trope M. Pulp revascularization of immature dog teeth with apical periodontitis. J Endod 2007; 33: 680–689.
5) Wang X, Thibodeau B, Trope M, Lin LM, Huang GT-J. Histologic characterization of regenerated tissues in canal space after the revitalization/revascularization procedure of immature dog teeth with apical periodontitis. J Endod 2010; 36: 56–63.
6) Torabinejad M, Milan M, Shabahang S, Wright KR, Faras H. Histologic examination of teeth with necrotic pulps and periapical lesions treated with 2 scaffolds: an animal investigation. J Endod 2015; 41: 846–852.
7) Londero CLD, Pagliarin CML, Felippe MCS, Felippe WT, Danesi CC, Barletta FB. Histologic analysis of the influence of a gelatin-based scaffold in the repair of immature dog teeth subjected to regenerative endodontic treatment. J Endod 2015; 41: 1619–1625.
8) Saoud TMA, Zaazou A, Nabil A, Moussa S, Aly HM, Okazaki K, Rosenberg PA, Lin LM. Histological observations of pulpal replacement tissue in immature dog teeth after revascularization of infected pulps. Dent Traumatol 2015; 31: 243–249.
9) Shimizu E, Jong G, Partridge N, Rosenberg PA, Lin LM. Histologic observation of a human immature permanent tooth with irreversible pulpitis after revascularization/regeneration procedure. J Endod 2012; 38: 1293–1297.
10) Martin G, Ricucci D, Gibbs JL, Lin LM. Histological findings of revascularized/revitalized immature permanent molar with apical periodontitis using platelet-rich plasma. J Endod 2013; 39: 138–144.
11) Nosrat A, Kolahdouzan A, Hosseini F, Mehrizi EA, Verma P, Torabinejad M. Histologic outcomes of uninfected human immature teeth treated with regenerative endodontics: 2 case reports. J Endod 2015; 41: 1725–1729.
12) Lei L, Chen Y, Zhou R, Huang X, Cai Z. Histologic and immunohistochemical findings of a human immature permanent tooth with apical periodontitis after regenerative endodontic treatment. J Endod 2015; 41: 1172–1179.
13) Torabinejad M, Nosrat A, Verma P, Udochukwu O. Regenerative endodontic treatment or mineral trioxide aggregate apical plug in teeth with necrotic pulps and open apices: a systematic review and meta-analysis. J Endod 2017; 43: 1806–1820.
14) Meschi N, Hilkens P, Lambrichts I, Van den Eynde K, Mavridou A, Strijbos O, Ketelaere MD, Gorp GV, Lambrechts P. Regenerative endodontic procedure of an infected immature permanent human tooth: an immunohistological study. Clin Oral Investig 2016; 20: 807–814.
15) Austah O, Joon R, Fath WM, Chrepa V, Diogenes A, Ezeldeen M, Couve E, Ruparel NB. Comprehensive characterization of 2 immature teeth treated with regenerative endodontic procedures. J Endod 2018; 44: 1802–1811.
16) Meschi N, Hilkens P, Van Gorp G, Strijbos O, Mavridou A, Cadenas de Llano Perula M, Lambrichts I, Verbeken E, Lambrechts P. Regenerative endodontic procedures post trauma: immunohistologic analysis of a retrospective series of failed cases. J Endod 2019; 45: 427–434.
17) Lui JN, Lim WY, Ricucci D. An immunofluorescence study to analyze wound healing outcomes of regenerative endodontics in an immature premolar with chronic apical abscess. J Endod 2020; 46: 627–640.
18) Torabinejad M, Turman M. Revitalization of tooth with necrotic pulp and open apex by using platelet-rich plasma: a case report. J Endod 2011; 37: 265–268.
19) Landesberg R, Roy M, Glickman RP. Quantification of growth factor levels using a simplified method of platelet-rich plasma gel preparation. J Oral Maxillofac Surg 2000; 58: 297–300.
20) Protocols schmorl's stein for reducing substances. https://www.stainsfile.com/protocols/schmorls-stain-for-reducing-substances/(cited 2000.5.1)
21) Lillie RD. Histopathological methods and practical histochemistry, 2nd ed. Blakiston: New York; 1954.
22) Hargreaves KM, Goodis HE, Tay FR. Seltzer and Bender's dental pulp. 2nd ed. Quintessence: Chicago; 2012. 141.
23) Edanami N, Yoshiba K, Shirakashi M, Belal RSI, Yoshiba N, Ohkura N, Tohma A, Takeuchi R, Okiji T, Noiri Y. Impact of remnant healthy pulp and apical tissue on outcomes after simulated regenerative endodontic procedure in rat molars. Sci Rep 2020; 10: 20967.
24) Saito K, Nakatomi M, Ida-Yonemochi H, Ohshima H. Osteopontin is essential for type I collagen secretion in reparative dentin. J Dent Res 2016; 95: 1034–1041.
25) Sonoyama W, Liu Y, Yamaza T, Tuan RS, Wang S, Shi S,

Huang GT-J. Characterization of the apical papilla and its residing stem cells from human immature permanent teeth: a pilot study. J Endod 2008; 34: 166–171.
26) Martin DE, De Almeida JFA, Henry MA, Khaing ZZ, Schmidt CE, Teixeira FB, Diogenes A. Concentration-dependent effect of sodium hypochlorite on stem cells of apical papilla survival and differentiation. J Endod 2014; 40: 51–55.
27) Trevino EG, Patwardhan AN, Henry MA, Perry G, Dybdal-Hargreaves N, Hargreaves KM, Diogenes A. Effect of irrigants on the survival of human stem cells of the apical papilla in a platelet-rich plasma scaffold in human root tips. J Endod 2011; 37: 1109–1115.
28) Smith AJ, Lesot H. Induction and regulation of crown dentinogenesis: embryonic events as a template for dental tissue repair? Crit Rev Oral Biol Med 2001; 12: 425–437.
29) Smith AJ, Tobias RS, Murray PE. Transdentinal stimulation of reactionary dentinogenesis in ferrets by dentine matrix components. J Dent 2001; 29: 341–346.
30) Murray PE, Smith AJ, Windsor LJ, Mjör IA. Remaining dentine thickness and human pulp responses. Int Endod J 2003; 36: 33–43.
31) Tomson PL, Grover LM, Lumley PJ, Sloan AJ, Smith AJ, Cooper PR. Dissolution of bio-active dentine matrix components by mineral trioxide aggregate. J Dent 2007; 35: 636–642.
32) Smith AJ, Lumley PJ, Tomson PL, Cooper PR. Dental regeneration and materials: a partnership. Clin Oral Investig 2008; 12: 103–108.
33) Diogenes A, Simon S, Law AS. Regenerative endodontics. Hargreaves KM, Berman LH. Cohen's pathways of the pulp. 1st ed. Elsevier: St. Louis; 2016. 447–473.

Original Article

ODEP 5 (1) : 44～53, 2025

Expression of Small Integrin-binding Ligand N-linked Glycoproteins During Early Pulp Wound Healing in Rat Molars (SIBLING Proteins in Early Pulp Healing)

Naoki EDANAMI, Kunihiko YOSHIBA*, Razi Saifullah Ibn BELAL, Nagako YOSHIBA*, Shoji TAKENAKA, Naoto OHKURA, Shintaro TAKAHARA, Takako IDA, Rosa BALDEON, Susan KASIMOTO, Pemika THONGTADE and Yuichiro NOIRI

Division of Cariology, Operative Dentistry and Endodontics, Department of Oral Health Science, Niigata University Graduate School of Medical and Dental Sciences
*Division of Oral Science for Health Promotion, Department of Oral Health and Welfare, Niigata University Graduate School of Medical and Dental Sciences

Abstract

Purpose: Vital pulp therapy induces extracellular matrix remodeling at the exposure site, resulting in reparative dentin formation. This study examined the spatiotemporal expression of three small integrin-binding ligand N-linked glycoproteins, namely bone sialoprotein (BSP), osteopontin (OPN), and dentin matrix protein-1 (DMP1), during pulpal healing after pulpotomy.

Methods: The Niigata University Committee on Animal Experimentation approved this study (Approval No. SA00903). Under anesthesia, pulpotomy was performed on the left maxillary first molars of 8-week-old Wistar rats. After irrigation with sodium hypochlorite and hydrogen peroxide, mineral trioxide aggregate was placed on the pulp exposure site, and cavities were sealed with composite resin. After the treated molars were extracted at 6 h, 1 day, 3 days, and 7 days, they were processed for histology, including hematoxylin and eosin staining, immunohistochemistry, and double immunofluorescence.

Results: Before reparative dentin formed, BSP, OPN, and DMP1 accumulated at the exposure site; however, their expression patterns differed. DMP1 was detected at 6 h, whereas BSP and OPN first appeared at day 1. OPN and DMP1 exhibited nearly identical spatial distributions, whereas BSP displayed a markedly more restricted pattern. Additionally, on days 3 and 7, colocalization of BSP, OPN, and DMP1 was observed.

Conclusion: Differences in the spatiotemporal expression of BSP, OPN, and DMP1 suggest they are derived from distinct cellular sources. In addition, their colocalization raises the possibility that a substrate capable of adsorbing these proteins is present at the exposure site.

Key words: vital pulp therapy, bone sialoprotein, osteopontin, dentin matrix protein-1

Corresponding author: Naoki EDANAMI, Division of Cariology, Operative Dentistry and Endodontics, Department of Oral Health Science, Niigata University Graduate School of Medical and Dental Sciences, 5274, Gakkocho-dori 2-bancho, Chuo-ku, Niigata 951-8514, Japan
TEL: +81-25-227-2866, FAX: +81-25-227-2864, E-mail: edanami@dent.niigata-u.ac.jp
Received for Publication: September 10, 2025/Accepted for Publication: October 30, 2025
DOI: 10.11471/odep.2025-005

Introduction

Dental pulp may be exposed to the external environment by deep caries, traumatic injury, or iatrogenic factors during dental procedures. Such exposure increases bacterial contamination and inflammation risks, potentially compromising pulp vitality[1].

Vital pulp therapy (VPT) is a treatment that preserves pulp vitality after exposure and serves as a less invasive alternative to root canal therapy[2]. Clinical studies have shown that teeth treated with VPT maintain long-term pulp vitality[3]. One specific case report demonstrated that VPT supports pulp healing even in deep caries with microabscess formation[4]. These findings support VPT as a biologically based approach for maintaining pulp health and function.

In VPT, biocompatible agents, such as calcium hydroxide (CH) and mineral trioxide aggregate (MTA), are placed on exposed pulp to protect tissue and stimulate reparative dentin formation. Although CH was historically regarded as the standard pulp-capping material[5], its high solubility, poor sealing ability, and tendency to induce reparative dentin with tunnel defects reduce clinical reliability[6]. MTA overcomes these limitations with lower solubility, improved sealing, and formation of a more homogeneous reparative dentin bridge[7]. Given these advantageous properties, MTA is now the preferred material for VPT[2].

VPT with CH or MTA induces extracellular matrix remodeling at the pulp exposure site, essential for pulpal healing[8–10]. Prior to reparative dentin formation, bone sialoprotein (BSP), osteopontin (OPN), and dentin matrix protein-1 (DMP1) accumulate at the exposure site[11–13]. These noncollagenous proteins belong to the small integrin-binding ligand N-linked glycoprotein (SIBLING) family and share common characteristics[14]. They contain a conserved arginine-glycine-aspartic acid (RGD) motif that interacts with integrins to modulate cell adhesion and signaling[15]. They also bind strongly to hydroxyapatite and act as regulators of biomineralization. Specifically, BSP promotes hydroxyapatite nucleation[16], OPN inhibits hydroxyapatite deposition and crystal growth[17], and DMP1 suppresses mineralization when in its native form but enhances it when cleaved or dephosphorylated[18].

Although their precise roles in VPT healing remain unclear, studies suggest that BSP, OPN, and DMP1 participate in reparative dentinogenesis. In rat molars, pulp capping with a BSP-enriched gelatin matrix induced the formation of thick, homogeneously mineralized tissue[19]. The application of a DMP1-containing collagen matrix was found to promote deposition of dentin-like hard tissue with a tubular structure[20]. Following cavity preparation in OPN-deficient mice, impaired type I collagen production in odontoblast-like cells and defective reparative dentin formation were observed[21]. *In vitro*, OPN was found to enhance the adhesion, proliferation, and odontoblastic differentiation of human dental pulp cells[22]. Collectively, these findings highlight BSP, OPN, and DMP1 as critical regulators of odontoblast-like cell differentiation and reparative dentin formation.

Studying BSP, OPN, and DMP1 expression at the pulp exposure site improves understanding of pulpal healing mechanisms and advances VPT. Rat molar studies have reported the immunoreactivity of BSP, OPN, and DMP1 following VPT. Kuratate et al.[11] detected OPN at the exposure site one day after MTA pulp capping. Shigetani et al.[12] found OPN and DMP1 accumulation beneath the necrotic layer 6 h after CH pulp capping. Xie et al.[13] reported BSP expression in the matrix at the exposure site 7 days after CH pulp capping. However, early BSP expression patterns, i.e., before 7 days, and the spatiotemporal relationships among BSP, OPN, and DMP1 during reparative dentinogenesis remain unclear.

This study investigated BSP, OPN, and DMP1 expression dynamics during early pulpal healing following MTA pulpotomy in rat molars, comparing their spatial and temporal localization. We hypothesized that BSP, OPN, and DMP1 exhibit distinct expression dynamics.

Methods

1. Ethical approval and animal care

All animal experiments followed the guidelines of the Committee on Animal Experimentation of Niigata University (approval number: SA00903) and complied with international, national, and institutional regulations. In total, 28 eight-week-old Wistar rats (Clea Japan, Tokyo, Japan) were used. They were maintained under controlled conditions (temperature: 23℃±2℃; humidity: 40–70%) with a 12/12-h light/dark cycle and had free

access to water and a pellet diet.

2. Pulpotomy procedure

Rats were anesthetized via intraperitoneal injection of medetomidine hydrochloride, midazolam, and butorphanol (Fujifilm Wako, Osaka, Japan). The surgical site was disinfected using a 10% povidone-iodine solution. A round tungsten carbide bur (E 0123 size 008; Dentsply, Tulsa, OK, USA) created an access cavity in the left maxillary first molar to expose the pulp chamber. Coronal pulp tissue was carefully removed, and the pulp stump was irrigated with 2.5% sodium hypochlorite and 3% hydrogen peroxide, followed by rinsing with normal saline. Hemostasis was achieved using a sterile cotton pellet. Subsequently, MTA (ProRoot MTA; Dentsply Sirona, York, PA, USA) was applied directly to the pulp stump as a capping material, and the cavity was sealed using a bonding system (Clearfil Universal Bond Quick; Kuraray, Tokyo, Japan) and flowable composite resin (Beautifil Flow; Shofu, Kyoto, Japan). To reduce fracture risk of the treated maxillary first molar, the corresponding mandibular first molar was extracted after pulpotomy.

3. Sample collection and tissue processing

Treated rats were euthanized via carbon dioxide inhalation at 6 h, 1 day, 3 days, and 7 days posttreatment (n=7 per time point). The left maxillary first molars with the surrounding maxillary bone were extracted, fixed in 4% paraformaldehyde for 24 h, and subsequently demineralized in an ethylenediaminetetraacetic acid solution (Osteosoft; Merck, Darmstadt, Germany) for 4 weeks. Demineralized tissues were dehydrated through a graded ethanol series, cleared in xylene, and embedded in paraffin. Serial 5-μm-thick sections were then prepared using a microtome (HistoCore Multicut R: Leica, Wetzlar, Germany).

4. Hematoxylin and eosin staining

For hematoxylin and eosin staining, sections were stained with Mayer's hematoxylin solution (Fujifilm Wako) for 5 min, followed by 1% Eosin Y solution (Fujifilm Wako) for 10 min.

5. Immunohistochemical staining

First, sections underwent heat-induced epitope retrieval in 70℃ citric acid buffer (10 mmol/L; pH 6.0) for 20 min. Endogenous peroxidase activity was then blocked with 0.3% hydrogen peroxide in phosphate-buffered saline for 30 min. Subsequently, sections were incubated with primary antibodies against BSP (WVID1; Developmental Studies Hybridoma Bank, Iowa City, IA, USA), OPN (18628; Immuno-Biological Laboratories, Gunma, Japan), or DMP1 (M176; Takara Bio, Shiga, Japan) for 2 h at room temperature. This was followed by incubation with horseradish peroxidase-conjugated secondary antibodies (Peroxidase AffiniPure Goat Anti-Mouse IgG [115-035-003; Jackson Immuno Research Laboratories, West Grove, PA, USA] or Peroxidase AffiniPure Goat Anti-Rabbit IgG[111-035-003; Jackson Immuno Research Laboratories]) for 1 h at room temperature. Immunoreactivity was visualized using a DAB substrate kit (Vector Laboratories Newark, CA, USA), and counterstaining was performed with hematoxylin for 1 min. The staining results were qualitatively assessed in a blinded manner by a trained observer, who was unaware of the experimental group or the observation period.

6. Double immunofluorescence staining

Initially, sections were incubated with a primary antibody mixture: mouse anti-OPN(MPIIIB10; Developmental Studies Hybridoma Bank) and rabbit anti-DMP1 (M176) antibodies, or mouse anti-BSP (WVID1) and rabbit anti-OPN (18628) antibodies. Secondary antibodies were then applied for 1 h at room temperature. For OPN and DMP1 staining, donkey Alexa Fluor 488-conjugated anti-mouse IgG (A21202; Invitrogen, Carlsbad, CA, USA) and donkey Alexa Fluor 546-conjugated anti-rabbit IgG (A10040; Invitrogen) were used; for BSP and OPN staining, donkey Alexa Fluor 546-conjugated anti-mouse IgG (A10036; Invitrogen) and donkey Alexa Fluor 488-conjugated anti-rabbit IgG (A21206; Invitrogen) were employed. Finally, sections were mounted using ProLong Diamond with DAPI (Thermo Fisher Scientific, Austin, TX, USA).

Results

1. Hematoxylin and eosin staining

At 6 h after pulpotomy, a thin necrotic layer was present at the pulp exposure site, with scattered inflammatory cells observed beneath it (Fig. 1-a). By 3 days, inflammation had largely subsided, spindle-shaped cells were evident below the necrotic layer (Fig. 1-e, i), and granulation-like tissue was present beneath the exposure site (Fig. 1-i). By 7 days, a thin dentin bridge had formed at the exposure site, accompanied by subjacent odontoblast-like cells (Fig. 1-m).

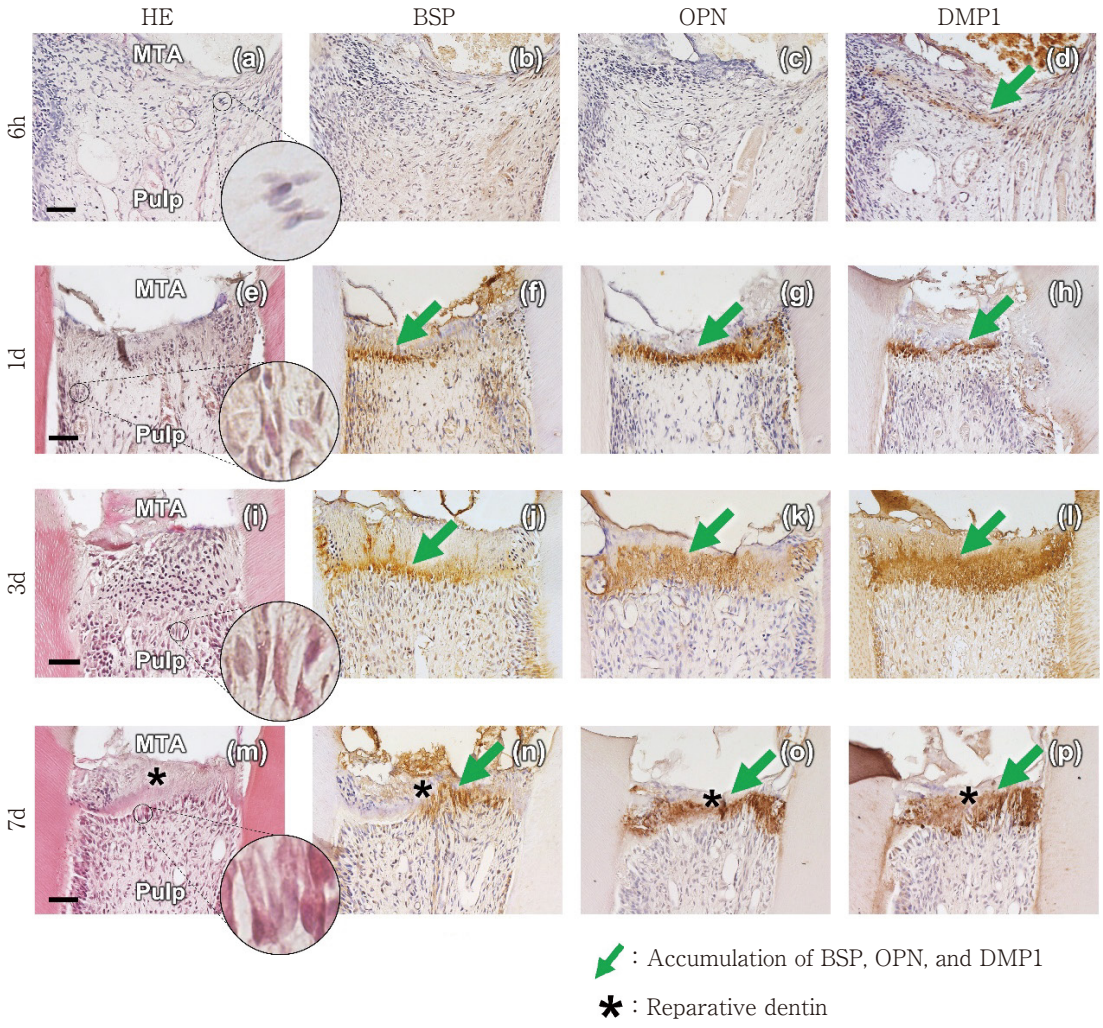

Fig. 1 Expression of bone sialoprotein (BSP), osteopontin (OPN), and dentin matrix protein-1 (DMP1) during reparative dentinogenesis

At 6 h, DMP1 immunoreactivity was observed at the pulp exposure site, whereas BSP and OPN immunoreactivity was absent. On days 1 and 3, all three SIBLING proteins showed immunoreactivity at the exposure site. By day 7, they were localized within reparative dentin. The BSP-positive area was narrower than the OPN- and DMP1-positive areas. HE: hematoxylin and eosin staining; MTA: mineral trioxide aggregate. Scale bars: 50 μm. The circle in (a) indicates an area containing inflammatory cells, the circles in (e) and (i) indicate areas containing spindle-shaped cells, and the circle in (m) indicates an area containing odontoblast-like cells.

2. Immunohistochemical staining

BSP, OPN, and DMP1 expression at the pulp exposure site is summarized in Table 1. At 6 h, a thin DMP1-immunopositive layer was observed in the matrix beneath the necrotic layer (Fig. 1-d), whereas BSP and OPN immunoreactivity was absent (Fig. 1-b, c). From day 1 onward, all three SIBLING proteins showed immunopositive reactions at the exposure site. On day 1, they were localized beneath the necrotic layer (Fig. 1-f-h); by day 3, they appeared within granu-

Table 1 Expression of bone sialoprotein (BSP), osteopontin (OPN), and dentin matrix protein-1 (DMP1) at the pulp exposure site

	6 h	1 day	3 days	7 days
BSP	0/7	1/7	4/7	6/7
OPN	0/7	2/7	7/7	7/7
DMP1	3/7	7/7	7/7	7/7

Values represent the number of positive specimens/total specimens examined.

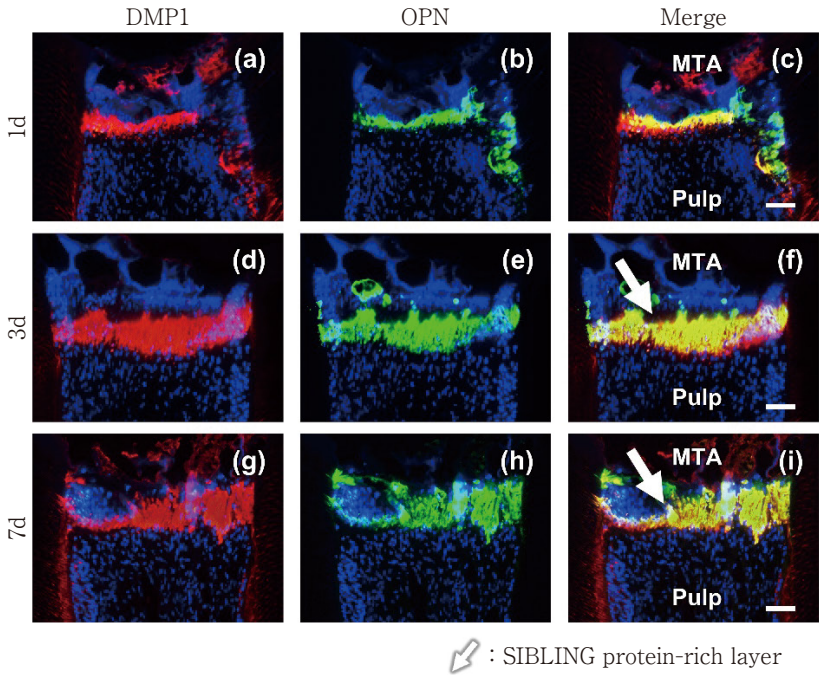

Fig. 2 Double immunofluorescence staining of dentin matrix protein-1 (DMP1) and osteopontin (OPN)

On day 1, DMP1 and OPN showed partly overlapping but distinct distributions. By days 3 and 7, their immunoreactive areas were expanded and nearly fully overlapped. MTA: mineral trioxide aggregate; SIBLING: small integrin-binding ligand N-linked glycoprotein. Scale bars: 50 μm.

lation-like tissue (Fig. 1-j-l); and by day 7, they were present in reparative dentin (Fig. 1-n-p).

3. Double immunofluorescence staining

On day 1, OPN and DMP1 exhibited slightly different distributions, with only partial overlap of immunoreactive areas (Fig. 2-a-c). By days 3 and 7, their immunoreactive regions had expanded and almost completely overlapped (Fig. 2-d-i). Similarly, BSP and OPN showed distinct distributions on day 1, with minimal overlap (Fig. 3-a-c). By days 3 and 7, BSP increasingly colocalized with OPN, in contrast to day 1 (Fig. 3-d-i), and the BSP-positive region was fully encompassed within the OPN-positive area (Fig. 3-f, i).

Discussion

In this study, considering the timing of protein accumulation onset and distribution at pulp exposure sites, BSP, OPN, and DMP1 exhibited distinct expression patterns. DMP1 accumulated as early as 6 h postoperatively, whereas OPN and BSP accumulated from the first postoperative day (Table 1 and Fig. 1). Although OPN and BSP accumulation showed similar onset times, their spatial distributions differed, with BSP confined to a more restricted area (Fig. 3). These findings indicate that SIBLING proteins' cellular sources may differ.

Rapid DMP1 accumulation within 6 h suggests that it likely originates from cells already present in the dental pulp. Pulp cells and odontoblasts reportedly express DMP1[23]; thus, they are plausible contributors. Additionally, DMP1 expression is known to increase in pulp cells cultured with MTA[24], suggesting that the MTA pulp-capping material may have promoted DMP1 accumulation.

OPN accumulation may involve dendritic cells and macrophages. In a mouse tooth transplantation model, MHC class II-positive immunocompetent cells with dendritic features deposited OPN at the dentin-predentin interface[25]. OPN-expressing macrophages are present in dental pulp and increase in abundance during inflammation[26]. Extracellular calcium ions also induce monocyte differentiation into macrophages and stimulate OPN production[27]. Therefore, OPN-producing dendritic cells and macrophages likely differentiate at the pulp

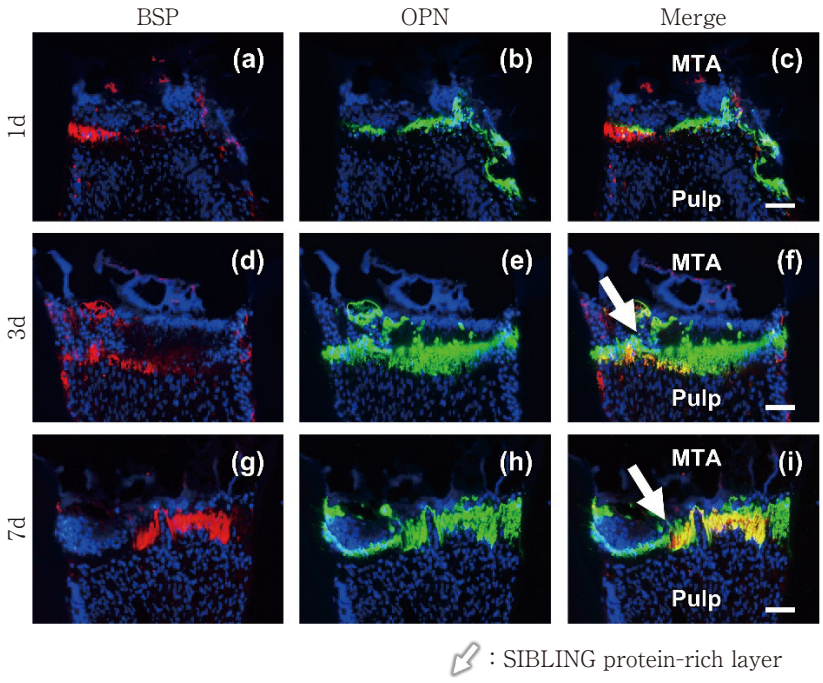

Fig. 3 Double immunofluorescence staining of bone sialoprotein (BSP) and osteopontin (OPN)

On day 1, BSP and OPN showed distinct distributions with minimal overlap. On days 3 and 7, the BSP-positive region was entirely enclosed within the OPN-positive area. MTA: mineral trioxide aggregate; SIBLING: small integrin-binding ligand N-linked glycoprotein. Scale bars: 50 μm.

exposure site in response to tissue injury and/or calcium ions from MTA[28], leading to OPN accumulation. This is supported by previous studies showing increased dendritic cell and macrophage counts in MTA- or CH-capped pulp[29,30].

BSP is an osteoblast marker[31]. Osteoblasts are normally absent from dental pulp, but appear under pathological conditions[32]. Severe pulp damage, which can occur after tooth replantation or transplantation, induces pulp cells to differentiate into osteoblastic cells producing BSP-positive bone-like tissue[33–35]. MTA pulp capping increases TGF-β production in pulp tissue[9], and TGF-β promotes BSP expression in pulp cells[36]. Therefore, the BSP detected in this study may have been produced by pulp cells undergoing osteoblastic differentiation in response to TGF-β stimulation.

By postoperative day 3, OPN and DMP1 distributions nearly overlapped (Fig. 2), and the BSP-positive region was entirely within OPN-positive areas on days 3 and 7 (Fig. 3). This pattern suggests that these SIBLING proteins were adsorbed onto a specific substrate rather than deposited randomly. BSP[37], OPN[38], and DMP1[39] strongly bind hydroxyapatite, and MTA induces rapid hydroxyapatite precipitation in adjacent tissue[40]. Our previous work showed that OPN and DMP1 accumulate beneath regions of hydroxyapatite deposition in MTA-capped pulp[41]. Collectively, these findings indicate that hydroxyapatite at the pulp exposure site may serve as a substrate for SIBLING protein accumulation, facilitating their colocalization.

Meanwhile, in pulp tissue capped with CH or MTA, fibroblasts produce new collagen fibrils, forming granulation-like tissue at the pulp exposure site[9,42,43]. Given that BSP[44], OPN[45], and DMP1[46] also bind collagen fibrils, the fibrils may offer an additional substrate for protein accumulation.

In this study, a SIBLING protein-rich layer containing BSP, OPN, and DMP1 formed prior to reparative dentin deposition (Figs. 2 and 3). Although their role remains unclear, RGD domains in SIBLING proteins serve as integrin recognition sites and activate intracellular signaling pathways[47]. Dentin phosphoprotein-derived peptides containing the RGD domain promote proliferation, odontoblastic differentiation, and mineralized matrix

deposition of dental pulp stem cells[48]. Thus, the SIBLING protein-rich layer may facilitate odontoblast-like cell differentiation and reparative dentin formation.

BSP, OPN, and DMP1 also activate the matrix metalloproteinases (MMPs): BSP activates MMP2, OPN activates MMP3, and DMP1 activates MMP9[49]. MMP3 promotes angiogenesis and reparative dentinogenesis in injured rat pulp[50], whereas MMP2 and MMP9 cleave latent TGF-β, releasing its active form[51,52], which induces odontoblastic differentiation of dental pulp stem cells[53]. Therefore, the SIBLING protein-rich layer observed in this study may also contribute to pulp healing via MMP activation.

The SIBLING protein-rich layer contains promoters and inhibitors of hydroxyapatite formation. BSP promotes hydroxyapatite crystal formation[16], OPN inhibits crystal growth[17], and DMP1 has multiple forms with differing effects (the N- and C-terminal fragments promote hydroxyapatite formation, whereas the chondroitin sulfate-linked N-terminal fragment acts as an inhibitor)[18]. Their coexistence in this layer suggests that mineralization is precisely regulated through their coordinated action, supporting effective tissue repair while preventing excessive calcification and compromised pulpal health.

This study has several limitations. In this study, we examined the spatial relationships between DMP1 and OPN, as well as BSP and OPN, using double immunofluorescence staining. However, the combination of DMP1 and BSP was not investigated. This was because DMP1 and OPN exhibited nearly identical localization patterns throughout the experimental period, and thus additional double staining for DMP1 and BSP was considered unlikely to provide new insights. Nevertheless, future studies using techniques such as iterative bleaching, which extends multiplexity[54] for triple staining of BSP, OPN, and DMP1, may help to clarify subtle differences in their localization and to better understand their origins and functions.

Another limitation of this study is that we did not identify the specific cell types responsible for the production of BSP, OPN, and DMP1. Because these proteins can be produced by multiple cell types[23–25,32], the predominant cellular sources at each stage of pulp healing remain unclear. Future studies employing co-immunostaining with cell-type markers or RNA *in situ* hybridization will be required to clarify which cells contribute to the expression of these proteins during the reparative process.

In addition, the mechanisms underlying the colocalization of BSP, OPN, and DMP1 remain unclear; however, detailed ultrastructural analysis using immunoelectron microscopy[55] may provide further insights into their precise localization and interactions with the surrounding matrix.

In summary, this study elucidated early BSP, OPN, and DMP1 expression dynamics in rat molar pulp following MTA pulpotomy, advancing our understanding of pulp wound healing. Our findings suggest that these proteins originate from distinct cellular sources and are adsorbed onto a substrate at the exposure site. Future studies should clarify the mechanisms of SIBLING protein accumulation at the pulp exposure site and determine whether modulating this process enhances reparative dentin formation.

Conclusion

BSP, OPN, and DMP1 exhibited distinct spatiotemporal expression patterns at the pulp exposure site following MTA pulpotomy, suggesting that they may originate from different cellular sources. The observed colocalization of these proteins further raises the possibility that a substrate capable of adsorbing them is present at the exposure site.

Acknowledgments

This work was supported by the CCRF of Niigata University. We thank Ms. Ayako Ikarashi for her valuable technical assistance. The monoclonal antibodies developed by M. Solursh and A. Franzen (WVID1 and MPIIIB10) were obtained from the Developmental Studies Hybridoma Bank, created by the NICHD of the NIH and maintained by the Department of Biology, The University of Iowa, Iowa City, IA 52242.

Conflicts of Interest

The authors have no conflicts of interest to declare.

References

1) Tani-Ishii N, Wang CY, Stashenko P. Immunolocalization of bone-resorptive cytokines in rat pulp and periapical lesions following surgical pulp exposure. Oral Microbiol

Immunol 1995; 10: 213–219.
2) Duncan HF. Present status and future directions—Vital pulp treatment and pulp preservation strategies. Int Endod J 2022; 55: 497–511.
3) Silva EJNL, Pinto KP, Belladonna FG, Ferreira CMA, Versiani MA, De-Deus G. Success rate of permanent teeth pulpotomy using bioactive materials: A systematic review and meta-analysis of randomized clinical trials. Int Endod J 2023; 56: 1024–1041.
4) Okamoto M, Duncan HF, Takahashi Y, Kuriki N, Matsumoto S, Hayashi M. Partial pulpotomy to successfully treat a caries-induced pulpal micro-abscess: A case report. Front Dent Med 2021; 2: 678632.
5) Sangwan P, Sangwan A, Duhan J, Rohilla A. Tertiary dentinogenesis with calcium hydroxide: a review of proposed mechanisms. Int Endod J 2013; 46: 3–19.
6) Cox CF, Sübay RK, Ostro E, Suzuki S, Suzuki SH. Tunnel defects in dentin bridges: their formation following direct pulp capping. Oper Dent 1996; 21: 4–11.
7) Parirokh M, Torabinejad M. Mineral trioxide aggregate: A comprehensive literature review—part I: Chemical, physical, and antibacterial properties. J Endod 2010; 36: 16–27.
8) Yoshiba N, Yoshiba K, Ohkura N, Hosoya A, Shigetani Y, Yamanaka Y, Izumi N, Nakamura H, Okiji T. Expressional alterations of fibrillin-1 during wound healing of human dental pulp. J Endod 2012; 38: 177–184.
9) Edanami N, Yoshiba N, Ohkura N, Takeuchi R, Tohma A, Noiri Y, Yoshiba K. Characterization of dental pulp myofibroblasts in rat molars after pulpotomy. J Endod 2017; 43: 1116–1121.
10) Yoshiba K, Yoshiba N, Nakamura H, Iwaku M, Ozawa H. Immunolocalization of fibronectin during reparative dentinogenesis in human teeth after pulp capping with calcium hydroxide. J Dent Res 1996; 75: 1590–1597.
11) Kuratate M, Yoshiba K, Shigetani Y, Yoshiba N, Ohshima H, Okiji T. Immunohistochemical analysis of nestin, osteopontin, and proliferating cells in the reparative process of exposed dental pulp capped with mineral trioxide aggregate. J Endod 2008; 34: 970–974.
12) Shigetani Y, Yoshiba K, Kuratate M, Takei E, Yoshiba N, Yamanaka Y, Ohshima H, Okiji T. Temporospatial localization of dentine matrix protein 1 following direct pulp capping with calcium hydroxide in rat molars. Int Endod J 2015; 48: 573–581.
13) Xie X, Ma S, Li C, Liu P, Wang H, Chen L, Qin C. Expression of small integrin-binding ligand n-linked glycoproteins (SIBLINGs) in the reparative dentin of rat molars. Dent Traumatol 2014; 30: 285–295.
14) Staines KA, MacRae VE, Farquharson C. The importance of the SIBLING family of proteins on skeletal mineralisation and bone remodelling. J Endocrinol 2012; 214: 241–255.
15) Kulkarni GV, Chen B, Malone JP, Narayanan AS, George A. Promotion of selective cell attachment by the RGD sequence in dentine matrix protein 1. Arch Oral Biol 2000; 45: 475–484.
16) Baht GS, O'Young J, Borovina A, Chen H, Tye CE, Karttunen M, Lajoie GA, Hunter GK, Goldberg HA. Phosphorylation of Ser136 is critical for potent bone sialoprotein-mediated nucleation of hydroxyapatite crystals. Biochem J 2010; 428: 385–395.
17) Hunter GK. Role of osteopontin in modulation of hydroxyapatite formation. Calcif Tissue Int 2013; 93: 348–354.
18) Gericke A, Qin C, Sun Y, Redfern R, Redfern D, Fujimoto Y, Taleb H, Butler WT, Boskey AL. Different forms of DMP1 play distinct roles in mineralization. J Dent Res 2010; 89: 355–359.
19) Decup F, Six N, Palmier B, Buch D, Lasfargues JJ, Salih E, Goldberg M. Bone sialoprotein-induced reparative dentinogenesis in the pulp of rat's molar. Clin Oral Investig 2000; 4: 110–119.
20) Almushayt A, Narayanan K, Zaki AE, George A. Dentin matrix protein 1 induces cytodifferentiation of dental pulp stem cells into odontoblasts. Gene Ther 2006; 13: 611–620.
21) Saito K, Nakatomi M, Ida-Yonemochi H, Ohshima H. Osteopontin is essential for type I collagen secretion in reparative dentin. J Dent Res 2016; 95: 1034–1041.
22) Tang J, Qiu Y, Li Z. Osteopontin facilitated dental pulp cell adhesion and differentiation: A laboratory investigation. ACS Appl Bio Mater 2025; 8: 1320–1329.
23) Qin C, D'Souza R, Feng JQ. Dentin matrix protein 1 (DMP1): new and important roles for biomineralization and phosphate homeostasis. J Dent Res 2007; 86: 1134–1141.
24) Chang SW, Lee SY, Kum KY, Kim EC. Effects of ProRoot MTA, bioaggregate, and micromega MTA on odontoblastic differentiation in human dental pulp cells. J Endod 2014; 40: 113–118.
25) Saito K, Nakatomi M, Ida-Yonemochi H, Kenmotsu S, Ohshima H. The expression of GM-CSF and osteopontin in immunocompetent cells precedes the odontoblast differentiation following allogenic tooth transplantation in mice. J Histochem Cytochem 2011; 59: 518–529.
26) Chen L, Zhu M, Zhang C, Wang Z, Lyu X, Xu W, Wu B. Osteopontin interacts with dendritic cells and macrophages in pulp inflammation: Comprehensive transcriptomic analysis and laboratory investigations. Int Endod J 2024; 57: 464–476.
27) Murthy S, Karkossa I, Schmidt C, Hoffmann A, Hagemann T, Rothe K, Seifert O, Anderegg U, von Bergen M, Schubert K, Rossol M. Danger signal extracellular

calcium initiates differentiation of monocytes into SPP1/osteopontin-producing macrophages. Cell Death Dis 2022; 13: 53.
28) Han L, Kodama S, Okiji T. Evaluation of calcium-releasing and apatite-forming abilities of fast-setting calcium silicate-based endodontic materials. Int Endod J 2015; 48: 124–130.
29) Takei E, Shigetani Y, Yoshiba K, Hinata G, Yoshiba N, Okiji T. Initial transient accumulation of M2 macrophage-associated molecule-expressing cells after pulpotomy with mineral trioxide aggregate in rat molars. J Endod 2014; 40: 1983–1988.
30) Zhang M, Kokabu S, Nakatomi C, Sugiyama G, Matsuo K, Jimi E. The distinct distributions of immunocompetent cells in rat dentin pulp after pulpotomy. Anat Rec 2015; 298: 741–749.
31) Bouleftour W, Juignet L, Bouet G, Granito RN, Vanden-Bossche A, Laroche N, Aubin JE, Lafage-Proust MH, Vico L, Malaval L. The role of the SIBLING, bone sialoprotein in skeletal biology—Contribution of mouse experimental genetics. Matrix Biol 2016; 52–54: 60–77.
32) Vijaykumar A, Dyrkacz P, Vidovic-Zdrilic I, Maye P, Mina M. Expression of BSP-GFPtpz transgene during osteogenesis and reparative dentinogenesis. J Dent Res 2020; 99: 89–97.
33) Hosoya A, Nakamura H, Ninomiya T, Hoshi K, Yoshiba K, Yoshiba N, Takahashi M, Okabe T, Sahara N, Yamada H, Kasahara E, Ozawa H. Hard tissue formation in subcutaneously transplanted rat dental pulp. J Dent Res 2007; 86: 469–474.
34) Zhao C, Hosoya A, Kurita H, Hu T, Hiraga T, Ninomiya T, Yoshiba K, Yoshiba N, Takahashi M, Kurashina K, Ozawa H, Nakamura H. Immunohistochemical study of hard tissue formation in the rat pulp cavity after tooth replantation. Arch Oral Biol 2007; 52: 945–953.
35) Takamori Y, Suzuki H, Nakakura-Ohshima K, Cai J, Cho SW, Jung HS, Ohshima H. Capacity of dental pulp differentiation in mouse molars as demonstrated by allogenic tooth transplantation. J Histochem Cytochem 2008; 56: 1075–1086.
36) Hwang YC, Hwang IN, Oh WM, Park JC, Lee DS, Son HH. Influence of TGF-β1 on the expression of BSP, DSP, TGF-β1 receptor I and Smad proteins during reparative dentinogenesis. J Mol Histol 2008; 39: 153–160.
37) Goldberg HA, Warner KJ, Li MC, Hunter GK. Binding of bone sialoprotein, osteopontin and synthetic polypeptides to hydroxyapatite. Connect Tissue Res 2001; 42: 25–37.
38) Wada T, McKee MD, Steitz S, Giachelli CM. Calcification of vascular smooth muscle cell cultures: inhibition by osteopontin. Circ Res 1999; 84: 166–178.
39) Gajjeraman S, Narayanan K, Hao J, Qin C, George A. Matrix macromolecules in hard tissues control the nucleation and hierarchical assembly of hydroxyapatite. J Biol Chem 2007; 282: 1193–1204.
40) Edanami N, Takenaka S, Ibn Belal RS, Yoshiba K, Takahara S, Yoshiba N, Ohkura N, Noiri Y. In vivo assessment of the apatite-forming ability of new-generation hydraulic calcium silicate cements using a rat subcutaneous implantation model. J Funct Biomater 2023; 14: 213.
41) Edanami N, Yoshiba K, Ibn Belal RS, Yoshiba N, Takenaka S, Ohkura N, Takahara S, Ida T, Baldeon R, Kasimoto S, Thongtade P, Noiri Y. Role of dystrophic calcification in reparative dentinogenesis after rat molar pulpotomy. Int J Mol Sci 2025; 26: 7130.
42) Yoshiba N, Edanami N, Tohma A, Takeuchi R, Ohkura N, Hosoya A, Noiri Y, Nakamura H, Yoshiba K. Detection of bone marrow-derived fibrocytes in human dental pulp repair. Int Endod J 2018; 51: 1187–1195.
43) Schröder U. Effects of calcium hydroxide-containing pulp-capping agents on pulp cell migration, proliferation, and differentiation. J Dent Res 1985; 64: 541–548.
44) Baht GS, Hunter GK, Goldberg HA. Bone sialoprotein-collagen interaction promotes hydroxyapatite nucleation. Matrix Biol 2008; 27: 600–608.
45) Zurick KM, Qin C, Bernards MT. Mineralization induction effects of osteopontin, bone sialoprotein, and dentin phosphoprotein on a biomimetic collagen substrate. J Biomed Mater Res Part A 2013; 101: 1571–1581.
46) He G, George A. Dentin matrix protein 1 immobilized on type I collagen fibrils facilitates apatite deposition in vitro. J Biol Chem 2004; 279: 11649–11656. doi: 10.1074/jbc.M309296200.
47) von Marschall Z, Fisher LW. Dentin matrix protein-1 isoforms promote differential cell attachment and migration. J Biol Chem 2008; 283: 32730–32740.
48) Hassan T, Qiu Y, Hasan MR, Saito T. Effects of dentin phosphophoryn-derived RGD peptides on the differentiation and mineralization of human dental pulp stem cells in vitro. Biomedicines 2022; 10: 2781.
49) Fedarko NS, Jain A, Karadag A, Fisher LW. Three small integrin binding ligand N-linked glycoproteins (SIBLINGs) bind and activate specific matrix metalloproteinases. FASEB J 2004; 18: 734–736.
50) Zheng L, Amano K, Iohara K, Ito M, Imabayashi K, Into T, Matsushita K, Nakamura H, Nakashima M. Matrix metalloproteinase-3 accelerates wound healing following dental pulp injury. Am J Pathol 2009; 175: 1905–1914.
51) Yu Q, Stamenkovic I. Cell surface-localized matrix metalloproteinase-9 proteolytically activates TGF-beta and promotes tumor invasion and angiogenesis. Genes Dev 2000; 14: 163–176.

52) Niwa T, Yamakoshi Y, Yamazaki H, Karakida T, Chiba R, Hu JC, Nagano T, Yamamoto R, Simmer JP, Margolis HC, Gomi K. The dynamics of TGF-β in dental pulp, odontoblasts and dentin. Sci Rep 2018; 8: 4450.
53) Bai Y, Cheng X, Liu X, Guo Q, Wang Z, Fu Y, He W, Yu Q. Transforming growth factor-β1 promotes early odontoblastic differentiation of dental pulp stem cells via activating AKT, Erk1/2 and p38 MAPK pathways. J Dent Sci 2023; 18: 87–94.
54) Radtke AJ, Chu CJ, Yaniv Z, Yao L, Marr J, Beuschel RT, Ichise H, Gola A, Kabat J, Lowekamp B, Speranza E, Croteau J, Thakur N, Jonigk D, Davis JL, Hernandez JM, Germain RN. IBEX: an iterative immunolabeling and chemical bleaching method for high-content imaging of diverse tissues. Nat Protoc 2022; 17: 378–401.
55) McKee MD, Nanci A. Secretion of osteopontin by macrophages and its accumulation at tissue surfaces during wound healing in mineralized tissues: a potential requirement for macrophage adhesion and phagocytosis. Anat Rec 1996; 245: 394–409.

Original Article

ODEP 5 (1) : 54～60, 2025

The Effects of Essential Amino Acids in the Wound Healing Process of Rat Gingival Tissue

Kosho KASHITANI, Hirohito KATO and Kazuya TOMINAGA*

Department of Periodontology, Osaka Dental University
*Department of Oral Pathology, Osaka Dental University

Abstract

Purpose: Essential amino acids (EAAs) are required for protein synthesis and tissue repair. However, their role in gingival tissue wound healing remains unclear. This study aimed to evaluate the effects of dietary EAA deficiency on gingival tissue wound healing in rats.

Methods: Seven-week-old Sprague-Dawley rats were divided into two groups: one was fed a standard diet containing EAAs (+EAA group) and the other was fed a diet without EAAs (−EAA group). Body weight and size were monitored throughout the experimental period. Standardized gingival wounds were created, and wound healing was assessed by measuring the wound area over time, histologically examining the connective tissue, and evaluating re-epithelialization.

Results: Rats in the −EAA group exhibited lower body weight gain and smaller overall body size than those in the +EAA group. Wound area measurements revealed delayed contractions and slower closures in the −EAA group. The results of histological analysis revealed impaired granulation tissue formation and reduced tissue organization in the −EAA group. Furthermore, re-epithelialization across the wound surface was significantly slower in the −EAA group than in the +EAA group, which showed continuous epithelial coverage and more organized connective tissue repair.

Conclusion: Dietary EAA deficiency adversely affects gingival tissue wound healing by impairing systemic growth, delaying wound closure, and suppressing tissue regeneration and re-epithelialization. These findings highlight the importance of adequate EAA intake in maintaining the healing capacity of the oral tissue and suggest that nutritional support could be a valuable addition to periodontal therapy.

Key words: essential amino acids, gingival tissue, wound healing

Corresponding author: Hirohito KATO, Department of Periodontology, Osaka Dental University, 8-1, Kuzuha-hanazono-cho, Hirakata, Osaka 573-1121, Japan
TEL: +81-72-864-3084, FAX: +81-72-864-3184, E-mail: kato-h@cc.osaka-dent.ac.jp
Received for Publication: September 15, 2025/Accepted for Publication: November 4, 2025
DOI: 10.11471/odep.2025-006

Introduction

Healing of gingival tissue directly influences the morphology and stability of gingival attachment, making it a critical process that determines the prognosis of periodontal treatment and periodontal tissue regeneration therapy[1,2]. Smooth progression of gingival connective tissue healing improves the overall stability of periodontal tissues and contributes to the restoration of masticatory function and aesthetics[3–5]. Therefore, elucidating the molecular mechanisms underlying gingival tissue wound healing is fundamentally and clinically important.

Wound healing requires the proliferation and migration of fibroblasts as well as the production of extracellular matrix components, primarily collagen[6,7]. These processes are influenced by local factors and by systemic nutritional status. In particular, amino acids are essential for protein synthesis and energy metabolism and have been reported to be strongly involved in maintaining cellular function and tissue repair[8–10]. Among them, essential amino acids (EAAs) cannot be synthesized within the body and must be obtained from the diet or other external sources. A deficiency of these amino acids has been suggested to reduce the overall repair capacity of tissue[11,12].

Our previous research demonstrated that under conditions of EAA deficiency, gingival fibroblast proliferation and migration are suppressed and collagen synthesis is decreased[13]. However, these findings were primarily limited to the cellular culture level, and the contribution of EAAs to gingival tissue wound healing at the tissue level has not been sufficiently investigated.

Therefore, in this study, we used a rat gingival tissue defect model to investigate the effects of EAAs intake on wound healing. The objective of this study was to clarify the role of EAAs in gingival tissue wound healing and elucidate their biological significance. This study provides new insights into the mechanisms underlying periodontal tissue healing from a nutritional perspective.

Materials and Methods

1. EAA-adjusted feed administration and animals

Shimizu Experimental Materials Co., Ltd. provided either a standard diet or feed lacking the EAAs present in the standard diet. Both feeds were solid diets, with the standard diet having an amino acid calorie content of 708 kcal/kg. To standardize the total caloric content between the standard diet and the experimental group feed, the caloric deficit caused by removing EAAs was adjusted using cornstarch to ensure uniform total caloric intake. Feeding was conducted in an environment that allowed free access to food. Thirty Sprague-Dawley rats aged 7 weeks were divided into two groups and fed either a standard diet containing EAAs (+EAA group) or a diet without EAAs (−EAA group). Body weight changes in the rats were measured over time (Fig. 1). All the animal experiments were approved by the Osaka Dental University Animal Experiment Committee (Animal Experiment Approval No. 25-04002).

2. Palatal wound creation

All rats were subjected to general anesthesia using a triple anesthetic combination (medetomidine, midazolam, and butorphanol). The volume of anesthetic solution administered was calculated based on body weight at 10 mL/kg. After confirming the effectiveness of anesthesia, local anesthesia was administered via lidocaine injection. Subsequently, an experimental gingival tissue defect was created bilaterally from the mesial palatal aspect of the first maxillary molar to the distal palatal aspect of the third molar using a scalpel (No. 15, Feather, Osaka, Japan), as previously reported[14].

3. Morphometric analysis

The healing area of the gingival connective tissue was photographed using a digital SLR camera (Nikon D7000) at a fixed magnification (1.1×) from approximately 70° toward the maxillary occlusal surface. The healing area was evaluated using ImageJ software (National Institutes of Health, MD, USA) by measuring the digital trace boundary of the non-epithelialized area. Percentage values represent the healing rate measured at each day relative to the gingival connective tissue defect on day 0.

4. Histological analysis

On postoperative days 0, 7, and 14, rats in the + EAA and −EAA groups were euthanized via excessive inhalation of isoflurane and perfused for fixation in 4% paraformaldehyde phosphate buffer solution (FUJIFILM Wako Pure Chemical Corporation, Osaka, Japan). Subsequently, the soft tissue surrounding the adminis-

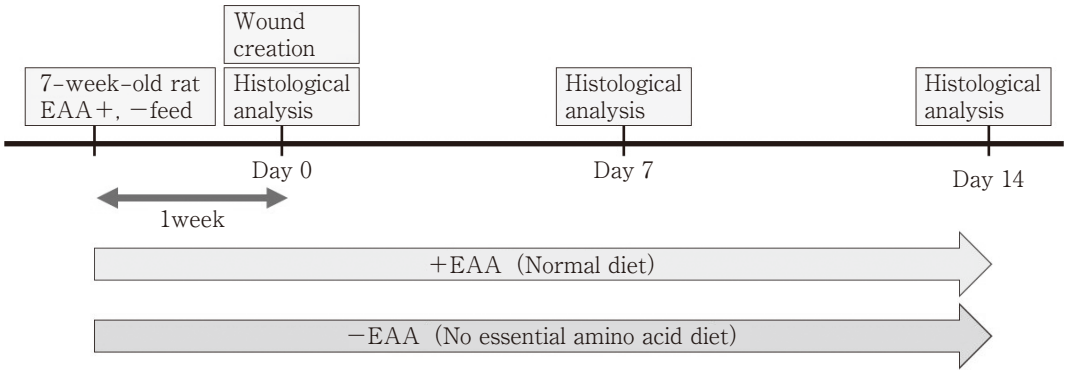

Fig. 1 Schedule for rats fed a standard diet containing essential amino acids (+EAA) or a diet without essential amino acids (−EAA)

Rats were fed a diet supplemented with or without essential amino acids for 1 week prior to surgery. Subsequently, gingival surgery was performed, and changes in gingival wound healing were observed at 7 and 14 days post-surgery.

tration site was excised as a single block with the maxillary bone. The collected specimens were fixed, demineralized, paraffin embedded according to standard procedures, and stained with hematoxylin and eosin (H-E). They were examined under an optical microscope to observe wound healing and inflammatory cell infiltration. For the evaluation of gingival tissue re-epithelialization, the width of the base of the gingival tissue defect was measured from H-E stained histological sections, and the proportion of re-epithelialized tissue was analyzed using ImageJ software.

5. Statistical analysis

Data are presented as mean±standard deviation. Parametric data for +EAA versus −EAA were analyzed using Student's *t*-test. Statistical analyses were performed using IBM SPSS Statistics Ver. 17 (IBM, IL, USA).

Results

1. Effects of EAA supplementation on body weight and body size in rats

This study evaluated body weight changes in rats in the +EAA and −EAA groups to assess systemic effects. At the start of rat rearing (Baseline), no changes in body weight were observed in either group. On postoperative day 0, both groups showed changes in body weight, but by postoperative day 2, they exhibited weight loss. However, from the third day onward, the −EAA group exhibited progressive weight loss over time whereas the +EAA group showed progressive weight gain over time (Fig. 2A). Changes in rat body size over time were examined. The −EAA group exhibited a clear reduction in body size. In particular, the limbs tended to become thinner. Each experiment was performed three times for statistical analysis (n=5) (Fig. 2B).

2. Macroscopic evaluation of gingival wound closure

Macroscopic evaluation of gingival connective tissue wound closure for 14 days showed that the −EAA group tended to have a reduced wound healing area compared with the +EAA group, with delayed wound closure (Fig. 3A). Quantification and comparison of the healing areas between the two groups also revealed a significantly smaller area in the −EAA group (Fig. 3B).

3. Histological analysis

The results were consistent with the macroscopic findings, showing a tendency toward suppressed wound healing in the −EAA group compared with the +EAA group. In the +EAA group, the wound site was completely closed and covered by epithelial tissue, whereas in the −EAA group, the wound remained open with exposed bone surfaces. Furthermore, while almost no inflammatory cell invasion of the gingival connective tissue was observed in the +EAA group, numerous inflammatory cells invaded the exposed bone surface and gingival connective tissue in the −EAA group. Collagen fibers stained with eosin were also observed, and collagen tended to be less abundant in the −EAA group (Fig. 4).

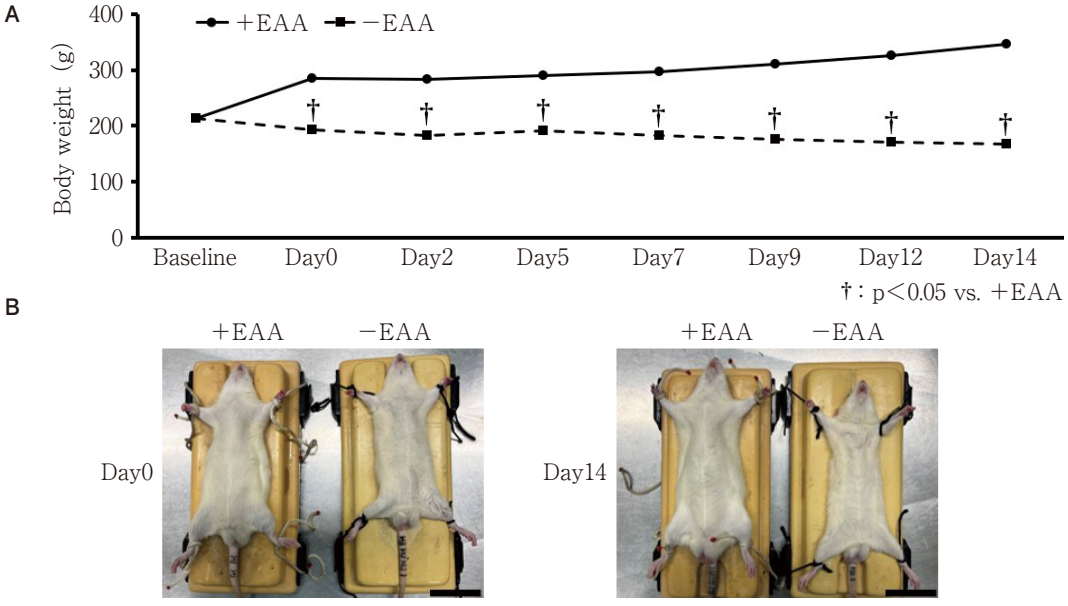

Fig. 2 Effects of essential amino acid supplementation on body weight of and physical changes in rats

(A) Changes in rat body weight were measured to assess the effect of essential amino acid supplementation. Both groups showed weight loss until day 2 post-surgery. However, from day 3 onward, the −EAA group exhibited continued weight loss whereas the +EAA group showed a progressive increase in body weight over time. For each day, a significant decrease in the −EAA group compared to the +EAA group is denoted as †: $p<0.05$.

(B) In terms of body size, the −EAA group tended to be smaller in size than the +EAA group. Scale bar: 5 cm.

4. Evaluation of epithelialization rate

Regarding the epithelial coverage rate during epithelial closure in the wound healing process, the −EAA group showed a tendency toward suppression compared with the +EAA group throughout the 14-day follow-up period. Delayed epithelialization was observed in the −EAA group, particularly on day 14 (Fig. 5).

Discussion

In this study, the −EAA group showed a marked delay in gingival tissue wound closure over the 14-day postoperative period. Histological evaluation revealed inadequate epithelial coverage at the wound site. Additionally, the wound failed to close completely in some cases, thereby exposing the bone surface. Persistent inflammatory cell infiltration was observed near the bone surface and within the gingival connective tissue.

Gingival wound healing progresses through inflammatory, proliferative, and maturation phases, with proper epithelialization and connective tissue regeneration ultimately determining the quality of healing[15]. The delayed epithelial closure observed in the −EAA group is thought to be associated with the reduced proliferation and migration of epithelial cells and fibroblasts. Leucine promotes cell proliferation, while arginine and lysine are essential for collagen synthesis and crosslinking formation[16,17]. Deficiencies in these EAAs likely impede smooth epithelial tissue migration and inhibit granulation tissue maturation and stable regeneration.

Furthermore, the healing and regeneration of periodontal tissues are generally known to be inhibited by inflammatory responses caused by bacterial pathogens and other factors[18,19]. The persistent inflammatory cell infiltration observed in the −EAA group is a significant finding, indicating the stagnation of gingival tissue healing and a tendency toward chronic inflammation.

Furthermore, the lack of collagen fiber formation was noteworthy. The proliferation of collagen fibers is essential for the maturation of connective tissue during periodontal tissue healing[20]. In the +EAA group, the proliferation and alignment of collagen fibers were observed, progressing toward mature connective tissue.

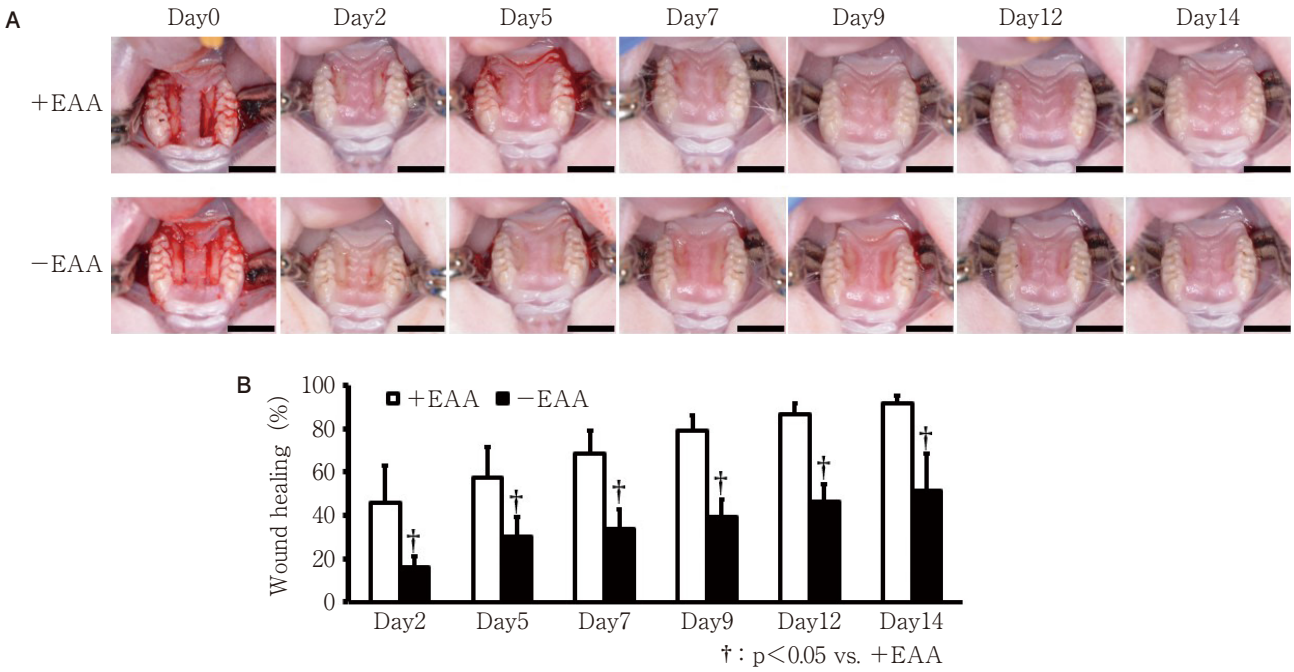

Fig. 3 Effect of essential amino acid supplementation on temporal changes in the wound healing area of gingival connective tissue

(A) Macroscopic evaluation of gingival connective tissue wound closure at postoperative days 0, 2, 5, 7, 9, 12, and 14. Scale bar: 5 mm.

(B) Quantification of wound healing area via ImageJ analysis of images obtained via single-lens reflex camera photography. A significant decrease compared with the +EAA group is denoted as †: $p<0.05$. Each experiment was performed three times for statistical analysis (n=5).

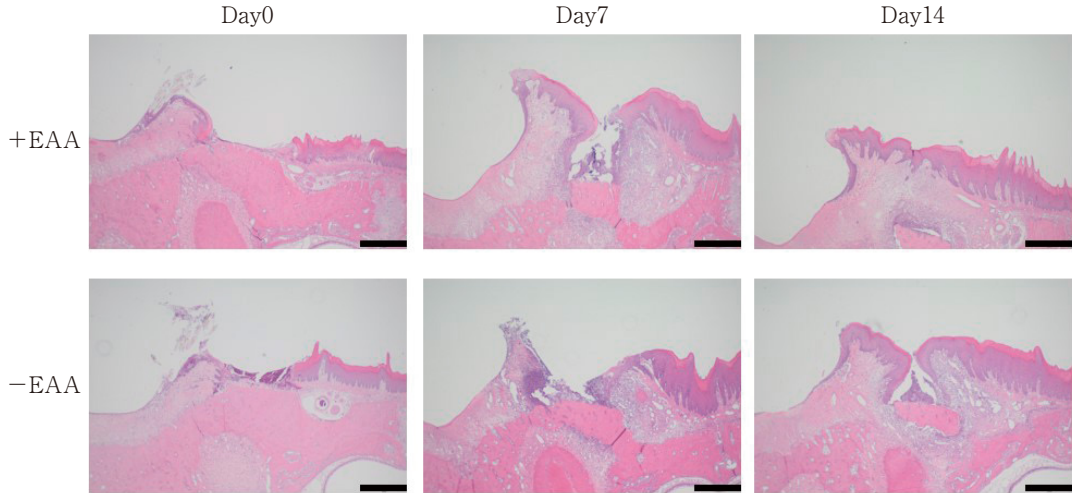

Fig. 4 Effect of essential amino acid supplementation on gingival tissue wound healing H-E staining

Magnification×40. Scale bar: 500 μm.

In contrast, collagen fiber proliferation was relatively reduced in the −EAA group. Consequently, the wound site failed to acquire fibrous strength, suggesting a significant difference not only in the speed but also in the quality of healing itself. Failure to achieve qualitative maturation of the connective tissue may lead to instability in gingival tissue wound healing and an increased risk of recurrence.

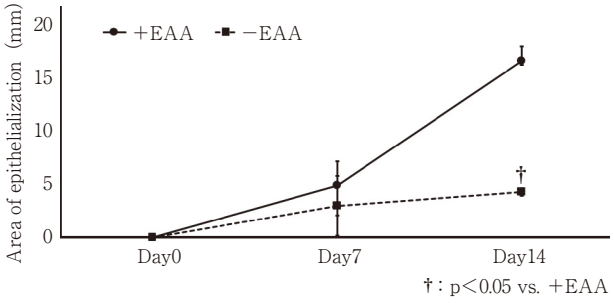

Fig. 5 Effect of essential amino acid supplementation on epithelialization of rat gingival wounds

Quantification of the epithelialization area was performed using ImageJ software. Data are shown as mean±standard deviation (n=5). A significant decrease compared with the +EAA group is denoted as †: p＜0.05.

This novel finding demonstrated that EAA deficiency inhibits multiple processes involved in gingival tissue wound healing, including epithelialization, connective tissue formation, and inflammation control. Particularly noteworthy is the finding that EAA deficiency not only profoundly results in delayed healing but also significantly affects the quality of healing itself, representing a novel finding in conventional periodontal research. Thus, this study provides new insights into the association between periodontal tissue healing and nutritional status.

EAA deficiency suggests that systemic nutritional status, alongside local treatment, plays a major role in promoting favorable postoperative healing in clinical procedures dependent on periodontal tissue healing, such as periodontal surgery and implant therapy. Future studies should explore the potential of nutritional interventions, including EAAs, to promote wound healing after periodontal surgery.

Conclusions

The results clearly demonstrate that wound healing in rat gingival tissue is inhibited under conditions of EAA deficiency. Therefore, the presence or absence of EAAs may influence gingival tissue healing.

Conflict of interest

The authors declare no conflicts of interest associated with this manuscript.

Acknowledgements

The authors would like to thank Dr. Masato Nakagawa and Dr. Yutian Wang, Osaka Dental University, Department of Oral Anatomy, for providing technical instructions regarding the animal experiments. This study was partially supported by Grants-in-Aid for Scientific Research from the Japan Society for the Promotion of Science (C) (23K19761 and 24K12922).

References

1) Sculean A, Gruber R, Bosshardt DD. Soft tissue wound healing around teeth and dental implants. J Clin Periodontol 2014; 41 Suppl 15: S6–S22.
2) Chen FM, Jin Y. Periodontal tissue engineering and regeneration: current approaches and expanding opportunities. Tissue Eng Part B Rev 2010; 16: 219–255.
3) Ercoli C, Tarnow D, Poggio CE, Tsigarida A, Ferrari M, Caton JG, Chochlidakis K. The relationships between tooth-supported fixed dental prostheses and restorations and the periodontium. J Prosthodont 2021; 30: 305–317.
4) Cortellini P, Tonetti MS. Clinical concepts for regenerative therapy in intrabony defects: surgical techniques and outcome measures. Periodontol 2000 2015; 68: 282–307.
5) Needleman I, McGrath C, Floyd P, Biddle A. Impact of oral health on the life quality of periodontal patients. J Clin Periodontol 2004; 31: 454–457.
6) Naruishi K. Biological roles of fibroblasts in periodontal diseases. Cells 2022; 11: 3345.
7) Chang HY, Chi JT, Dudoit S, Bondre C, Rijn MVD, Botstein D, Brown PO. Diversity, topographic differentiation, and positional memory in human fibroblasts. Proc Natl Acad Sci USA 2002; 99: 12877–12882.
8) Kelly B, Pearce EL. Amino assets: How amino acids support immunity. Cell Metab 2020; 32: 154–175.
9) Kamei Y, Hatazawa Y, Uchitomi R, Yoshimura R, Miura S. Regulation of skeletal muscle function by amino acids. Nutrients 2020; 12: 261.
10) Corsetti G, D'Antona G, Saverio F, Rezzani R. Topical application of dressing with amino acids improves cutaneous wound healing in aged rats. Acta Histochem 2010; 112: 497–507.
11) Enomoto T. The effects of protein-free diet on the hearing of skin incision suture wounds in rats-with special reference to weight, blood components, tensile strength and histopathological findings for different postoperative feeding starting times. J Nihon Univ Sch Dent 1987; 61: 429–438.
12) Yokogawa T. The effects of hypoproteinemia on the skin

incision suture wounds in rats—with special reference to changes in time lapse of their tensile strength of the tissue. J Oral Sci 1984; 58: 467–485.
13) Yoshimura K, Kato H, Azuma H, Nakata T, Takahashi T, Umeda M. Biological impacts of essential amino acid deficiency on human gingival fibroblast. J Hard Tissue Biol 2025; 34: 29–34.
14) Kominato H, Takeda K, Mizutani K, Mikami R, Kido D, Buranasin P, Saito N, Takemura S, Nakagawa K, Nagasawa T, Iwata T. Metformin accelerates wound healing by Akt phosphorylation of gingival fibroblasts in insulin-resistant prediabetes mice. J Periodontol 2022; 93: 256–268.
15) Smith PC, Cáceres M, Martínez C, Oyarzún A, Martínez J. Gingival wound healing: an essential response disturbed by aging? J Dent Res 2015; 94: 395–402.
16) Fujiwara T, Kanazawa S, Ichibori R, Tanigawa T, Magome T, Shingaki K, Miyata S, Tohyama M, Hosokawa K. L-arginine stimulates fibroblast proliferation through the GPRC6A-ERK1/2 and PI3K/Akt pathway. PLoS One 2014; 20: e92168.
17) Gonçalves EM, Gomes-Marcondes MC. Leucine affects the fibroblastic Vero cells stimulating the cell proliferation and modulating the proteolysis process. Amino Acids 2010; 38: 145–153.
18) Ren F, Zheng S, Luo H, Yu X, Li X, Song S, Bu W, Sun H. Fibroblast-derived C3 promotes the progression of experimental periodontitis through macrophage M1 polarization and osteoclast differentiation. Int J Oral Sci 2025; 17: 30.
19) Huang Y, Tang Y, Zhang R, Wu X, Yan L, Chen X, Wu Q, Chen Y, Lv Y, Su Y. Role of periodontal ligament fibroblasts in periodontitis: pathological mechanisms and therapeutic potential. J Transl Med 2024; 22: 1136.
20) Smith A, Martínez SE, Martínez G, McCulloch CA. Role of fibroblast populations in periodontal wound healing and tissue remodeling. Front Physiol 2019; 10: 270.

Original Article

ODEP 5 (1) : 61～69, 2025

Investigation of the Impact of Rheumatoid Arthritis on Pulp Healing Following Direct Pulp Capping

Masahito YAMANE, Kazuhiro ITONAGA, Shiori YAMAZAKI,
Nobuyuki TANI-ISHII and Noriko MUTOH

Department of Endodontics, Kanagawa Dental University

Abstract

Purpose: Rheumatoid arthritis (RA) is an autoimmune disease characterized by chronic inflammation and systemic immune dysregulation, which are induced by an exaggerated immune response against self-antigens. Although the involvement of autoimmune disease in pulpitis and periodontitis pathogenesis has been reported, the effects of autoimmune diseases on the healing process remain poorly understood. This study aimed to elucidate the influence of autoimmunity on pulp healing following direct pulp capping using a murine model of RA.

Methods: Female SKG mice (RA model, n=24) and BALB/c mice (controls, n=24) were subjected to direct pulp capping with mineral trioxide aggregate (MTA) on the maxillary first molars following pulp exposure at 8 weeks old. Histological analyses of hematoxylin-eosin staining, nestin immunostaining, terminal deoxynucleotidyl transferase dUTP nick-end labeling, and macrophage marker (i.e., F4/80 and CD206) staining were performed at 7 and 14 days post-treatment.

Results: All data were statistically analysis by the Kolmogorov-Smirnov test, ANOVA and Tukey test ($p < 0.05$). Compared with BALB/c mice, SKG mice exhibited sustained inflammatory cell infiltration, persistent necrosis, lower nestin expression indicative of suppressed odontoblast regeneration, and higher levels of apoptosis. Macrophage polarization skewed toward a pro-inflammatory M1-like phenotype, with delayed recruitment of F4/80- and CD206-positive cells, which were significantly more abundant by day 14.

Conclusions: Immune dysregulation associated with RA may contribute to prolonged inflammation, impaired apoptotic clearance, and suppressed tissue regeneration in the dental pulp, ultimately disrupting the healing process after direct pulp capping.

Key words: dental pulp, apoptosis, pulpitis, direct pulp capping, rheumatoid arthritis

Corresponding author: Noriko MUTOH, Division of General Dentistry 1, The Nippon Dental University Hospital, 2-3-16, Fujimi, Chiyoda-ku, Tokyo 102-8158, Japan

TEL: +81-3-3261-4041, E-mail: mutoh77@tky.ndu.ac.jp

Received for Publication: September 15, 2025/Accepted for Publication: December 1, 2025

DOI: 10.11471/odep.2025-007

Introduction

Endodontic treatment aims to restore and maintain the health of the dental pulp in cases of hard tissue disease, thereby preventing the onset of pulpal pathology. When pulpal disease becomes irreversible, the affected pulp is removed to prevent the development of apical periodontitis, and thorough root canal treatment is performed to eliminate the cause of infection and to restore the health of the periapical tissues. Ultimately, the goal of endodontic treatment is to preserve teeth in a healthy and functional state within the oral cavity[1]. Beyond the local effects, progression of root canal infection may allow microorganisms and their by-products to disseminate into the systemic circulation, potentially contributing to various systemic infections. Elevated levels of inflammatory cytokines, including interleukin-6 (IL-6), tumor necrosis factor-alpha (TNF-α), and C-reactive protein (CRP), have been associated with exacerbation of systemic conditions such as cardiovascular disease and diabetes mellitus. Therefore, appropriate endodontic treatment that eradicates local infections may play a role in reducing systemic inflammatory burden[2].

Vital pulp therapy (VPT) is critical in preserving the physiological functions of the dental pulp and supporting mastication[3]. In patients with systemic diseases, particular attention is required when performing invasive dental procedures, underscoring the importance of VPT in caries treatment[4,5]. Previous studies using wild-type Wistar rats demonstrated that direct pulp capping with mineral trioxide aggregate (MTA) for deep caries results in mild inflammatory and necrotic changes beneath the exposure site, followed by the initiation of calcific bridge formation within 7 days[6]. Autoimmune diseases such as type 1 diabetes mellitus and rheumatoid arthritis (RA) can disrupt local inflammatory responses owing to systemic immune dysfunction, which may affect tissue healing. For instance, in type 1 diabetes, chronic inflammation induced by hyperglycemia alters immune pathways through adipocytes[7]. It has also been reported that macrophages are excessively activated upon infection in patients with autoimmune diseases, leading to exacerbated inflammatory responses[8]. In RA, chronic inflammation is sustained by dysregulated immune cell activity and aberrant cytokine production[9].

Our previous work showed that bacterial infection of the pulp in various autoimmune disease models results in prolonged inflammation[10,11]. The SKG mouse, an RA model, harbors a point mutation in the ZAP-70 gene, leading to impaired T cell receptor signaling and Th17-mediated autoimmunity induction. These mice do not spontaneously develop disease under specific pathogen-free conditions but exhibit arthritis upon administration of β-glucan[12]. Recent studies have revealed that pulpitis healing is delayed and apical periodontitis is prolonged in SKG mice compared with wild-type controls, likely owing to impaired macrophage function and lower levels of apoptosis[10].

However, the pathological features of pulpitis and the dentin regeneration process following VPT in the context of RA remain largely unexplored. The objective of this study was to investigate the histopathological changes in inflamed pulp tissue following direct pulp capping in SKG mice, with the aim of elucidating how RA influences the pulp healing process.

Materials and Methods

1. Dental cavity preparation and direct pulp capping

Five-week-old female RA model mice (SKG mice; experimental group, n=24) and mice with normal immune function (BALB/c mice; control group, n=24) were used in this study. A pronounced sex difference has been observed in the incidence of RA, with women being affected approximately three times more frequently than men. Furthermore, it has been suggested that female sex hormones may contribute to disease onset by activating immune cells. Therefore, in the present study, female mice were used to facilitate a detailed analysis of disease-related inflammatory responses and immune cell activation in this RA model[13]. SKG mice and BALB/c mice were purchased from Japan CLEA (Tokyo, Japan). At 6 weeks old, SKG mice received an intraperitoneal injection of laminarin (30 mg in 0.3 mL of 100 mg/mL solution), a β-glucan used to induce arthritis. At 8 weeks old, mice were anesthetized intraperitoneally with a mixture of medetomidine (0.75 mg/kg; Fujifilm Wako Pure Chemical, Osaka, Japan), midazolam (4 mg/kg; Sandoz, Tokyo, Japan), and butorphanol tartrate (5 mg/kg; Fujifilm Wako Pure Chemical). All

instruments were sterilized in an autoclave, and sterilized cotton pellets and gauze were used throughout the procedure. Using water cooling and a stereomicroscope (Olympus SZ61 stereomicroscope, Tokyo, Japan, zoom range 6.7×to 45×), we mechanically exposed the occlusal surfaces of the bilateral maxillary first molars using an air turbine handpiece equipped with a tungsten 1/4 round carbide bur (Φ 0.5 mm) thereby establishing a pulp exposure model. The cavity was prepared to a depth corresponding to half the diameter of a bur. Pulp exposure was confirmed by stereomicroscope and #15 K-file[10, 14]. All groups received direct pulp capping with MTA (ProRoot MTA, Dentsply Sirona)[15]. Placement of MTA and subsequent sealing were also carried out under a stereomicroscope. The sealing with glass ionomer cement was applied using an explorer, carefully avoiding the inclusion of air bubbles. All experimental protocols were approved by the Animal Ethics Committee of Kanagawa Dental University (approval number: 23-017).

2. Tissue preparation

Samples were collected from SKG mice (n=12) and control mice (n=12) at 7 and 14 days after pulp capping. Mice were deeply anesthetized using the same anesthetic regimen described above. After intracardiac perfusion with physiological saline, fixation was performed with 4% paraformaldehyde in phosphate buffer (Fujifilm Wako Pure Chemical). Maxillary bones were harvested and immersed in the same fixative at 4℃ for 24 hours. The specimens were then decalcified in 0.5 mol/L ethylenediaminetetraacetic acid for 3 weeks, embedded in paraffin, and sectioned at a 4-μm thickness[10].

3. Histopathological analysis

1) Histological assessment of pulp tissue

Time-course changes in the pulp tissue were evaluated based on the extent of polymorphonuclear leukocyte (PMN) infiltration. Hematoxylin-eosin staining was used to assess the progression of pulpitis and necrotic areas. PMN counts were measured using ImageJ software (version 1.53e, NIH, Bethesda, MD, USA)[10,16].

2) Analysis of odontoblast activity via nestin immunostaining

Odontoblast activity was evaluated via nestin immunostaining. After deparaffinization, sections were incubated with a primary monoclonal anti-rat nestin antibody (MilliporeSigma, St. Louis, MO, USA; 1：200, MAB353), followed by processing with the EnVision system (Dako Japan, Tokyo, Japan) as the secondary antibody. Visualization was performed with 3,3′-diaminobenzidine (DAB; Dojindo, Tokyo, Japan), and counterstaining was performed with Carazzi hematoxylin. Nestin-positive areas along the dentin-pulp border in the coronal pulp were quantified using ImageJ[10,11,16].

3) Analysis of macrophage dynamics

To evaluate macrophage dynamics, we performed immunostaining for F4/80 (M1 and M2 macrophages) and CD206 (M2 macrophages). Sections were incubated with the primary antibodies anti-F4/80 (Novus Biologicals, Centennial, CO, USA; 1：250, NB600-404) and anti-CD206 (Abcam, Tokyo, Japan; 1：1000, ab64693), and incubated with secondary antibody EnVision FLEX-IgG (Dako Japan). Staining was visualized with DAB (Fujifilm Wako Pure Chemical). The percentage of positive staining at the dentin-pulp interface was quantified using ImageJ[16,17].

4) Analysis of apoptotic cells by terminal deoxynucleotidyl transferase dUTP nick-end labeling assay

We detected apoptotic cells in the pulp tissue via terminal deoxynucleotidyl transferase dUTP nick-end labeling (TUNEL) assay. After they were subjected to deparaffinization and antigen retrieval with recombinant proteinase K (Ambion, Austin, TX, USA; 1：100, AM2548), sections were stained using the ApopTag Peroxidase In Situ Apoptosis Detection Kit (Millipore, Billerica, MA, USA; S7100), and visualized with DAB. The area containing TUNEL-positive cells was quantified using ImageJ[10,11,16].

5) Statistical analysis

All data were expressed as means±standard errors. Normality was assessed using the Kolmogorov-Smirnov test, and one-way analysis of variance (ANOVA) was first applied. Intergroup comparisons were analyzed using the Tukey test. Statistical significance was set at $p<0.05$. Analyses were performed using SPSS software (version 26; IBM, Tokyo, Japan).

Results

1. Histopathological changes in pulp tissue

The histological findings from the MTA-treated group are shown in Figures 1-a and c, and those from the control group in Figures 1-b and d. Seven days after direct pulp capping, the experimental group showed inflammatory cell infiltration predominantly composed

of PMNs immediately beneath the capping site. The underlying pulp tissue exhibited partial loss of vascular structures and the odontoblast layer (Fig. 1-a). In the control group, the number of inflammatory cells was lower than in the experimental group; however, the inflammatory infiltrate extended beyond the area beneath the cavity floor and was widely distributed throughout the pulp chamber (Fig. 1-b). At day 14, the experimental group still exhibited PMN infiltration extending from the central radicular pulp to the apical pulp (Fig. 1-c); in the control group, inflammation extended up to the middle third of the root but the apical pulp maintained normal histology (Fig. 1-d). PMN migration was observed in both groups at day 7. Although necrotic tissue was not identified at day 14, signs of pulp healing were present in both groups (Fig. 2-a).

2. Odontoblast dynamics

Nestin-positive odontoblast dynamics following direct pulp capping are shown in Figure 1-e–h. At day 7, nestin-positive cells were observed in the coronal pulp immediately beneath the capping site in both groups (Fig. 1-e, f). At day 14, positive cells were observed primarily in the apical third (Fig. 1-g, h). The proportion of nestin-positive areas relative to the entire dentin-pulp interface decreased over time in the control group but showed an increasing trend in the experimental group (Fig. 2-b).

3. Apoptotic cell dynamics

TUNEL-positive apoptotic cells are shown in Figure 1-i–l. On day 7, both groups had positive cells beneath the capping site (Fig. 1-i, j). On day 14, apoptotic cells were observed in the coronal pulp in both groups (Fig. 1-k, l). In the experimental group, the number of apoptotic cells significantly increased from day 7 to day 14, whereas in the control group it significantly decreased. Quantitative changes are shown in Figure 2-c.

4. Macrophage dynamics

Macrophage dynamics (F4/80-positive M1/M2 macrophages) are shown in Figure 1-m–p. In the experimental group, F4/80-positive cells were observed from the region beneath the capping site to the central radicular pulp at day 7, and the percentage positive for F4/80 significantly increased by day 14 (Fig. 1-m, o; Fig. 2-d). In contrast, the control group showed a significant decrease in F4/80-positive cells between 7 and 14 days (Fig. 1-n, p; Fig. 2-d).

5. M2 macrophage dynamics

CD206-positive M2 macrophages are shown in Figure 1-q–t. In the experimental group, positive cells were observed from the coronal pulp beneath the capping site to the upper third of the root pulp at day 7 and spread throughout the pulp chamber by day 14, although the difference was not statistically significant (Fig. 1-q, r; Fig. 2-e). In the control group, the number of positive cells was significantly higher than in the experimental group at day 7 but significantly lower by day 14 (Fig. 1-s, t; Fig. 2-e).

Discussion

Previous studies have demonstrated prolonged inflammation and enhanced bone resorption in the settings of pulpitis and apical periodontitis in SKG RA mice compared with immunocompetent mice, with greater PMN infiltration at the lesion site. In the present study, we investigated the influence of RA on pulp healing following direct pulp capping with MTA in SKG mice. Consistent with earlier reports, SKG mice exhibited prolonged PMN infiltration and increased apoptosis compared with BALB/c controls. This sustained inflammation was associated with damage in odontoblasts, which are a critical component of the healing process. Moreover, significant polarization shifts in macrophage phenotypes were observed in the SKG group.

Direct pulp capping aims to preserve the vitality and function of the dental pulp, particularly in cases of deep carious lesions. MTA has high biocompatibility and excellent sealing ability, with consistent reports of favorable outcomes in VPT[18]. MTA, primarily composed of tricalcium silicate and dicalcium silicate, has been widely used for direct pulp capping owing to its excellent biocompatibility and sealing ability. During the setting process, MTA undergoes hydration reactions; moreover, even after setting, the material continues to absorb moisture and gradually produces calcium hydroxide. As a result, calcium and hydroxide ions are continuously released into the surrounding environment. Furthermore, when MTA is placed in a phosphate-containing environment, the released calcium ions react with phosphate ions, leading to the formation of apatite crystals on the material surface. These physicochemical properties of MTA create a favorable environment for dentin bridge formation, modulation of pulpal

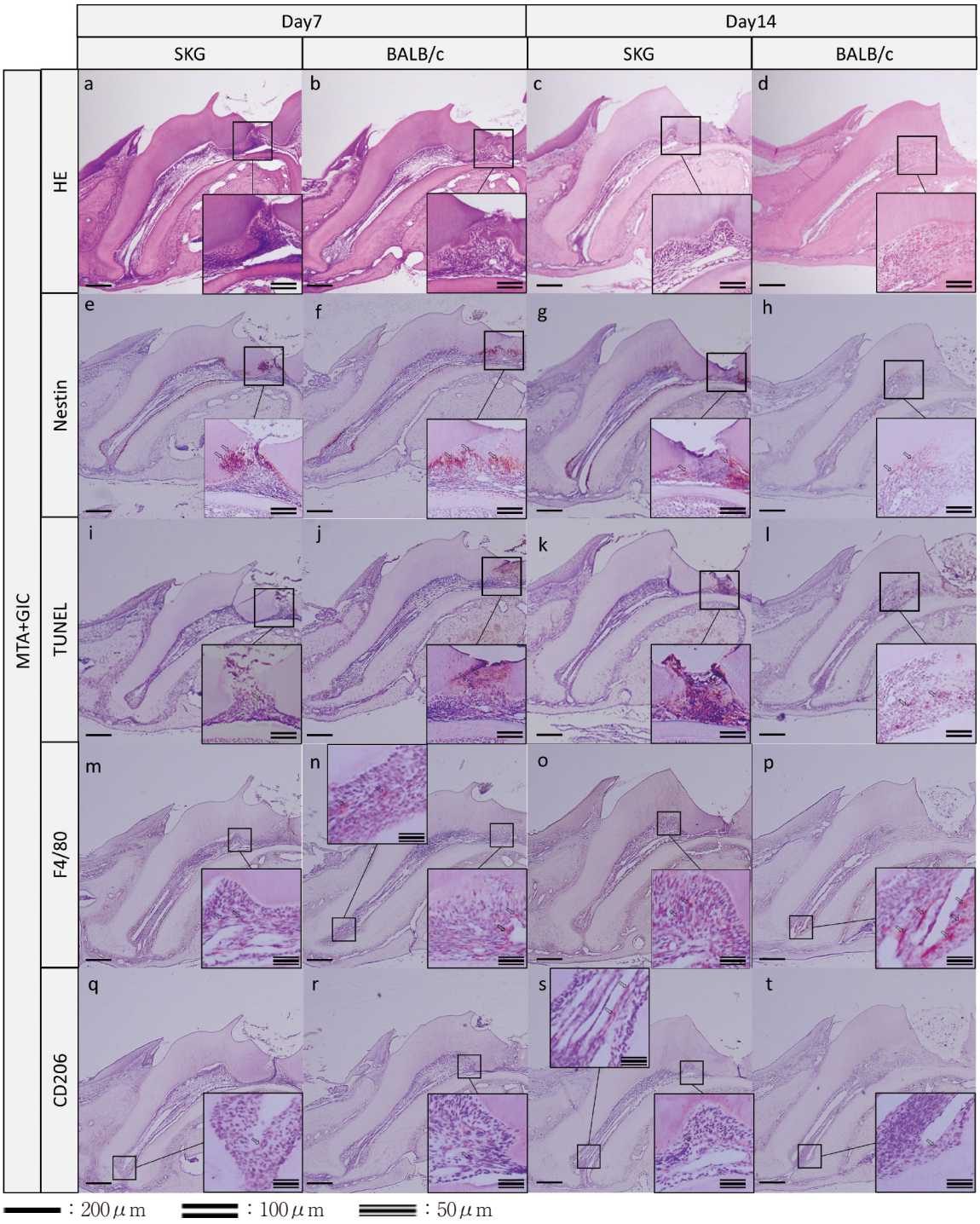

Fig. 1 Histological and immunohistochemical analysis of pulp tissue at days 7 and 14 after direct pulp capping

HE staining reveals inflammatory cell infiltration, pulp necrosis, and bone resorption in the apical region (a–d). Nestin immunostaining demonstrates the arrangement and staining intensity of odontoblasts at the dentin-pulp interface (e–h). TUNEL staining shows the distribution of apoptotic cells in the pulp and apical regions (i–l). Immunohistochemical analysis of macrophage phenotypes via F4/80 (M1 and M2 macrophages) (m–p) and CD206 (M2 macrophages) staining at 7 and 14 days post-treatment (q–t). In SKG mice, F4/80-positive cells (m, o) increased and CD206-positive cells (q, s) decreased in the pulp and apical tissues. HE, hematoxylin-eosin; TUNEL, terminal deoxynucleotidyl transferase dUTP nick-end labeling.

Scale bars: HE=200 μm and 100 μm, nestin/TUNEL=200 μm and 100 μm; macrophage markers=200 μm and 50 μm.

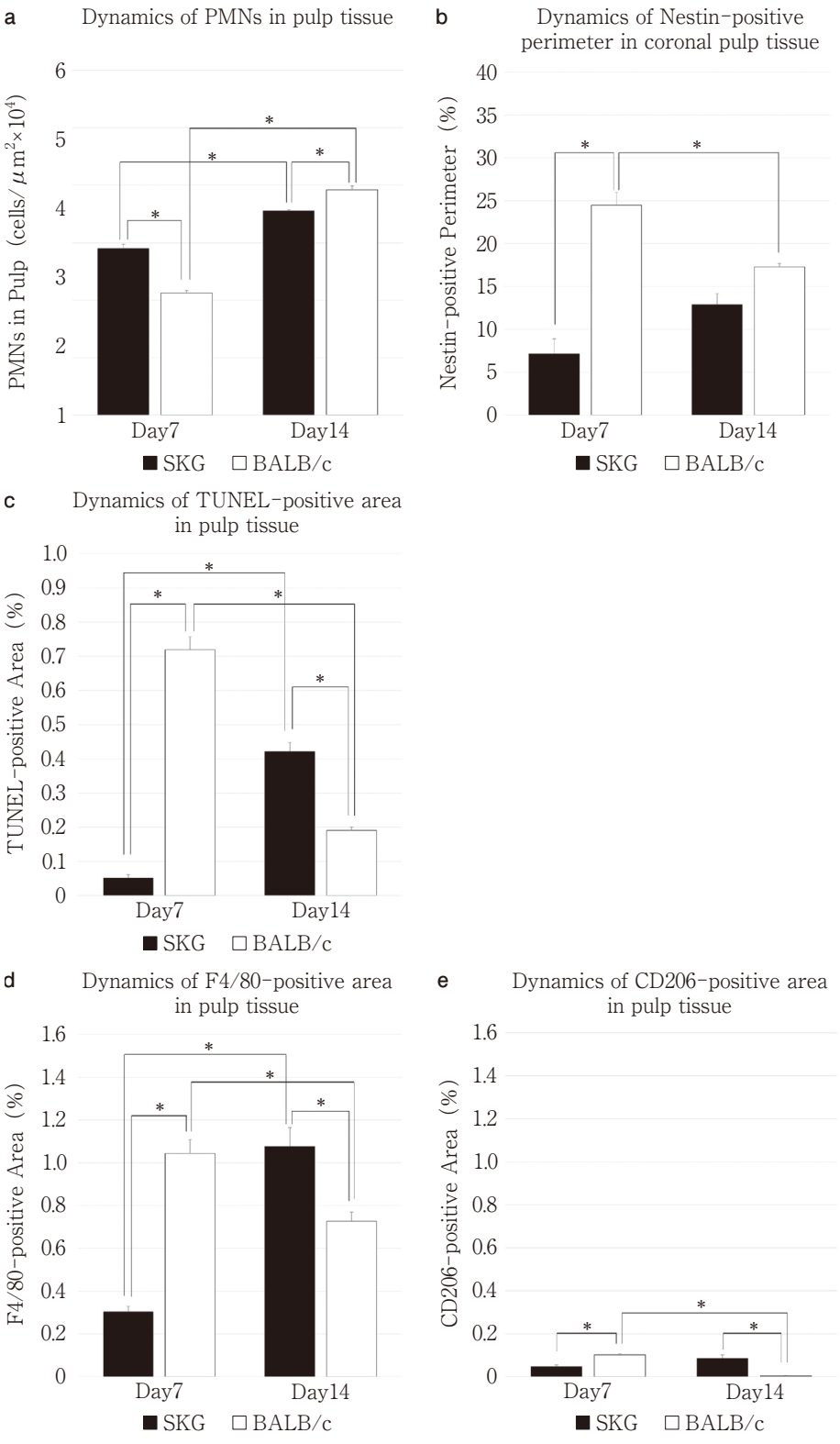

Fig. 2 Quantitative analysis of cellular dynamics (of PMNs, apoptotic cells, and odontoblasts) and inflammatory parameters (necrotic and bone resorption areas) in the pulp tissue of SKG and BALB/c mice at 7 and 14 days post-treatment

Quantification of PMNs in the pulp tissue (a), nestin-positive areas along the entire dentin-pulp border (b), TUNEL-positive apoptotic cells (c), F4/80-positive macrophages (d), and CD206-positive macrophages (e). ＊denotes significant differences between SKG and control groups ($p<0.05$). PMN, polymorphonuclear leukocyte; TUNEL, terminal deoxynucleotidyl transferase dUTP nick-end labeling.

inflammation, and recruitment of progenitor cells, thereby promoting pulp healing and regeneration[19–21]. MTA promotes early odontoblast differentiation and mineralization, typically within 7 days.

In the present study, BALB/c mice demonstrated a typical healing pattern characterized by localized inflammation in the coronal and middle radicular pulp, preservation of normal apical pulp tissue, and early odontoblast rearrangement-findings consistent with the previous literature[15]. In contrast, SKG mice exhibited persistent inflammatory cell infiltration composed predominantly of PMNs, extending to the apical pulp even at day 14. RA is characterized by aberrant activation of lymphocytes against autoantigens and chronic production of cytokines, including TNF-α, IL-6, and IL-17, which activate macrophages and induce tissue destruction. These mechanisms may also be involved in pulp inflammation in the SKG model[19,20]. The marked reduction in nestin-positive odontoblasts observed in SKG mice may reflect impaired stem cell differentiation owing to Th17-mediated immune dysregulation and autoantibody interference[21]. Increased apoptosis in the infected pulp and periapical tissues of SKG mice has also been reported[7]. In RA, dysregulation of apoptosis and efferocytosis (clearance of apoptotic cells) contributes to synovial hyperplasia and chronic inflammation[22,23]. A similar mechanism may underlie the immunopathology observed in the dental pulp. TUNEL-positive apoptotic cells are normally eliminated by macrophages; however, in autoimmune conditions, phagocytic capacity is impaired, leading to an accumulation of apoptotic debris[24,25]. In our study, the number of TUNEL-positive apoptotic cells significantly increased in SKG mice at day 14, indicating persistent inflammation accompanied by impaired clearance.

RA is also associated with macrophage activation syndrome, a condition characterized by excessive immune activation and a cytokine storm involving the overproduction of inflammatory cytokines[8]. Our analysis of macrophage dynamics and polarization showed that inflammatory F4/80-positive macrophages increased from day 7 to 14 in SKG mice; anti-inflammatory CD206-positive macrophages also increased during this period. In contrast, both F4/80- and CD206-positive cells decreased in the control group over time. In the control group, inflammation was restricted to the coronal pulp at day 7, with signs of resolution in the radicular pulp by day 14. The early migration of M2 macrophages (day 7) and their subsequent decline (day 14) were consistent with tissue healing. In SKG mice, however, the ratio of F4/80-positive to CD206-positive cells indicated a predominance of M1-type macrophage polarization, reflecting the chronic inflammatory milieu of RA and a breakdown in local immune regulation, which may hinder pulp healing[26]. In RA, impaired resolution of inflammation has been reported[10].

In the present study, which simulates a clinical situation of direct pulp capping, the extent of pulpal inflammation is assumed to be localized. It has been reported that, in SKG mice, the development of RA as a defined pathological condition becomes evident within 3 to 17 weeks after administration of β-glucan (laminarin), during which clinical signs of arthritis can be observed[27]. In the present study, because our target was the dynamics of pulp tissue from the pre-disease stage through the early phase of disease onset, the observed cellular responses occurred only at a very limited frequency. If the pathological condition were to progress further, although the healing period may be prolonged compared with that under healthy conditions, dentin bridge formation is expected to occur, and the inflammatory response is likely to subside over time. However, if the inflammatory area expands or extensive infection develops, complete resolution of inflammation may be difficult to achieve. This should be recognized as a limitation of the present study, and further investigations are warranted to clarify these aspects.

Conclusion

In conclusion, the inflammatory pathophysiology of RA may impair pulp healing following direct pulp capping. These findings suggest the need to consider prolonged inflammation and impaired healing in patients with autoimmune diseases undergoing VPT.

Acknowledgments

We thank Amanda Holland, PhD, from Edanz (https://jp.edanz.com/ac) for editing a draft of this manuscript.

Conflicts of Interest

There are no conflicts of interest to disclose regarding this study.

References

1) Kyaw MS, Kamano Y, Yahata Y, Tanaka T, Sato N, Toyama F, Noguchi T, Saito M, Nakano M, Harada F, Saito M. Endodontic regeneration therapy: current strategies and tissue engineering solutions. Cells 2025; 14: 422.
2) Gomes MS, Hugo FN, Hilgert JB, Sant'Ana Filho M, Padilha DMP, Simonsick EM, Ferrucci L, Reynolds MA. Apical periodontitis and incident cardiovascular events in the Baltimore Longitudinal Study of Aging. Int Endod J 2016; 49: 334–342.
3) Moretto C, Kopper PMP, Münchow EA, Scarparo RK. Association between patient age and vital pulp therapy outcomes: a systematic review and meta-analysis of prognostic studies. Int Endod J 2025; 58: 809–832.
4) Cushley S, Duncan HF, Lundy FT, Nagendrababu V, Clarke M, El Karim I. Outcomes reporting in systematic reviews on vital pulp treatment: a scoping review for the development of a core outcome set. Int Endod J 2022; 55: 891–909.
5) Tong HJ, Seremidi K, Stratigaki E, Kloukos D, Duggal M, Gizani S. Deep dentine caries management of immature permanent posterior teeth with vital pulp: a systematic review and meta-analysis. J Dent 2022; 124: 104214.
6) Ohkura N, Edanami N, Takeuchi R, Tohma A, Ohkura M, Yoshiba K, Ida-Yonemochi H, Ohshima H, Okiji T, Noiri Y. Effect of pulpotomy using mineral trioxide aggregate on prostaglandin transporter and receptors in rat molars. Sci Rep 2017; 7: 6870.
7) Baldeon-Gutierrez R, Ohkura N, Yoshiba K, Yoshiba N, Tohma A, Takeuchi R, Belal RSI, Edanami N, Takahara S, Gomez-Kashimoto S, Ida T, Noiri Y. Wound-healing processes after pulpotomy in the pulp tissue of type 1 diabetes mellitus model rats. J Endod 2024; 50: 196–204.
8) Cope AP. Exploring the reciprocal relationship between immunity and inflammation in chronic inflammatory arthritis. Rheumatology (Oxford) 2003; 42: 716–731.
9) Talal N, Flescher E. Rheumatoid arthritis: an editorial perspective based on cytokine imbalance. J Autoimmun 1988; 1: 309–317.
10) Yamazaki S, Hayashi R, Mutoh N, Ohshima H, Tani-Ishii N. Effects of rheumatoid arthritis on the progression of pulpitis and apical periodontitis in SKG mice. J Endod 2023; 49: 1501–1507.
11) Hayashi R, Yamazaki S, Mutoh N, Hashimoto T, Ohshima H, Tani-Ishii N. Influence of IgA nephropathy on the progression of pulpitis and apical periodontitis in HIGA mice. J Oral Biosci 2024; 66: 98–104.
12) Napier RJ, Lee EJ, Vance EE, Snow PE, Samon KA, Dawson CE, Moran AE, Stenzel P, Davey MP, Sakaguchi S, Rosenzweig HL. Nod2 deficiency augments Th17 responses and exacerbates autoimmune arthritis. J Immunol 2018; 201: 1889–1898.
13) Oliver JE, Silman AJ. Why are women predisposed to autoimmune rheumatic diseases? Arthritis Res Ther 2009; 11: 252.
14) Song M, Kim S, Kim T, Park S, Shin KH, Kang M, Park NH, Kim R. Development of a direct pulp-capping model for the evaluation of pulpal wound healing and reparative dentin formation in mice. J Vis Exp 2017; 12: 54973.
15) Xu D, Mutoh N, Ohshima H, Tani-Ishii N. The effect of mineral trioxide aggregate on dental pulp healing in the infected pulp by direct pulp capping. Dent Mater J 2021; 40: 1373–1379.
16) Itonaga K, Yamane M, Yamazaki S, Tani-Ishii N, Mutoh N. Investigation of dentin regeneration via neurotransmitters and innate immune regulation during pulp healing. ODEP 2024; 4: 46–53.
17) Sano H, Nakakura-Ohshima K, Quispe-Salcedo A, Okada Y, Sato T, Ohshima H. Intentionally perforating the pulp chamber floor promotes M2 macrophage polarization in the dental pulp following tooth replantation in mice. J Oral Biosci 2025; 67: 100681.
18) Ashouri JF, Hsu LY, Yu S, Rychkov D, Chen Y, Cheng DA, Sirota M, Hansen E, Lattanza L, Zikherman J, Weiss A. Reporters of TCR signaling identify arthritogenic T cells in murine and human autoimmune arthritis. Proc Natl Acad Sci USA 2019; 116: 18517–18527.
19) Okiji T, Yoshiba K. Reparative dentinogenesis induced by mineral trioxide aggregate: A review from the biological and physicochemical points of view. Int J Dent 2009; 2009: 464280.
20) Parirokh M, Torabinejad M. Mineral trioxide aggregate: A comprehensive literature review—Part III: Clinical applications, drawbacks, and mechanism of action. J Endod 2010; 36: 400–413.
21) Camilleri J. Characterization of hydration products of mineral trioxide aggregate. Int Endod J 2008; 41; 408–417.
22) Shiomi A, Usui T, Ishikawa Y, Shimizu M, Murakami K, Mimori T. GM-CSF but not IL-17 is critical for the development of severe interstitial lung disease in SKG mice. J Immunol 2014; 193: 849–859.
23) González MA, Gonzalez-Rey E, Rico L, Büscher D, Delgado M. Treatment of experimental arthritis by inducing immune tolerance with human adipose-derived mesenchymal stem cells. Arthritis Rheum 2009; 60: 1006–1019.
24) Kotake S, Nanke Y, Kawamoto M, Yago T, Udagawa N, Ichikawa N, Kobashigawa T, Saito S, Momohara S, Kamatani N, Yamanaka H. T-cell leukemia translocation-associated gene (TCTA) protein is required for

human osteoclastogenesis. Bone 2009; 45: 627–639.
25) Raptopoulou AP, Bertsias G, Makrygiannakis D, Verginis P, Kritikos I, Tzaedi M, Klareskog L, CatrinaAI, Sidiropoulos P, Boumpas DT. The programmed death 1/programmed death ligand 1 inhibitory pathway is up-regulated in rheumatoid synovium and regulates peripheral T-cell responses in human and murine arthritis. Arthritis Rheum 2010; 62: 1870–1880.
26) Perlman H, Georganas C, Pagliari LJ, Koch AE, Hained 3rd K, Pope RM. Bcl-2 expression in synovial fibroblasts is essential for maintaining mitochondrial homeostasis and cell viability. J Immunol 2000; 164: 5227–5235.
27) Yoshitomi H, Sakaguchi N, Kobayashi K, Brown GD, Tagami T, Sakihama T, Hirota K, Tanaka S, Nomura T, Miki I, Gordon S, Akira S, Nakamura T, Sakaguchi S. A role for fungal β-glucans and their receptor Dectin-1 in the induction of autoimmune arthritis in genetically susceptible mice. J Exp Med 2005; 201: 949–960.

Case Report

ODEP 5 (1) : 70～76, 2025

Severe Root Resorption with Pulp Fibrosis Despite Normal Responses to Pulp Sensibility Tests: A Case Report

Daisuke TAKEGAWA, Yoshihito NAITO[1], Koichi KANI[2], Takaaki TSUNEMATSU[3], Hitomi KURAMOTO[4] and Tadashi NAKANISHI

Department of Conservative Dentistry, Tokushima University Graduate School of Biomedical Sciences
[1]Sweden Dental Clinic Kokufu
[2]Department of Oral Medicine, Tokushima University Graduate School of Biomedical Sciences
[3]Department of Oral Pathology, Tokushima University Graduate School of Biomedical Sciences
[4]Department of Pediatric Dentistry, Tokushima University Graduate School of Biomedical Sciences

Abstract

Purpose: We report a rare case of atypical external root resorption in the mid-root region of a mandibular molar following direct pulp capping(DPC), despite the tooth consistently exhibiting normal responses to pulp sensibility tests. We discuss the diagnostic challenges presented by such cases, focusing on the limitations of conventional pulp testing, the potential role of pathological pulp fibrosis, and the importance of cone-beam computed tomography (CBCT) in early detection and accurate diagnosis.

Case: A 38-year-old male patient presented with a chief complaint of chronic discomfort and distal gingival swelling in the right mandibular second molar. The tooth had undergone DPC with calcium hydroxide nine years earlier due to pulp exposure following complete caries removal. Clinical examination revealed mild gingival swelling and slight tenderness to percussion, with normal periodontal probing depths. The electric pulp test (EPT) and cold test showed normal responses, which were consistent with the results from a previous visit six years earlier. A dental radiograph taken six years earlier showed no abnormalities; however, comparison with the radiograph obtained at presentation revealed extensive external root resorption localized to the mid-root area of the mesial root. CBCT images confirmed that the resorption had perforated the dentin and reached the pulp chamber, accompanied by substantial loss of lingual alveolar bone. The prognosis was ultimately deemed poor, and the tooth was extracted. The extracted tissue was subjected to histopathological examination using hematoxylin and eosin staining. Histopathological analysis revealed extensive fibrosis in the pulp tissue without bacterial infection. In addition, chronic inflammatory granulation tissue, mainly with neutrophil infiltration, was observed in the area of external root resorption.

Discussion: This case highlights the limitations of relying solely on pulp sensibility tests for assessing pulp health. Especially in teeth with a history of DPC and chronic symptoms, underlying pathological changes, such as fibrosis, may not alter nerve responses until later stages. Atypical external root resorption can occur secondary to these changes, potentially progressing significantly without typical symptoms or radiographic signs on conventional 2D imaging. CBCT proved useful for identifying the precise location, extent, and perforation of the resorption lesion, underscoring its value in diagnosing complex endodontic-periodontal conditions.

Conclusion: Early use of CBCT should be considered in teeth with persistent symptoms after DPC, even in patients with normal pulp sensibility tests results, to facilitate timely diagnosis and appropriate management.

Key words: root resorption, electric pulp test (EPT), cone-beam computed tomography (CBCT)

Corresponding author: Daisuke TAKEGAWA, Department of Conservative Dentistry, Tokushima University Graduate School of Biomedical Sciences, 3-18-15, Kuramoto-cho, Tokushima 770-8504, Japan
TEL: 088-633-7340, FAX: 088-633-9127, E-mail: d-takegawa@tokushima-u.ac.jp
Received for Publication: July 3, 2025/Accepted for Publication: October 1, 2025
DOI: 10.11471/odep.2025-008

Introduction

Root resorption is a pathological condition where the hard tissues of a tooth are resorbed by osteoclast-like cells. In permanent teeth, it is broadly classified into internal resorption and external resorption. Internal resorption involves the resorption of dentin from the pulp side and is categorized into inflammatory and replacement types. External resorption, on the other hand, originates from the periodontal ligament side and is subclassified into surface resorption, inflammatory resorption, and replacement resorption[1]. Among these, external inflammatory resorption is triggered by the activation of osteoclasts due to bacterial toxins leaking through the apical foramen following pulp necrosis or root canal infection, leading to rapid destruction of dentin and cementum. High concentrations of proinflammatory cytokines, such as IL-1α and TNF-α, are expressed at the lesion site, with IL-1α being considered a promising early biomarker for external resorption after trauma[2].

Early diagnosis is the most critical factor influencing the prognosis of root resorption. However, external resorption often progresses asymptomatically; thus, the lesion may already be advanced by the time the patient reports symptoms, making clinical detection of initial lesions difficult[3]. Traditionally, dental radiographic images have been used for diagnosing root resorption, but their accuracy is limited for small lesions or those obscured by complex anatomical structures. The advent of cone-beam computed tomography (CBCT) has significantly improved the detection sensitivity of minute resorption lesions using three-dimensional imaging. Experimental models have reported that minute lesions detected at a rate of about 35% with dental radiography showed an increased detection rate of 47% with CBCT, and for smaller lesions specifically, the detection rate reached 96% with CBCT[4]. Thus, the use of CBCT is recommended for early diagnosis and accurate assessment of the pathological state of root resorption lesions[1].

As the condition of the dental pulp is deeply involved in the progression of root resorption, accurate diagnosis of the pulp status is necessary. Clinically, pulp sensibility tests, such as the electric pulp test (EPT) and cold test, are used. However, these assess the sensory response of nerves and do not directly evaluate the actual vitality or blood flow status of the pulp[5]. Regarding the diagnostic accuracy of pulp sensibility tests, the cold test is reported to have a sensitivity of approximately 83% and specificity of approximately 93%, whereas EPT has a sensitivity of about 72%. Both tests are known to have false-negative and false-positive results[6]. Especially in elderly patients or teeth with a history of trauma, calcification or fibrosis within the pulp space can progress, often leading to false-negative results (negative response despite vital pulp)[7]. False-positive results can also occur due to stimulus conduction through dental restorative materials or to adjacent teeth, even in non-vital teeth[5]. Therefore, sensibility tests have limitations in pulp diagnosis. Recently, methods for measuring pulp blood flow, such as laser Doppler flowmetry and pulse oximetry, have been proposed to overcome these limitations. These methods can assess the physiological vitality of the pulp with higher accuracy than sensibility tests and are gaining attention as auxiliary tools to enhance diagnostic precision[8].

Direct pulp capping (DPC) is a commonly employed pulp preservation technique in which exposed pulp tissue is covered with a medicament to maintain its vitality. The treatment aims to reduce inflammation at the exposure site and form a dentin bridge, preserving the pulp[9]. The success rate of DPC varies greatly depending on the cause of exposure and the infection status of the pulp. While it shows a high success rate (about 92%) for healthy accidental exposures, the success rate is lower (about 33%) in cases of carious exposure[10]. Clinically, even without infection after DPC, chronic aseptic inflammation or pathological fibrosis may progress within the pulp, leading to a long-term decrease in pulp responsiveness or transition to necrosis in some cases[11]. Moreover, if micro-infection or microleakage persists after capping, chronic inflammation can continue, ultimately increasing the risk of pulp necrosis and periapical lesions[12].

Pulp diagnosis, monitoring temporal changes in the pulp after DPC, and diagnosing root resorption present complex challenges that often complicate clinical decision-making. Herein, we present a rare case where, following DPC with calcium hydroxide after complete caries removal and pulp exposure, the tooth maintained normal pulp sensibility responses for an extended

Fig. 1 Chronological clinical and radiographic findings of the lower right second molar
A：Radiographic image of the same tooth before the onset of root resorption, taken in 2015.
B：Mild gingival swelling observed around the lower right second molar.
C：Radiographic image showing loss of tooth substance in the central part of the root of the lower right second molar, taken in 2021.

period; however, irreversible root damage occurred due to pathological pulp fibrosis and atypical external root resorption originating from the mid-root area. We report the features of this case and discuss the limitations of pulp diagnosis, the influence of pathological pulp fibrosis on resorption lesions, and the importance of CBCT imaging in diagnosis. This report aims to contribute to improving the accuracy and quality of pulp and root resorption diagnosis in clinical dentistry.

Case Report

A 38-year-old man visited the Dental Clinic of Tokushima University Hospital complaining of chronic discomfort in the right mandibular second molar that had continued for several years and the recent appearance of gingival swelling on the distal surface of the tooth. The patient had no significant systemic medical history.

According to the patient's interview, the affected tooth had been treated for dental caries nine years prior to this visit. Although the details of the procedure are unknown, the tooth had a history of pulp exposure following complete caries removal. Therefore, the patient underwent DPC using calcium hydroxide. Following treatment, the patient began to experience intermittent discomfort in the affected tooth and initially visited our clinic six years earlier. Radiographic examination using X-ray (Fig. 1A) and pulp sensibility tests were performed, revealing no abnormalities. The patient was placed under observation.

Six years later, the patient complained of gingival swelling. Intraoral examination revealed mild gingival swelling on the distal surfaces of the teeth (Fig. 1B). No other acute symptoms were evident. The tooth showed slight tenderness to percussion, but no mobility was observed. Periodontal examination revealed pocket depths of 2–3 mm, with no clear signs of periodontal disease. The EPT and cold test showed normal pulp responses. However, X-ray imaging revealed extensive resorption of dentin in the middle part of the mesial root of the right mandibular second molar (Fig. 1C). Comparison with the X-ray taken six years earlier, which showed no abnormalities (Fig. 1A), revealed rapid progression of root resorption. Therefore, CBCT (MCT-HN; J. Morita Mfg. Corp., Kyoto, Japan; 99.0 kV, 8.0 mA, 9.4 s, isotropic voxel size 0.960 mm) was performed for further investigation. This revealed significant root resorption in the mid-portion of the mesial root, confirming communication between the pulp space and the external environment via the resorptive cavity. Extensive bone resorption was also observed on the lingual side (Fig. 2).

Considering the extensive root and bone resorption, the prognosis for the tooth was judged to be extremely poor, even with aggressive endodontic treatment. The treatment options after extraction were explained in detail to the patient, including the increased burden on abutment teeth and potential negative long-term prognosis with a bridge, versus the potential for improved long-term prognosis with implant therapy[13]. After consultation, the patient opted for implant therapy.

The extraction was performed under intravenous sedation combined with local anesthesia (3.6 mL of 2% lidocaine with 1：73,000 epinephrine). An incision was made from the buccal aspect of the right mandibular

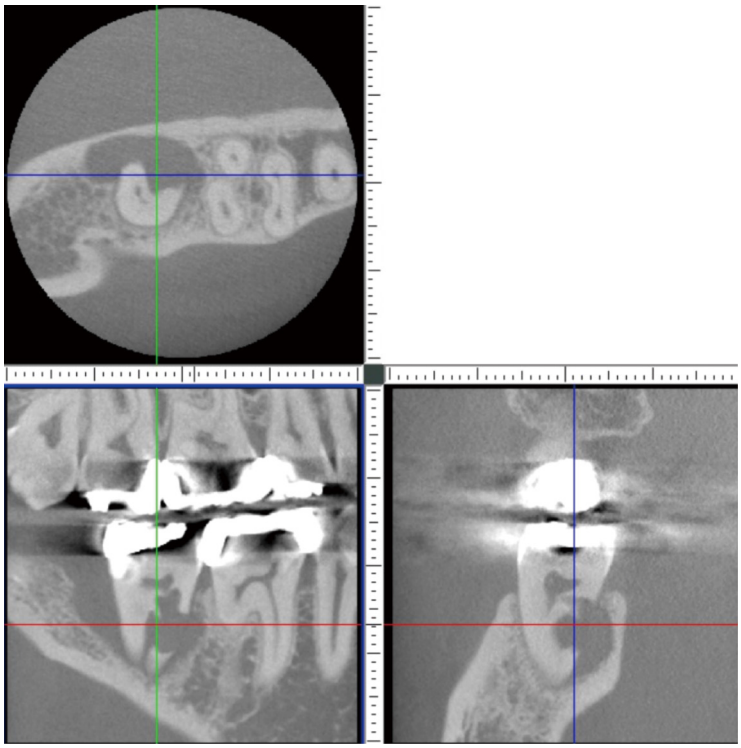

Fig. 2 CBCT imaging showing external root resorption affecting the mesial root in the middle third with communication between the pulp chamber and the external environment and extensive bone loss on the lingual aspect of the affected tooth

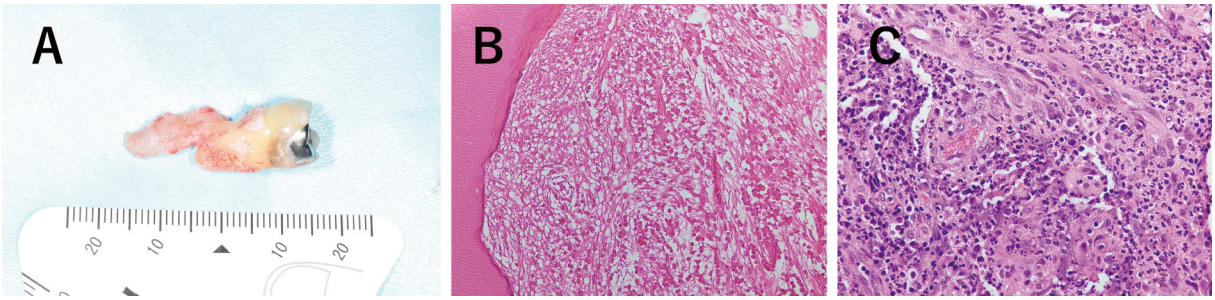

Fig. 3 Macroscopic findings and corresponding histopathological features of the extracted lower right second molar
A：Extraction of the lower right second molar with associated apical lesion.
B：Microscopic view of fibrosis in the pulp chamber（H&E；original magnification×400）.
C：Inflammatory granulation tissue at the site of bone resorption（H&E；original magnification×400）.

first molar to the cervical region of the second molar, and a mucoperiosteal flap was elevated and reflected. The problematic tooth and surrounding lesion (Fig. 3A) were extracted. The extraction socket was carefully curetted, and an atelocollagen sponge（TERUPLUG; Terumo Corp., Tokyo, Japan）was placed to promote healing, followed by suture closure of the wound with VICRYL sutures（Ethicon, Inc., Raritan, NJ, USA）.

The extracted tissue was fixed in 10% neutral buffered formalin for histopathological evaluation. Observation under a light microscope（NIKON ECLIPSE 80i, Nikon Corp., Tokyo, Japan）after hematoxylin and eosin staining revealed pathological fibrosis progressing within the pulp space without signs of bacterial infection（Fig. 3B）. The granulation tissue from the bone resorption area showed chronic inflammatory cell infil-

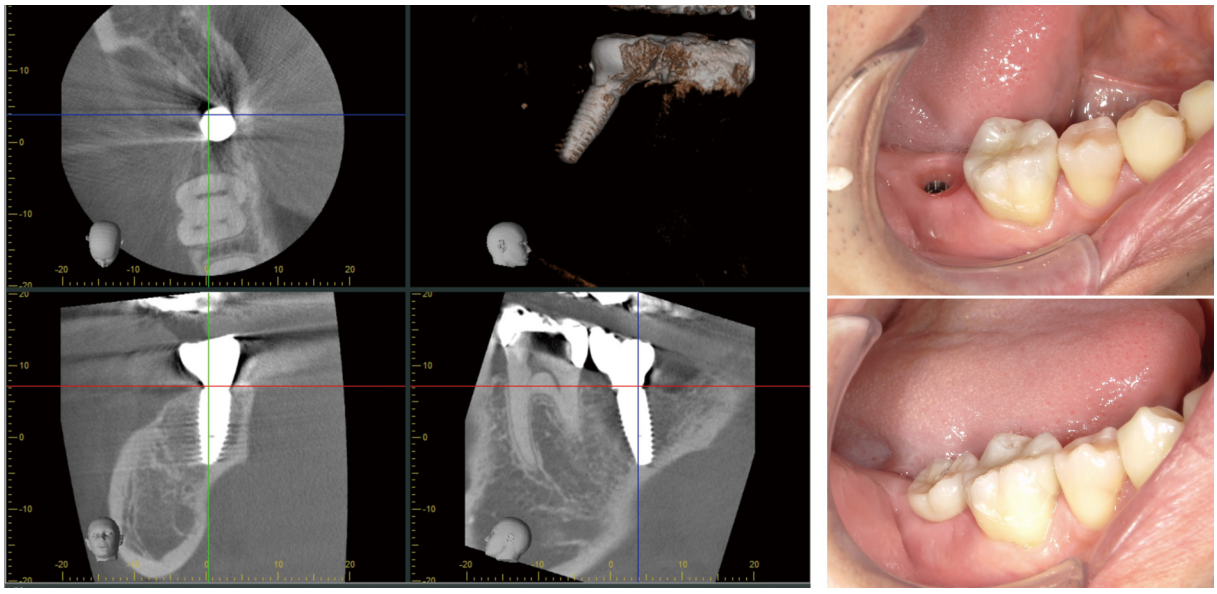

Fig. 4 CBCT scans (left panel) and intraoral photographs (right panel) taken six months post-implant placement, demonstrating proper osseointegration and prosthetic function

tration, predominantly neutrophils (Fig. 3C); however, no neoplastic changes or malignant findings were observed. Based on these clinical, imaging, and pathological evaluations, the final diagnosis was established as chronic inflammatory granuloma associated with root resorption.

The post-extraction healing process was uneventful. Primary implant placement surgery was performed approximately six months after extraction. No notable issues were observed during the subsequent six-month follow-up period. The peri-implant tissues remained stable and functional, and the patient continued to attend follow-up appointments (Fig. 4).

Discussion

The extensive external root resorption observed in this case, originating from the mid-root area, represents an atypical pathology that differs from the more common inflammatory resorption, which typically begins in the apical region. External root resorption is often associated with trauma or bacterial infection following pulp necrosis[3]; however, the present case showed normal responses to pulp sensibility tests. Rapid resorption progressed from the mid-root area without involvement of apical lesions. This idiopathic external resorption localized in the mid-root region is extremely rare, and elucidating its pathogenesis and underlying factors remains challenging.

The common causes of external resorption in permanent teeth include pulp necrosis, periodontitis, trauma, and orthodontic forces[3,14]. The present patient had no history of trauma or orthodontic treatment, nor were there clinical findings suggestive of chronic periodontitis, such as deep periodontal pockets. Gross observation of the extracted specimen revealed extensive resorption on the external surface of the root, exhibiting the morphology of external resorption. CBCT images also suggested that the lesion had expanded from the external root surface. Thus, this case was considered to be an idiopathic external resorption. However, because the defect was extremely large, it was difficult to precisely identify the initial site or pattern of progression. In other words, the possibility of internal or combined resorption could not be completely excluded. It should be recognized that when root resorption progresses, as in this case, there are certain limitations to diagnosing whether it is internal or external.

A particularly interesting finding in the histopathological examination was the presence of pathological pulp fibrosis, despite the absence of any signs of bacterial infection in the pulp cavity. In this case, chronic discomfort persisted even after DPC was performed 9 years earlier. This suggests that persistent irritation associated with non-infectious pulp fibrosis may have contributed to disturbances in blood circulation and

subsequent resorption, although this remains a possible association rather than a definitive mechanism. The pulp cavity and the periodontal ligament tissue are separated by dentin. It is generally considered unlikely that pathological conditions within the pulp space directly cause cementum damage or root resorption on the PDL side[15]. However, if the anatomical root canal is present, it may be a route for this[16]. In the present case, root resorption had progressed to the point where the pulp cavity and the periodontal ligament were directly connected, but because the lesion was extremely large, it was not possible to determine whether a pre-existing pathway had originally been present. The mid-root resorption observed in this case might have been related to long-standing non-infectious pulp inflammation and intrapulpal fibrosis after DPC, which could have altered intrapulpal circulation and the tissue environment. Although this remains speculative, such changes may have facilitated the progression of resorption once communication between the pulp cavity and the periodontal ligament occurred.

Regarding pulp sensibility tests, both the EPT and cold test showed normal responses over a long period, despite the progression of extensive pathological fibrosis within the pulp space. Since sensibility tests evaluate the neural response of the pulp, they may not accurately reflect the overall pathological state, especially in fibrotic pulps. Partially surviving nerves can yield false-negative or seemingly normal responses[5,6]. Molars often show normal responses even if only one of their multiple root canals is healthy. These false-negative responses can hinder the early detection of pathology. When pathological pulp fibrosis is suspected, it is necessary to use auxiliary diagnostic methods, such as pulp blood flow measurement and 3D imaging, in conjunction with sensibility tests.

In imaging diagnostics, conventional two-dimensional radiography has limitations in the early detection of mid-root resorption lesions[4]. In the present case, the root resorption lesion was not clearly visible on the X-ray taken six years earlier; however, progression of the lesion became apparent in the subsequent imaging. Three-dimensional evaluation using CBCT was necessary to identify the extent of the lesion and perforation to the external environment. Previous studies have reported the high sensitivity and specificity of CBCT in the diagnosis of root resorption[17]. Especially in atypical cases, such as the present case, early implementation of CBCT examination is desirable for early detection and appropriate intervention.

Regarding the treatment strategy for non-inflammatory idiopathic resorption, conventional root canal treatment aimed solely at eliminating intracanal infection is often ineffective. Surgical approaches are generally required to directly manage the resorption defect and seal it with biocompatible materials such as MTA or bioceramics[1]. However, in the present case, the resorption was already so extensive that the structural integrity of the root was compromised, making functional restoration difficult through conservative treatment and therefore necessitating extraction.

If the lesion had been detected earlier with CBCT, tooth preservation might have been possible. Therefore, this case underscores the importance of detailed imaging examinations, including early CBCT, when chronic symptoms persist after DPC, rather than relying solely on clinical symptoms and conventional imaging. Furthermore, incorporating pulp blood flow measurements in addition to sensibility tests could lead to earlier detection of root resorption and improved success rates for conservative treatments in future clinical practice.

Conclusion

This case report describes a rare pathology where, despite normal responses to pulp sensibility tests following DPC, pathological fibrosis progressed within the pulp space concurrently with idiopathic external root resorption originating in the mid-root area, leading to complete dentin destruction and communication between the pulp space and the periodontal ligament side.

This case highlights the critical importance of not relying solely on conventional pulp sensibility tests when chronic discomfort or symptoms persist after DPC. Proactive utilization of three-dimensional imaging diagnostics, such as CBCT, is important for the early detection of lesions involving the periodontal ligament side. Further accumulation of similar cases is needed to elucidate the pathogenesis, establish diagnostic criteria, and refine treatment strategies for idiopathic external root resorption.

Conflict of Interest

The authors declare no conflicts of interest associated with this manuscript, and the patient's consent to publish the material was obtained.

Acknowledgment

This work was supported by JSPS KAKENHI Grant Number 24K03557.

References

1) Aidos HFA, Diogo P, Santos JM. Root resorption classifications: A narrative review and a clinical aid proposal for routine assessment. Eur Endod J 2018; 3: 134–145.
2) Galler KM, Grätz EM, Widbiller M, Buchalla W, Knüttel H. Pathophysiological mechanisms of root resorption after dental trauma: a systematic scoping review. BMC Oral Health 2021; 21: 163.
3) Kotuła J, Kuc A, Nawrocki J, Babczyńska A, Sarul M, Lis J. External root resorption of a permanent tooth: Case study. J Dent Probl Solut 2022; 9: 20–24.
4) Huamán SD, Arnez MFM, Oliveira FMMPC, De Rossi A, Silva LAB, Paula-Silva FWG. In vivo detection of external apical root resorption induced by apical periodontitis using periapical radiography and cone-beam computed tomography. Pesqui Bras Odontopediatria Clín Integr 2022; 22: e210163.
5) Chen E, Abbott PV. Dental pulp testing: A review. Int J Dent 2009; 2009: 365785.
6) Petersson K, Soderstrom C, Kiani-Anaraki M, Lévy G. Evaluation of the ability of thermal and electrical tests to register pulp vitality. Endod Dent Traumatol 1999; 15: 127–131.
7) Siddiqui SH, Mohamed AN. Calcific metamorphosis: A review. Int J Health Sci (Qassim) 2016; 10: 437–442.
8) Patro S, Meto A, Mohanty A, Chopra V, Miglani S, Das A, Luke AM, Al Hadi D, Meto A, Fiorillo L, Karobari MI, Wahjuningrum DA, Pawar AM. Diagnostic accuracy of pulp vitality tests and pulp sensibility tests for assessing pulpal health in permanent teeth: A systematic review and meta-analysis. Int J Environ Res Public Health 2022; 19: 9599.
9) Islam R, Islam MRR, Tanaka T, Alam MK, Ahmed HMA, Sano H. Direct pulp capping procedures—Evidence and practice. Jpn Dent Sci Rev 2023; 59: 48–61.
10) Al-Hiyasat AS, Barrieshi-Nusair KM, Al-Omari MA. The radiographic outcomes of direct pulp-capping procedures performed by dental students: A retrospective study. J Am Dent Assoc 2006; 137: 1699–1705.
11) Karkoutly M, Alnour A, Alabdullah J, Abu Hasna A, Nam OH, Jalloul D, Al Kurdi S, Bshara N. Analysis of pulp histological response to pulpotomy performed with white mineral trioxide aggregate mixed with 2.25% sodium hypochlorite gel in humans: a randomized controlled clinical trial. Sci Rep 2024; 14: 31471.
12) Fuks AB, Bielak S, Chosak A. Clinical and radiographic assessment of direct pulp capping and pulpotomy in young permanent teeth. Pediatr Dent 1982; 4: 240–244.
13) Torabinejad M, Anderson P, Bader J, Brown LJ, Chen LH, Goodacre CJ, Kattadiyil MT, Kutsenko D, Lozada J, Patel R, Petersen F, Puterman I, White SN. Outcomes of root canal treatment and restoration, implant-supported single crowns, fixed partial dentures, and extraction without replacement: A systematic review. J Prosthet Dent 2007; 98: 285–311.
14) Patel S, Kanagasingam S, Pitt Ford T. External cervical resorption: A review. J Endod 2009; 35: 616–625.
15) Darcey J, Qualtrough A. Resorption: part 1. Pathology, classification and aetiology. Br Dent J 2013; 214: 439–451.
16) Tanaka M, Arai K, Kitajima K, Igarashi M, Kawasaki K. A preliminary investigation on the presence of accessory foramina in human mandibular molar furcations with gutter shaped roots by micro-CT analysis. Jpn J Conserv Dent 2007; 50: 530–538.(in Japanese)
17) Durack C, Patel S. Cone beam computed tomography in endodontics. Braz Dent J 2012; 23: 179–191.

Case Report

ODEP 5 (1) : 77～87, 2025

A Case of Periodontal Tissue Regeneration Therapy for a Tooth with Mobility Due to Traumatic Root Resorption and Vertical Bone Resorption from Severe Chronic Periodontitis

Hiroko IGARASHI-TAKEUCHI and Yukihiro NUMABE

Department of Periodontology, The Nippon Dental University School of Life Dentistry at Tokyo

Abstract

Introduction: This report describes the case of a patient with severe chronic periodontitis complicated by traumatic root resorption and tooth mobility due to vertical bone defects. Periodontal tissue regeneration therapy achieved favorable treatment outcomes at the 10-year follow-up.

Case: A 55-year-old woman had sustained a severe blow to the face in a traffic accident three years earlier. Four days prior to presentation, the patient had experienced pain in the upper front teeth and occlusal discomfort. Radiographic examination revealed external root resorption resulting in an inverted crown-to-root ratio, and vertical bone loss extending to the apex was observed on the distal aspect of tooth #12. In addition to the chief complaint site, redness and swelling were observed at other locations. Sites with probing depths (PD) ≥6 mm accounted for 1.9%, and bleeding on probing was positive at 30.2% of sites. Grade I furcation involvement was noted on the buccal aspect of tooth #26. Plaque control record score at the initial visit was 50.8% and oral hygiene was poor. In addition, implants had been placed in the regions corresponding to teeth #47, #46, #36, and #37. PDs were ≥3 mm and radiographic examination revealed vertical bone loss around the implants at sites #36 and #37. Based on these findings, generalized severe chronic periodontitis, stage III, grade C, was diagnosed.

Course: Following initial periodontal therapy, periodontal regenerative therapy was applied to tooth #21. At tooth #15, flap operation was carried out. At tooth #16, flap operation combined with odontoplasty for removal of an enamel pearl, osteoplasty, and autogenous bone grafting were performed. Due to gingival recession in the maxillary anterior region and the desire of the patient for esthetic improvement, crown shape modification was performed. For implant sites with PD ≥4 mm, meticulous plaque control as well as scaling and root planning were performed. Notably, radiographic examination of the implants corresponding to teeth #36 and #37 demonstrated bone flattening and the presence of an alveolar lamina dura. Subsequently, the case was transitioned to supportive periodontal therapy (SPT).

Conclusion: In this case, root resorption caused by a traffic accident resulted in an unfavorable crown-to-root ratio and severe vertical bone resorption extending to the apex in a tooth with severe chronic periodontitis. Approximately 10 years have passed since the transition to SPT, and the condition has been maintained in a favorable state.

Key words: periodontal tissue regeneration therapy, crown-to-root ratio, traumatic root resorption, severe chronic periodontitis

Corresponding author: Hiroko IGARASHI-TAKEUCHI, Department of Periodontology, The Nippon Dental University School of Life Dentistry at Tokyo, 1-9-20, Fujimi, Chiyoda-ku, Tokyo 102-8159, Japan

TEL & FAX: +81-3-3261-5937, E-mail: hiroko.p0324@gmail.com

Received for Publication: September 15, 2025/Accepted for Publication: October 22, 2025

DOI: 10.11471/odep.2025-009

Introduction

Chronic periodontitis is a chronic inflammatory disease in which plaque acts as the primary etiological factor, initiating inflammation in the marginal gingiva and subsequently leading to attachment loss and alveolar bone resorption[1]. The disease often progresses asymptomatically, and advanced bone destruction may be present at the time of diagnosis.

Initial periodontal therapy is the first step in the management of periodontitis[2]. This involves assessing the oral hygiene status of the patient, providing oral hygiene instruction to establish effective plaque control, and performing scaling and root planing (SRP). Patient motivation is essential for the success of these interventions[3]. Teeth that are deemed non-restorable serve as plaque-retentive factors and may be extracted during initial therapy[2]. Following re-evaluation after initial therapy, residual deep periodontal pockets with bleeding may require periodontal surgical intervention, and periodontal regenerative therapy may be applied to vertical bony defects.

This report describes the case of a patient with generalized severe chronic periodontitis who presented with mobility of teeth affected by root resorption secondary to trauma and concurrent chronic periodontitis. Comprehensive periodontal therapy was performed throughout the dentition, and periodontal regenerative treatment using autogenous bone grafts and enamel matrix derivative was applied to deep vertical bony defects. Favorable clinical outcomes were observed following these interventions.

Written informed consent for publication of this case report was obtained from the patient, and all drugs and materials used were approved by the Ministry of Health, Labour and Welfare.

Case Report

1. Clinical presentation

A 55-year-old Japanese woman presented with pain and occlusal discomfort in the anterior maxillary region. The patient had sustained facial trauma in a traffic accident 3 years earlier. Four days prior to presentation, she noted pain and occlusal discomfort in the maxillary anterior teeth. The patient's general dentist had recommended extraction of teeth #11 and #21, and was referred to our clinic in May 2014. The patient recently reported swelling and bleeding from the gingiva in the left posterior maxillary region. Teeth #36, #37, #46, and #47 had previously been extracted due to apical periodontitis, with the edentulous areas restored using removable partial dentures. Two years earlier, implants had been placed in these regions. To adjust the crown length at the time of implant placement, full-cast crowns were placed on teeth #26 and #27, and endodontic treatment was performed on tooth #26. The patient had received annual maintenance for her implants. Tooth #34 had fractured 20 years earlier due to a trauma incident at a swimming pool.

The medical history of the patient included surgery for uterine fibroids, gallbladder, and polyps 6 years earlier. The patient was 150 cm tall, weighed 55 kg, and had a body mass index of 24.44 (within normal range). The family history regarding periodontitis was unknown. The patient's father was deceased, and her mother had died of gastric cancer. The four siblings of the patient (older sister, older brother, younger brother, younger sister) were all in good health; her younger sister had undergone surgery for an ovarian tumor. The patient had no history of smoking. The patient used an electric toothbrush twice daily (morning and before bedtime), had previously received oral hygiene instruction, and occasionally used dental floss.

Clinical examination revealed mild supragingival calculus on the interproximal surfaces of the mandibular anterior lingual region (Fig. 1). Mild erythema was observed on the buccal gingiva of the maxillary posterior teeth. The patient had a short labial frenum and a narrow oral vestibule. At the time of initial examination, 27 teeth were present (16 in the maxilla, 11 in the mandible), and four implants had been placed in the mandible.

Probing depth (PD) ranged from 1 to 12 mm (mean 3.3 mm). Sites with a PD of 4–5 mm accounted for 30.9% (50/162 sites), while sites with PD ≥6 mm accounted for 1.9% (3/162 sites). Bleeding on probing (BOP) was positive at 30.2% of sites (49/162 sites). On the buccal aspect of tooth #26, a grade I furcation defect was observed according to Lindhe's classification. Tooth mobility, assessed using Miller's criteria, was grade 1 for teeth #12, #11, #22, #32, and #41, and grade 2 for teeth #21 and #26.

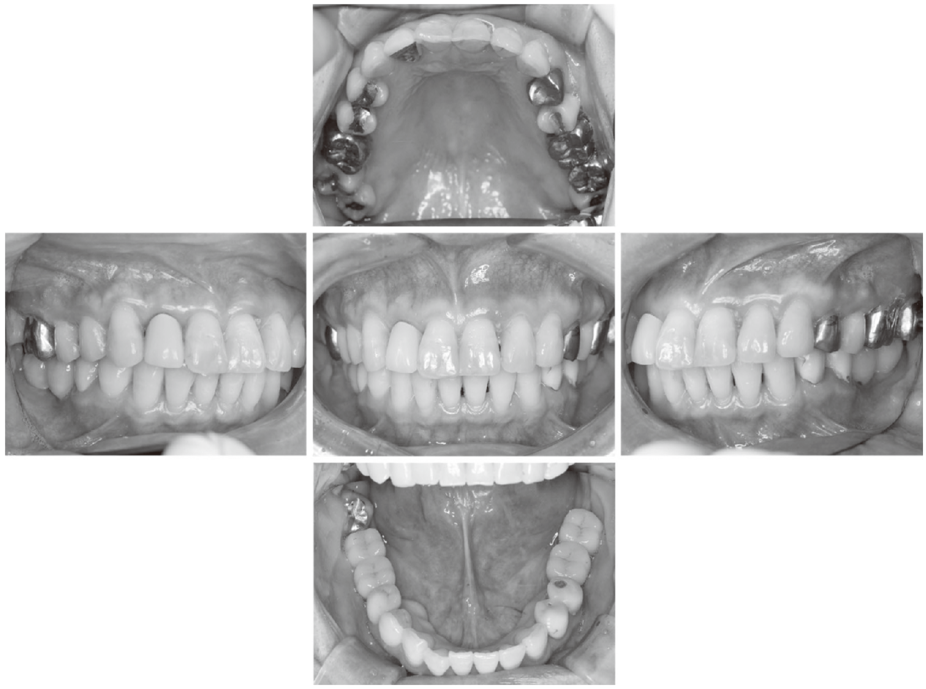

(a) Intraoral photographs

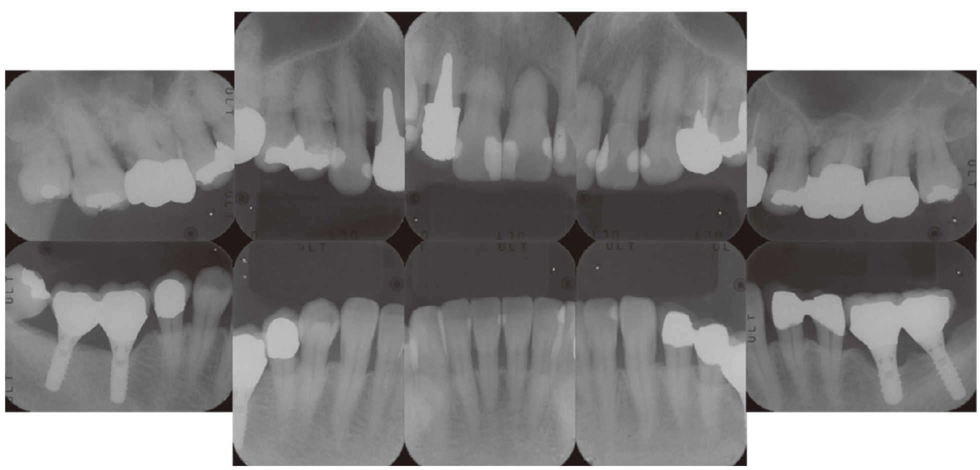

(b) Radiographic images

PCR																
Mobility	0	0	0	0	0	0	1	1	2	1	0	0	0	2	0	0
Furcation														I		
PD B	4 4 4	4 3 4	4 3 4	4 3 4	4 3 3	3 3 3	3 2 3	3 2 4	4 3 8	5 3 4	3 2 3	4 3 4	4 3 4	4 3 4	5 3 4	5 4 4
PD P	4 3 5	6 3 4	4 3 3	4 3 4	4 3 3	5 2 3	3 2 3	3 2 3	3 5 12	3 3 3	3 3 3	3 3 3	3 3 4	4 3 4	3 3 4	3 4 4
	8	7	6	5	4	3	2	1	1	2	3	4	5	6	7	8
	8	7	6	5	4	3	2	1	1	2	3	4	5	6	7	8
PD L	4 3 3	4 3 3	3 2 4	4 3 4	3 3 3	3 2 3	2 2 3	3 2 3	3 2 3	2 2 2	2 2 3	3 2 3	3 3 3	4 3 4	3 3 3	
PD B	4 4 4	3 3 3	3 3 4	3 4 3	3 3 3	3 2 3	3 2 2	3 1 2	2 1 3	2 1 2	3 2 3	3 3 4	4 3 4	5 4 5	4 3 4	
Furcation																
Mobility	0	0	0	0	0	0	0	1	1	0	0	0	0	0	0	
PCR																

Stage	Initial examination
Date	2014/05
Number of teeth	27
Implants	4
Mean PD	3.3 mm (162 sites)
1 - 3 mm	109 (67. 3%)
4 - 5 mm	50 (30. 9%)
PD ≥ 6 mm	3 (1. 9%)
BOP (+)	49 (30. 2%)
PISA PESA	642. 1 mm² 1629. 1 mm²
PCR	50. 8%

Bleeding on probing (BOP)

(c) Periodontal examination

Fig. 1 Initial examination (May 2014)

Panoramic and periapical radiography showed generalized short roots, with teeth #11 and #12 exhibiting inverted crown-to-root ratios due to root resorption. Vertical bone loss extending to the apex was observed on the distal aspect of tooth #12. Generalized moderate to severe alveolar bone loss was noted throughout the dentition. The roots of the maxillary molars were close together, appearing partially fused. Slight radiolucencies were observed at the furcation areas of teeth #16 and #26, and a cup-shaped bone defect was present at tooth #36.

The dental arches were generally parabolic, although tooth #18 was palatally displaced. Mandibular tori were observed. Restorations included amalgam fillings on the occlusal surfaces of teeth #18 and #28, inlays on teeth #16–14, #24, and #48, full-cast crowns on teeth #16, #12, #24, #26, and #27, and splinted crowns on teeth #34 and #35. Composite resin restorations were present on the interproximal surfaces of teeth #13, #11–23, #31, #32, #42, and #41. Implants had been placed in the regions corresponding to teeth #37, #36, #47, and #46. The occlusion was Angle Class I bilaterally. The patient has a small mouth and limited mouth opening.

Plaque control, as measured by the O'Leary plaque control record (PCR) at the initial visit, was 50.8%, indicating poor oral hygiene. Based on these findings, a diagnosis of generalized severe chronic periodontitis, stage III, grade C, was established.

2. Case management

A treatment plan was established with the primary objective of controlling inflammation of the periodontal tissues. The first step consisted of initial periodontal therapy. Following oral hygiene instruction using the Bass technique and interdental brushes, SRP was performed. Re-evaluation included periodontal examination, dental radiography, and comparison with initial PCR scores. Sites with residual PD ≥4 mm and BOP-positive sites were selected for periodontal surgical intervention (teeth #18–13, #11, #21, #22, #24–28, #35, #48, #45). Flap surgery was planned, and periodontal regenerative therapy was applied to sites exhibiting vertical bone defects. After an appropriate healing period, re-evaluation was conducted to compare periodontal conditions before and after surgery. Subsequently, the patient was placed on a regular maintenance program for ongoing monitoring of periodontal and peri-implant status.

3. Clinical outcomes

Following periodontal examination, the patient received oral hygiene instruction using the Bass technique and adjunctive cleaning devices, and SRP was performed (May–August 2014). Although the patient had been receiving annual maintenance for the implant sites, PD ≥3 mm with BOP-positive sites were observed, and thorough plaque control and debridement were performed. Tooth #21 responded positively to electric pulp testing, and no pain was noted after the initial visit. Although root resorption was observed, maintaining the tooth without endodontic treatment is considered a treatment option when the pulp remains intact[4]. Because vital teeth show a higher survival rate than non-vital teeth, preservation of pulp vitality was prioritized whenever possible. Occlusion of the mobile left maxillary central incisor was evaluated, and occlusal adjustment was carried out. Re-evaluation revealed improvement in oral hygiene, with resolution of erythema in the marginal gingiva. The PCR score decreased by 33.9% compared with the initial visit, and BOP decreased by 26.5% (Fig. 2). Residual PD ≥4 mm with BOP-positive sites were selected for periodontal surgical intervention. Tooth #26 exhibited persistent BOP and mobility. The patient was therefore informed again that, due to limited root divergence, short roots, and apical alveolar bone loss, treatment of this tooth would be challenging, and consent for extraction was obtained.

For the narrow three-wall intrabony defect at the distal aspect of tooth #21 extending to the apical region, periodontal regenerative therapy using enamel matrix derivative (Emdogain gel, Straumann Basel, Switzerland) was selected to promote periodontal tissue regeneration (Fig. 3). A three-wall intrabony defect at tooth #16, which exhibited residual PD ≥4 mm and BOP-positive sites after re-evaluation, underwent flap surgery to ensure thorough access to the root surface and pocket removal. Odontoplasty was performed for enamel pearl removal, and alveolar bone contouring was performed to restore the thick, shelf-like marginal bone to a normal shape (Fig. 4-a). For the approximately 3 mm-wide three-wall intrabony defect located just beneath the enamel pearl, autogenous bone harvested from buccal alveolar bone using a bone scraper was grafted to promote periodontal regeneration (Fig. 4-b). Tooth #15 underwent flap surgery to ensure root surface access

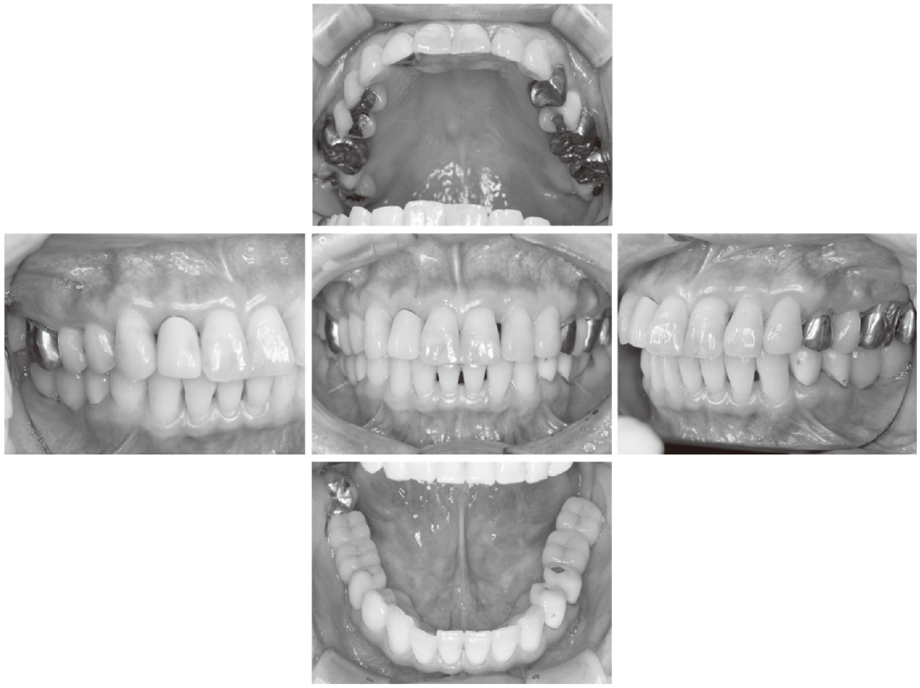

(a) Intraoral photographs

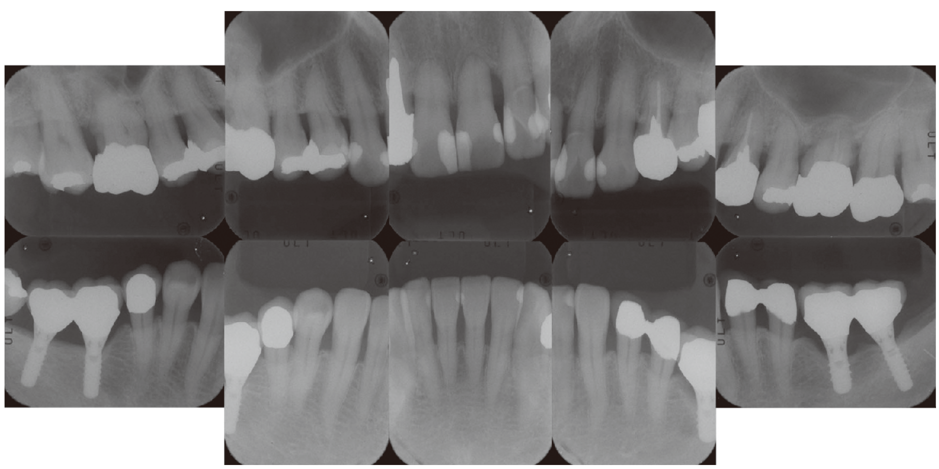

(b) Radiographic images

PCR																
Mobility	0	0	0	0	0	0	1	1	1	1	0	0	0	2	0	0
Furcation														I		
PD B	3 2 3	3 2 3	4 3 3	3 2 3	3 2 3	3 2 3	3 2 3	3 3 3	2 3 4	3 2 3	3 2 3	3 2 3	4 2 3	3 3 3	3 4 3	3 3 3
PD P	4 3 4	4 3 4	5 3 3	4 2 4	4 2 3	3 2 3	3 2 3	3 2 3	3 2 6	4 2 3	3 2 3	3 3 3	3 2 3	3 3 4	3 3 3	3 3 3
	8	7	6	5	4	3	2	1	1	2	3	4	5	6	7	8
	8	7	6	5	4	3	2	1	1	2	3	4	5	6	7	8
PD L	3 3 4	3 3 3	3 3 3	3 2 3	3 2 3	3 2 3	2 2 2	2 2 2	3 2 3	3 2 3	2 2 2	2 2 2	2 2 2	3 4 3	3 3 3	
PD B	3 3 4	3 3 3	3 3 3	3 2 3	3 2 2	2 2 3	3 2 2	2 2 2	2 1 2	3 1 2	2 1 2	2 1 3	3 2 3	4 3 4	3 3 3	
Furcation																
Mobility	0	0	0	0	0	0	0	1	1	0	0	0	0	0	0	
PCR																

Stage	After initial periodontal therapy
Date	2014/09
Number of teeth	27
Implants	4
Mean PD	2.7 mm (162 sites)
1 - 3 mm	145 (89. 5%)
4 - 5 mm	16 (9. 9%)
PD ≥ 6 mm	1 (0. 6%)
BOP (+)	6 (3. 7%)
PISA PESA	76. 6 mm² 1345. 2 mm²
PCR	16. 9%

Bleeding on probing (BOP)

(c) Periodontal examination

Fig. 2 Periodontal examination after the initial periodontal therapy (September 2014)

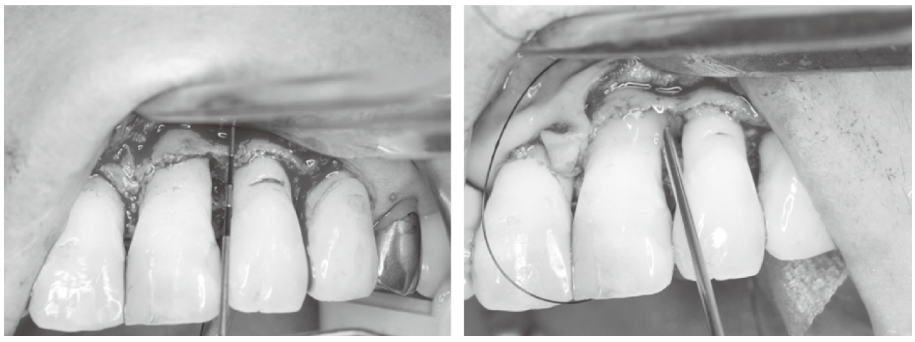

Fig. 3 Periodontal surgery (September 2014)
For the three-wall intrabony defect on the distal aspect of tooth #21, periodontal tissue regeneration therapy was performed using an enamel matrix derivative (Emdogain) with the aim of promoting periodontal regeneration.

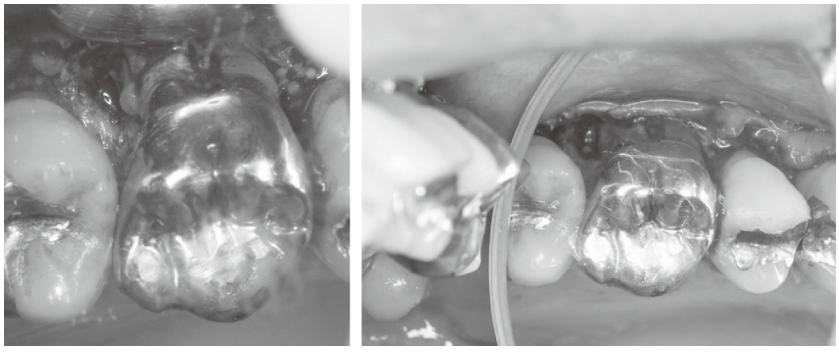

(a)

(b)

Fig. 4 Periodontal surgery (October 2014)
(a) The enamel pearl on tooth #16 was removed. In addition, osteoplasty was carried out to reshape the thick, shelf-like alveolar bone margin and restore a more physiological contour.
(b) For the three-wall intrabony defect, an autogenous bone graft was performed by harvesting cortical bone from the buccal alveolar bone using a bone scraper, with the aim of promoting periodontal regeneration. For tooth #15, flap surgery was performed to achieve adequate access to the root surface and to eliminate the periodontal pocket.

and pocket removal. Tooth #26 was extracted. After healing from periodontal surgery, re-evaluation was performed (March 2015). In tooth #21, radiographic examination showed disappearance of the apical defect and evidence of bone regeneration. Compared with the periodontal examination after the initial periodontal

Fig. 5 Oral rehabilitation (April–June 2015)
For the embrasure spaces between teeth #11, #21, #22, and #23, direct composite resin restorations were performed to improve the crown morphology. In addition, a porcelain jacket crown was placed on tooth #12. At that time, the patient was instructed to clean between teeth #12, #11, and #21 with dental floss, and between teeth #21 and #22 with an interdental brush. Following the extraction of tooth #26, a fixed prosthesis (bridge) was fabricated using teeth #25 and #27 as abutments. The margins were placed supragingivally, and the bridge was designed to allow insertion of an interdental brush.

therapy, an attachment gain of approximately 4 mm was achieved. In tooth #16, an attachment gain of approximately 2 mm was obtained. Following extraction of tooth #26, 26 teeth remained. Two sites exhibited PD of 4 mm, but all BOP-positive sites were eliminated, and the PCR score was 9.2%. The patient thus proceeded to oral functional rehabilitation.

Due to gingival recession in the maxillary anterior region and the desire of the patient for esthetic improvement, direct composite resin restorations were placed to adjust the crown morphology of the interdental spaces between teeth #11, #21, #22, and #23, and a porcelain jacket crown was placed on tooth #12. The patient was instructed to use dental floss between teeth #12, #11 and #21, and interdental brushes between teeth #21 and #22. Following extraction of tooth #26, a fixed bridge using teeth #25 and #27 as abutments was placed with a supragingival margin, designed to allow insertion of interdental brushes (Fig. 5). Re-evaluation of oral functional rehabilitation revealed a PCR score of 9.2%, representing a 7.7% reduction compared with preoperative values, and BOP was 0%. Two sites with PD of 4 mm remained, but were BOP-negative. The patient was transitioned to supportive periodontal therapy (SPT) (Fig. 6).

After transitioning to SPT, the full cast crown on tooth #24 became dislodged, and caries were detected on the abutment tooth. Core build-up was therefore performed, followed by prosthetic restoration using a porcelain-fused-to-metal crown. Currently, the patient attends SPT visits every 3 months (Fig. 7). The PCR score has been maintained at 7.5% and BOP remains 0%. At each visit, oral hygiene is assessed, probing is performed, and supragingival scaling is carried out. In addition, to prevent root caries associated with gingival recession, high-concentration fluoride varnish has been applied. Since no gingival pain during toothbrushing has been observed, the patient was instructed to use a small-headed, soft-bristled toothbrush to allow adequate access to the molar region and to perform the Bass technique for oral hygiene. The patient was also advised to pay attention to brushing pressure. As supplemental cleaning devices, an end-tuft toothbrush has been used to clean the cervical areas and distal surfaces of the terminal molars, while interdental brushes and super floss have been employed for interdental cleaning. With these preventive measures in place, the areas with PD $\geq$4 mm are being carefully monitored during follow-up. The prognosis remains favorable under continuous SPT.

Discussion

Permanent teeth are normally resistant to resorption, and unlike primary teeth, root resorption does not usually occur. However, in permanent teeth, trauma, infec-

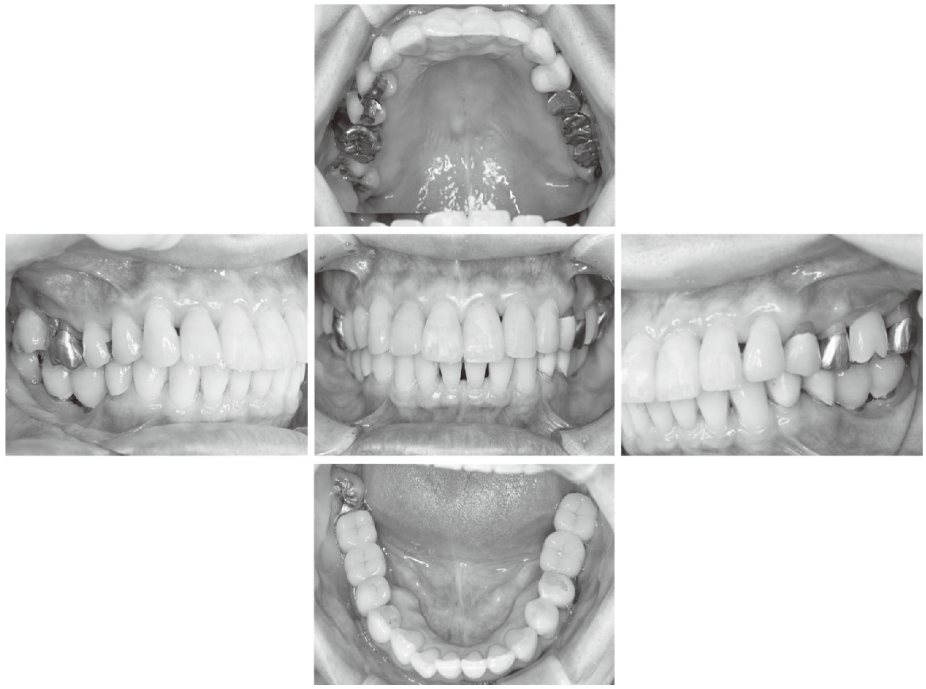

(a) Intraoral photographs

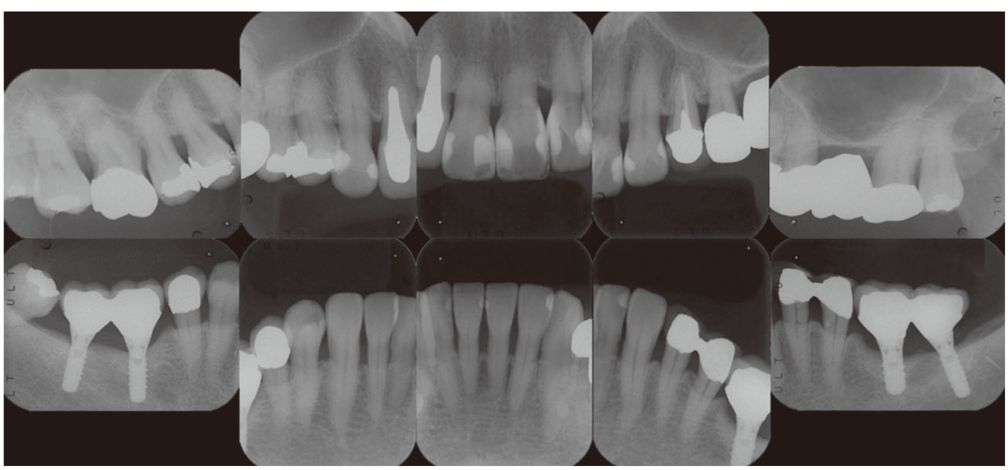

(b) Radiographic images

PCR																
Mobility	0	0	0	0	0	0	0	0	0	0	0	0	0		0	0
Furcation																
PD B	3 2 3	3 2 3	3 2 3	3 2 2	2 2 3	3 2 3	2 1 2	2 1 2	2 1 2	2 1 2	2 2 3	2 2 2	2 2 2		3 3 4	3 3 3
PD P	3 2 3	3 2 3	3 2 3	2 2 2	2 2 3	2 2 2	2 1 2	2 1 2	2 1 2	2 1 2	2 2 2	2 2 2	2 2 2		3 2 3	3 2 3
	8	7	6	5	4	3	2	1	1	2	3	4	5	6	7	8
	8	7	6	5	4	3	2	1	1	2	3	4	5	6	7	8
PD L	3 2 3	3 3 3	3 3 3	3 2 4	3 2 2	2 2 2	2 1 2	2 1 2	2 2 2	2 2 2	2 2 3	3 2 3	3 2 3	3 3 3	3 3 3	
PD B	3 2 3	3 3 3	3 3 3	3 2 2	2 2 2	2 2 2	2 1 2	2 1 2	2 1 2	2 2 2	2 2 2	3 2 3	3 2 3	3 3 3	3 3 3	
Furcation																
Mobility	0	0	0	0	0	0	0	1	1	0	0	0	0	0	0	
PCR																

Stage	The start of SPT
Date	2015/08
Number of teeth	26
Implants	4
Mean PD	2.2 mm (156 sites)
1-3 mm	154 (98. 7%)
4-5 mm	2 (1. 3%)
PD ≥ 6 mm	0 (0. 0%)
BOP (+)	0 (0. 0%)
PISA PESA	0. 0 mm^2 1024. 9 mm^2
PCR	9. 2%

(c) Periodontal examination

Fig. 6 At the start of SPT (August 2015)

Re-evaluation of oral functional rehabilitation revealed a PCR score of 9.2%, representing a 7.7% reduction compared with preoperatively, and BOP was 0%. Two sites with PD of 4 mm remained, but were BOP-negative. The patient was therefore transitioned to SPT.

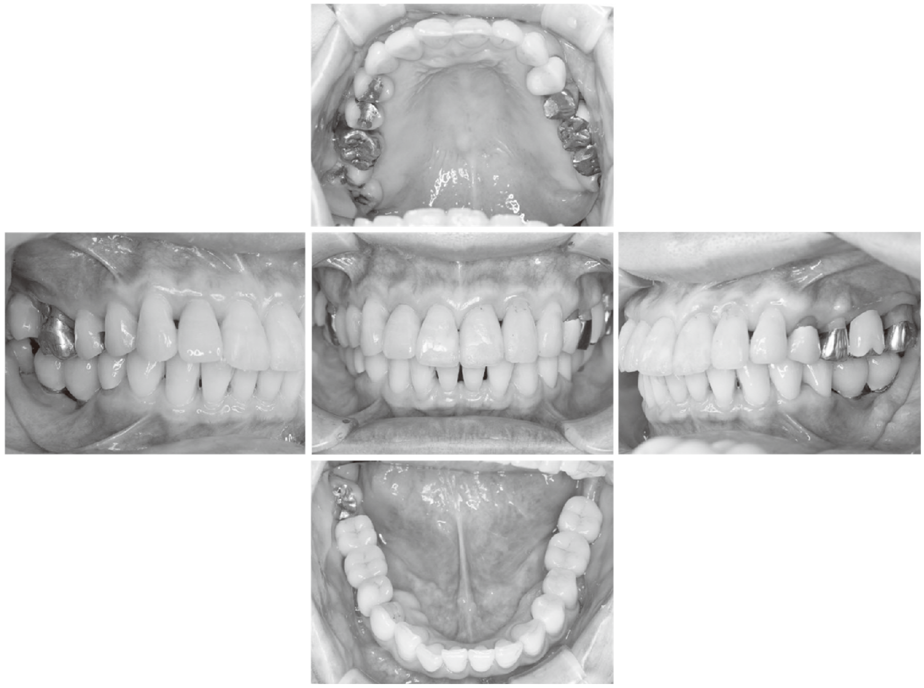

(a) Intraoral photographs

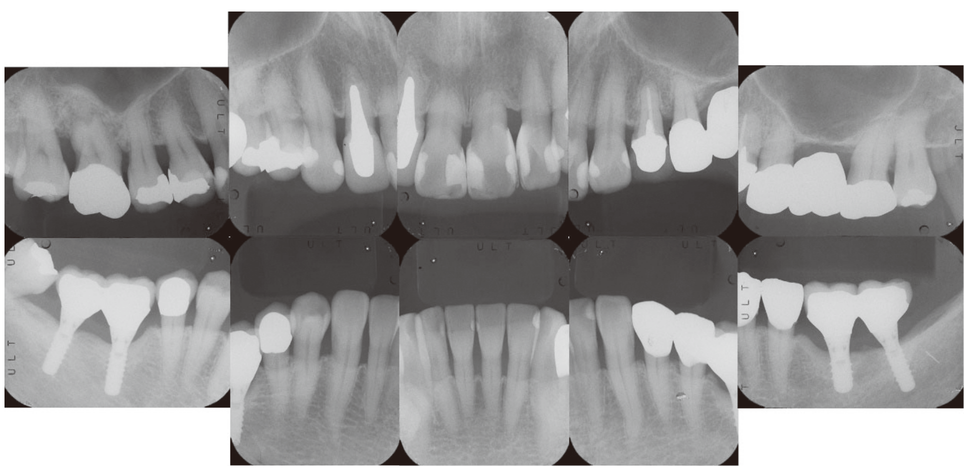

(b) Radiographic images

PCR																
Mobility	0	0	0	0	0	0	0	0	0	0	0	0	0		0	0
Furcation																
PD B	3 2 3	3 2 3	3 2 3	3 2 2	2 2 3	3 2 3	2 1 2	2 1 2	2 1 2	2 1 2	2 2 2	2 2 2	2 2 2		3 3 3	3 3 3
PD P	3 2 3	3 2 3	3 2 3	2 2 2	3 2 3	2 2 2	2 1 2	2 1 2	2 1 2	2 2 2	2 2 2	2 2 2	2 2 3		3 2 3	3 3 3
	8	7	6	5	4	3	2	1	1	2	3	4	5	6	7	8
	8	7	6	5	4	3	2	1	1	2	3	4	5	6	7	8
PD L	3 2 2	3 3 3	3 3 3	3 2 4	3 2 3	3 2 2	2 1 2	2 1 2	2 2 2	2 2 2	2 2 2	2 2 2	2 2 3	3 3 3	3 3 3	
PD B	3 3 3	3 2 3	3 2 3	3 2 2	2 2 2	2 1 2	2 1 2	2 1 2	2 1 2	2 1 2	2 1 2	2 2 3	2 2 3	3 3 3	3 3 3	
Furcation																
Mobility	0	0	0	0	0	0	0	0	0	0	0	0	0	0	0	
PCR																

Stage	The latest SPT
Date	2025/08
Number of teeth	26
Implants	4
Mean PD	2.2 mm (156 sites)
1 - 3 mm	155 (99. 4%)
4 - 5 mm	1 (0. 6%)
PD ≥ 6 mm	0 (0. 0%)
BOP (+)	0 (0. 0%)
PISA PESA	0. 0 mm^2 1003. 2 mm^2
PCR	7. 5%

(c) Periodontal examination

Fig. 7 At the latest SPT (August 2025)

Table 1 Association between PISA, PESA, BOP, and PCR during Treatment

	Initial exam	After initial periodontal therapy	At the start of SPT	Latest SPT
PCR (%)	50.8	16.9	9.2	7.5
BOP (%)	30.2	3.7	0.0	0.0
PISA (mm^2)	642.1	76.6	0.0	0.0
PESA (mm^2)	1,629.1	1,345.2	1,024.9	1,003.2

tion, orthodontic forces, or pressure from impacted teeth can damage the cementum on the root surface, leading to external root resorption[5]. In this patient, the maxillary anterior teeth exhibited short roots relative to crown length, resulting in an inverted crown-to-root ratio. Vertical bone defects extending to the apex were observed, contributing to grade 2 mobility.

Periodontitis is an inflammatory disease affecting the periodontal tissues. At initial presentation, generalized erythema and swelling were observed. Initial periodontal therapy was therefore performed to remove and control bacterial plaque as a local risk factor. Periodontal inflammatory burden was quantified using periodontal epithelial surface area (PESA) and periodontal inflamed surface area (PISA)[6,7]. PESA represents the total epithelial surface area of the periodontal pockets, calculated based on pocket depth and attachment loss, and is expressed in square millimeters. PISA represents the area of inflamed pocket epithelium, calculated by extracting only BOP-positive sites from PESA. At the initial examination, the PISA was 642.1 mm^2 and the PESA was 1,629.1 mm^2. At the most recent SPT, the PISA had decreased to 0 mm^2, while the PESA remained at 1,003.2 mm^2. Based on the relationship between PCR and BOP, these findings indicate that inflammation had been successfully controlled (Table 1).

Initially, periodontal surgery was planned for teeth #25, #26, and #27. Tooth #26 exhibited frequent acute exacerbations and increased mobility, was deemed unsalvageable, and extraction was performed. Teeth #25 and #27 showed reduced PD and were not indicated for surgery. Fixed prostheses using teeth #25 and #27 as abutments were later placed for oral functional rehabilitation. During periodontal surgery, an enamel pearl was observed on the buccal-distal root of tooth #16, with an underlying three-wall bone defect. Enamel pearls are a known risk factor for localized periodontitis[8]. The enamel pearl was removed via odontoplasty, and autogenous cortical bone harvested from the buccal alveolar bone was grafted to promote regeneration. Cortical bone contributes to both osteoconduction and direct incorporation of the grafted bone[9]. Grade I buccal furcation involvement was carefully treated with SRP, and alveolar bone contouring was performed. For the narrow vertical defect of the left maxillary central incisor with PD $\geq$6 mm, enamel matrix derivative (Emdogain) was applied for periodontal regenerative therapy, promoting tissue regeneration via amelogenins secreted from Hertwig's epithelial root sheath[9]. Sites treated with regenerative therapy demonstrated bone formation on radiographs, PD reduction to 2 mm, and physiological mobility, consistent with the study by Giannobile and Somerman[10], who reported superior attachment gain and PD reduction when Emdogain is combined with flap surgery. Autogenous bone grafting also produced significant improvement, consistent with reports by Froum et al.[11].

PDs $\leq$3 mm and negative BOP were achieved, although grade 1 mobility persisted at teeth #32 and #41. The patient was transitioned to SPT. Tooth #16 exhibited PD reduction postoperatively due to gingival recession, with partial exposure of the furcation; epithelial attachment was obtained and clinical stability was maintained. Careful observation remains necessary.

Interestingly, non-surgical treatment of implant sites exhibiting BOP and cup-shaped bone defects on radiographs at initial presentation resulted in favorable outcomes. Thorough plaque control and debridement were performed using rubber cups, polishing paste, floss, interdental brushes, and plastic instruments, which are softer than titanium and do not damage implant surfaces[12]. Peri-implantitis is a multifactorial disease sharing many clinical features and risk factors with periodontitis[13,14]. Treatment is divided into two phases: 1) anti-infective and 2) regenerative. The anti-infective phase focuses on mechanical decontamination of the

implant surfaces, while the regenerative phase aims to establish conditions suitable for re-osseointegration[15]. In this patient, meticulous plaque control and SRP resolved inflammation and allowed bone flattening in some areas.

The patient has maintained SPT for 10 years, and had achieved stable outcomes as of August 2025. The patient has demonstrated an understanding of oral status and actively participates in SPT visits every 3 months. At each visit, oral hygiene instruction, professional mechanical tooth cleaning, scaling, and application of high-concentration fluoride for root surface protection are provided. Even during the Covid-19 pandemic in 2020, the patient continued to attend visits, reflecting a strong patient-clinician relationship. Continued SPT is planned to maintain long-term periodontal and peri-implant health.

Conclusion

This case demonstrated that periodontal regenerative therapy can achieve favorable outcomes in severe chronic periodontitis with external root resorption caused by trauma, inverted crown-to-root ratios, and vertical bone defects extending to the apex. Further, thorough plaque control and SRP contributed to flattening of vertical bone defects and stabilization of peri-implant tissues. The patient remains motivated, and careful SPT will continue to ensure long-term periodontal and peri-implant health.

Conflicts of Interest

The authors declare no conflicts of interest related to this article.

Acknowledgments

This paper is related to the presentation that won the 2022 Specialist Physician Outstanding Case Presentation Award at the 156th Spring Scientific Meeting of the Japanese Society of Conservative Dentistry, 2022, with the latest clinical data added.

References

1) The Japanese Society of Periodontology. Clinical practice guideline for the periodontal treatment 2015. Ishiyaku Publishers: Tokyo; 2015. 8.
2) Yamamoto M. Chapter 5, Ⅰ: Periodontal disease treatment methods. Numabe Y, Saito A, Umeda M, Yamamoto M, Iwata T. The periodontology. 4th ed. Nagasue Shoten: Kyoto; 2019. 105–110.
3) Weinstein P, Milgrom P, Melnick S, Beach B, Spadafora A. How effective is oral hygiene instruction? Results after 6 and 24 weeks. J Public Health Dent 1989; 49: 32–38.
4) Consolaro A, Bittencourt G. Why not to treat the tooth canal to solve external root resorptions? Here are the principles! Dental Press J Orthod 2016; 26: 20–25. doi: 10.1590/2177-6709.21.6.020-025.oin.
5) Levin L, Trope M. Root resorption. Hargreaves KM, Goodis HE. Seltzer and Bender's dental pulp. 3rd ed. Quintessence Publishing: Hanover Park; 2001. 425–447.
6) Nesse W, Abbas F, van der Ploeg I, Spijkervet FK, Dijkstra PU, Vissink A. Periodontal inflamed surface area: quantifying inflammatory burden. J Clin Periodontol 2008; 35: 668–673.
7) Hujoel PP, White BA, García RI, Listgarten MA. The dentogingival epithelial surface area revisited. J Periodontal Res 2001; 36: 48–55.
8) Zenóbio EG, Vieira TR, Bustamante RPC, Gomes HE, Shibli JA, Soares RV. Enamel pearls implications on periodontal disease. Case Rep Dent 2015; 236462.
9) Japanese Society of Periodontology. Guidelines for regenerative therapy in patients with periodontal disease, 2012. Ishiyaku Publishers: Tokyo; 2012. 37–42.
10) Giannobile WV, Somerman MJ. Growth and amelogenin-like factors in periodontal wound healing. A systematic review. Ann Periodontol 2003; 8: 193–204.
11) Froum SJ, Ortiz M, Witkin RT, Thaler R, Scopp IW, Stahl SS. Osseous autografts. III. Comparison of osseous coagulum-bone blend implants with open curetage. J Periodontol 1976; 47: 287–294.
12) Matarasso S, Quaremba G, Coraggio F, Vaia E, Cafiero C, Lang NP. Maintenance of implants: An in vitro study of titanium implant surface modifications subsequent to the application of different prophylaxis procedures. Clin Oral Implants Res 1996; 7: 64–72.
13) Heitz-Mayfield LJA., Lang NP. Comparative biology of chronic and aggressive periodontitis vs. peri-implantitis. Periodontol 2000 2010; 53: 167–181.
14) Berglundh T, Zitzmann NU, Donati M. Are peri-implantitis lesions different from periodontitis lesions? J Clin Periodontol 2011; 38: 188–202.
15) John V, Shin D, Marlow A, Hamada Y. Peri-implant bone loss and peri-implantitis: A report of three cases and review of the literature. Case Rep Dent 2016; 19: 2491714.

Case Report

ODEP 5 (1) : 88～98, 2025

Treatment of Extensive Apical Periodontitis Associated with Cemental Tears: A Case Report

Ryo SAKO, Hiroki IWASAWA, Kana EGAWA, Chie TAKAHARA, Hinako SEKIYA, Momoko BAMBA, Yoshiaki FURUSAWA, Yoshihiko AKASHI*, Kei NAKAJIMA* and Rie FUJII

Department of Endodontics, Tokyo Dental College
*Department of Pathology, Tokyo Dental College

Abstract

Apical periodontitis is highly prevalent among dental diseases. Accurate diagnosis requires a combination of clinical symptoms, radiographic findings, and histopathological examination. While most cases are managed with root canal treatment, surgical apicoectomy is indicated when conservative therapy fails.

Case: A 27-year-old male presented with persistent discomfort in the mandibular left central incisor. Clinical examination revealed no tenderness to percussion or apical palpation, and a sinus tract was present on the labial gingiva. Radiography showed diffuse radiolucency around the root apex. A diagnosis of chronic suppurative apical periodontitis was made, and non-surgical root canal treatment was performed. Despite completion of root canal filling, the sinus tract persisted. Postoperative radiographs revealed periapical radiolucency in the mandibular right central incisor, suspected to be the source of the persistent sinus tract. Cone-beam computed tomography (CBCT) identified a cemental tear near the apex of the left central incisor and an untreated canal in the right central incisor, with contiguous periapical lesions affecting both teeth. Retreatment of the right incisor improved periapical tissues, but the sinus tract in the left incisor remained. Apicoectomy was subsequently performed. Histopathological examination confirmed necrotic cementum and a radicular cyst.

Course: Postoperatively, both central incisors were asymptomatic, and periapical radiolucency decreased, indicating favorable healing.

Conclusion: Careful assessment of clinical signs, imaging, and treatment outcomes enabled minimally invasive management and successful healing. Continued follow-up is planned.

Key words: apical periodontitis, cemental tear, apicoectomy

Corresponding author: Ryo SAKO, Department of Endodontics, Tokyo Dental College, 2-9-18, Kanda-Misakicho, Chiyoda-ku, Tokyo 101-0061, Japan
TEL: +81-3-6380-9136, E-mail: sakoryou@tdc.ac.jp
Received for Publication: August 14, 2025/Accepted for Publication: October 27, 2025
DOI: 10.11471/odep.2025-010

Introduction

Apical periodontitis is diagnosed and treated very frequently in everyday dental practice, with approximately half of the world's population believed to have at least one affected tooth[1]. Various classifications are based on clinical symptoms, X-ray findings, and histopathological features. However, it is often difficult to match all the findings of an actual case to a single diagnostic category. The treatment plan is determined based on the diagnosis, but because radicular cysts and radicular granulomas have similar X-ray findings, pathological examination of tissue removed during apicoectomy is important for a definitive diagnosis[2].

In most cases, apical periodontitis in the jawbone is evaluated using clinical examination and X-ray imaging. Dental radiographs and cone-beam computed tomography (CBCT) are mainly used for endodontic imaging. CBCT can detect periapical bone destruction more accurately than conventional radiographs[3,4] and is often used to assess the relationship between the lesion and surrounding anatomical structures, as well as to plan apical surgery. However, the size of an apical radiolucency on a radiograph cannot determine the specific disease or whether the tooth can be preserved, which often makes treatment planning difficult.

Root canal treatment is usually the first choice for treating apical periodontitis because of its high success rate[5,6]. When the results are unsatisfactory owing to complex root canal morphology, surgical endodontic treatment is commonly performed[7].

In this report, we present a case in which apical periodontitis affecting both lower central incisors was successfully managed through gradual treatment over time, minimizing invasiveness while preserving the affected teeth. The patient agreed to the publication of this report.

Case Report

The patient was a 27-year-old male. One year earlier, he had undergone root canal treatment for both mandibular central incisors at a local dental clinic. He later visited Tokyo Dental University Suidobashi Hospital with discomfort in the mandibular left central incisor (#31). No systemic medical conditions requiring special consideration for dental treatment were identified. Both mandibular central incisors had been restored with composite resin from the incisal edge to the lingual surface. Intraoral examination findings from the first visit are summarized in Table 1. Tooth #31 exhibited no tenderness to percussion or apical palpation, and a sinus tract was noted on the labial gingiva (Fig. 1-a). The periodontal pocket depth was within 2 mm. Dental radiographs showed diffuse radiolucency around the apical region of #31 (Fig. 1-b). Based on these findings, a diagnosis of chronic suppurative apical periodontitis was made, and non-surgical root canal treatment was planned.

During treatment, a rubber dam was used for moisture control; however, owing to crowding in the lower anterior teeth, the clamp did not fit properly. The rubber dam sheet was therefore secured to the cervical region with dental floss and caulking material (Dent-to-Dam, MEDICLUS, Cheongju, Korea). Composite resin was removed using an air turbine and diamond point, and remaining caries were removed with a steel round bur and excavator. The gutta-percha points were mechanically removed from the root canal using a K-file. The removed gutta-percha showed brownish fragments suspected to be softened dentin (Fig. 2, arrow heads), along with discoloration (Fig. 2, arrows). During root canal exploration with K-files, softening was observed in the wall of root canal #31. The patient's history revealed no prior experience with rubber dam isolation. Root canal irrigation was performed with 10% sodium hypochlorite solution (Neo Cleaner, Neo Pharmaceutical, Tokyo, Japan) and 17% EDTA (17% EDTA Liquid, PENTRON JAPAN, Tokyo, Japan) using irrigation syringes. Calcium hydroxide paste (Calvital, Neo Pharmaceutical) was applied, and the tooth was temporarily sealed with glass ionomer cement (Base Cement, Shofu, Kyoto, Japan). One month later, at the second visit, #31 showed no spontaneous pain, but vertical percussion pain and a sinus tract on the labial gingiva were noted. The same sterile isolation procedure was followed, and root canal enlargement, shaping, and irrigation were performed under a dental operating microscope (OPMI pico, Carl Zeiss Meditech Co., Ltd., Tokyo, Japan) with K-files and ultrasonic instruments (VARIOS, Nakanishi, Tochigi, Japan). During electronic root canal length measurement with a #25 K-file, the value was 17 mm and it was considered shorter than

Table 1 Findings from the initial examination of teeth with suspected symptoms.

Tooth No. (FDI)	Cold test	Electric pulp test	Percussion pain	Spontaneous pain	Sinus tract	Probing depth	Remarks
#42	+	+	−	−	−	2 mm	
#41	−	−	+	−	−	2 mm	
#31	−	−	+	−	+	2 mm	Root canal caries with blackened gutta-parcha point
#32	+	+	−	−	−	2 mm	

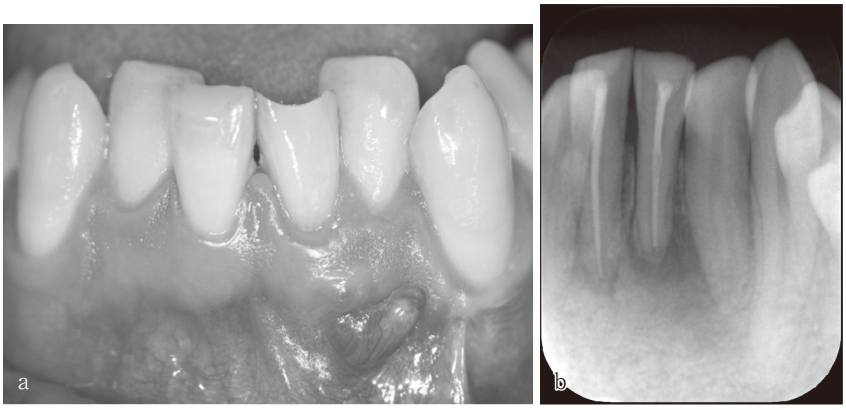

Fig. 1 Oral photograph and radiograph before starting treatment

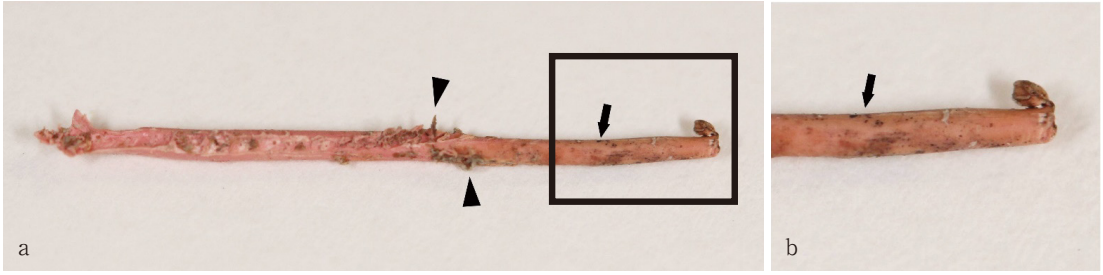

Fig. 2
a : Gutta-percha point from the lower left central incisor. b : Enlarged view of the area outlined in a.

that estimated from the radiograph; thus, a radiograph was taken with the K-file in place (Fig. 3). The tip of the K-file appeared short of the apex (17 mm), possibly owing to a laterally opened apical foramen caused by external resorption or the presence of exudate. The working length was to be remeasured at the next visit.

During the third visit, one month after the previous treatment, a trace of a sinus tract was observed on the labial apical gingiva of #31. However, no exudate was detected within the root canal. Electronic root canal length measurement again indicated the same result as before, confirming that the apical foramen was open laterally owing to external resorption. The working length was set 1 mm shorter than the measured value (16 mm) and the master apical file was set as #55. Following enlargement of the root canal using K-files, an ultrasonic scaler and a micro-excavator until the sticky sensation on the canal walls disappeared, it was confirmed that the sodium hypochlorite solution filling the canal did not effervesce. Cleaning was performed using EDTA, followed by lateral condensation root canal filling using gutta-percha points and a magnesium oxide-based root canal sealer (MGO Sealer, Neo Pharmaceutical). The lateral condensation filling was performed using the master point of the master apical file size (PIERCE, META BIOMED, Cheongju, Korea), the

Fig. 3 Confirmation of root canal length using radiography

Fig. 4 Radiograph after root canal filling of the lower left central incisor

accessory point of the fine-medium size (GC, Tokyo, Japan), and the 04 taper spreader (YDM, Tokyo, Japan).

After applying root canal sealer to the master point surface with the half of working length of #31, the master point was carefully inserted into the root canal. During insertion, the sealer was applied by tracing the entire circumference of the root canal wall with the master point. Subsequently, lateral pressure was applied to the master point using a spreader to create a gap. The subsequent procedure involved the insertion of an accessory point, to which a sealer had been applied to the tip, into the aforementioned gap. This was followed by the re-application of pressure with the spreader. The process of applying pressure with the spreader and inserting the accessory point was repeated until the insertion length of each reached approximately half the root canal length, and until sealer adhered to the surface of the spreader upon its removal from the root canal. Post-obturation radiographs showed an opaque image suggestive of sealer extrusion from the apical foramen of #31 and a radiolucent area around the apex of the mandibular right central incisor (#41) (Fig. 4). A possible cause of sealer extrusion from the apical foramen was thought to be that the sealer viscosity had become significantly higher than the standard. Although #41 showed no percussion pain or gingival tenderness, the periapical radiolucency had enlarged compared to previous images, raising suspicion of apical periodontitis. One month after root canal filling of #31, a sinus tract and pus discharge persisted in the labial gingiva of the lower anterior region. As #31 had been asymptomatic at the time of obturation, apical periodontitis in #41 was suspected as the cause. #41 had no spontaneous pain, and was diagnosed with chronic suppurative apical periodontitis. The patient was informed that #41 may require retreatment and that apicoectomy of #31 might be necessary. Dental CBCT was scheduled for further assessment. CBCT revealed radiolucency with labial cortical bone loss around the apex of #31 (Fig. 5-a). A fragment-like opaque image was also observed in the mesial apical region of #31, suggestive of cementum detachment (Fig. 5-b). In #41, an untreated lingual canal was identified (Fig. 5-c, d). Because #41 could be clamped, standard rubber dam isolation was performed with caulking material. Under a dental microscope, the untreated lingual canal was accessed. The labial and lingual canals including isthmus suspected of infection were unified using a U-file ISO30 (Nakanishi). The gutta-percha points removed by H-file showed deposits and discoloration, suspected to be sources of persistent infection. The instruments, irrigants, and medicaments used for root canal treatment in #41 were identical to those employed for treatment in #31. Root canal treatment was performed over multiple sessions, and root canal filling was completed once symptom resolution was confirmed. Radiographs taken during trial fitting and after root canal filling showed a radiolucent area on the mesial side of #31 (Fig. 6), possibly related to the recurrent sinus tract. As orthodontic treatment of the mandible was planned, consultation with an orthodon-

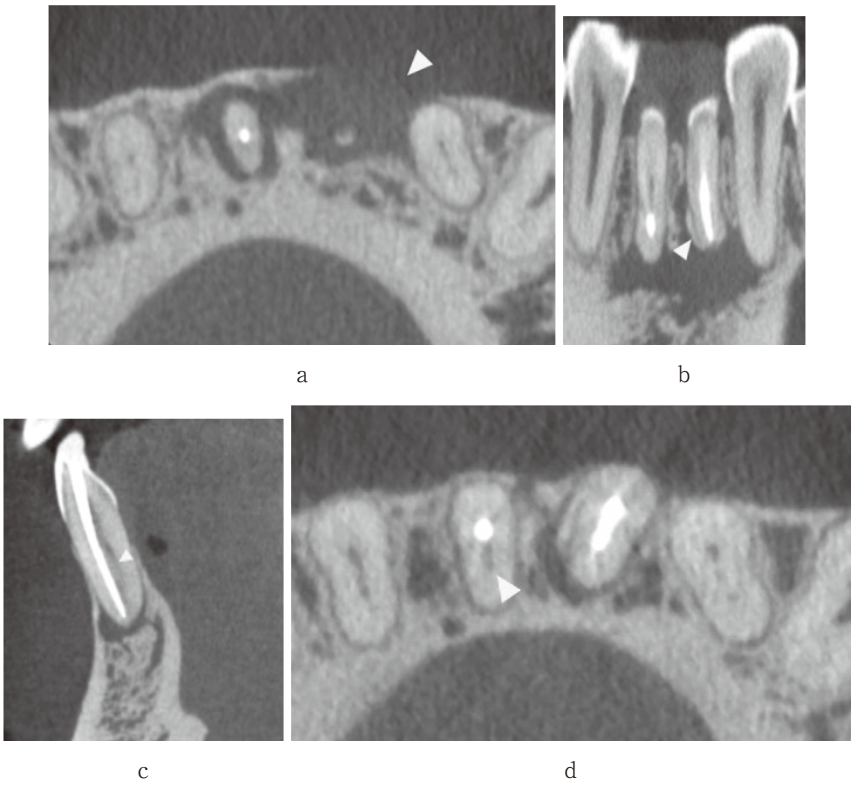

Fig. 5 CBCT images of the lower anterior region
a : Axial section. Arrowhead indicates loss of labial cortical bone. b : Coronal section. Arrowhead indicates cemental tear. c : Sagittal section of the lower right central incisor. Arrowhead indicates an untreated root canal. d : Axial section of the lower right central incisor. Arrowhead indicates an untreated root canal.

tist was conducted, and a 6-month observation period was set to evaluate healing after root canal treatment.

Six months after root canal filling of #41, the lower anterior teeth were re-evaluated. #41 showed no oral symptoms. #31 presented with percussion pain, with a sinus tract on the labial gingiva. Most periodontal pockets at site #31 measured 2 mm, except for the central labial area, which showed a depth of 10 mm. Dental radiographs revealed that the periapical radiolucency in #41 had resolved with formation of alveolar bone, while #31 showed an enlarged radiolucent area extending toward the crown on the mesial side (Fig. 7). Based on the course to date, apical inflammation associated with apical granuloma, apical cyst, or cementum detachment in #31 was suspected as the cause of the persistent sinus tract. The expansion of periapical inflammation raised concerns about a potential transition of combined endodontic and periodontal lesions. Apicoectomy was indicated to remove the infection source and inflammatory tissue around the apex.

After surface anesthesia with ethyl aminobenzoate (BEEZOCAINE Dental Jelly, BEE BRAND MEDICO DENTAL CO., LTD., Osaka, Japan) on the labial gingiva of the lower anterior teeth, infiltration anesthesia was administered using 2% lidocaine with 1/80,000 adrenaline (EPILIDO Combination Injection Dental Cartridges, NIPRO CORPORATION, Osaka, Japan). Once anesthesia had taken effect, an interproximal papilla protection incision was made between the mandibular lateral incisors, and the mucoperiosteal flap was elevated. Adherent areas between the flap and the periapical inflammatory tissue were separated with a scalpel blade. The inflammatory tissue was detached from the bone cavity wall using a spoon excavator and removed in one piece. During removal, a hard fragment suspected to be detached cementum from the root surface of #31 was collected (Fig. 8). Pathological examination was requested for both the soft and hard tissue specimens.

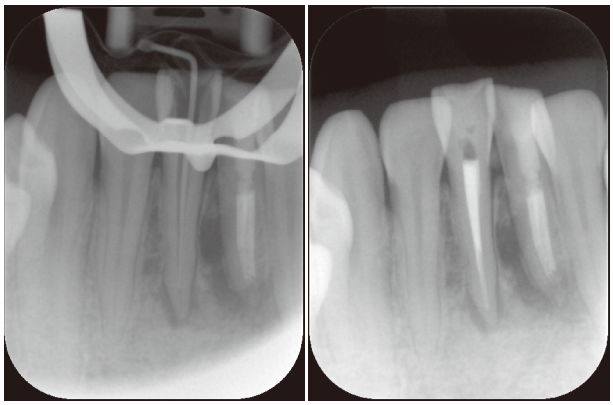

Fig. 6 Radiographs related to root canal filling of the lower right central incisor
a : Trial fitting of the gutta-percha point. b : After root canal filling.

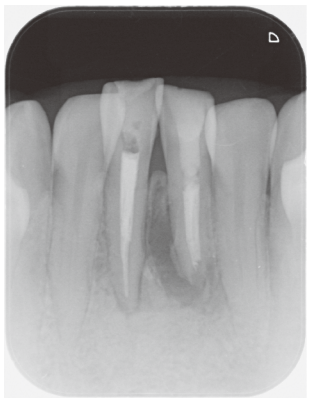

Fig. 7 Evaluation of periapical radiolucency after root canal filling
The lower left incisor at 1 year post-treatment ; the lower right incisor at 6 months post-treatment.

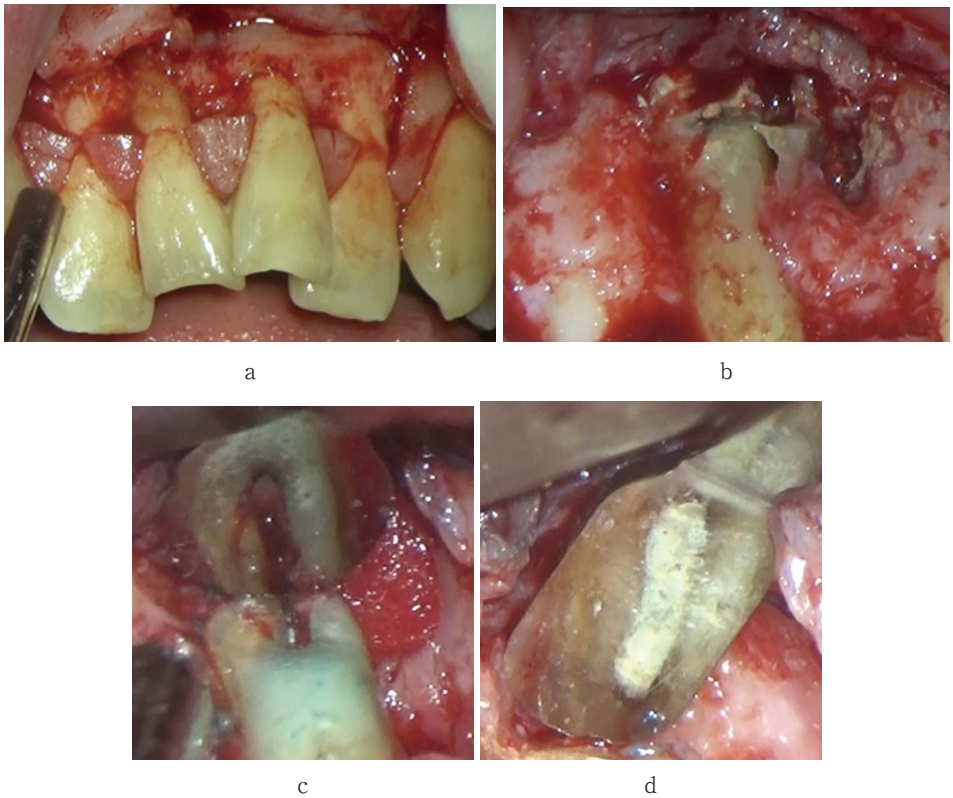

a b c d

Fig. 8
a : Following complete lamina separation. b : Cemental tear observed on the root apex surface. c : Immediately after retrograde root canal filling cavity preparation. d : Following retrograde root canal filling.

As #41 was healing radiographically and only the apex of #31 was exposed in the bone cavity after soft tissue removal, apicoectomy was performed only on #31. The root was cut 3 mm from the apex.

Cementum that appeared easy to detach was also observed and was removed as much as possible. The retrograde root canal cavity was prepared to 3 mm using an ultrasonic tip (E32D, Nakanishi) and filled with

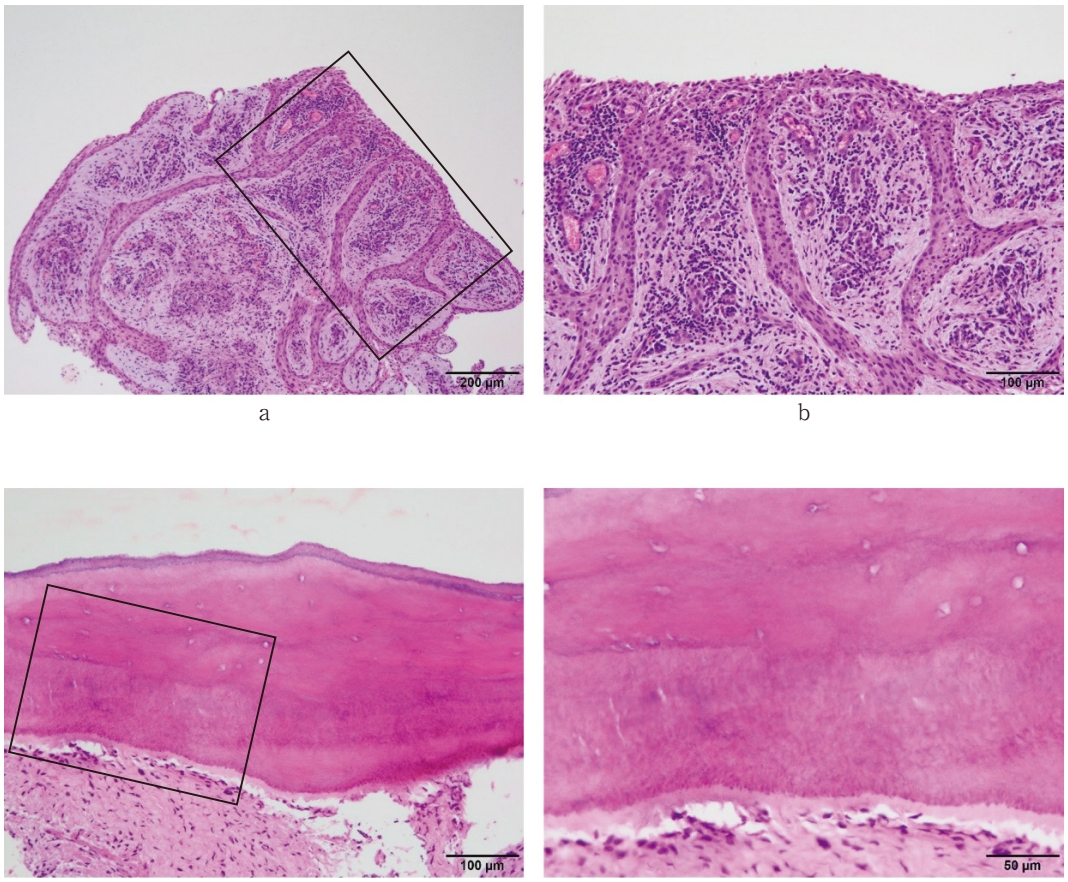

a b c d

Fig. 9 Histopathological images of tissue removed from the periapical area of the lower left central incisor

Tissue was stained using H-E staining.

a : Soft tissue at low magnification. b : Soft tissue at high magnification. c : Cemental tear fragment at low magnification. d : Cemental tear fragment at high magnification.

reinforced zinc oxide-eugenol cement (Super EBA Cement, MOKUDA DENTAL, Hyogo, Japan). The flap was sutured with 6-0 nylon. Penicillin-based antibiotics were prescribed for infection prevention and analgesics were prescribed for pain control. The suture was removed 6 days after apicoectomy. The gingiva showed no swelling or bleeding, and the sinus tract had resolved. Histopathology with H-E staining revealed that the excised soft tissue was lined with non-keratinized stratified squamous epithelium with nail-like projections, inflammatory cell infiltration, and collagen fiber bundles, consistent with a radicular cyst. The hard tissue exhibited cemental cavities and Sharpey's fiber structures, confirming it as necrotic cementum detached from the root surface (Fig. 9). Given the favorable clinical course, periodic radiographic evaluation of alveolar bone healing around the apex was planned.

Shortly after apicoectomy, dental radiographs revealed a radiolucent area extending from the periapical region to the crown side on the mesial aspect of #31 (Fig. 10-a). Six months later, #31 showed no mobility, percussion pain, or sinus tract with pus discharge, and #41 also remained asymptomatic. Radiographs demonstrated a reduction in the radiolucent area around #31 compared to the immediate postoperative image, and no radiolucency was observed around #41 (Fig. 10-b). Six months later, #31 remained symptom-free, and the periodontal pocket depth, which had been 10 mm preoperatively, had improved to 3 mm. A radiolucent area persisted on the mesial side of #31's apex (Fig. 10-c), but given the extent of preoperative alveolar bone loss, the tooth was considered to be in the healing phase.

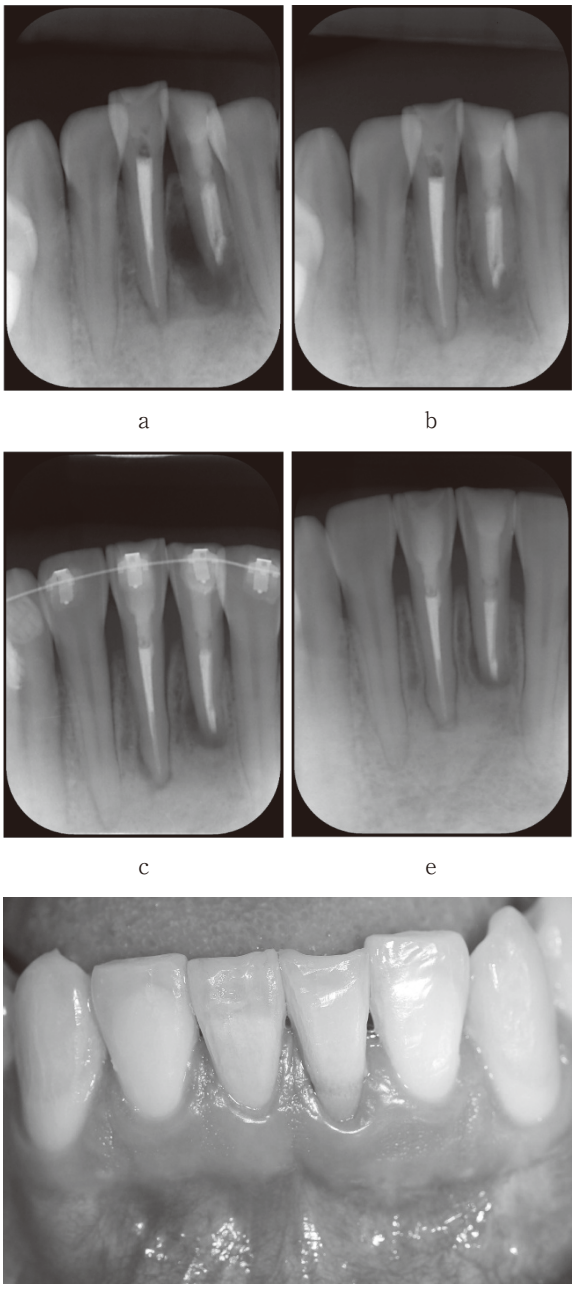

Fig. 10 Changes in periapical radiolucency after apicoectomy

a : Day of apicoectomy. b : Six months after apicoectomy. c : Lower left incisor at 1 year after apicoectomy ; lower right incisor at 1 year and 6 months after root canal filling. d : The sinus tract disappeared from the gingiva. e : Lower left incisor at 2 years after apicoectomy ; lower right incisor at 2 years and 6 months after root canal filling.

Meanwhile, #41 showed widening of the periodontal ligament space owing to orthodontic forces, but the periapical region was judged to be healed. Two years after apicoectomy of #31, and two and a half years after root canal treatment of #41, both teeth remained free of symptoms (Fig. 10-d). Comparison with previous radiographs showed further reduction in periapical radiolucency of #31 and normalization of the periodontal ligament space in #41 (Fig. 10-e). Based on these findings, both mandibular central incisors were judged to be healing well. However, as further monitoring is necessary, annual follow-up examinations are planned.

Discussion

X-ray imaging has long been used to examine endodontic diseases, but diagnostic accuracy has improved with the advent of CBCT[3]. However, while the radiographic appearance varies depending on the nature of the bone defect, complete agreement with the histopathological diagnosis is often difficult. Apical periodontitis also tends to progress slowly, making it hard to determine the point at which it becomes refractory. Therefore, conservative treatment of the affected tooth, usually by root canal therapy, is generally performed first. Based on the course of symptoms and radiographic findings, surgical endodontic therapy may then be considered if necessary[8].

Determining the timing for root canal filling upon completion of treatment requires the resolution of all symptoms in the affected tooth following the establishment of control of infection within the root canal. In this case, as it was difficult to identify the causative tooth for the sinus tract, #31 required surgical endodontic treatment after root canal therapy due to the possibility of extra-canal bacterial infection or cementum detachment, and root canal treatment for tooth #41, which was thought to be connected to the sinus tract based on the periapical radiolucency. As long-term follow-up was anticipated for both teeth, root canal filling was performed on tooth #31 despite residual gingival swelling, which was thought to be a trace of the sinus tract. Progressing with root canal treatment on #31 and #41 also offered the prospect that, as the extensive periapical inflammation improved, the causative tooth for the sinus tract might be identified. However, continuing to apply calcium hydroxide paste within the

root canal of #31 during the treatment of #41 risked increasing the tooth's fragility and causing coronal leakage[9]. To avoid these risks, despite deviating from standard practice, the root canal of #31 was sealed with root canal filling material. Furthermore, as #31 exhibited symptoms including a recurrent sinus tract following root canal treatment, it was decided to proceed with the anticipated apicoectomy. Given that the presence of a gutta-percha point within the retrograde filling cavity is considered essential for adequate retrograde filling, the decision not to use calcium hydroxide for temporary filling until the sinus tract resolved may have been effective in this case. In the present case, #41 healed with infected root canal treatment, whereas #31 required apicoectomy. This highlights the importance of stepwise treatment planning that takes into account invasiveness to the patient.

In #31, an opaque image suggestive of sealer extrusion was observed in radiographs taken during root canal filling. However, subsequent radiographs showed no signs of residual sealer, and none was found in the periapical bone cavity during apicoectomy. The root canal sealer used in this case contained zinc oxide, magnesium oxide, bismuth oxide, methyl salicylate, and guaiacol. Its tissue reaction has demonstrated safety comparable to that of resin-based sealers and calcium hydroxide-based sealers[10]. There are various reports on the clinical significance of sealer extrusion. Some indicate that eliminating the infection source within the canal and sealing the apex are more important than addressing extrusion outside the foramen[11]. Although some cases have healed following surgical removal[12] of extruded material, many reports describe overflow of filling material beyond the apical foramen[13], and perceptions of such overflow have changed over time.

MGO sealer requires evenly squeezing out the base paste and catalyst paste from their respective tubes and kneading them together. However, since the catalyst paste has higher fluidity than the base paste, more of it may be squeezed out, even when handled identically. Mixing in this state will result in the kneaded sealer having higher fluidity than intended. In this case, the cause of root canal sealer overflowing beyond the apical foramen was considered to be inadequate adjustment of consistency during mixing, or enlargement of the apical foramen due to external resorption of the root. The sealer, which overflowed beyond the apical foramen due to higher than normal fluidity, was thought to have been expelled through the recurrent sinus tract before its setting had completed. Therefore, immediate surgical intervention for the extrusion was avoided, which was considered appropriate. However, because foreign bodies outside the apical foramen may place stress on the healing process[14,15], close monitoring and appropriate treatment planning remain important.

In this case, both teeth showed periapical radiolucency extending mesiodistally and labially on CBCT images. When a wide periapical inflammatory lesion involves the apices of two teeth, it is referred to as a "lesion including two apices," and it has been reported that identifying the causative tooth is often challenging despite various diagnostic examinations[16,17]. In the present case, the apical periodontitis of tooth #31 appeared to have expanded to involve the apex of tooth #41, corresponding to a Type 1–2 lesion. Because the adequacy of the previous endodontic treatment was questionable, retreatment of both teeth was considered necessary at our institution. The treatment sequence was determined to begin with tooth #31, as its apex was closest to the sinus tract and primarily involved in the periapical radiolucency, followed by endodontic treatment of tooth #41. As a result, tooth #41 was successfully separated from the original periapical abscess cavity, and surgical endodontic intervention was limited to tooth #31. Following standard procedures, the laterally open apical foramen was removed, and the apical region was sealed, which is believed to have achieved infection control. Furthermore, a cemental fracture was observed near the apex of #31, which may have contributed to the persistent symptoms, including deepening of the periodontal pocket. In general, localized deep periodontal pockets raise suspicion of vertical root fracture. However, in this case, CBCT revealed no findings suggestive of a fracture line, leading to its exclusion.

Cemental tear has been reported to be more common in males and in incisors, with causes thought to include age-related changes and occlusal trauma[18]. Both cemental tear and vertical root fracture have been associated with common etiological factors such as occlusal trauma, excessive occlusal forces, structural loss during endodontic treatment, prosthetic or post placement, root morphology, and age-related changes. In this context, the design of the final restoration or

prosthesis and appropriate occlusal adjustment should be considered crucial in minimizing excessive stress concentration, thereby potentially preventing both cementum detachment and vertical root fracture. In the present case, there was no history of occlusal trauma, but the patient was male and the affected tooth was a mandibular central incisor. CBCT and microscopic examination revealed cementum detachment, and easily detachable cementum was removed during apicoectomy. Following removal of the apical infection, necrotic tissue, and inflammatory substances in #31, the sinus tract remaining in the gingiva disappeared, and improvement in the periodontal pocket was also observed due to regeneration of the remaining periodontal ligament.

Various criteria for evaluating healing after endodontic treatment have been reported[19]. However, because of the risk of recurrence, long-term follow-up is important; a follow-up period of at least 4 years is generally recommended[20]. This case was reported within 3 years of treatment, but because a clear trend toward healing was observed, it may serve as a useful reference for planning minimally invasive treatment. At present, both teeth are progressing well, but regular follow-up based on clinical and radiographic findings is planned. If apical periodontitis recurs, the cause will be re-evaluated, and the need for non-surgical or surgical endodontic therapy will be carefully considered.

Conclusion

In managing extensive apical periodontitis associated with cemental tears, it is essential to adopt a stepwise, tooth-preserving treatment strategy, to evaluate clinical and radiographic changes after each intervention, and to adjust the treatment plan according to the healing response.

Acknowledgements

We express our gratitude to Professor Kenichi Matsuzaka of the Department of Pathology, Tokyo Dental College, for his involvement in the pathological diagnosis of the extracted specimen in this case report. We would like to thank Editage (www.editage.jp) for English language editing.

Conflicts of Interest

There are no conflicts of interest to disclose in relation to this case report.

References

1) Tiburcio-Machado CS, Michelon C, Zanatta FB, Gomes MS, Marin JA, Bier CA. The global prevalence of apical periodontitis: a systematic review and meta-analysis. Int Endod J 2021; 54: 712–735.
2) Syed Ismail PM, Apoorva K, Manasa N, Rama Krishna R, Bhowmick S, Jain S. Clinical, radiographic, and histological findings of chronic inflammatory periapical lesions—a clinical study. J Family Med Prim Care 2020; 9: 235–238.
3) Patel S, Dawood A, Mannocci F, Wilson R, Pitt Ford T. Detection of periapical bone defects in human jaws using cone beam computed tomography and intraoral radiography. Int Endod J 2009; 42: 507–515.
4) Mostafapoor M, Hemmatian S. Evaluation of the accuracy values of cone-beam CT regarding apical periodontitis: a systematic review and meta-analysis. Oral Radiol 2022; 38: 309–314.
5) Natkin E, Oswald RJ, Carnes LI. The relationship of lesion size to diagnosis, incidence, and treatment of periapical cysts and granulomas. Oral Surg Oral Med Oral Pathol 1984; 57: 82–94.
6) Nair PN. New perspectives on radicular cysts: do they heal? Int Endod J 1998; 31: 155–160.
7) Bucchi C, Rosen E, Taschieri S. Non-surgical root canal treatment and retreatment versus apical surgery for apical periodontitis: a systematic review. Int Endod J 2023; 56: 475–486.
8) Karamifar K, Tondari A, Saghiri MA. Endodontic periapical lesion: an overview on the etiology, diagnosis and current treatment modalities. Eur Endod J 2020; 5: 54–67.
9) Sunlakawit C, Chaimanakarn C, Srimaneekarn N, Osiri S. Effect of calcium hydroxide as an intracanal medication on dentine fracture resistance: a systematic review and network meta-analysis. J Endod 2024; 50: 1714–1724 e6.
10) Nakano K, Tomida M, Sato M, Matsuura S, Yamamoto A, Kasahara E, Kawakami T. Histopathological safety evaluation of newly-developed MgO sealer. Eur J Med Res 2011; 16: 526–530.
11) Malagnino VA, Pappalardo A, Plotino G, Carlesi T. The fate of overfilling in root canal treatments with long-term follow-up: a case series. Restor Dent Endod 2021; 46: e27.
12) Ektefaie MR, David HT, Poh CF. Surgical resolution of chronic tissue irritation caused by extruded endodontic

filling material. J Can Dent Assoc 2005; 71: 487–490.
13) Abulhamael A, Lim D-Y, Chiang K, Alghamdi F, Roges R. The prevalence of cases with apical sealer extrusion published in recent articles of the endodontic literature. Ann Dent Spec 2022; 10: 62–64.
14) Sari S, Duruturk L. Radiographic evaluation of periapical healing of permanent teeth with periapical lesions after extrusion of AH Plus sealer. Oral Surg Oral Med Oral Pathol Oral Radiol Endod 2007; 104: e54–59.
15) Aminoshariae A, Kulild JC. The impact of sealer extrusion on endodontic outcome: a systematic review with meta-analysis. Aust Endod J 2020; 46: 123–129.
16) Yoshioka T, Sakaue H, Yoshioka T. Periapical lesion around the maxillary lateral incisor: part 1. JJEA 2015; 36: 69–74.
17) Yoshioka T, Sakaue H, Yoshioka T. Periapical lesion around the maxillary lateral incisor. part 2: a lesion including 2 root apices of both an endodontically treated tooth and an intact tooth. JJEA 2015; 36: 121–125.
18) Lin HJ, Chan CP, Yang CY, Wu CT, Tsai YL, Huang CC, Yang KD, Lin CC, Chan SH, Jeng JH. Cemental tear: clinical characteristics and its predisposing factors. J Endod 2011; 37: 611–618.
19) Rajasekhar R, Soman S, Sebastian VM, Muliyar S, Cherian NM. Indexes for periapical health evaluation—a review. Int Dent Res 2022; 12: 97–106.
20) Strindberg LZ. The dependence of the results of pulp therapy on certain factors—an analytical study based on radiographic and clinical follow-up examination. Acta Odontol Scand 1956; 14: 1–175.

Submission Guidelines for *ODEP*

1. *ODEP* aims to develop conservative dentistry (operative dentistry, endodontology, and periodontology) through the publication of research and reviews on the following topics: (1) General dental medicine, clinical practice, and education on conservative dentistry; and (2) Conservative dentistry.
2. Papers are categorized into the following four types: (1) Original articles (reports on unique research discoveries); (2) Reviews (discussions on research questions and objectives to indicate future directions, or summaries of the contents of existing papers to propose new ideas); (3) Mini reviews (concise summaries of recent topics; mini reviews include papers awarded with prizes); and (4) Case and clinical reports (analysis of clinical records useful for dental care practice and development of the field of conservative dentistry). Reviews and mini reviews are categorized into the following: (1) Papers requested by the editorial board; and (2) Submitted papers.
3. Original articles and case and clinical reports are limited to the following: (1) Papers that have not been published in other journals; (2) Papers that are not presently submitted to another journal; and (3) Papers that are not presently scheduled for publication.
4. Acceptance or rejection of papers is determined through peer review (except for papers requested by the editorial board).
5. Submitted papers should be concisely written in English.
6. In principle, original articles should be organized as follows: (1) Abstract; (2) Introduction; (3) Materials and Methods; (4) Results; (5) Discussion; (6) Conclusion; (7) References; (8) Figure legend; (9) Figures and Tables. In principle, papers other than original articles should conform to the style format of original articles.
7. In principle, *ODEP* is published once a year in December. In addition, special issues are published when appropriate.
8. The Japanese Society of Conservative Dentistry provides a certain amount of support for the listing fees of papers. For cases in which the lead author is not a member of the Japanese Society of Conservative Dentistry, such support is not provided. For cases in which the lead author is a member, but the co-authors include a non-member, partial support is provided. The cost to be borne by the authors is determined based on the number of non-members. The costs for figures, tables and photographs, for dispatching and offprints, and for creating the J-STAGE registration data are borne by the authors. In the case of papers requested by the editorial board, such costs are exempted.
9. Date of submission is the date when the submitted manuscript arrives at the secretariat of the Japanese Society of Conservative Dentistry. Date of acceptance is the date when the reviewers determine that the submitted manuscript can be published.
10. The listing order is the order of acceptance. A certification of publication will be issued upon request.
11. Manuscripts are to be submitted via the Japanese Society of Conservative Dentistry's website, e-mail, or postal mail. Manuscripts submitted for publication should be addressed to the secretariat of the Japanese Society of Conservative Dentistry.
12. In principle, authors can proofread their manuscript a maximum of two times. Extensive changes, additions, or deletions made to the contents of the manuscript cannot be accepted. Proofs should be returned by the designated date. If the authors do not need to proofread their manuscript, they should mention this on the left side of the cover page.
13. The copyrights for articles published in *ODEP* belong to the Japanese Society of Conservative Dentistry.
14. Matters not mentioned in these guidelines will be independently determined by the editorial board.
15. Authors' final manuscripts or publisher's versions (PDF) may be registered in the institutional repository from the time of electronic publication of the issue. The source must be indicated.

Submission of your manuscript for publication must conform to the following "Submission Guidance" as well as "Submission Guidelines."

The publishing charge is 10,000 yen for a Journal page including tables and figures. Extra charges for such as figures and tables preparation, color printing of photographs will also be paid by the authors. If authors do not pay publishing charge, the article may be retracted.

Submission Guidance (applied as of the Issue 1 of Vol. 4)

Manuscript organization

1. In principle, original articles should be organized into the following sections: (1) cover page; (2) abstract; (3) Main text (Introduction, Materials and Methods, Results, Discussion, and Conclusion); (4) References; and (5) Figure and table captions. Page numbering should start with the cover page. In principle, manuscripts, such as reviews or case reports, other than original articles should be organized in the same format as that of original articles.
2. Manuscript sections
   1) Title: The title should concisely describe the contents of the manuscript. The subtitle should also clearly describe the contents, and should not consist of only numbers.
   2) Introduction: The introduction should clearly describe the background, novelty, purpose, and significance of the study.
   3) Materials and Methods: This section should provide detailed information on the materials, equipment, or methods used along with clear instructions so that the experiments can be reproduced by others. Parameter settings, number of specimens, extraction methods, statistics processing, and others should comply with the purpose of the study.
   4) Results: This section should simply present the findings without bias or interpretation. Measurement results should show characteristic values including mean values and standard deviations.
   5) Discussion: This section should carefully consider the materials and methods, results, and others referring to relevant literature. Please note that it should not be overly assertive and should avoid off-topic points. The discussion should stay focused on the study purpose and not digress into a general discussion.
   6) Conclusion: The section should precisely summarize the results obtained and relate them to the purpose of the study and hypothesis as presented in the Introduction.
3. Manuscripts should be prepared using A4-size paper. The suggested length of each typed page is 80 alphanumeric characters per line×25 lines per page using a 12-point font. Top/bottom/left/right margins should be approximately 25 mm. Non-Japanese names and places should be in their original names.
4. For the manuscript style, refer to the latest issue of the journal.

Ethics code

1. Each report on the result of clinical research (clinical trial or observational research) or research involving any specimen collected from a human body must include a clear statement that it was approved by the head of the affiliated institution or by the research ethics review board assigned by the institution's head, in order to expressly indicate that the research was conducted in compliance with all applicable guidelines and laws, including the Declaration of Helsinki and the medical research guidelines, etc. issued by the Ministry of Health, Labour and Welfare including the following:
   1) Ethical Guidelines for Life Science and Medical Research Involving Human Subjects;
   2) Guidelines for Gene Therapy and Other Clinical Research; and
   3) Clinical Trials Act.
2. Each report on the result of research on, or a case concerning, regenerative medicine technology, etc. as defined

in the Act on the Safety of Regenerative Medicine must include a clear statement that the technology was provided to the patients in compliance with the aforementioned Act.

3. Each report on a case of a therapeutic method involving any off-label drug or device, or any pharmaceutical, medical device, regenerative medicine, or other related product not domestically approved must include a clear statement that the use was approved by the committee concerned (research ethics review board, review board for unapproved new drugs, etc.) at the affiliated institution or that the case report was approved for publication by *ODEP's* Clinical and Epidemiological Ethics Committee.
4. In each instance of publication of an academic paper, all personal information must be thoroughly protected so that none of the research subjects (patients) can be identified from it.
5. In each instance where a patient's clinical photo or X-ray image is included in an academic paper for publication, a clear statement must be provided that the consent of each such patient (or a parent, guardian, or proxy if the patient is a minor or in case it is otherwise difficult to obtain consent from the patient) was duly obtained.
6. Each report on the result of research involving animal subjects must include a clear statement that the research was approved by the animal experiment committee, etc. at the affiliated institution.

Cover page

1. The title, authors' names, institutional affiliations, and corresponding author's contact address should be centered, with a new line for each item, on the cover page.
2. The title should be in upper and lowercase letters, where the first letter of each word is uppercased and the remaining letters are lowercased. Articles, prepositions, conjunctions, and commonly used technical terms are lowercased. For hyphenated compound words, the letters following the hyphen should be lowercased.
3. The corresponding author's contact details should include the following information: one author's name, institutional affiliation, postal address, telephone and fax numbers, and e-mail address.

Abstract

1. The abstract should be a maximum of 400 words organized into four sections with the following headings: Purpose, Methods, Results, and Conclusion. Approximately three keywords should be placed at the end of the abstract.
2. Contributors should put considerable effort into preparing the abstract as it may determine whether or not the reader continues with the manuscript. When necessary, abstracts should be checked by a native English reviewer (preferably with expertise in dental medicine).

Main text

1. Introduction, Materials and Methods, Results, Discussion, and Conclusion are the main headings and are not numbered.
2. Subparagraphs should be numbered in the following order: 1. 2. 3. …; 1) 2) 3) …; (1) (2) (3) …; ① ② ③ …; and a. b. c. …
3. English characters should be written in the following manner:
   1) Generally, only the last name should be used to indicate a person.
   2) When the name of a product or manufacturer must be in the original language, the first letter of each word should be uppercased and the remaining letters lowercased.
      In principle, "generic name (product name, company name, city [state in the case of U.S.], country)" should be used in English manuscripts. Trademark and registration symbols ® and ™ are not required.
   3) Regarding common nouns in German or Latin, the first letter should be uppercased and the remaining letters lowercased. For common nouns in English and French, all letters should be lowercased.
   4) Regarding binominal nomenclature, the first letter of the genus should be uppercased and the remaining letters lowercased. The names of all genera and species should be italicized. When the same genus

appears frequently, it is acceptable to replace the name with the initial after the first use.

Example: *Streptococcus mutans* → *S. mutans*

5) For nouns that must be in their original language, other than German, Latin, English or French, all letters should be lowercased, except for commonly used technical terms.

4. In principle, SI units are used for measurements.
5. Any conflicts of interests (COI) must be declared after the conclusions. When there is no COI, the statement "The authors declare no conflict of interest related to this paper" should be included.
6. Acknowledgments for all sources supporting this study including grant funds should be added after of COI.

References

1. References must be listed at the end of the main text, and numbered in the same order as they appear in the text.
2. In the main text, a cited reference should appear with a superscript numeral and closing parenthesis. When two references are cited, a comma should be used to separate them; more than two references should be connected by an en dash between the first and last numeral.
   Examples: "by authors[3)]", "…is reported[7,8)]", "previous studies[10–15)]show"
3. Examples of Reference

a. Journal articles

Number) Last name and first name of all authors with a comma separating each author. Title of paper. Name of journal and publishing year in the Christian era; Volume number: Inclusive page numbers of paper.

Example:

1) Clark AB, Erickson D, Hamilton FG. Tensile bond strength and modulus of elasticity of several composite resins. J Dent Res 1992; 37: 618–621.

b. Book

Number) Author (co-authors). Title of book. First/last volume. Edition. Publisher's name: Publisher's location (City); Publishing year in the Christian era. Cited pages.

Example:

2) Phillips RW. Skinner's science of dental materials. 9th ed. WB Saunders: Philadelphia; 1991. 219–221.

c. Book with co-authors

Number) Contributor's name. Title of contributed article. Name of editor (editor-in-chief). Book title. First/last volume. Edition. Publisher's name: Publisher's location (City); Publishing year in the Christian era. Cited pages.

Example:

3) Torneck CD. Dentin-pulp complex. Ten Cate AR. Oral histology. 5th ed. Mosby: St. Louis; 1998. 150–196.

For cases in which each author's contribution is not separately indicated, the author's name and the title of the contributed article should not be listed.

Number) Name of editor (editor-in-chief). Title of book. First/last volume. Edition. Publisher's name: Publisher's location (City); Publishing year in the Christian era. Cited pages.

d. Other writing styles

・Abstracts of scientific meeting

Number) Presenter (all presenters should be cited. A comma should be used to separate the authors in the case of co-presentations.). Title of abstract. Name of journal and publishing year in the Christian era; Volume number: Inclusive page numbers, abstract number.

Example:

4) Marais JT. Cleaning efficacy of a new root canal irrigation material. J Dent Res 1998; 77: 669, Abst. No. 300.

・Journal articles in press

In principle, the same style as that of a regular journal article should be used; however, when the inclusive page

numbers are not known, they can be omitted. The statement "in press" should be shown at the end.

Example:

5) Sato K. Effect of toothbrushes on gingival abrasion. J Periodont Res 1994; 29: in press.

・Electronic journal

In principle, the same style as that of a regular journal article should be used; however, when the inclusive page numbers are not known, the DOI and other indicators should be shown. When papers are published in electronic journals before printing, the statement [Epub ahead of print] should be shown after the publishing year and month.

Example:

6) Sunada N, Ishii R, Shiratsuchi K, Shimizu Y, Tsubota K, Kurokawa H, Miyazaki M. Ultrasonic measurement of the effects of adhesive application and power density on the polymerization behavior of core build-up resins. Acta Odontol Scand; doi: 10.3109/00016357.2011.654252

・Internet website

Page publisher. Title of page. URL address. (Access date)

Example:

7) World Health Organization. Continuous improvement of oral health in the 21st century. http://www.who.int/oral_health/en/ (cited 2005. 10. 1)

4. In principle, journal names should be abbreviated in accordance with the format used by the journal.

Figures and tables

1. Figures, photographs, and tables are categorized into figures and tables, and then numbered. Paper size should be A4, and each figure and table should be printed on a separate page. The numbers allocated for the figures and tables should be consistent with those referred to in the text.
2. Figures and tables should be accompanied by explanations that are easily understandable. Explanations of figures/tables are presented as captions and explanations for tables/tables should be presented as footnotes.
3. If authors wish to have the figures shown in color, color data should be attached; if authors wish to have the figures shown in black and white, black-and-white data should be attached.

   Notes on creating imaging data:

   ・The jpg data format should be used if possible.

   ・Image size should correspond to the layout; image resolution should be at least 300 dpi for photographs and at least 1,200 dpi for line drawings.
4. If authors wish to reprint a figure from another publication, should be responsible for confirming whether permission is required from that publication, and obtaining permission if necessary. In addition, the source should be clearly stated in the explanatory text of each figure.

Sending manuscript intended for publication

1. The manuscript (cover page, abstract, main text, references, and figure and table captions are created as one file) should be formatted as a Microsoft Office Word (hereafter "Word") document.
2. Figures should be provided in jpg or pdf format.
3. Tables should be provided in Microsoft Office Excel, jpg, pdf, or Word format.
4. File titles should be as follows: "author name"_"university name (name after department is not needed)"_"manuscript/figure/table/submission form"_".filename extension (indicating file type)".

   Example) Nihon Tarou_Nihon University/manuscript.docx; Nihon Taro_Nihon University_Figure.jpg; Nihon Taro_Nihon Univesity_Table.xlsx; Nihon Taro_Nihon University_submission form.pdf

   Also, pdf files with embedded fonts for all contents are acceptable for submission. In such cases, file names should be as follows: Nihon Taro_Nihon University_comprehensive manuscript.pdf
5. E-mail title (subject) should be "Submitted papers for ODEP".

6. Submitted papers should be sent to the e-mail address of Oral Health Association of Japan: hensyu6@kokuhoken.or.jp. For safety, also send as a CC to hensyu5@kokuhoken.or.jp.
7. When e-mail submission is difficult for such reasons as the file size is too large, submission via an FTP server and other methods are acceptable. In such cases, the intent of submission should be informed by e-mail. In the e-mail, information regarding the site and other methods for downloading the file should be provided.
8. The submission form of *ODEP* provided on the Japanese Society of Conservative Dentistry's home page (https://www.kokuhoken.or.jp/form/ jscd/form-pub/) can be used for submission.

歯科接着用レジンセメント

Tokuyama

ESTECEM Ⅱ

BONDMER Lightless Ⅱで簡単前処理、術式の統一

BoSE Technology × Contact Cure

CR充填時のボンディング

支台築造時の前処理

補綴物・補綴装置の前処理

セメンティング時の前処理

補綴物も歯質も操作はひとつ

塗布後の待ち時間も光照射も不要！

エステセムⅡ

- CAD/CAMハイブリッドレジンも安定した接着力。
- 垂れにくく、余剰セメントも除去しやすいペースト。
- 無機フィラー74wt%で高強度を実現。

歯科接着用レジンセメント **エステセム Ⅱ** ボンドマー ライトレス Ⅱ セット （管理医療機器）認証番号228AFBZX00129000

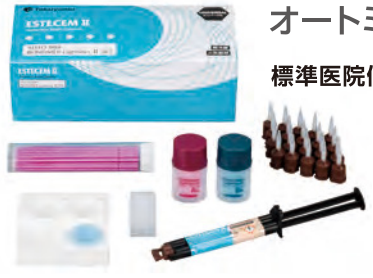

オートミックスセット

標準医院価格 ￥20,500／セット

ハンドミックスセット

標準医院価格 ￥20,500／セット

詳細は特設サイトで！ https://www.tokuyama-dental.co.jp/bondmer2

株式会社トクヤマデンタル
本　社　〒110-0016 東京都台東区台東1-38-9
お問い合わせ・資料請求
インフォメーションサービス
0120-54-1182
受付時間
9:00～12:00/13:00～17:00（土日祝日は除く）

Webにもいろいろ情報載っています!!
トクヤマデンタル　検索

●札 幌 TEL011-812-5690　●仙 台 TEL022-717-6444　●東 京 TEL03-3835-7201　●名古屋 TEL052-932-6851　●大 阪 TEL06-6386-0700　●福 岡 TEL092-412-3240

Thinking ahead. Focused on life.

MORITA

Spaceline EX

スペースライン EXが iFデザイン賞の金賞を受賞

ドイツのiFデザイン賞は、50年以上の歴史を有し、各国から選ばれた審査員によって厳正に選考される世界的に権威のあるデザイン賞です。世界中から6,400以上のエントリーが有った中、最優秀デザインとして75件に授与される金賞（ iF GOLD AWARD ）をスペースライン EXが受賞しました。人間工学に基づき緻密に計算されたデザインは、患者さんだけでなく術者にも理想的で洗練されたデザインであると評価されました。

iF GOLD AWARD 2018

発売
株式会社 モリタ

大阪本社　大阪府吹田市垂水町3-33-18
〒564-8650 T 06. 6380 2525
東京本社　東京都台東区上野2-11-15
〒110-8513 T 03. 3834 6161
お問合せ　お客様相談センター 歯科医療従事者様専用
T 0800. 222 8020（フリーコール）

製造販売・製造
株式会社 モリタ製作所

本社工場　京都府京都市伏見区東浜南町680
〒612-8533 TEL 075-611-2141
久御山工場　京都府久世郡久御山町市田新珠城190
〒613-0022 TEL 0774-43-7594

販売名：スペースライン
一般的名称：歯科用ユニット
機器の分類：管理医療機器（クラスⅡ）
特定保守管理医療機器
医療機器認証番号：228ACBZX00018000

www.dental-plaza.com